# Extensional development and contractional reactivation of salt walls: examples from the southeastern Paradox Basin (SW Colorado) and the Eastern Prebetic Zone (SE Spain)
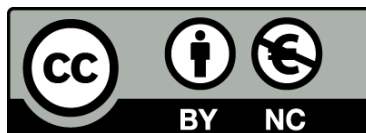
Frederic Oriol Escosa Bernal

# EXTENSIONAL DEVELOPMENT AND CONTRACTIONAL REACTIVATION OF SALT WALLS:

## EXAMPLES FROM THE SOUTHEASTERN PARADOX BASIN (SW COLORADO) AND THE EASTERN PREBETIC ZONE (SE SPAIN)

Institut de Recerca Geomodels
Grup de Geodiàmica i Anàlisi de Conques
Departament de Dinàmica de la Terra i de l'Oceà
Universitat de Barcelona

Frederic O. Escosa Bernal
Ph.D. Thesis
Juny 2019
Supervisor: Dr. Eduard Roca i Abella

Institut de Recerca Geomodels

Grup de Recerca de Geodinàmica i Anàlisi de Conques

Departament de Dinàmica de la Terra i de l'Oceà

UNIVERSITAT DE BARCELONA

# Extensional development and contractional reactivation of salt walls: examples from the southeastern Paradox Basin (SW Colorado) and the Eastern Prebetic Zone (SE Spain)

Memòria de Tesi Doctoral -com a compendi d'articles- presentada per **Frederic Oriol Escosa Bernal** per optar al grau de Doctor en Ciències Geològiques per la Universitat de Barcelona.

Aquesta memòria ha estat realitzada dintre del Programa de Doctorat de Ciències de la Terra (H0Z01–HDK09) sota la direcció del **Dr. Eduard Roca i Abella**.

Frederic O. Escosa Bernal

Barcelona, Juny 2019

Dr. Eduard Roca i Abella

*A la meua família, amics i amigues*

# Agraïments/Acknowledgements

Són moltes les persones que d'alguna manera o altra han fet possible l'inici i el desenvolupament d'esta tesi, i ara que s'acosta el final d'esta etapa cal nombrar i agrair. Quede dit per endavant, que mentre estic escrivint estes línies no puc evitar que se m'escape algun somriure entremesclat amb una mica de nostàlgia pels records innumerables que em venen al cap.

En primer lloc, m'agradaria donar les gràcies al meu director de tesi, l'Eduard Roca, per les ensenyances i coneixements transmesos durant tots aquests anys. Eduard, com a alumne teu, sobretot em quedo amb la teva meticulositat alhora d'entendre i transmetre la geologia la qual cosa m'ha permès, com també a tants altres abans que jo, ser una mica millor geòleg estructural. Definitivament has creat una escola. Gràcies també per la llibertat, la confiança i per les oportunitats que m'has anat donant durant aquests anys. Se que en més d'un moment has pensat que anava pel camí equivocat. Però tot i així has deixat que m'equivoqués o l'encertés perquè sabies que això em forjava com a científic. Per això i molt més, moltes gràcies.

En segon lloc m'agradaria donar les gràcies a l'Oriol Ferrer per "reclutar-me" en aquell llunyà treball de final de llicenciatura del 2012. Oriol, se que per a tu vaig ser un mal de cap més quan et disposaves, entre altres coses, a acabar la teua tesi. En canvi, aquell fet va significar un abans i un després. Estic segur que sense aquella primera experiència amb la modelització analògica, jo no estaria on estic ara. Així doncs, gràcies també per tots aquests anys de suport i amistat, tant professional com personal, sempre disposat a acompanyar-me al camp o a revisar articles quan més ho he necessitat.

En tercer lloc, donar les gràcies particularment al Josep Antón Muñoz, i en general a l'Institut de Recerca Geomodels, al Departament de Dinàmica de la Terra i de l'Oceà i al Grup de Geodinàmica i Anàlisi de Conques. Pel seu suport logístic i financer i per facilitar tot allò que he necessitat durant aquests anys de recerca. Així mateix, agrair especialment a la Teresa Beamud i a la Ana Romera per posar-ho en pràctica i fer-ho possible sempre amb un somriure. Sense aquesta amabilitat rebuda de ben segur que els resultats que es presenten en aquest volum no serien els mateixos.

A big thanks is owed to Kate Giles and Mark Rowan who helped me through the first part of this study in the Paradox Basin. Working with you has been an awesome and rewarding experience. Kate, thank you for your generosity, for the financial support of the Institute of

Tectonic Studies and the Salt-Sediment Interaction Research Consortium. Thank you also for proposing me to do field-work in the Gypsum Valley Diapir and to letting me become part of your group as well as for sharing your knowledge about the geology of the Paradox Basin and your lessons during the field-work campaigns. Too many things to knowledge, but c'mon Kate they are all true! Many thanks especially to Mark Rowan for your unselfish assistance from the beginning of the Gypsum Valley project. Thank you for your advices and meticulous corrections during the construction of the geological map and cross-sections of the SE termination of the Gypsum Valley salt wall. But also, during the writing process of the first paper enclosed in this thesis. I really appreciate your help, which at the same time helped and encouraged me to become a better scientist.

Als companys de feina i també amics del Departament de Dinàmica de la Terra i de l'Oceà i de la Facultat de Geologia que durant tots aquests anys han sigut un suport important, tant personal com professional. Gràcies també per escoltar i per "perdre" el temps intentant resoldre els meus dubtes i/o qüestions sempre que ho he necessitat. Així doncs, gràcies a la Maria Roma, Oriol Pla, Luís Valero, Núria Carrera, Mireia Butillé, Esther Izquierdo, Marco Snidero, Pau Arbués, Òscar Gratacós, Fani Górriz, Jordi Miró, Daniel Bello, Pablo Granado, Pablo Santolaria, Marco de Matteis, Patricia Cabello, Marina Nebot, Rodolfo Uranga, Elisabeth Wilson, Joana Mencos, i altres que segur que em deixo. Gràcies especialment a la Mireia Butillé per estar sempre disposada a resoldre dubtes sobre qualsevol programari; a la Núria Carrera que, compartint "pupitre" al meu costat, ha tingut sempre a punt la resposta adient a les meues preguntes imprevistes; a l'Oscar Gratacós per la seva ajuda logística a la sala 226 i pels bons consells sobre disseny i geologia; al Daniel Bello per la seva inestimable ajuda amb el Petrel i el pas a profunditat de la sísmica; a la Fani per la infinitat d'hores de camp junts fent campanyes de MT o recollint dades estructurals i fent mapa al Prebetic oriental. I finalment agrair a la Maria Roma i a l'Oriol Pla per la seva amistat i recolzament durant aquests anys, tant en els bons com els mal moments. Sempre hem dit que vam començar sense saber ben bé on es posàvem, però crec que, mirat en perspectiva, hem fet plegats un molt bon treball.

A big thanks to my friends in El Paso. To Kyle Deatrick, Evey Gannaway, Ally Mast, Rachelle Kernen, Rib Langford and the other Pasoans. Thank you for your warm welcome the first time I arrived in town, and also for the successive ones. With you and a margarita in our hands, the life in the desert was much more pleasant. I'd like to give special thanks to Kyle Deatrick and Evey Gannaway who helped me in so many ways. Thank you, for always offering

me a place to stay in the city. Kyle, thank you for your tremendous help doing field work in the Gypsum Valley. Also, for our running sessions climbing the Franklins, our dirtbag trips to climb at Indian Creek or Hueco Tanks, or that time we tried to attempt the summit of the Mount Tukuhnikivatz with snow covering up to our chests. Definitely, all of you have made me to keep a fantastic memory of my time in the Western United States.

Gràcies també als companys i companyes de fatigues del Trail Roquetes i la Joca Club Alpí. Per les sessions d'escalada, per les sortides i expedicions arreu, per les rises, pels quilòmetres correguts, caminats o rodats i sobretot per la desconnexió que això ha suposat i que tant necessària ha estat al llarg d'aquests anys i que tant he agraït.

Gràcies als companys de la carrera que em van ajudar amb les primeres campanyes de camp: al Lluís Camps, l'Héctor Carmona i el Gerard Montardit. Així com també als amics de Roquetes, sense els quals aquests anys definitivament haguessin sigut molt més durs de passar.

Gràcies infinites als meus pares, la meua germana i a la meua àvia per la vostra estima demostrada. Per suport i comprensió que m'heu donat durant tots aquests anys i per recolzar-me en els moments que més ho he necessitat. També, gràcies per encoratjar-me sempre amb tot allò que m'he proposat fer. Finalment, voldria agrair d'una manera molt especial a la Núria, a qui li ha tocat patir la part més fotuda de la tesi: el final. Tot i això gràcies per fer-ho tot més fàcil, sempre amb un somriure i per enredar-me en el món de l'esquí, el descens de barrancs, les vies ferrates,... en definitiva gràcies per la teva estima.

Per tot això, aquesta tesi és també en part vostra.

12 de Juny de 2019

# Table of Contents

# List of Figures and Tables

# CHAPTER 2

## CHAPTER 3

# ABSTRACT

This thesis uses a field-based approach complemented with geophysical and well data to investigate the controlling factors on the geometry and kinematics of salt walls developed above extensional faults whose movement occurs during or after the deposition of salt; and the behavior of these precursor diapiric structures when are involved in a subsequent thin-skinned contractional deformation. This is an investigation that has been carried out by defining the geometric and temporal relationships between the structure of the salt walls and their adjacent strata in two distinct field-work areas: the southeastern Paradox Basin (SW Colorado) and the Eastern Prebetic Zone at the Jumilla region (SE Spain).

At the SE Paradox Basin, the analyzed salt wall is the Gypsum Valley Diapir, which was mostly driven by differential sedimentary loading and developed above a pre-existing subsalt fault without significant regional extension or contraction. The early style of diapirism was that of single-flap active NW-trending salt wall, with a thinned roof bounded by a suprasalt counterregional fault over its northeastern edge. Erosion of the thinned diapiric roof triggered the salt breakthrough and the onset of passive diapirism. Subsequent evacuation of deep salt into the growing diapir generated diapir-flanking depocenters with progressive rotation of the southwestern flank into the megaflap geometry and consequent widening of the diapir. Therefore, the present-day structure of the salt wall is characterized by a highly asymmetric stratal architecture on its northeastern and southwestern flanks, with thicker, deeper, gently dipping strata in the depositionally proximal (NE) minibasin and thinned older strata rotated to near-vertical in a megaflap on the distal (SW) side. The megaflap terminates to the SE through a progressive decrease of the bedding dip and ultimately truncation by a pair of radial faults bounding a down-dropped block with lower dips. East of these faults, the salt wall termination is a moderately plunging nose of salt overlain by a gently southeast-dipping strata separated from the down-dropped NE minibasin by a counterregional fault.

At the Jumilla region instead, the studied salt walls and salt-related structures correspond to diapirs, made up of pre-kinematic salt, triggered by thick-skinned extension during the development of a passive margin (i.e. the Mesozoic Iberian margin of the Maghrebian Tethys), which was later incorporated into the external part of the eastern Betic foreland fold-and-thrust belt. In this scenario, the initial extension led to a major decoupling of the deformation with planar subsalt extensional faults overlain by monoclinal drape folds and suprasalt faults and extensionally triggered diapirs (salt walls). After extension, this inherited sub- and suprasalt structure together with the formed diapirs controlled the subsequent contractional deformation

in such a way that: 1) determined a stepped geometry for the salt and therefore for the future décollement level where the thin-skinned contractional deformation is propagated; and 2) allowed the development of a series of fault-bend folds where the salt walls and salt-related structures concentrated the major part of the thin-skinned contractional deformation. This deformation was resolved first by narrowing and squeezing of the preexisting salt structures (i.e. cryptic shortening) and then, when secondary welds were developed, by the formation of thrust faults at their pedestals.

The results of these investigations have permitted to propose a series of simple end-member models addressing the extensional formation and later contractional reactivation of the studied salt walls developed above a thick-skinned extended basement. These simple models together with the discussion conducted in this thesis suggest that the geometry and kinematics of salt walls triggered by thick-skinned extension are strongly controlled by: 1) the geometry of the subsalt faults; 2) the spatial and temporal thickness variations of the overburden; 3) the salt thickness variations and the available deep salt budged to flow into the forming salt walls; 4) the lateral changes in the syn-kinematic sedimentary loading induced by the subsalt fault motion; and, 5) the position of the salt breakthrough and the pre-kinematic salt wall piercement geometry. And, in relation to a later thin-skinned contractional reactivation of these salt walls, this investigation points out that the resulting structure is largely determined by: 1) the subsalt structure defined by the dip, dip direction and the displacement magnitude of the subsalt faults; 2) the thickness/strength and 3) the structure of the pre-contractional overburden adjacent to the contractionally reactivated salt wall; 4) the ratio between amount of shortening and the initial width of the diapir; and finally, 5) other factors like the length, shape and orientation of the precursor salt wall, the possible linkage between adjacent diapiric structures and the lithological composition of the evaporitic sequence.

# RESUM EN CATALÀ

Aquesta tesi doctoral utilitza treball de camp complementat amb dades geofísiques i de pous d'exploració per tal d'investigar els factors que controlen la geometria i la cinemàtica de les parets salines desenvolupades a sobre de falles extensionals –el moviment de les quals ocorre durant i després la deposició de la sal. Així mateix, també analitza el comportament d'aquestes parets salines preexistents quan es sotmeten a una deformació contractiva posterior de pell fina. Per tant, aquesta és una investigació que s'ha dut a terme definint la geometria i les relacions temporals entre l'estructura de les parets salines analitzades i els estrats adjacents en dos zones de camp situades a: la regió sud-est de la Conca de Paradox (SW del Colorado) i a la part est del Prebetic a la zona de Jumilla (SE d'Espanya).

Al sud-est de la Conca de Paradox, la paret salina analitzada és el Gypsum Valley Diapir, el qual es va formar principalment per diferència de càrrega sedimentaria a sobre d'una falla subsalt preexistent. Una falla que no va tenir moviment extensiu o contractiu significatiu durant la formació de la paret salina. L'estil inicial de diapirisme va ser del tipus actiu i single-flap, caracteritzat per un sostre aprimat delimitat al nord-est per una falla de tipus counterregional i suprasalt. L'erosió d'aquest sostre diapiric desencadenà la perforació de la sal i l'inici del diapirisme passiu. Posteriorment, l'evacuació de la sal cap al diapir va generar la formació de depocentres sedimentaris flanquejant la paret salina. Durant aquest procés, els estrats localitzats al flanc sud-oest del diapir van anar rotant progressivament, formant així una geometria en forma de megaflap, al mateix temps que l'amplada la paret salina anava incrementant. Per tant, l'estructura actual de la paret salina es caracteritza per ser asimètrica i per tenir: un costat nord-est amb una successió sedimentaria potent, profunda i amb cabussaments suaus; i un costat sud-oest amb una successió sedimentaria aprimada, somera i amb cabussaments que progressivament es van verticalitzant per tal de formar un megaflap. Cap al sud-est, aquest megaflap desapareix a mesura que el seu cabussament va disminuint on finalment queda trucat per un parell de falles radials que delimiten un graben situat al límit sud de la paret salina. Finalment, a l'est de les falles radials, la paret salina presenta una terminació de sal recoberta per estrats sedimentaris descrivint conjuntament cabussaments graduals cap al sud-est. Una terminació, que està separada del costat nord-est, per una falla de tipus counterregional i suprasalt.

Per altra banda, a la regió de Jumilla, les parets y altres estructures salines estudiades corresponen a diapirs constituïts per salt pre-cinemàtica. Aquestes es van desenvolupar a partir de l'extensió de pell gruixuda de l'escorça continental durant la formació d'un marge passiu, concretament el marge Ibèric del Tethys magrebí durant el Mesozoic. Posteriorment, aquest

marge va ser incorporat en un sistema de plegament formant així la part externa i més oriental de la Serralada Bètica. En aquest sentit, l'extensió inicial donà lloc a un desacoblament de la deformació tectònica amb falles planars i extensionals de tipus subsalt recobertes per una cobertora sedimentaria deformada per plecs monoclinals, per falles de tipus suprasalt i per diapirs i parets salines. Després d'aquesta etapa d'extensió, l'estructura heretada conjuntament amb els diapirs desenvolupats varen controlar la deformació contractiva posterior de manera que: en primer lloc, van determinar una estructura esglaonada del nivell salí i per tant del futur nivell de desenganxament on la deformació contractiva de pell fina es podia propagar; i en segon lloc, van facilitar el desenvolupament d'una sèrie de plecs de tipus fault-bend a la cobertora sedimentaria on les parets i les altres estructures salines van concentrar la major part de la deformació de pell fina. Concretament, aquesta deformació es va resoldre amb l'escanyament de les estructures salines preexistents (escurçament críptic), la formació de cicatrius salines secundaries pel tancament de les tiges d'aquests diapirs, i finalment, amb la formació d'encavalcaments la seva base.

Els resultats d'aquestes investigacions han permès proposar una sèrie de models geològics que tenen com a objectiu abordar la formació extensiva i la posterior deformació contractiva de les parets salines estudiades. Aquest models, conjuntament amb la discussió inclosa en aquesta tesi, suggereixen que la geometria i la cinemàtica de parets salines desenvolupades a partir de l' extensió de pell gruixuda estan controlades per: 1) la geometria de les falles subsalt; 2) les variacions en l'espai i el temps del gruix de la cobertora sedimentaria; 3) les variacions de gruix del nivell salí i la quantitat de sal disponible per tal de fluir cap a la paret salina en formació; 4) els canvis laterals en la diferencia de càrrega sedimentaria sin-cinemàtica promoguda pel moviment de la falles de tipus subsalt; i finalment 5) la posició al llarg del sostre del diapir aprimat on té lloc la extrusió de la sal i la geometria pre-cinemàtica prèvia a la perforació del diapir. A més a més, aquesta investigació indica que la posterior reactivació contractiva de pell fina de parets salines preexistents ve determinada per: 1) l'estructura subsalt, la qual està definida pel cabussament, la direcció de cabussament i la magnitud de desplaçament de les falles subsalt; 2) el gruix/resistència i 3) l'estructura pre-contractiva de la cobertora sedimentaria adjacent a les parets salines reactivades; 4) la relació entre la quantitat d'escurçament de pell fina i l'amplada inicial del diapir; i finalment, 5) altres factors de control com la longitud, la forma i orientació de la paret salina precursora, així com la interconnexió amb altres parets salines veïnes i la composició litològica de la seqüència evaporítica involucrada durant el diapirisme.

# PREFACE

**Motivation and objectives**
**Structure and organization of the thesis memoir**

*The cover photo of the Preface depicts an overview of the basecamp installed in the SE termination of the Gypsum Valley salt wall during the successive field-work campaigns.*

# Motivation and objectives

Together with salt stocks, salt walls are the most classic of salt structures. In map-view, they are elongated diapirs that form the fundamental building blocks of many sedimentary basins containing mobile salt (e.g. Zechstein Basin, Atlas Mountains, Newfoundland, Sverdrup Basin, La Popa Basin or Nordkapp Basin). Their abundance is equally remarkable. For example, the Precaspian Basin alone contains about 1,800 named stocks and walls (Volozh et al., 2003).

These salt bodies and the corresponding flanking strata have become increasingly interesting for the hydrocarbon exploration because they can bear economically exploitable hydrocarbon gas and oil fields. For example, in the northern Gulf of Mexico, along the South Atlantic margins or in the Persian Gulf, hydrocarbon reservoirs flanking steep-sided salt diapirs account for significant oil and gas reserves (e.g. Kirkland & Evans, 1981; McGee et al., 1994; Alsharhan and Nairn, 1997; Warren, 2006; Wagner, 2010). Like the other salt structures, salt walls create structural hydrocarbon traps, control the reservoir and facies distribution, affect the fluid migration pathways, and regarding the petroleum systems, they impact on the maturation and generation of hydrocarbons. However, despite their great affluence in the salt-bearing sedimentary basins and their economic importance for the oil and mining industry, many aspects of their growth and development have been misunderstood for decades.

The structure of salt walls and adjacent strata as well as the lithological and sedimentological features of the involved rocks are critical factors during exploration, development and risk assessment. The resolution limitations of the seismic reflection data which hardly image steep surfaces, the complexity of developing velocity models for depth conversions and the one-dimensional well sampling may difficult, during the exploration process, the recognition of the salt body boundaries as well as the geometry of the subsalt strata, leading to missed opportunities or failed wells (Jackson & Lewis, 2012; Fiduk et al., 2014; Rowan et al., 2016). These issues, along with the reservoir prediction and risk assessment, reinforce the need for field-based studies of analogue outcropping salt structures. Thus, the integrated approach combining field mapping and structural analysis with seismic reflection and well data of outcropping salt walls improve the ability to interpret the three-dimensional structure and evolution of analogue structures imaged in seismic reflection data from many salt-bearing sedimentary basins. Therefore, the results of the present study have implications for providing a better understanding of the processes controlling the three-dimensional structure and development of salt walls, and thus improving the risk assessment in

hydrocarbon exploration.

The geometry and kinematics of salt walls are controlled by the driving mechanism (differential sedimentary loading, regional extension and/or contraction), and any younger deformation in which the basin might be involved. In this regard, salt walls like the other salt bodies, constitute the weakest part of the cover and consequently they tend to localize any ulterior deformation occurring in the area (e.g. Nilsen et al., 1995; Roca et al., 2006; Rowan & Vendeville, 2006; Callot et al., 2007; Dooley et al., 2015). Nevertheless, previous geological studies and scaled physical models mainly aimed at only one specific tectonic setting and more rarely at case studies with superposition of driving mechanisms (e.g. in the Great Kavir, Jackson et al., 1990; the Santos Basin, Jackson et al., 2014; La Popa Basin, Rowan et al., 2003; the Bicorb-Quesa salt wall, Roca et al., 1996, 2006). In addition, they were focused on cross-sectional views of near-diapir deformation and thus were primarily two-dimensional (e.g. Fletcher et al., 1995; Giles & Lawton, 2002; Giles & Rowan, 2012). While these studies stressed the relevance of salt-sediment interaction, rarely field data from several salt walls developed in different tectonic settings have been combined to obtain global factors controlling the geometry of salt walls and their adjacent strata as well as their kinematics.

To this end, the main objectives of this thesis are three-fold: (1) to document, from a field-based approach, the three-dimensional structure of salt walls developed by thick-skinned extension and affected by adjacent differential sedimentary loading and followed by a later contractional deformation; (2) to define the existing relationships between the geometry of the diapir and the flanking strata; and finally, (3) to establish a series of factors controlling the geometric and kinematic evolution of salt walls resulting from thick-skinned extension whether it occurs during or after the deposition of salt; and finally, to determine the constrains on the geometry and kinematic evolution of these precursor salt walls when they are affected by a subsequent thin-skinned contractional deformation.

To achieve these goals, field work has been performed in the Gypsum Valley salt wall at the southeastern Paradox Basin (SW Colorado, USA), and in the diapirs and salt-cored structures of the Jumilla region at the Eastern Prebetic Zone (SE Spain; **Fig. I.I**). The Gypsum Valley salt wall was mostly driven by differential sedimentary loading and developed above a basement fault without significant regional extension or contraction. At the Jumilla region, instead, the salt walls correspond to diapirs triggered by thick-skinned extension during the development of a passive margin, which was later incorporated into the external part of the Betic foreland fold-and-thrust belt.
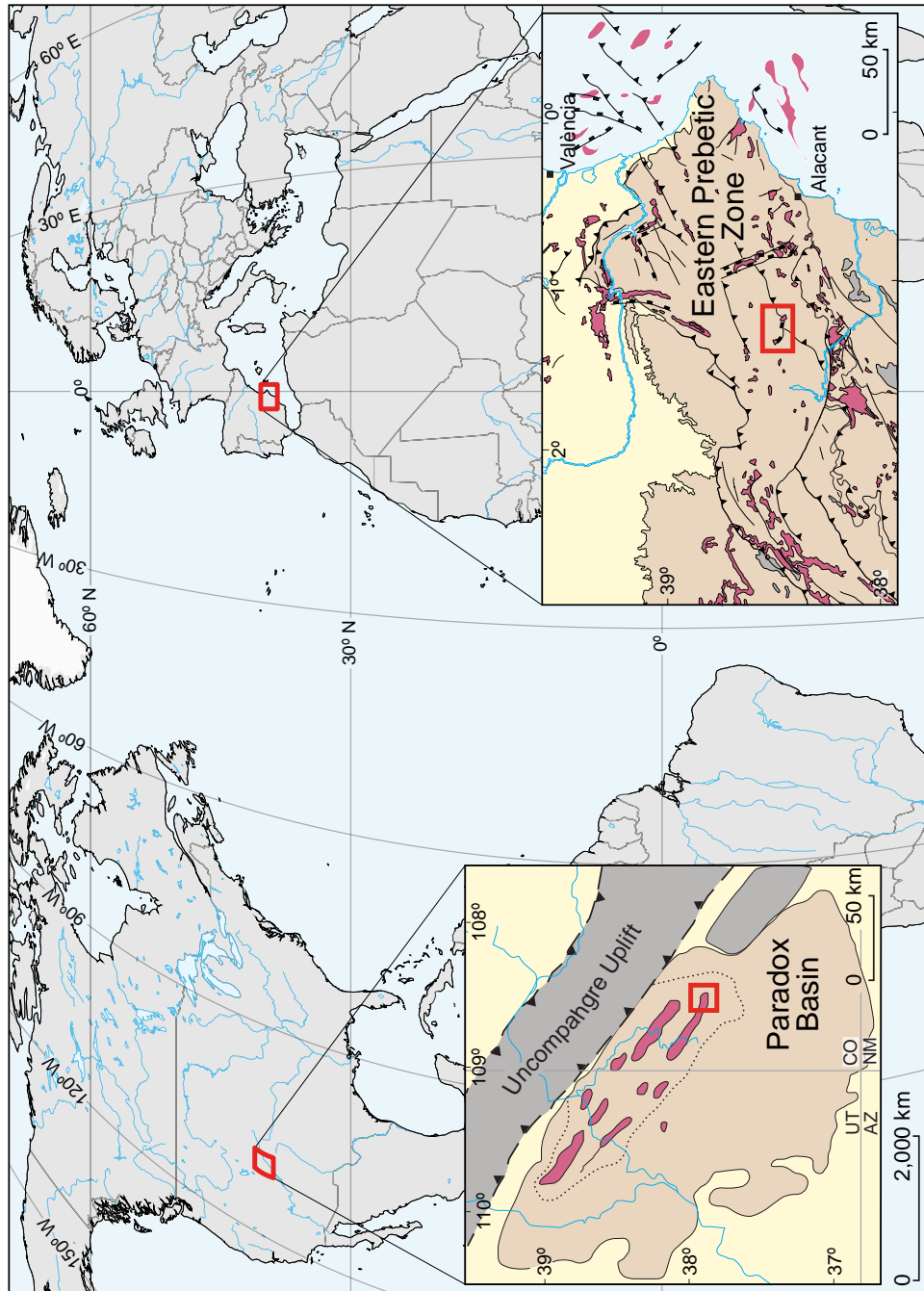
**Figure I.I.** Equal-area pseudocylindrical projections (courtesy of Tom Patterson) showing the location of the studied areas and respective magnified maps depicting the main geological features. Note displayed in pink the location of the salt structures outcropping in both studied areas. Red squares indicate the salt walls and salt-cored structures that have been analyzed in this thesis.

## Structure and organization of the thesis memoir

This PhD thesis has been designed as a compilation of scientific articles published in journals that are indexed by the Journal Citations Reports  and integrated with the Web of Science (https://www.fecyt.es/es/recurso/web-science). On the basis of the previous outlined approach, the present memoir has been organized in the following chapters:

**Chapter 1** introduces the fundamental aspects of the diapiric emplacement under three tectonic scenarios (extension, contraction and differential sedimentary loading), details the particular geometries of salt walls and adjacent strata during the diapiric evolution, and describes different reactivation mechanisms for salt walls and the types of flanking faults that form in each scenario. Thereby, this chapter provides the readership not versed in salt tectonics with the essential tools to easily understand the next chapters comprised in this memoir. After this general introduction, a summary of the methodological workflow followed during the investigation is also presented. Importantly, the terminology used to describe location with respect to autochthonous salt include the following terms: "overburden" (noun) and "suprasalt" (adjective) for designating the sedimentary pile and/or deforming structures that are lying above the autochthonous salt; "basement" (noun) and "subsalt" (adjective) for indicate strata and/or deforming structures located beneath the autochthonous salt layer; and "cover" (noun) when referring the entire sedimentary pile above crystalline basement including presalt strata, salt, and overburden. In addition to this, a specific color pattern has been used along the figures included in chapters 1 and 3 for consistency and a better understanding. Thereby, the blue–green colors indicate deposition of sediments prior to salt movement (i.e. pre-kinematic strata), and the red–orange–yellow colors indicate synchronous deposition of sediments during salt movement (i.e. syn-kinematic strata).

**Chapter 2** represents the core of this thesis including the main results of the investigation, which were materialized in three published articles (see **Annexes 1**, **2**, and **3**): the first paper was devoted to the Gypsum Valley salt wall at the Paradox Basin (SW Colorado, USA), and the other two were dedicated to the diapirs and salt-cored structures of the Jumilla region at the Eastern Prebetic Zone (SE Spain). Accordingly, this chapter is subdivided in two sections, in which the geological setting of each studied area is presented before summarizing the main results obtained from these investigations.

So, after a brief introduction, **Chapter 2.2** is inspired by the first article with the following complete reference:

- Escosa, F. O., Rowan, M. G., Giles, K. A., Deatrick, K. T., Mast, A. M., Langford, R. P., Hearon IV, T. E., & Roca, E. (2018c). Lateral termination of salt walls and megaflaps: An example from Gypsum Valley diapir, Paradox Basin, Colorado, USA. *Basin Research*, *31*, 191–212. doi:10.1111/bre.12316 (**Annex 1**)

The aim of this paper (Escosa et al., 2018c) is to present new data from the southeastern end of the Gypsum Valley salt wall (SW Colorado), in order to evaluate the structural styles and associated controls on lateral termination of salt walls and megaflaps developed by differential sedimentary loading. So, we produced a detailed geological map and six cross-sections of the SE-termination of the Gypsum Valley salt wall, allowing us to characterize the 3D structure and kinematic evolution of the salt wall and associated megaflap. Then, we compared these findings with other salt walls in the Paradox Basin, and to analogous counterregional systems in the northern Gulf of Mexico in order to establish simple models for the lateral terminations of salt walls and megaflaps.

And **Chapter 2.3** contains a summary of the main results and conclusions of the other two articles with the following complete references:

- Escosa, F. O., Ferrer, O., & Roca, E. (2018a). Geology of the Eastern Prebetic Zone at the Jumilla region (SE Iberia). *Journal of Maps*, *14*, 77–86. doi:10.1080/17445647.2018.1433562 (**Annex 2**)

- Escosa, F. O., Roca, E., & Ferrer, O. (2018b). Testing thin-skinned inversion of a prerift salt-bearing passive margin (Eastern Prebetic Zone, SE Iberia). *Journal of Structural Geology*, *109,* 55–73. doi:10.1016/j.jsg.2018.01.004 (**Annex 3**)

The first paper (Escosa et al., 2018a) presents a geological map and cross-sections at 1: 50,000 scale of the Eastern Prebetic Zone at the Jumilla region (SE Spain); documents printed at A1 size and enclosed at the end of this memoir. The geological map is accompanied with an explanation of the stratigraphic units and the general structure cropping out in the study area. This allowed to decipher the tectonic history of the Eastern Prebetic Zone at the Jumilla region, and then to discuss the Upper Jurassic to present day geodynamic evolution

considering the geological framework of the western Mediterranean.

The second article (Escosa et al., 2018b) includes the main results deriving out of the analysis and interpretation of surface and subsurface data from the Eastern Prebetic Zone at the Jumilla region (SE Iberia). The main objective of this study is to determine the role played by the pre-kinematic salt in the development of the proximal part of the South Iberian passive margin and its subsequent incorporation into the external part of the Betic fold-and-thrust belt. We first document and analyze the architecture of the existing salt walls and salt-related structures and adjacent strata. Then, we determine the structural styles and associated controls on the development of salt structures during thick-skinned extension and their reaction to a subsequent thin-skinned contractional deformation.

**Chapter 3** includes a discussion of the generic controls on the geometric and kinematic evolution of salt walls developed above subsalt faults whose movement occurs during of after the deposition of salt. And addresses the constrains on the geometry and kinematic evolution of these precursor salt walls when they are affected by a subsequent thin-skinned contractional deformation.

**Chapter 4** lists the partial and general conclusions of this thesis, stating the global factors controlling the geometric and kinematic evolution of salt walls in the above outlined tectonic settings. Finally, the **Reference** chapter details the bibliographic works mentioned along the thesis memoir.

# CHAPTER 1. INTRODUCTION

*The cover photo of Chapter 1 depicts the Klondike Ridge and, outcropping in its northwestern face, the Permian to Jurassic strata thinning-out and overlying the southeastern termination of the salt wall.*

## 1.1. Introduction to salt walls

Salt diapirs are composed of a ductile mass of evaporites and other types of rocks that have pierced their initial roof and have discordant contacts with the encasing overburden (Mrazec, 1907). They can display variable map-view shapes and when they are steep-sided are classified according to two end-members: stocks and walls (Jackson & Hudec, 2017). Salt stocks include pluglike bodies having equant or sub-circular planforms (**Fig. 1.1a**). Conversely, salt walls have clearly elongated planforms (**Fig. 1.1b**). When the diapir is subtle or little elongated, such classification becomes rather subjective and both names have been used indiscriminately to describe the corresponding salt bodies. To solve this discrepancy, Hudec & Jackson (2011) proposed to term these as salt stocks when the planform axial ratio is less than 2, and salt walls when it is greater than 2 (Trusheim, 1960; **Fig. 1.1**); but, as is indicated by the same authors (Jackson & Hudec, 2017), this is an arbitrary value and therefore disputable.
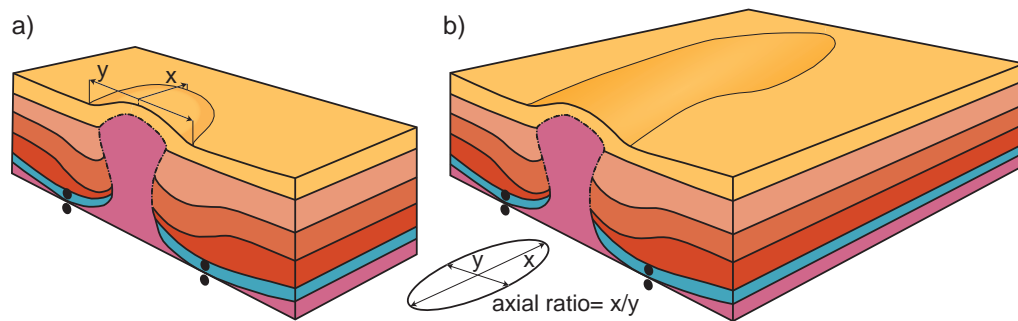
**Figure 1.1.** Block diagrams showing the main differences between a salt stock and a salt wall. x: length of the diapir in plan-view; y: width of the diapir in plan-view. All diapirs have discordant contacts against their overburden. Modified from Jackson & Hudec (2017).

It is important to not confuse salt walls and salt anticlines. Both are salt ridges (i.e. elongated salt bodies in map-view), but the latter are not diapirs because they do not pierce the overlying suprasalt strata. Therefore, defined by DeGolyer (1925), salt anticlines are elongated (planform axial ratio of two or more) upwellings of salt having concordant overburden (e.g. see the buckle anticline from the southern North Sea in **Fig. 1.2**).

## 1.2. Salt wall formation

The diapiric emplacement of buried salt and, hence the formation of any salt wall, is driven by removing or displacing the brittle overlying strata. Global tectonics can trigger salt
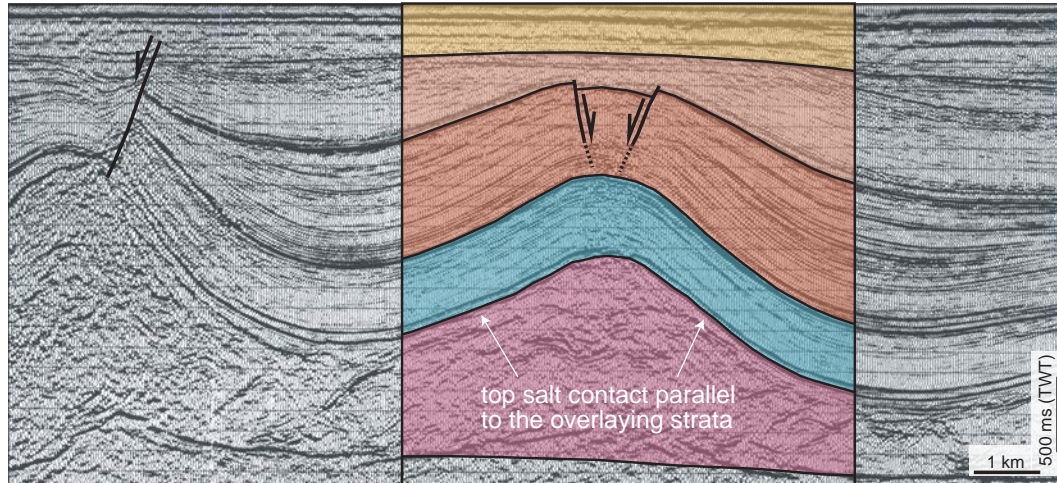
**Figure 1.2.** Two-dimensional time-migrated seismic profile depicting an example of a salt-cored buckle fold in Silverpit Basin (southern North Sea). Note that the top salt contact is parallel to the overlying strata. Modified from Stewart (2007).

movement, whether under extension, contraction and/or strike-slip deformation. But even in the absence of a tectonic drive, salt can begin to move and pierce the overburden if there are differences in the hydraulic head above salt (Vendeville & Jackson, 1992a; Hudec & Jackson, 2007; **Fig. 1.3**). Hydraulic head includes two components: elevation head and pressure head. Individually or in combination, both can trigger salt flow and consequently diapir initiation as long as the resulting hydraulic head is great enough to overcome the strength of the overburden and the viscous drag effects in the salt layer.

Lateral changes in the hydraulic head can be triggered by regional tectonics but also by depositional and erosional processes. Considering the geological settings of the studied salt walls in this thesis, three of the most common generators of salt flow are briefly described below.
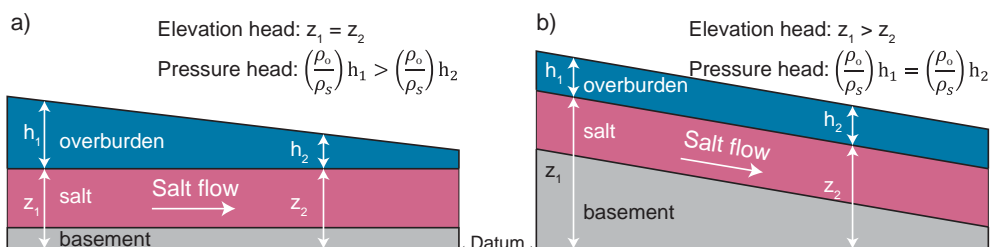


**Figure 1.3.** For simple geometries, the initial direction of salt flow can be inferred from hydraulic heads. Salt flow driven by a) pressure head or by elevation head b), whether or not the overburden is denser than salt. Modified from Hudec & Jackson (2007).

## 1.2.1. Extension

According to the structural and sedimentological analysis of salt basins (e.g. Zechstein Basin, Mohr et al., 2005; Krzywiec, 2006; Atlas Mountains, Saura et al., 2014; Martín-Martín et al., 2016; Newfoundland, Balkwill & Legall, 1989) combined with scaled physical models (Vendeville & Jackson, 1992a; Jackson & Vendeville, 1994), regional extension may initiate and control the growth of salt walls. This is because extension modifies the overall hydraulic head of the system and favors salt migration and the subsequent development of diapirs. Furthermore, because of the rectilinear trace of the extensional faults in map-view, this scenario favors the formation of salt walls rather than circular salt stocks. Considering the scaled physical models, diapirism may undergo three evolutionary stages: reactive, active, and passive diapirism (**Fig. 1.4**). Accordingly, lengthening and thinning of the overburden creates a graben at the surface and a reactive diapir at depth (**Fig. 1.4a**), thus salt reacts to extension by overall thinning and by passively filling the space beneath the graben. The result is a reactive diapir, triangular in cross-section and elongate in map-view, flanked by growth faults that are younger towards the center of the graben. If the diapir is tall enough and the overburden is thinned and weakened, the diapir will actively punch through to the surface (i.e. active stage; **Fig. 1.4a**). Once at the surface, the diapir will grow passively as surrounding suprasalt strata subside into and displace the salt in the source layer towards the diapir (Nelson, 1989; **Fig. 1.4a**).
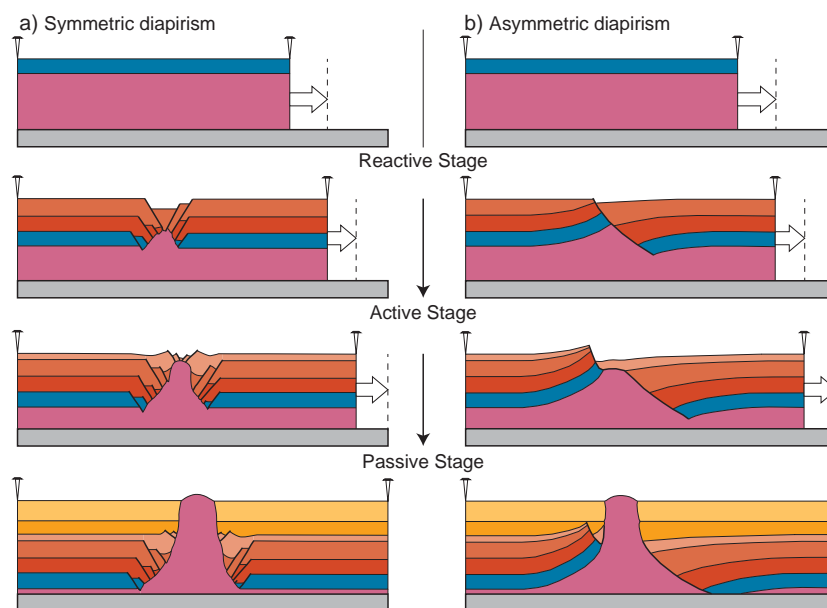


**Figure 1.4.** Schematic cross-sections illustrating the a) symmetric and b) asymmetric evolution of diapiric piercement through syn-kinematic overburden during thin-skinned extension. Symmetric diapiric evolution modified from Vendeville & Jackson (1992a).

In the reactive stage, the diapir may be controlled by symmetric and conjugated growth faults (**Fig. 1.4a**) or by a single asymmetric extensional fault with a salt roller in its footwall (**Fig. 1.4b**). In general, the symmetry of the diapir is controlled by the geometry of the salt detachment (Stewart, 1999). So, the formation of salt walls during extension may result from the gravitational failure of a tilted passive margin (**Fig. 1.5a**), or alternatively from crustal extension (e.g. thick-skinned extension in rift basins) affecting both the overburden and subsalt rocks (Jackson & Vendeville, 1994; **Fig. 1.5b**). Particularly, this latter trigger mechanism was the responsible for the development of the salt structures studied at the Eastern Prebetic Zone. In this scenario, the presence of an autochthonous salt layer decoupled the deformation affecting the overburden and the underlying subsalt strata. Thereby, controlling the general structural style of the overburden above a basement fault during thick-skinned extension. According to Withjack & Callaway (2000), see their figure 14, the degree of structural coupling between the basement and the overburden is constrained by: the thickness and viscosity of salt, the thickness and the cohesive strength of the suprasalt strata and the total displacement of the subsalt fault accommodating thick-skinned extension.
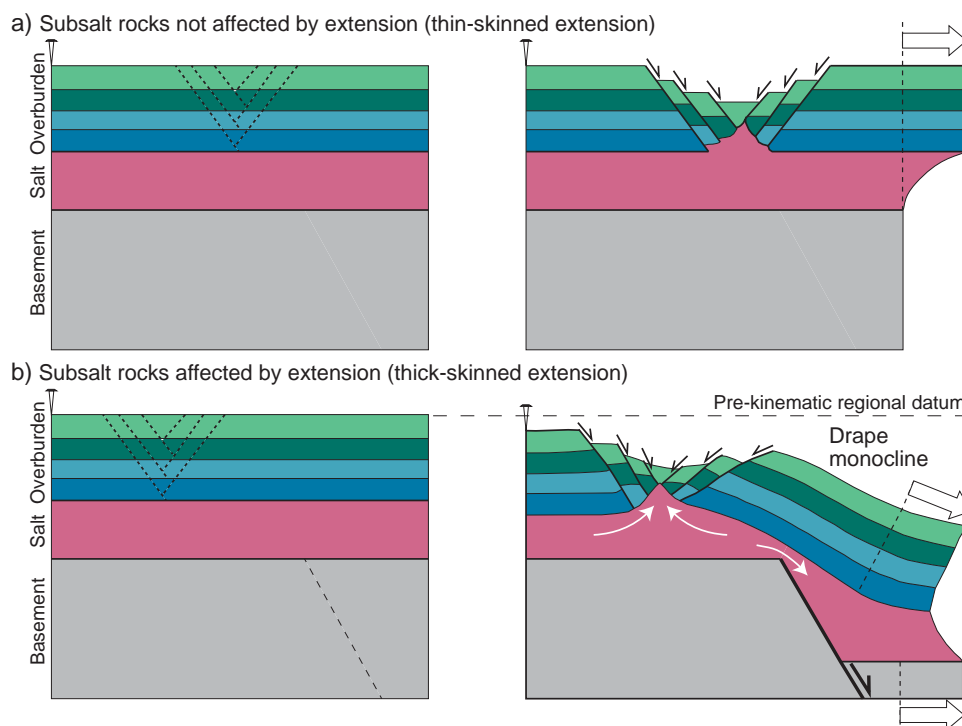


**Figure 1.5.** a) Thin-skinned extension may promote the rise of a reactive diapir through the pre-kinematic overburden. Further extension may promote the evolution from a reactive to a passive salt wall. b) Partially decoupled synrift extension in which the overburden drapes over a basement fault; stretching in the outer arc of the monoclinal drape fold creates a graben in the overburden, which initiated a reactive diapir. Further extension may promote the evolution from a reactive to a passive diapir above the footwall of a basement fault. Modified from Jackson & Vendeville (1994).

## 1.2.2. Contraction

Salt walls may also result during contraction (e.g. Sverdrup Basin, Harrison & Jackson, 2014; Sivas Basin, Kergaravat et al., 2016). If the suprasalt strata is tectonically thickened (**Fig. 1.6a)**, the differential load is insufficient, and its thickness and strength is too great for a diapir to initiate and grow. Conversely, if the suprasalt strata is thin (**Fig. 1.6b**), contraction above a salt décollement also generates detachment folds that may be eroded and/or weakened by local extension (e.g. fold crests deformed by outer arc extensional faults; **Figs. 1.7c**).
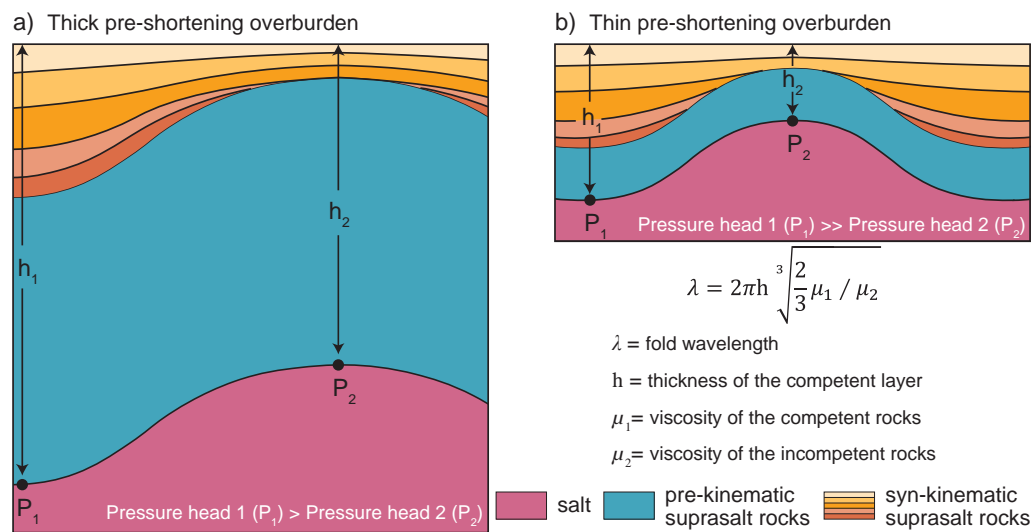


**Figure 1.6.** A thicker pre-kinematic overburden and a lower differential sedimentary load in a) prevents a diapir to rise. Conversely, a thinner pre-kinematic overburden with a greater differential sedimentary load in b), promotes the diapiric rise. Equation for the formation of buckle folds obtained from Ramberg (1960).

The combination of these processes favors the thinning of the overburden, so salt may break through to the surface and subsequently grow as a diapir (Coward & Stewart, 1995; Sans & Koyi, 2001). During contraction, erosion affecting detachment folds enhances salt piercement allowing passive salt extrusion (**Fig. 1.7d**). However, erosion may be local and heterogeneous, thus promoting the formation of elliptical salt stocks rather than salt walls (e.g. Cardona diapir; Sans, 2003). Nevertheless, outer arc extension at the anticline crests, more continuous in map-view, may trigger the development of more elongated diapirs (e.g. salt walls).

Another factor that controls the formation of salt walls during contraction is the syn-tectonic sedimentation in the adjacent synclines (Duerto & McClay, 2009; Pichot & Nalpas, 2009; Izquierdo-Llavall et al., 2018; **Fig. 1.8**). According to scaled physical models, the syn-

kinematic sedimentation promotes an increase of the hydraulic head of salt favoring the development of salt walls at the crests of the detachment anticlines (Pla et al., 2015; **Fig. 1.8b**). Additionally, a thick syn-kinematic overburden tends to preserve tight isoclinal salt-cored anticlines with vertical to overturned limbs of pre-kinematic strata (**Fig. 1.8c**).
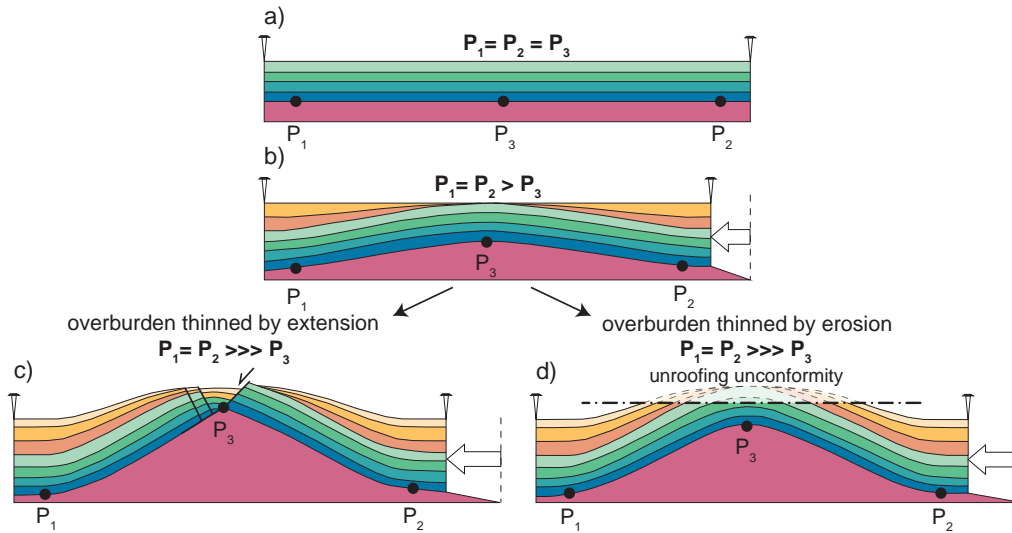


**Figure 1.7.** Given an initial situation in a) with an horizontal overburden, the syn-kinematic sedimentation at the synclines in b) combined with the extension of a buckling salt-cored fold in c) and erosional unroofing in d), may trigger the development of a salt wall at the anticline crest. Modified from Coward & Stewart (1995).
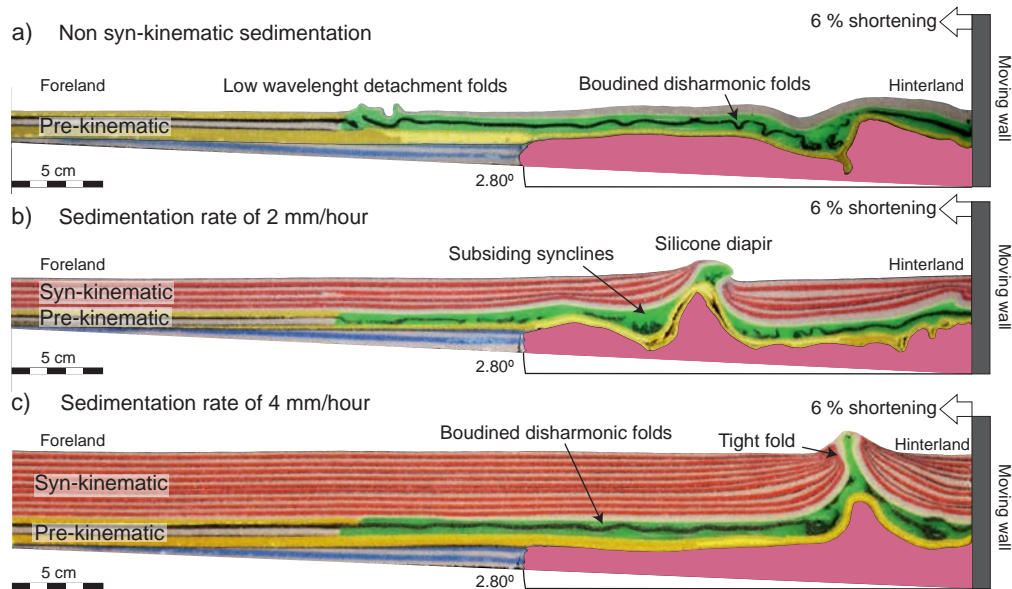


**Figure 1.8.** Vertical slices of three different scaled physical models from Pla et al. (2015), investigating the influence of syn-kinematic sedimentation during thin-skinned shortening. Note that syn-kinematic sedimentation prevents deformation to migrate towards the foreland and nucleates the formation of salt walls towards the hinterland.

## 1.2.3. Differential sedimentary loading

Salt walls may also form by differential sedimentary loading, in the absence of extension or contraction (e.g. Paradox Basin, Trudgill, 2011; La Popa Basin, Rowan et al., 2003; Nordkapp Basin, Rowan & Linsø, 2017). In this scenario, the pattern of the depositional loading might be asymmetric, especially when a foreland basin is progressively filled by syn-orogenic sediments shed from the hinterland (**Fig. 1.9**).
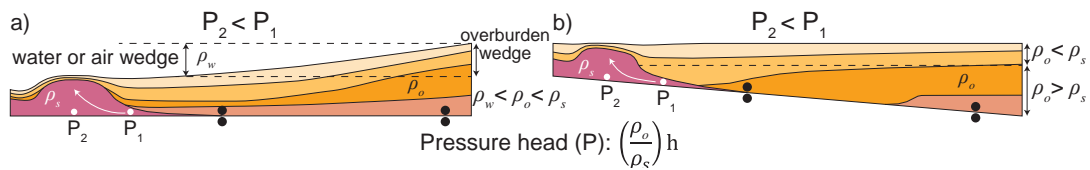


**Figure 1.9.** a) Active diapirism can be driven by topographic variation creating a wedge of water (or air); a diapir can rise actively even though the cover is less dense than salt. Modified from Jackson & Hudec (2017). b) active diapirism can be developed when a foreland basin is progressively filled by syn-contractional sediments.

When this occurs, the progradation of sediment over mobile salt develops a pressure head. Even if the overburden is less dense than the salt, it is denser than the adjacent water or air. Thereby, the area beneath the sediment wedge will sink until the salt is welded, at which point the depocenter shifts basinward (**Fig. 1.10**). The shifting load of advancing sediment displaces the underlying salt (**Fig. 1.10b**). As also occurs in salt walls resulting from contraction, salt inflation promotes arching of the overburden above the subsalt faults to from crestal faults, which initiate active diapirism. Erosion of the crest causes further thinning of the suprasalt strata leading salt breakthrough and passive growth of a salt wall by simply downbuilding (Nelson, 1989; Jackson & Talbot, 1991; **Figs. 1.10c** and **1.10d**).
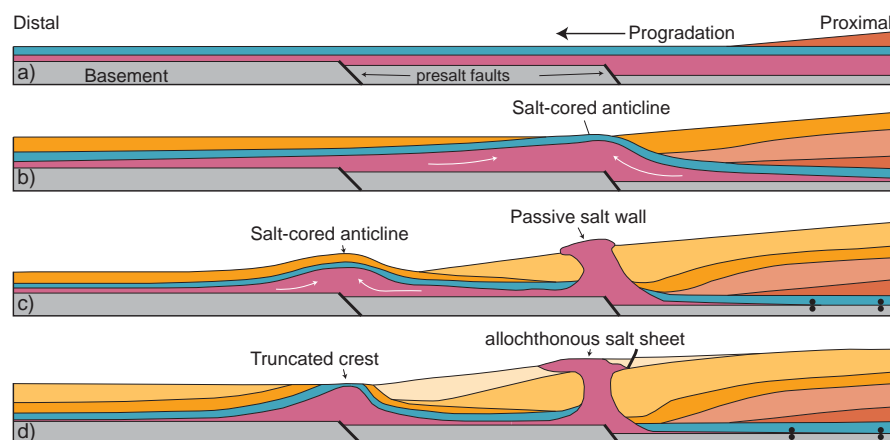


**Figure 1.10.** Vertical slices of scaled physical models showing the schematic evolution of salt structures during progradation above a salt basin underlain by a stepped basement. Modified from Ge et al. (1997).

Despite the great variety of tectonics scenarios where salt walls can be developed, the present study assumes that in most cases, regardless of the triggering mechanism, salt walls grow as passive diapirs once the salt has pierced its initial roof.

## 1.3. Salt wall and pre-kinematic piercement geometries

Regardless of the triggering mechanism, the brittle pre-kinematic strata adjacent to salt walls may depict different geometries depending on the shape of the diapir and its evolutionary stage (**Fig. 1.11**). As is explained above, a reactive diapir may be controlled by several symmetric faults (Vendeville & Jackson, 1992a; **Fig. 1.4a**) or by a single asymmetric fault with a salt roller in its footwall (**Fig. 1.4b**). Depending on the shape of the reactive diapir, the adjacent pre-kinematic strata also depict symmetrical (**Fig. 1.11a**) or asymmetrical geometries (**Fig. 1.11b**), respectively. For example, pre-kinematic strata may be faulted down toward the center of a graben; or may be broken in two parts by a single listric fault.

In all scenarios, if the pre-kinematic overburden is thinned and weakened enough because is situated above the regional datum where is exposed to erosion, the salt wall will actively rise (Vendeville & Jackson, 1992a; Schultz-Ela et al., 1993). Specifically, for a symmetrical diapir, the active rise will promote the progressive folding of the pre-kinematic strata together with the rotation of the conjugate faults (**Fig. 1.11a**).
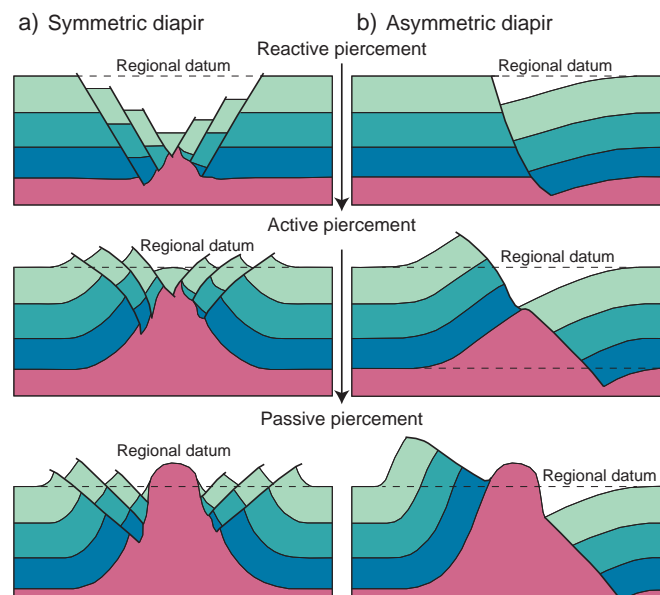


**Figure 1.11.** Schematic cross-sections illustrating the a) symmetric and b) asymmetric evolution of diapiric piercement through pre-kinematic overburden during thin-skinned extension. Symmetric diapirism modified from Vendeville & Jackson (1992a).

The active rise of an asymmetrical diapir will promote folding of the pre-kinematic strata located in the footwall of the listric fault (**Fig. 1.11b**). The fault plane will be also folded as the diapir progressively rises and breaks the thinned pre-kinematic strata. Despite this, the deeper strata located in the hanging wall will remain slightly undeformed and will be progressively covered by syn-kinematic sediments. Once at the surface, the diapir will grow passively as surrounding suprasalt strata subside into and displace the salt in the source layer (Nelson, 1989). At this point, regional deformation is preferentially accommodated by weak salt flowing into widening salt walls (i.e. cryptic extension; Vendeville & Jackson, 1992a). So, regardless of the diapir geometry, the extensional faults that initiated diapirism will be no longer active and will remain attached at the diapir walls.

The pre-kinematic strata adjacent to passive diapirs may also be folded over wider zones with variable amounts of structural relief (Rowan et al., 2016). In extreme cases, termed megaflaps, the deeper minibasin strata may extend far up the sides of steep diapirs or their equivalent welds (Giles & Rowan, 2012; Graham et al., 2012; Rowan et al., 2016; **Fig. 1.12**). The width of folding and vertical relief of megaflaps span multiple kilometers, with the maximum bedding attitude ranging from near-vertical to completely overturned beneath an allochthonous salt sheet. The megaflap strata may be constant thickness or convergent and the oldest part is usually concordant to the top salt or slightly onlapping. This description is purely geometric and implies nothing about the genesis, kinematics or evolution of the verticalized strata neither de diapir (Rowan et al., 2016).
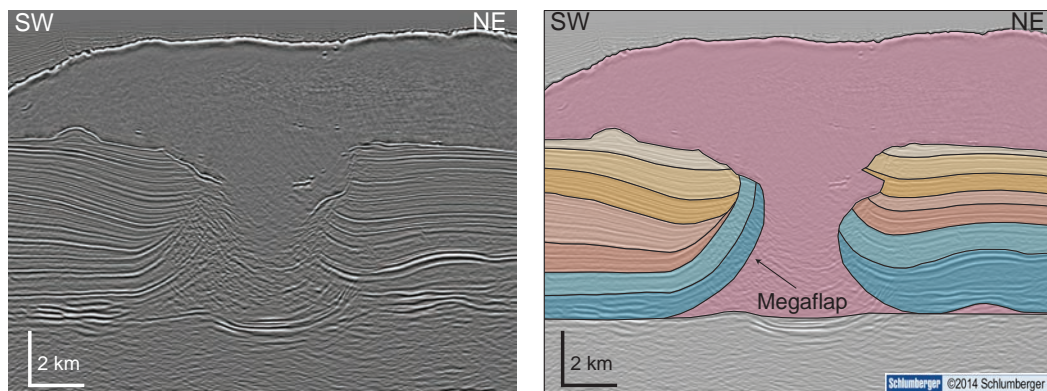


**Figure 1.12.** Uninterpreted and interpreted 3D prestack depth-migrated seismic reflection profile using well ties of a diapir flanked by a megaflap in the northern Gulf of Mexico. No vertical exaggeration. Modified from Rowan et al. (2016).

## 1.4. Syn-kinematic stratal geometries flanking salt walls

The growth of a salt wall, described in the previous section 1.3, is accompanied by the deposition of syn-kinematic sediments recording the diapiric evolution. The geometrical analysis of the syn-kinematic strata adjacent to salt walls allow to decipher the driving mechanism for diapirism, to determine the shape of the salt wall, and to infer the geometry of the pre-kinematic strata when, for example, they are not well imaged in the seismic reflection data.

From this structural analysis, two main groups of syn-kinematic stratal geometries can be distinguished depending on the moment in which sedimentary deposition occurs in relation to the evolutionary stage of the diapir. That is, when sediments are deposited synchronous to salt inflation and prior to piercement of the diapir's roof (i.e. reactive and/or active diapir growth), or when deposition occurs after salt breakout and synchronous to salt extrusion (i.e. passive diapir growth). During reactive diapirism, the syn-extensional sediments thicken in the grabens as they are progressively developed above a reactive salt wall (Vendeville & Jackson, 1992a; **Fig. 1.13a**). In this scenario, the stratal geometries will depend on the shape of the extensional faults bounding the graben and the relationship between sedimentation rate and the fault slip rate (Jackson & Hudec, 2017). During the active rise of a diapir, the resulting syn-kinematic stratal geometries are similar to those located adjacent to detachment folds formed by limb rotation (e.g. Poblet & Hardy, 1995; **Fig. 1.13b**). Thereby, the syn-kinematic sediments onlap and overlap the diapir's roof (i.e. pre-kinematic strata) as it is being rotated and uplifted during the active rise of the diapir. Note that in the limb-rotation model, straight fold limbs rotate and steepen maintaining constant limb length and fold hinges and axial surfaces remain fixed during the growth of the active diapir (Poblet & McClay, 1996).
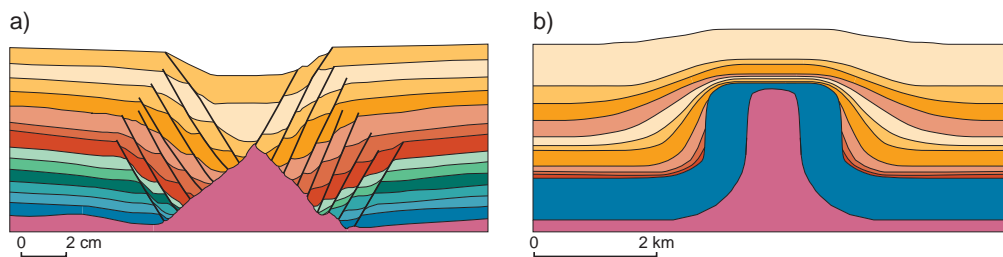


**Figure 1.13.** a) Syn-kinematic growth faults above a reactive diapir (scaled physical model by Bruno Vendeville; Jackson & Hudec, 2017). b) syn-kinematic growth wedges above an active diapir (modified from Poblet & Hardy, 1995).

Finally, passive diapirism undergo multiple phases of active rise, as ephemeral diapiric roofs are successively pierced by the rising salt (Barton, 1933; Nelson, 1989; Vendeville & Jackson, 1992a; Schultz-Ela et al., 1993). The repeated phases of uplift and salt breakout produce syn-kinematic folded beds that are preserved and stacked to form halokinetic sequences adjacent to passive diapirs (Giles & Rowan, 2012). This type of syn-kinematic stratal geometries are described from field exposures in Mexico (e.g. Rowan et al., 2003; Giles & Rowan, 2012; Andrie et al., 2012), South Australia (e.g. Kernen et al., 2012; Hearon et al., 2015) and more recently from subsurface seismic analogues in the northern Gulf of Mexico (e.g. Hearon et al., 2014; **Fig. 1.14**), the Nordkapp Basin (Rojo & Escalona, 2018), or the Santos Basin (Coleman et al., 2018).
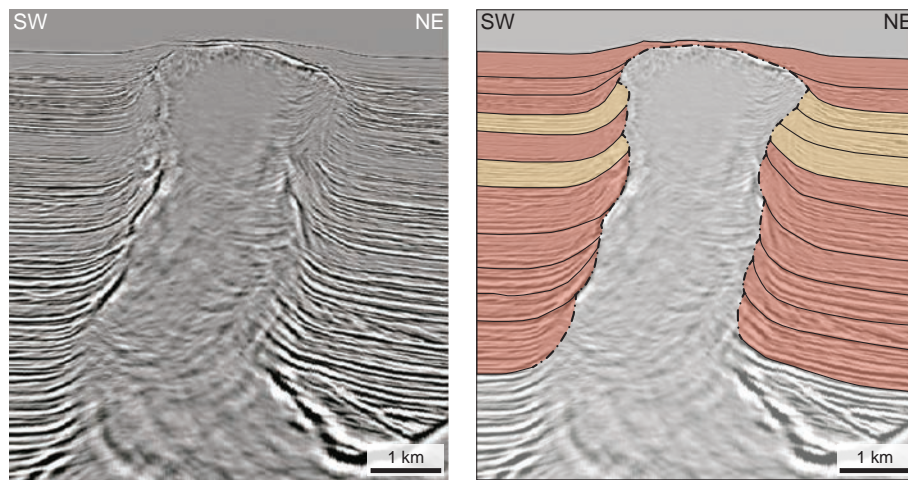


**Figure 1.14.** Uninterpreted and interpreted 3D wide-azimuth, prestack depth-migrated seismic profile across the center of the Auger diapir showing the vertical distribution of tapered (orange) and tabular (yellow) composite halokinetic sequences. No vertical exaggeration. Modified from Hearon et al. (2014).

The halokinetic sequences are localized (<1 km wide), unconformity-bound successions of growth strata that form as a drape fold due to the interplay between salt-rise rate (R) and sediment-accumulation rate (A; Giles & Lawton, 2002; Rowan et al., 2003; Giles & Rowan, 2012). Two types of halokinetic sequences, wedges and hooks (**Fig. 1.15**), are defined geometrically depending on changes in topography above an active rising diapir. The topographic relief is controlled by the interplay between salt inflation/deflation rates and sedimentation rates (Rowan et al., 2003). Hook halokinetic sequences have narrow and steep drape-fold geometries (**Fig. 1.15a**). Beds fold and thin over a distance of 50–200 m from the diapir with bed rotation of up to, but not surpassing, 90°. Bounding unconformities are correspondingly highly angular (<70°) with up to 90° of angular discordance but become conformable within 200 m of the

diapir (**Fig. 1.15a**). In contrast, wedge halokinetic sequences have broad and gentle drape-fold geometries (**Fig. 1.15b**). Folding and thinning occurs over a wider zone of 300–1,000 m, with only minor or gradual bed rotation. Bounding unconformities have low-angle truncation (5–10°), but commonly extend for more than 500 m away from the diapir edge before becoming conformable.

a)

Minibasin

Diapir

Hook

50 - 200 m

- Drape-folding in zone 50–200 m wide.
- Up to 90° angular unconformity.
- Near-diapir abrupt facies change.
- Results from relatively slow agradation.

b)

Minibasin

Diapir

Wedge

300 - 1000 m

- Drape-folding in zone 300–1000 m wide.
- Up to 30° angular unconformity.
- Broad zone of facies changes.
- Results from relatively fast agradation.
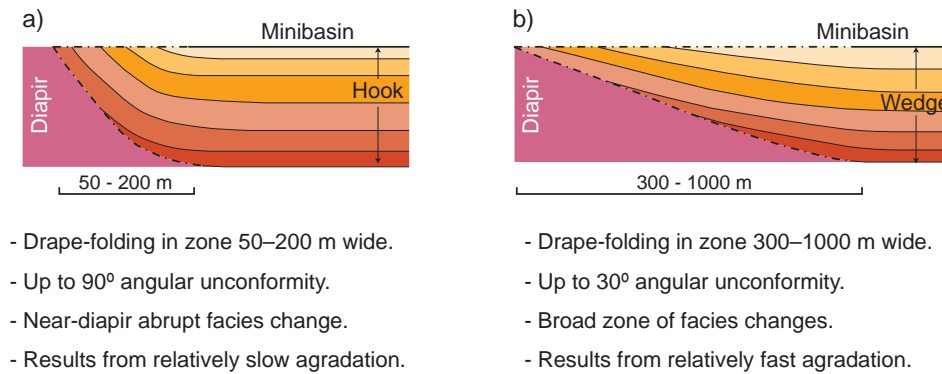
**Figure 1.15.** End-member styles of halokinetic sequences with their corresponding specifics: a) hook halokinetic sequence, and b) wedge halokinetic sequences, respectively. Modified from Giles & Rowan (2012).

Halokinetic sequences stack stratigraphically into two end-member types of composite sequences (**Fig. 1.16**): tabular and tapered, which form under relatively high and low ratios, respectively, of R and A (**Figs. 1.17a** and **1.17b**). Tabular CHS form by vertically staking hook sequences (**Fig. 1.16a**), creating a large-scale package with tabular form (**Fig. 1.17a**). Stratal thinning and drape-fold monoclines within individual hook halokinetic sequences are slightly offset from each other at the halokinetic sequence boundaries but are confined to a narrow zone (50–200 m) trending roughly parallel to the diapir margin. Minor cusps form where the unconformities intersect the diapir. In contrast, tapered CHS form by stacking wedge

a)

Zone of stacked monoclinal axial traces

Diapir

Hook HS

Hook HS

Hook HS

Hook HS

Tabular CHS

50 - 200 m

- Subparallel base and top boundaries.
- Narrow zone of thinning near diapir.
- Axial trace of monocline near diapir &
  forms zone parallel to diapir margin.

b)

Zone of stacked monoclinal axial traces

Diapir

Wedge HS

Wedge HS

Wedge HS

Wedge HS

Tapered CHS

300 - 1000 m

- Convergent base and top boundaries.
- Broad zone of thinning toward diapir.
- Axial trace of monocline progressively
  inclined from diapir.

**Figure 1.16.** Vertical stratigraphic stack of halokinetic sequences forming a) tabular and b) tapered end-member composite halokinetic sequence (CHS) types with their corresponding specifics. Modified from Giles & Rowan (2012).

sequences (**Fig. 1.16b**), creating a large-scale package with a broadly folded tapered form (**Fig. 1.17b**). The lower boundary is folded over a distance of 300–1,000 m from the diapir so that thinning towards the diapir occurs over a wider zone. The axial traces of stacked drape-fold monoclines trend at an incline away from the margin of the diapir and are slightly curved. In addition, salt walls growing along contractional anticlines could have adjacent folded zones affecting the halokinetic sequences as much as 3 km wide (Rowan et al., 2003).
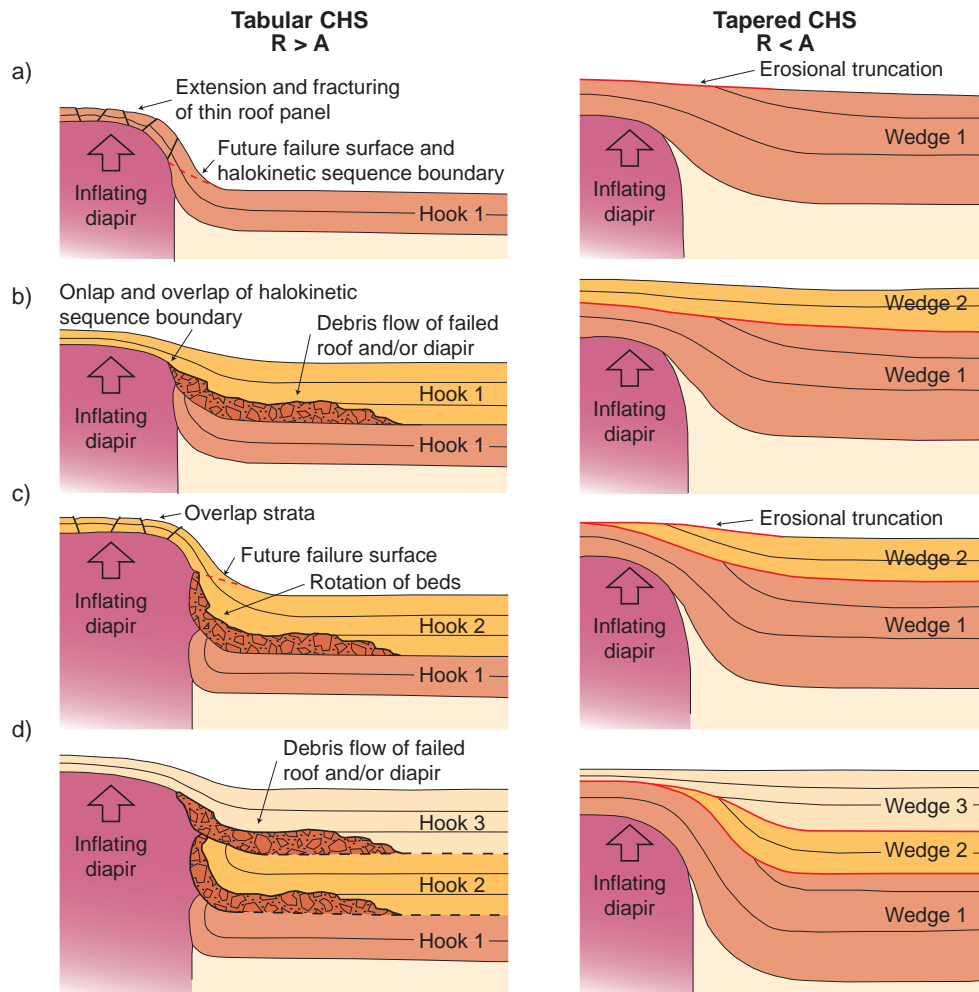
**Figure 1.17.** Genetic models for the development of tabular and tapered CHS as a function of the relative rates of salt rise (R) and sediment accumulation (A). Modified from Giles & Rowan (2012).

Finally, syn-kinematic sediments may be coevally deposited adjacent to a developing megaflap (**Fig. 1.12**). Thereby, they onlap and overlap the pre-kinematic strata as a megaflap is progressively formed. Two end-member geometries characterize these types of syn-kinematic strata (Rowan et al., 2016; **Fig. 1.18**): progressive wedging and/or pronounced onlap depending on the kinematic process for megaflap formation (limb-rotation and/or kink-band migration respectively), which are analogous to those involved during the development of detachment

folds (Poblet & McClay, 1996; Poblet et al., 1997; Suppe et al., 1997). Therefore, the resulting geometry of these specific syn-kinematic strata is ultimately controlled by the interplay between deformation rate and sediment-accumulation rate as well as by the kinematic process for megaflap development, which can be also a combination of the two folding mechanisms mentioned above (Rowan et al., 2016).
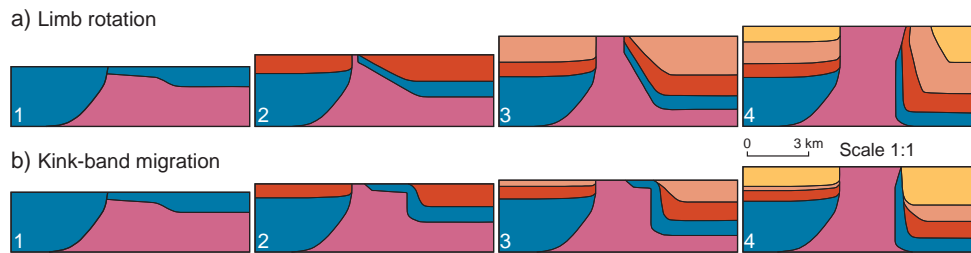


**Figure 1.18.** Forward-kinematic models with the same initial geometry and developing megaflap formations by a) limb rotation and b) kink-band migration. Models modified from Rowan et al., (2016) incorporating compaction and preserving bed lengths.

## 1.5. Reactivation of salt walls

Precursor salt walls are commonly reactivated by later extension and/or contraction. Salt walls, like the rest of salt bodies, are the weakest part of the rock volume and consequently localize any ulterior deformation occurring in the area (e.g. Nilsen et al., 1995; Roca et al., 2006; Rowan & Vendeville, 2006; Callot et al., 2007; Dooley et al., 2015). In this sense, they are very sensitive to any change of the tectonic regime, thus they are the first structures to record such changes. The deformation style of salt walls during newly stablished tectonic scenarios can vary considerably but shows some distinctive features whenever it is produced during extension, contraction or strike-slip. Below are summarized the principal key features during the extensional and contractional reactivation of salt walls. Note that the influence of strike-slip reactivation on precursor salt walls is beyond the scope of this investigation, and thus not detailed in this memoir (see further details in Jackson & Hudec, 2017; their Chapter 12).

## 1.5.1. Extensional reactivation

Regional extension promotes the widening of salt walls with time because it is easier than faulting the adjacent stronger sedimentary overburden. As long as there is enough salt supply from the source layer, the diapir can widen and grow at the same time by internal flow without

visible extensional faulting (i.e. "cryptic extension"; Vendeville & Jackson, 1992a). The diapir height can decrease or increase in function of the ratio between the extension and salt supply rates (Schultz-Ela, 1992; Vendeville & Jackson, 1992b; **Fig. 1.19**). Thereby, if there is enough salt coming from the source layer, the salt wall will maintain or even increase its height (**Fig. 1.19a**). Despite this, if the salt supply is insufficient to fill the accommodation space generated by continued extension, the diapir will start to fall (Vendeville & Jackson, 1992b; **Fig. 1.20**). Independently of extension, the diapir will collapse if the source layer is depleted and primary welds form beneath the adjacent subsiding minibasins.
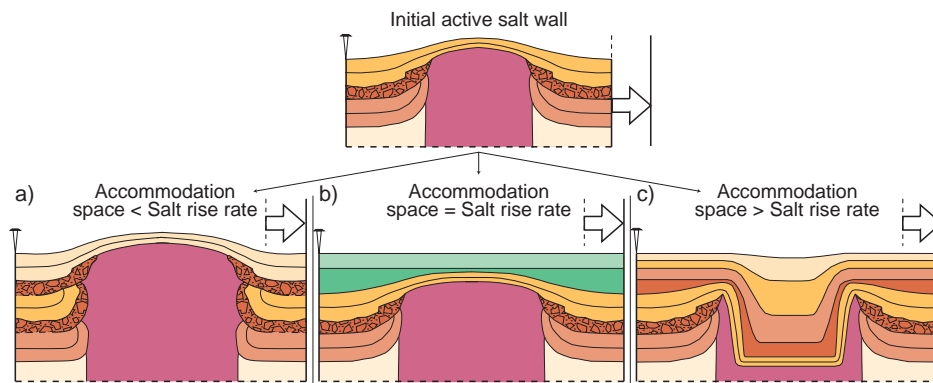


**Figure 1.19.** The relationship between accommodation space and salt rise rate controls the height of an initial active salt wall covered with a thin roof. a) Low ratios promote the further growth of the diapir; b) equant rates tend to stop the diapir growth; and finally, c) high ratios foster the salt wall collapse and the formation of a younger depocenter.
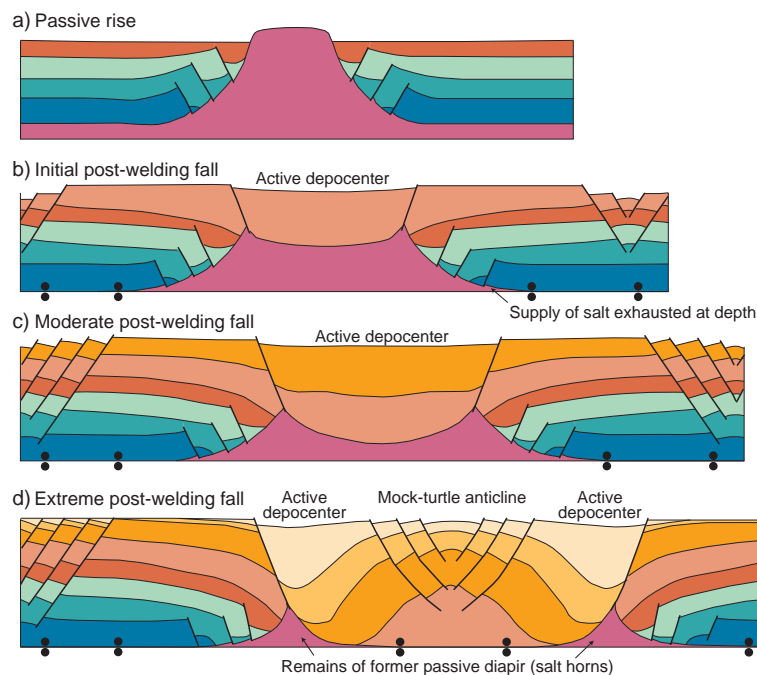


**Figure 1.20.** Extensional fall of a salt wall may create a muck-turtle anticline. Modified from Vendeville & Jackson (1992b).

The collapse or fall of a salt wall results in the formation of a younger depocenter in the form of an elongated minibasin over what was the diapiric high (**Fig. 1.19c**). This newly created minibasin, surrounded by salt horns, can evolve to a "mock-turtle" anticline when a primary weld is created beneath the depocenter of the subsiding minibasin and regional extension continues. As it is folded, a crestal graben may be developed in the center of the former minibasin, which is now subdivided in two separated active depocenters that migrate laterally as salt horns are progressively depleted (Vendeville & Jackson, 1992b; **Fig. 1.20d**).

## 1.5.2. Contractional reactivation

Precursor salt walls may be also affected by regional shortening. Again, as the weakest part of the cover, they narrow by internal flow localizing shortening strain without visible contractional faulting (i.e. "cryptic shortening"; Vendeville & Nilsen, 1995; Gottschalk et al., 2004). So, they affect the style of the contractional deformation in the way that shortening reduces the width of the salt walls, increases the rate of salt extrusion meanwhile the rest of the cover remains almost undeformed.

Regional shortening can rejuvenate dormant salt walls even if their roof is thick, the source layer is depleted, or the diapir is denser than its overburden (Vendeville & Nilsen, 1995). Shortening promotes the narrowing of salt walls by squeezing them and arching their roofs (**Figs. 1.21a** and **1.21b**). In this point, if the diapiric roof is thin and/or weak enough, rising salt may disrupt the overlying strata, allowing salt to break through the surface and to extrude passively as a salt sheet (**Figs. 1.21c**, **1.21d** and **1.21e**). If shortening increases, the salt wall's stem may be depleted, until the development of secondary welds (**Fig. 1.21f**) that can link two remnant diapirs (e.g. "Q-tip" structure; Rowan & Vendeville, 2006; **Fig. 1.22**). Eventually, tilted secondary welds dipping favorably to the shortening propagation can evolve into thrust-welds if compression progresses (e.g. Callot et al., 2007; **Figs. 1.21g** and **1.21h**).

As occurs in the extensional reactivation, the salt wall orientation and distribution exert a strong influence in the location and strike of folds and thrusts developed during shortening (e.g. Fars province of the Zagros Mountains in Iran, Letouzey & Sherkati, 2004; Jahani et al., 2009; Callot et al., 2012; or the Atlas Mountains of Algeria, Letouzey et al., 1995; **Fig. 1.23**). The influence of salt walls on the surrounding stress pattern recedes away from the diapir termination, so thrust faults are more prevalent along the termination of the salt walls tending to be perpendicular to regional shortening (**Fig. 1.23**).
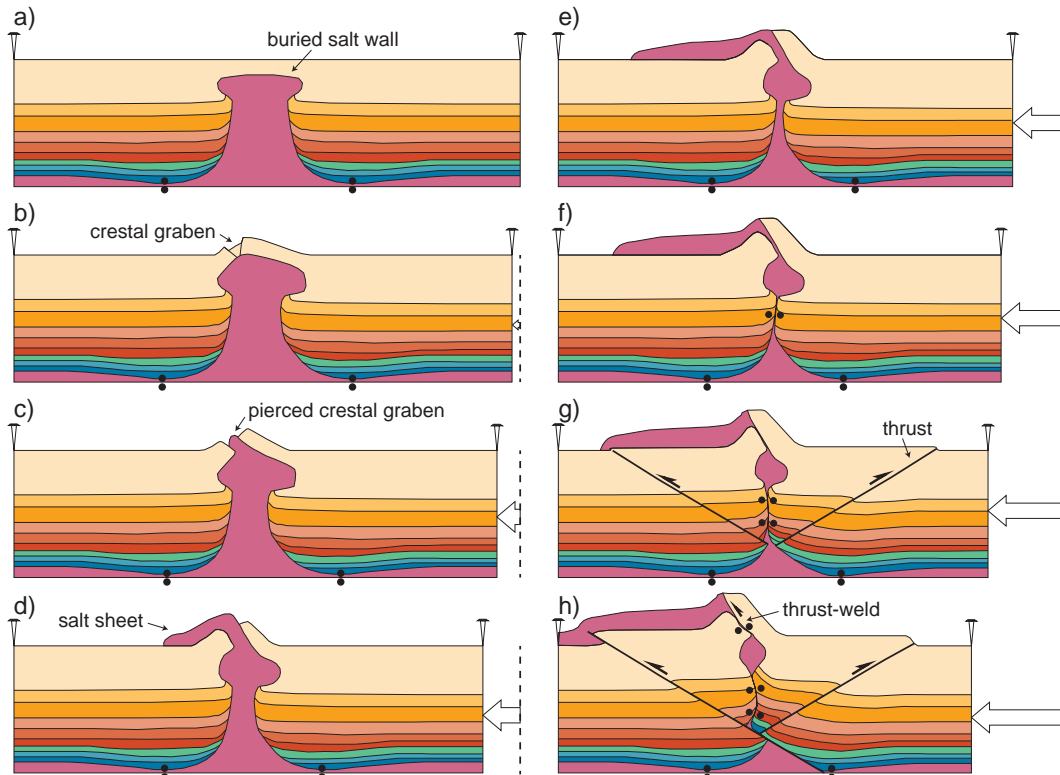
**Figure 1.21.** Conceptual evolutionary model, obtained from scaled physical models, for the contractional reactivation of a buried salt wall without syn-kinematic sedimentation and erosion. a) initial stage; b) narrowing of the buried diapir and arching of its roof with formation of a keystone graben (crestal graben); c) narrowing of the diapir and piercement of its roof along the crestal graben; d) narrowing of the diapir, increase of the dip of the roof shoulders and development of a salt sheet; e) narrowing of the diapir, and the increase in size of the salt sheet as a consequence of the continued extrusion of salt. f) complete closure of the diapir stem and formation of a secondary weld. g) nucleation of a short-cut and a back-thrust in the upper part of the diapir pedestal and incipient development of a box-fold antiform. h) amplification of the box-fold antiform and formation of a thrust-weld along favorable dipping portions of the primary weld. Modified from Ferrer (2012).
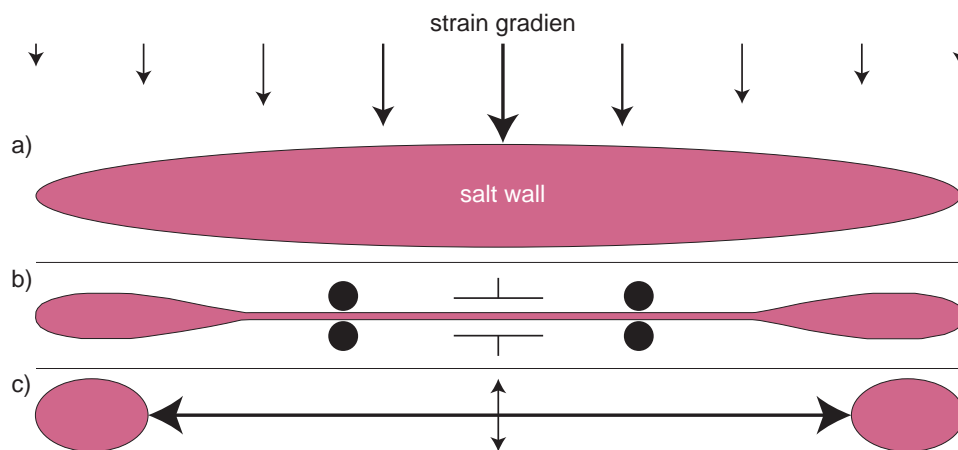


**Figure 1.22.** Plan-view evolution of a salt wall under compression. a) the relative weakness of the salt and the strength of the rocks around the salt wall tips promotes the development of a strain gradient. As a result, the central part of the salt wall is squeezed more than its terminations. b) with enough shortening, a vertical secondary weld is formed linking two remnant diapirs that have not been squeezed. c) if the two remnant diapirs together with the secondary weld are covered, the result may be an anticline with a central culmination and plunging in both directions. Modified from Rowan & Vendeville (2006).

**CHAPTER 1**
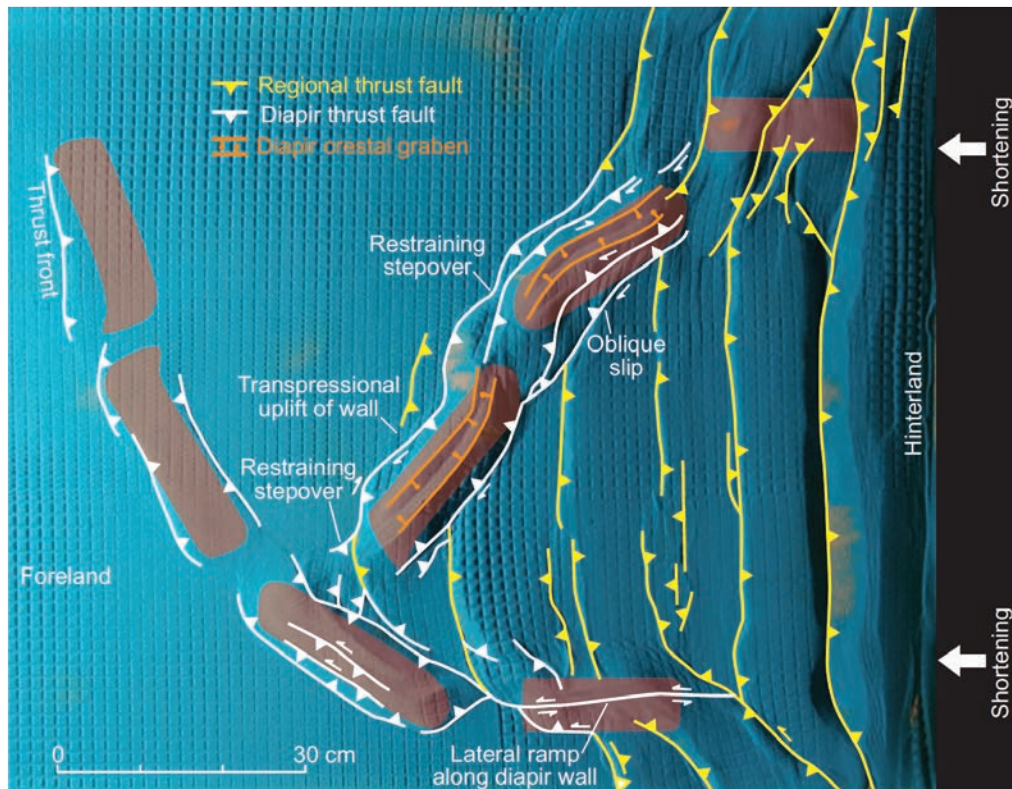
**Figure 1.23.** Salt walls oblique to regional shortening affect the resulting structural style of the deformed cover. The deformed salt walls are typically bounded by oblique-slip transpressional faults and crowned by oblique-slip transtensional grabens. Scaled physical model published in Jackson & Hudec (2017) courtesy of Tim Dooley.

## 1.6. Salt wall-flanking faults

The mode of diapirism as well as the tectonic regime are controlling factors on the type of the resulting syn-kinematic faults flanking the reactivated salt walls. Thus, the adjacent fault patterns will be different according to the geometry in plan-view of the salt wall (Link, 1930; Parker & McDowell, 1955; Withjack & Scheiner, 1982; Sims et al., 2013), but also depending on the specific stage of the diapir evolution in which faulting occurs (Vendeville & Jackson, 1992a and 1992b; Schultz-Ela, et al., 1993). That is, during the reactive stage, the active rise of the diapir or any ulterior reactivation.

## 1.6.1. Syn-kinematic faults developed during reactive diapirism

The structural style of a salt province affected by thin-skinned extension is a function of the salt detachment geometry, whenever it is horizontal or tilted basinwards (Stewart, 1999). When the salt detachment is horizontal, classic reactive diapirism is usually symmetrical,

in which conjugate thin-skinned faults develop over the reactive diapir (e.g. **Fig. 1.4a**). As extension progresses, younger extensional faults are developed toward the center of the graben. If the overburden is thinned and weakened enough, the diapir will actively rise through to the surface and the preexisting set of extensional faults will become inactive as they are rotated and shouldered aside (**Fig. 1.4a**).

Conversely, in regional dipping salt detachment scenarios, the thin-skinned faults typically dip in the same direction than the detachment (e.g. **Fig. 1.4b**), having in plan-view, maximum displacements near the center of the faults and zero at the fault tips. The center of the fault usually shows a greater salt roller than at the fault tips. If extension progresses, is likely in this position where the salt will break the thinned overburden if there is enough salt to flow and differential load established by faulting and syn-kinematic sedimentation. Once this occurs, a passive diapir is developed and the former extensional faults are abandoned and rotated on one side of the diapir (**Fig. 1.4b**).

## 1.6.2. Syn-kinematic faults developed during active diapirism

The active diapiric rise is characterized by the uplift and arching of the diapir's roof above the regional level (Jackson et al., 1994, Schultz-Ela et al., 1993; **Fig. 1.4**). This process promotes thinning and lengthening of the sedimentary roof as is drape-folded over the rising diapir leading to the formation of several types of extensional faults, that are not necessarily linked to regional extension. In arched roofs, small-scale deformation can be widespread and their response to deformation depends on strain intensity and the lithology of the involved rocks (Davison, 2000).

The geometry of the faults affecting the roof is strongly dependent on the plan-view edge of the salt wall (Link, 1930; Parker & McDowell, 1955; Withjack & Scheiner, 1982; Sims et al., 2013). Thereby, they will be longitudinal faults when the curvature of the diapir edge is zero, that is a diapir with a rectangular outline in plan-view; or radial faults when the curvature is different to zero. Nevertheless, during the active rise of a diapir, both types of faults are indistinctly developed when the overburden is drape-folded to form hook and/or wedge halokinetic sequences adjacent to the salt wall. Additionally, a third type of syn-kinematic faults can be found adjacent to active salt walls in counterregional-style systems (e.g. northern Gulf of Mexico, Diegel et al., 1995; Rowan & Inman, 2005; Rowan et al., 1999; Trudgill

& Rowan, 2004; or Paradox Basin, Escosa et al., 2018c). In this case, the counterregional faults accommodate part of the differential subsidence adjacent to the diapirs and extend into the overburden away from the diapir termination. Note that this model requires no regional extension to be accommodated by the faults, only differential sedimentary loading adjacent to the growing diapir (Schuster, 1995).

### 1.6.2.1. Longitudinal faults

These are faults parallel to the long axis of the salt wall (i.e. the x axis in **Fig. 1.1**) and are caused by regional extension and/or differential sedimentary loading adjacent to the diapir or by local doming (e.g. **Fig. 1.24**). In cross-section view, they depict different geometries (e.g. listric, planar…) and are rooted at the top of the diapir (Schultz-Ela et al., 1993).

Additionally, if the volumetric flux of salt along the long axis of the diapir is not homogeneous (e.g. culminations and subsiding areas along the topographic surface of the salt wall), longitudinal faults may be relayed by oblique transversal faults that are also detached above the salt wall.

### 1.6.2.2. Radial faults

Radial faults may originate in arched roofs above active raising diapir terminations (e.g. **Fig. 1.24**). They have large net slips at the crest and zero at the edge of the diapir (Stewart, 2006; Yin & Groshong, 2007). These faults can also extend radially from the edge of the salt body into the flanking strata. This may be caused as the overburden is drape-folded around a curved edge of salt and the resultant concentric tensile (hoop) stress regime (e.g. Rowan et al., 2003; Stewart, 2006; Escosa et al., 2018c). The hoop extension is proportional to the strike curvature of the salt-sediment interface, which is why radial faults are more prevalent at the end of salt walls where the radius of curvature is higher (Withjack & Scheiner, 1982; Davison et al., 2000; Stewart, 2006; Sims et al., 2013). Additionally, Coleman et al. (2018) suggested that the causal mechanism for radial faults on a salt stock (both affecting the roof and/or the entire overburden adjacent to the diapir) is dependent on the thickness variations of the roof during the active/passive phases of the diapiric rise.
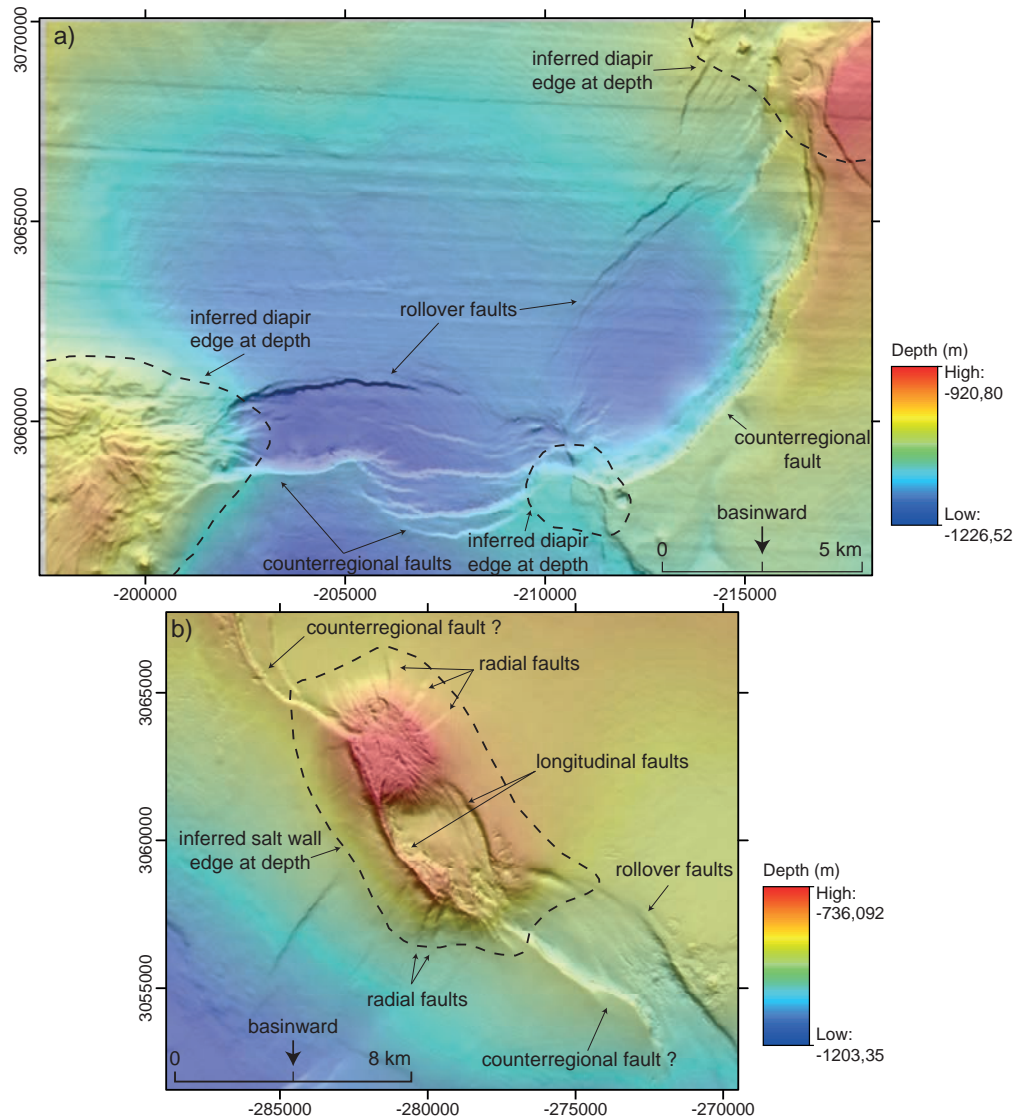
**Figure 1.24.** Examples of: a) landward dipping faults (counterregional) linking buried diapirs; and an b) active salt wall with radial and longitudinal faults and possible counterregional faults extending off the ends of the diapir. BOEM Northern Gulf of Mexico deepwater hillshaded bathymetry obtained from 3D seismic data (vertically exaggerated by 5x). Courtesy of U.S. Bureau of Ocean Energy Management (https://www.boem.gov/Gulf-of-Mexico-Deepwater-Bathymetry/).

## 1.6.2.3. Counterregional faults

In counterregional-style systems like the northern Gulf of Mexico, the largest differential subsidence is centered adjacent to the diapirs (Rowan & Inman, 2005). However, differential subsidence may still be significant along strike from the diapirs, where it is accommodated by slip on counterregional faults that merge into the proximal edges of the diapirs (Rowan et al., 1999; Trudgill & Rowan, 2004; Rowan & Inman, 2005; e.g. **Fig. 1.24**). These faults dip towards the source of the prograding sediment (landward-dipping) and curve into the proximal edge

of the diapirs (Diegel et al., 1995; Schuster, 1995). The deeper portions of the faults are actually welds since the salt evolves from linear, low relief walls to high-relief stocks (Trudgill & Rowan, 2004). As fault displacement decreases along strike, the differential subsidence is increasingly accommodated by folding, until only monoclinal folding records the deformation around the landward and lateral margins of the minibasin. They are typical of asymmetric diapirs flanked by thicker and deeper strata in one side and thinner and shallower strata in the other side (e.g. **Fig. 1.4b**).

## 1.6.3. Salt dissolution related faults

All evaporites are dissolved by undersaturated surface or groundwater, so salt walls close to the erosional regional level are prone to salt dissolution (Bosák et al., 1998; Talbot, 1998; Warren, 2006).

When the dissolved salt is not replaced by the rising diapir, the upper part of a salt wall will start to subside (Jackson & Hudec, 2017). In this scenario, the salt dissolution promotes the development of different types of salt dissolution related structures above the collapsing diapir. For example, when the salt wall is exposed or covered by a thin roof, the salt dissolution may promote the development of tight folds bounded by diapir-parallel extensional faults at the diapir margins. Both the extensional faults and the folds are interpreted as different manifestations of shoulder collapse due to halite dissolution and the formation of caprock. Note that a salt shoulder is a diapir margin geometry where the edge steps relatively abruptly inward (e.g. McFarland et al., 2015; Giles et al., 2017; Escosa et al., 2018c).

Conversely, when the salt wall is totally covered by a thicker roof, the salt dissolution may promote the development of extensional faults parallel to the diapir margin deforming the diapir's roof. Additionally, scaled physical models suggest that these extensional faults verticalize in depth to became contractional thrusts before rooting at the edges of the collapsing diapir (Ge & Jackson, 1998; **Fig. 1.25**). The spacing of the resulting faults depends on the initial geometry of the salt wall. Regardless of the diapir geometries, extension of the normal faults at the upper part is balanced by shortening of the reverse faults in the lower part of the collapsing diapir. Besides this, the presence of contractional zones helps to differentiate the collapsed roofs from those structures resulting from the extensional reactivation of a diapir (Jackson & Hudec, 2017).
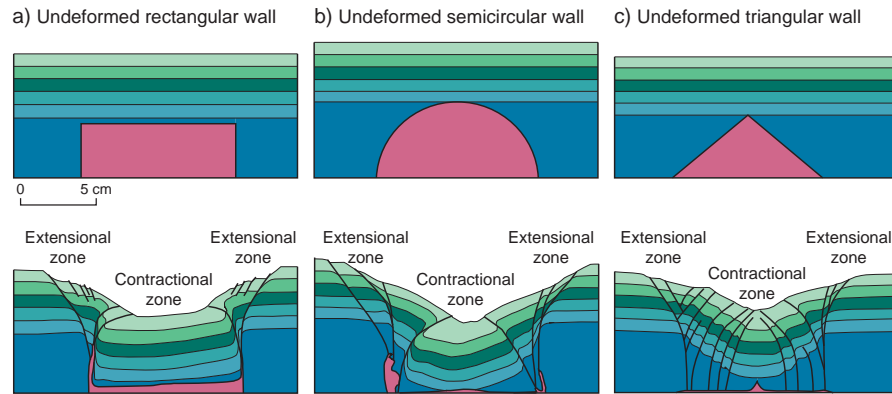
**Figure 1.25.** Three different scenarios of roofs collapse for salt diapirs displaying different geometries a), b) and c) when they are dissolved. Modified from scaled physical models by Ge & Jackson (1998).

## 1.6.4. Salt wall reactivation related faults

### 1.6.4.1. Faults developed during the extensional fall of salt walls

Extensional faults can be developed above collapsing salt walls when the rate of extension exceeds the rate of salt supply (Vendeville & Jackson, 1992b; Jackson & Hudec 2017; e.g. **1.19c**). In this process, crestal fault blocks indent the top of the diapirs. Depending on the geometry of the extensional faults accommodating the roof collapse, the indenting fault blocks can form half-grabens or symmetric grabens above the falling diapirs (e.g. **Figs. 1.20b - 1.20c**). These grabens are usually flanked by planar or listric faults with hornlike projections of salt in the footwall of each fault. So, as the salt wall progressively collapses and syn-kinematic sedimentation continues, the diapirs and their indented grabens become wider and lower as the flanking faults increase its height (e.g. Schultz-Ela, 1992). This process finishes when the salt stem is depleted, and the bottom of the graben touches down to form a primary weld.

### 1.6.4.2. Faults developed during the contractional reactivation of salt walls

Contractional and extensional faults can be developed above buried salt walls affected by thin-skinned shortening. The characteristics of these faults are mainly controlled by the diapir's width, profile and orientation, thickness of the diapir's roof and the shortening magnitude (Vendeville & Nilsen 1995; Gottschalk et al. 2004; Rowan et al. 2004; Roca et al. 2006; Jackson et al. 2008; Dooley et al. 2009; Callot et al., 2012; Duffy et al., 2018).

Essentially, the thinner the roof relative to the height of the underlying diapir, the tighter and more localized is the deformation affecting the arched roof by shortening (Callot et al., 2012). Accordingly, if the roof is thin and weak, rising salt disrupts the roof affected by ephemeral extensional and/or contractional faults, allowing salt to break through to the surface and to rise passively. Conversely, if the roof above a squeezed diapir is thick and mechanically strong, scaled physical models suggest that different structures may be developed as the diapir is contractionally reactivated (Dooley et al., 2009; Duffy et al., 2018). At the beginning, before the adjacent overburden shows signs of shortening, far-field shortening pressurizes the salt source and an inward plume inflates the diapir's stem. This promotes arching of the overlying roof and the nucleation of outer-arc extensional faults at the crest of the folded roof. Further shortening promotes the formation of a thrust salient on the foreland side and a backthrust on the hinterland side of the diapir. Additionally, the continued extensional thinning over the crest of the diapir triggers the development of a crestal graben flaked by roof flaps (**Fig. 1.21b**). Finally, once the diapir has pinched shut and shortening progresses, one flank may override the other as a thrust fault, offsetting the two halves of the diapir from each other (e.g. **Fig. 1.21h**).

## 1.7. Methodology

This section summarizes the methodological workflow followed during this investigation (**Fig. 1.26**), which comprehends the collection of data, their processing and their incorporation into the present analysis, to finally obtain the results of this PhD thesis. Thereby, the present investigation has carried out from surface data supported whenever it has been possible by the available subsurface data (2D seismic reflection, well, and gravimetric data). At the same time, this study builds on the preexisting knowledge of the studied areas (published articles and geological maps) and utilizes the concepts of salt tectonics and the structural geology to characterize different salt walls in the respective investigated areas.

Therefore, the research carried out during the last five years has resulted in the construction of a geometric and kinematic model for the studied salt walls as well as in the identification of global factors that control these salt structures driven by extension and/or differential loading and affected by a subsequent thin-skinned contractional deformation. The outcomes of this study have been reflected in three articles published in journals indexed by the Journal Citation Reports (JCR), the present thesis memoir, several oral and poster presentations at international

CHAPTER 1
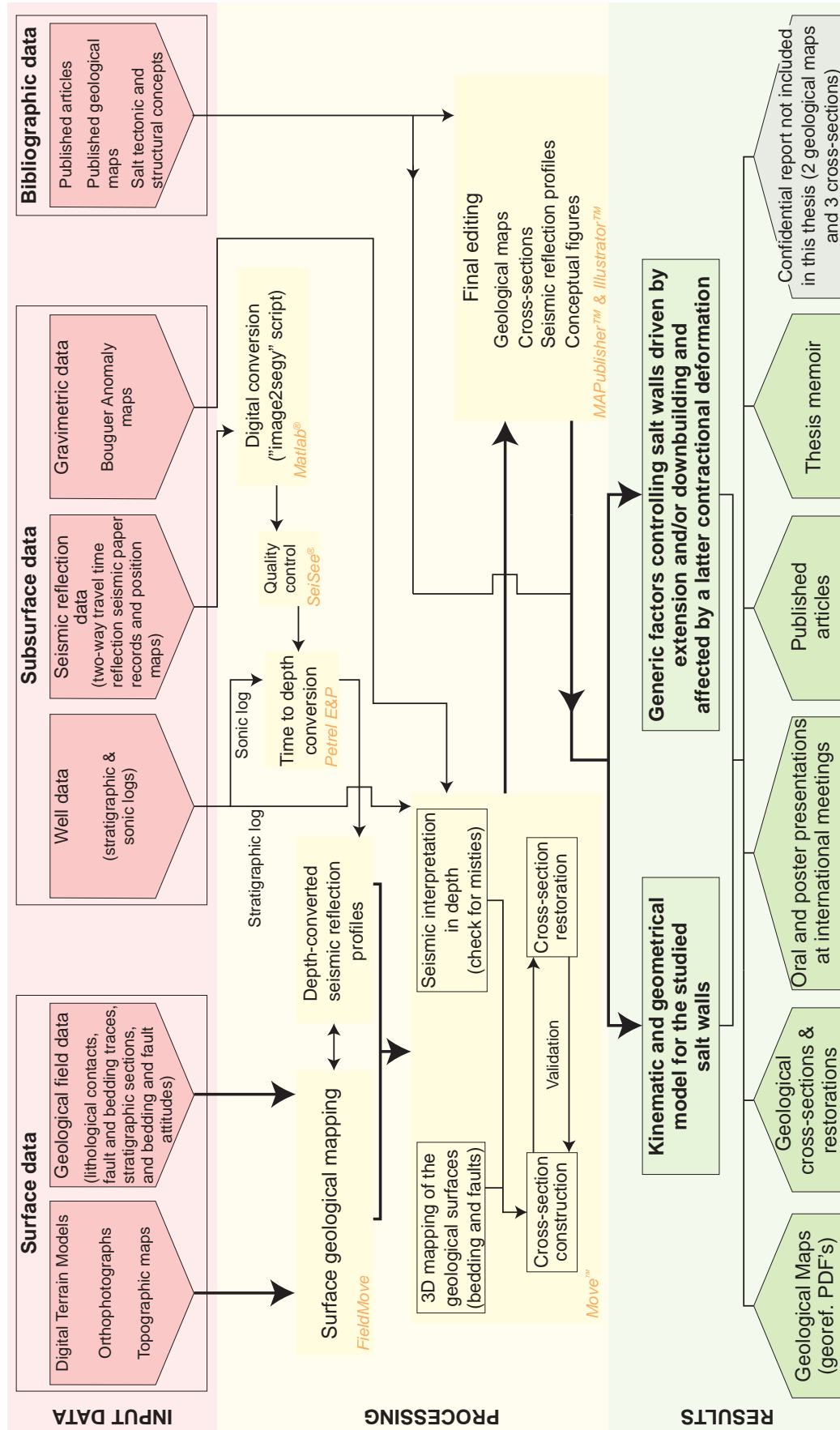


**Figure 1.26.** Methodological workflow followed during this investigation. To comprehend the chronological order, read first from top to bottom and then from left to right.

meetings, and a report of the Cofrentes-Ayora region which is not included in this thesis memoir due to confidential agreements with the company. Nevertheless, among the results presented in this thesis, there are three geological maps, ten cross-sections and one cross-section restoration at scales ranging from 1:50,000 to 1:1,000.

## 1.7.1. Input data

### 1.7.1.1. Surface data set

The surface data set used in this thesis consists of cartographic and geological field data. The cartographic data include digital terrain models (DTM), orthophotographs, topographic maps, and previously published geological maps. The digital terrain models and orthophotographs pertaining to SE Spain have downloaded from the *Centro Nacional de Información Geográfica* (https://www.cnig.es/) and the geological maps have downloaded from the *Instituto Minero y Geológico de España* (http://www.igme.es/). The topographic and geologic maps of SW Colorado (USA) have been supplied by professor Richard P. Langford of the University of Texas at El Paso. In this case, the corresponding digital terrain models and orthophotographs have downloaded from a Global Mapper™ repository.

The geological field data include localization and mapping of the different outcropping stratigraphic or lithological units, the tracing of the outcropping geological contacts (stratigraphic or tectonic), and the acquisition of structural and stratigraphic data. The collection of this data set has been done by using an iPad and the FieldMove software in three different field-work areas: SW Colorado (USA), Jumilla and Cofrentes-Ayora regions (SE Spain). During this process, more than 11, 400 (11,464) bedding and fault/fold attitude data have been collected from the investigated areas using a compass-clinometer. However, the data set and corresponding results from the latter studied area (Cofrentes-Ayora region) are not included in this memoir because of confidential agreements with the company.

### 1.7.1.2. Subsurface data set

The subsurface data located in the two studied areas (SW Colorado and Jumilla region; see their respective locations in **Figs. 1.27** and **1.28**) consist of 17 wells (13 from SW Colorado and 4 from the Eastern Prebetic Zone), 16 two-dimensional seismic reflection profiles (2 from SW Colorado and 14 from the Eastern Prebetic Zone), and bouguer anomaly maps (**Fig. 1.26**).
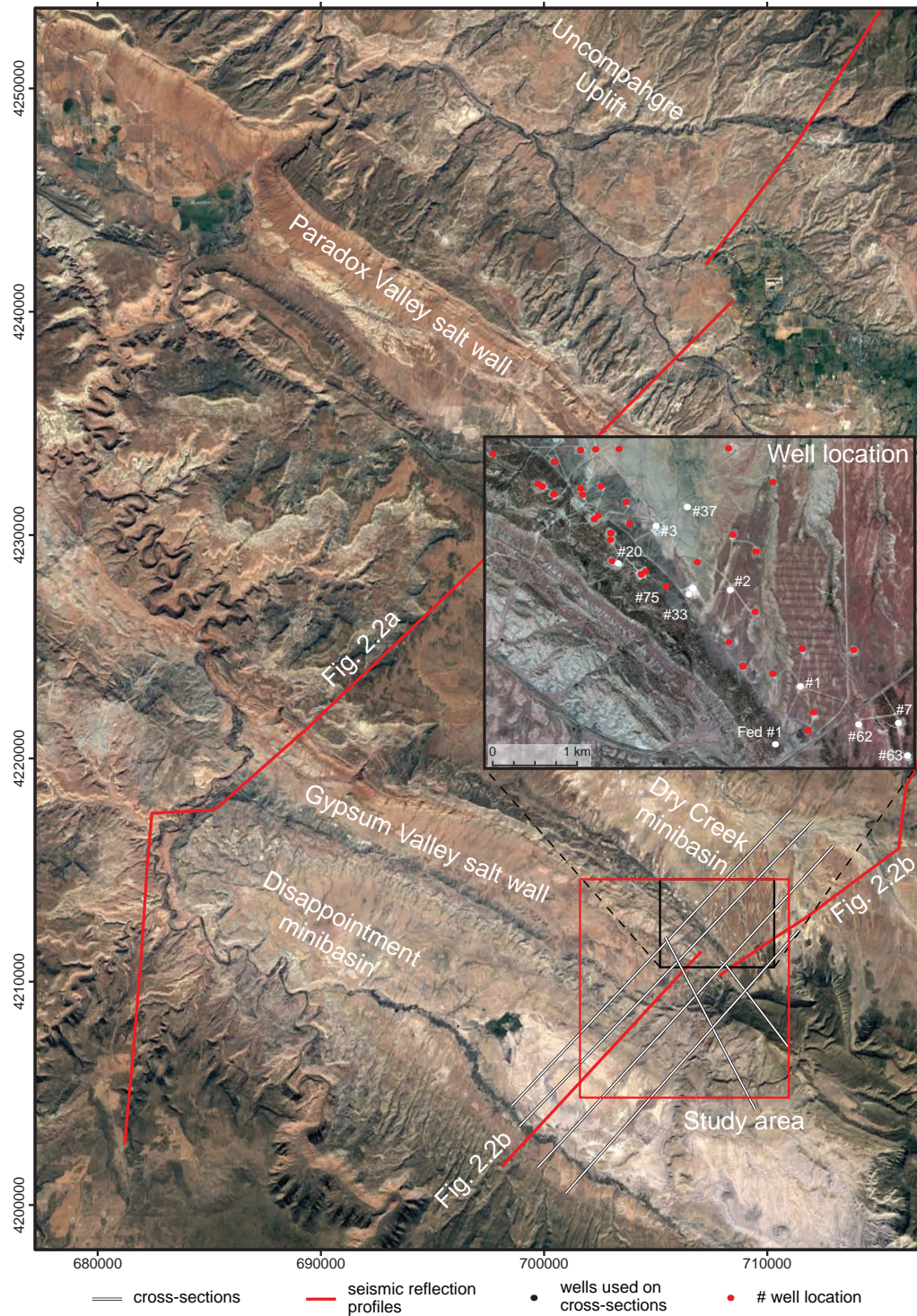
**Figure 1.27.** Location of the seismic refection and well data used in this thesis as well as the position of the constructed cross-sections in the southeastern Paradox Basin (SW Colorado). Red square points out the location of the studied area. Coordinates are in meters in Universal Transverse Mercator, zone 12 northern hemisphere and datum NAD83.
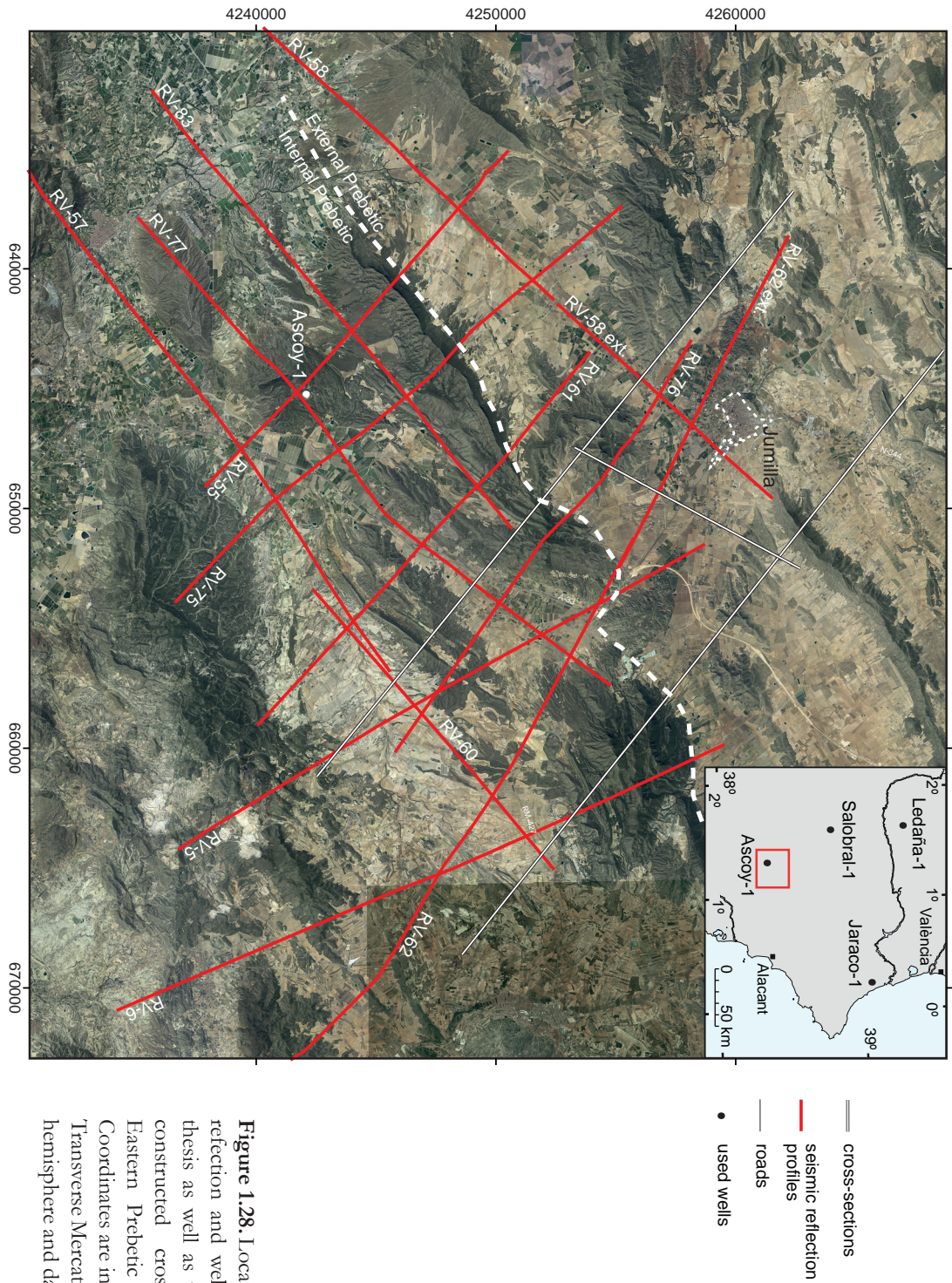
**Figure 1.28.** Location of the seismic reflection and well data used in this thesis as well as the position of the constructed cross-sections in the Eastern Prebetic Zone (SE Spain). Coordinates are in meters in Universal Transverse Mercator, zone 30 northern hemisphere and datum ED50.

The source of the gravity data from the Prebetic Zone is field data downloaded from the *Instituto Minero y Geológico de España* (http://www.igme.es/) combined with additional gravimetric data collected by Castaño (1993). The used reference density is 2.67 g/cm$^3$ and the topographic correction has been implemented. The source of the gravity data from SW Colorado is field and spatial data downloaded from the Regional Geospatial Service Center at the University of Texas at El Paso (http://gis.utep.edu/data.html). The used reference density is also 2.67 g/cm$^3$ and the topographic correction has also been implemented.

The reflection seismic and well data from SE Spain has been supplied in paper copy by the *Archivo Técnico de Hidrocarburos* (*Ministerio de Economía, Industria y Competitividad*) of the Spanish Government, and in digital copy by the *Instituto Geologico y Minero de España* (Lanaja et al., 1989). The seismic reflection data set is composed of the vintage "RV" seismic survey acquired between 1982–1985 by CGG and BP, using dynamite as a seismic source and a receptor array composed by 36 geophones. These seismic reflection data were provided in time, simple-stacked but not migrated to time. Despite this, during the processing stage, multichannel deconvolution was applied by the operating companies to avoid possible seismic diffractions. Regarding the exploratory wells, they were drilled between 1965–1989 by different companies (Enpensa, Enpasa, Tenneco, Repsol…). From them, we only have a complete data set of the closest well to the Jumilla region (Ascoy-1). This data set includes the well tops and the lithological, sonic, gamma ray, resistivity, ciberdip and dipmeter logs. For the other wells, only the well tops and the lithologoical logs are available.

The original subsurface data from SW Colorado have been directly supplied in digital format by Conoco-Phillips. The seismic reflection data set is composed of two lines shot in the 1970s using dynamite. They were time-processed data converted to depth using average velocities of four units dividing the stratigraphic section: surface to top Honaker Trail, Honaker Trail, Paradox Fm., and basement. The velocities were based on check-shot data from the Burkholder #1 well near Castle Valley (located in central Paradox Basin). In this instance, the well data set consisted of well tops and lithological logs. As a result of the confidentiality agreements with the company that supplied the data, only the line drawings of the seismic reflection profiles are included in this memoir and in the corresponding compiled article (see **Annex 1**).

## 1.7.2. Processing

### 1.7.2.1. Digital and time-to-depth conversions of the seismic reflection data

Fourteen paper-based seismic reflection profiles of the Eastern Prebetic Zone have been processed to obtain standard digital SEG-Y files. For that purpose, they have been scanned and the corresponding seismic trace lines have been georeferenced and then digitized from a seismic trace position map to obtain the X/Y UTM coordinates of the seismic navigation files. The chosen methodology is the one developed by Farran (2008) in the *Grup de Geologia Marina* (ICM) and *Institut de Ciències del Mar* (CMIMA-CSIC) to save seismic paper records as fully conforming SEG-Y digital data files. This methodology is embodied a Matlab® script called "image2segy" (Farran, 2008) which associates the pixels of the scanned seismic images with the geographical and geophysical information included in their corresponding seismic navigation files.

The obtained SEG-Y digital data files have been subsequently checked by a quality control to detect possible mistakes. Common encountered errors were mostly related to the X/Y UTM coordinate locations and sporadically to the shot points, common depth points or the sample interval. If detected, the errors have been corrected by adjustments introduced in the trace headers of the SEG-Y files using the Seisee software.

The time to depth conversion of the resulting digital seismic reflection profiles has been performed with a calculated velocity model and using a depth conversion algorithm included in the Petrel E&P software. Such model is based on the sonic log of the Ascoy-1 well, which allow to define interval and average velocities as well as a time to depth conversion curve. The processing datum used along this process is located at 1050 m above the mean sea level. Therefore, this is a velocity model only constrained by a unique data set and, consequently, susceptible to generate results with appreciable margins of error in areas placed away from the Ascoy-1 well; specially, in those areas located in other paleogeographic domains (i.e. External Prebetic; **Fig. 1.28**). Nonetheless, this issue is minimized because most of the seismic reflection profiles are in the same paleogeographic domain than the exploratory well (i.e. the Internal Prebetic). Accordingly, the interpretable seismic stratigraphy should be similar to the one intersected by the well, and thus little deviations are expected between the real and calculated depths.

## 1.7.2.2. Map construction

The georeferenced cartographic and field data have been transferred into a three-dimensional digital environment (Move™ software from Midland Valley; **Fig. 1.26**). Both orthophotographs and geological field data (i.e. differentiated geological contacts and structural data) have been overlain over the digital terrain models, and following the methodology developed by Fernández (2005), the mapping of the geological surfaces has been completed in three-dimensions.

The fault symbols depicted on the geological maps have been stablished by taking as a reference the bedding (i.e. datum) surfaces located at both faulted blocks and classifying the faults as extensional or contractional depending if the involved strata are lengthened/thinned or shortened/thickened respectively (Norris, 1958; Suppe, 1985; Groshong, 2006). The color charts used for designating the geological units, both on the maps and cross-sections of the Paradox Basin and the Eastern Prebetic Zone, follow respectively the Institute of Tectonic Studies (ITS) convention and the Commission for the Geological Map of the World (http://www.ccgm.org). Finally, the resulting maps have been edited using MAPublisher™ in Adobe Illustrator™ and are presented in this memoir as georeferenced PDF files.

## 1.7.2.3. Seismic interpretation

The depth-converted seismic reflection profiles have been transferred into a Move™ project along with the geological field data. In this software, they have been interpreted simultaneously to the construction of the geological maps. This interpretation is constrained by the stratigraphic information provided by well data and the collected surface data (bedding attitudes, outcropping lithologies and tectonic/stratigraphic contacts).

Due to confidential agreements, the interpretation of the 2D depth-converted seismic reflection data from SW Colorado is based on line-drawings previously interpreted by Mark G. Rowan and Thomas E. Hearon. Despite this, the interpretation in depth is constrained by horizon tops from 13 wells. Conversely, in the Eastern Prebetic Zone (SE Spain), the seismic interpretation has been accomplished directly on the SEG-Y digital data files and constrained by the Ascoy-1 well logs. This borehole is located 2 km northwest from the seismic reflection profile RV-57 (**Fig. 1.28**), so according to the information provided by the dipmeter log, the well tops have been properly projected into the seismic reflection profile RV-57 (**Fig. 1.29**).
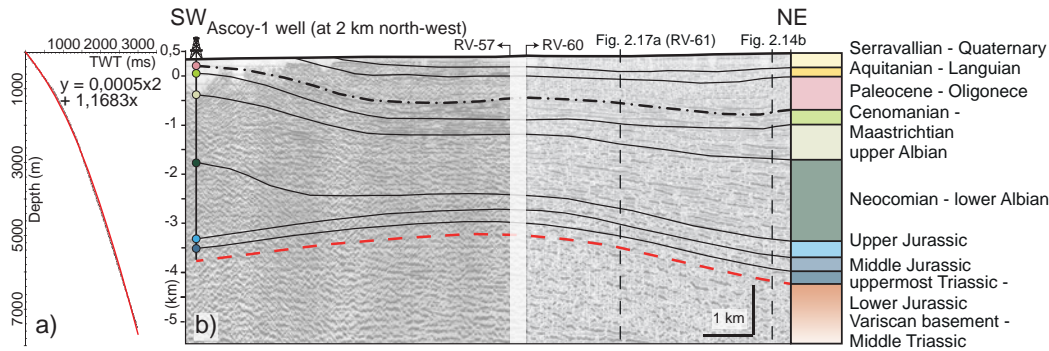
**Figure 1.29.** a) Time-depth curve used to perform the depth conversion of the seismic profiles in the Eastern Prebetic Zone (see the specifics of the time-to-depth conversion in Chapter 1.7.2.1). b) Seismostratigraphy of the Mesozoic and Cenozoic cover at the Ascoy-1 well (see the location of the well and the seismic profiles RV-57 and RV-60 in **Fig. 1.28**). Colored dots indicate the base of the stratigraphic units intersected by the well.

This procedure has allowed to identify the characteristic seismic facies of each sedimentary unit and to determine the position in depth of following horizon tops (**Fig. 1.29**): Lower Jurassic, Middle Jurassic, Upper Jurassic, lower Albian, upper Albian and Maastrichtian. Therefore, this has facilitated the interpretation of the intersecting seismic reflection profiles but also of those profiles located away from the Ascoy-1 well by comparing the seismic facies. Besides this, from the seismic interpretation and the surface data, some vertical mis-ties have been detected at profile intersections between time-equivalent lateral seismic reflections. These incoherencies have been minimized by applying a bulk shift (Z axis correction) for each seismic reflection profile.

## 1.7.2.4. Cross-section construction and restoration

Several geological cross-sections have been constructed to depict the structure of the studied areas. They have been designed perpendicularly to the main trend of the structures, but in some cases, they have also been constructed parallel to these to depict the structural variations along strike. Accordingly, the cross-sections have been built from the lithological contacts and fault traces cut by the vertical plane of the cross-sections and from the projected strike and dip data located less than 200 m from the cross-section trace. Additionally, they are also constrained by the geometrical relationships between stratigraphic units that are laterally observed in other cross-sections, seismic reflections and/or geological maps. The projection of the dip attitudes of bedding and faults into the cross-sections has been done accordingly to the calculated projection vectors which are parallel to the plunge of the intersected geological structures (DePaor, 1988; Groshong, 2006; Fernández et al., 2003). Thereby, depending if

they cut cylindrical (e.g. Ramsay, 1967; Wilson, 1967; Bengston, 1980; Groshong, 2006) and non-cylindrical or conical folded structures (e.g. Stauffer, 1964; Ramsay, 1967; Wilson, 1967; Webb & Lawrence, 1986; Langenberg et al., 1987; Nicol, 1993), different projection vectors have been calculated for each segment of the cross-sections.

Using also Move™ software, the interpolation and extrapolation of the projected data has been done according to the widely used constrains in both extensional and contractional tectonic settings (e.g. Dahlstrom, 1969; Elliott, 1976; Hossack, 1983 and 1995; Suppe, 1983; Woodward et al., 1985; Rowan & Kligfield, 1989; Schultz-Ela, 1992; Rowan, 1993; Rowan et al., 1996; Hudec & Jackson, 2004; Rowan & Ratliff, 2012) and also considering the following assumptions for the subsalt, salt and suprasalt units.

For the suprasalt structure, these assumptions are: 1) to maintain constant thicknesses of the sedimentary units except if it is contrarily indicated by the sub- and surface data; 2) to make gradual and progressive thickness variations of the suprasalt units; and 3) to stablish the fold geometry according to its relationship with subsalt faults or salt detachments (e.g. Jamison, 1987; Mount et al., 1990; Hardy & Poblet, 1994; Poblet & Hardy, 1995).

During the construction of the salt structures we have assumed that: 1) the presence of sediments covering piercing salt diapirs is indicative of that the underlying salt structure is no longer active, and thus is either surrounded in depth by primary welds or squeezed with secondary welds; 2) the gradual thinning of syn-kinematic units within sedimentary basins, suggests the progressive depletion of the salt source layer and the formation of primary welds beneath the principal depocenters; 3) thickened young suprasalt strata lying directly on top of previously salt inflated areas are indicative of diapiric extensional collapse; and finally 4), considering the regional context in which the studied salt structures were formed (i.e. the proximal segment of an extensional developing passive margin in the Eastern Prebetic Zone, SE Spain; and the distal part of a foreland basin in the Paradox Basin, SW Colorado), the style of early diapirism in the first case was that of reactive diapiric rise (Jackson & Vendeville, 1994); and for the second case was that of single-flap active diapiric rise because no regional extension nor shortening was involved (Schultz-Ela et al., 1993).

And for the subsalt units, depth-to-basement calculations are made using the suprasalt stratigraphic thicknesses both obtained from well and field data and combined with the interpreted seismic data. In addition to these constrains, we also accept the following

assumptions for the construction of the subsalt structure: 1) the brittle behavior of the basement in the studied areas; 2) the location of the synclinal fold hinges determines the position of the basement roof as long as the fold hinge coincides with a primary weld in depth; and 3) the monoclinal flexures of the overburden coinciding with sharp changes in the elevation of the regional datum (defined as the level where strata, deposited at the synclines after primary welding, have not gone up or down due to local deformation; Hossack, 1995) are interpreted as related to basement faults –whose extensional or contractional nature would be defined according to its age and the regional context. In all cases, the interpretation considers the geometry of the syn-kinematic sediments because their structural analysis provides valuable information not only for the kinematic evolution of the structures but also for their geometry in depth (e.g. Medwedeff, 1989, 1992; Mount et al., 1990, DeCelles et al., 1991; Bloch et al., 1993, Shaw & Suppe, 1994; Poblet & Hardy, 1995).

Finally, one of the obtained cross-sections has been qualitatively restored to illustrate the Alpine evolution of the South Iberian passive margin at the studied area in the Eastern Prebetic Zone. It is a restoration based on the Rowan (1993) methodology in which: 1) the bed length of the supra- and subsalt layers is maintained in all restoration steps (Rowan & Ratliff, 2012); 2) the suprasalt beds are considered to be deformed by flexural slip; 3) the salt area is not maintained assuming that salt migration could occur out of the cross-section plane; 4) the fault displacement is maintained along the fault planes; 5) the salt structures are restored individually and then merged to the contiguous ones; and 6) unknown "cryptic" extension and/or shortening is assumed during the restoration of the salt structures (see further details in chapter 1.5.1 and 1.5.2). The explained methodology and procedure have been done by using the tools and algorithms included in the Move™ software. This process encompassed multiple iterations to finally obtain regional consistent and kinematically plausible restoration steps. In this regard, the restoration process has been proven to be a powerful tool to detect incongruences in the original cross-sections, that obligate to modify and thus improve the final result. Finally, as the other illustrations included in this memoir, the cross-sections and corresponding restoration have been edited and exported in a PDF file by using Adobe Illustrator™.
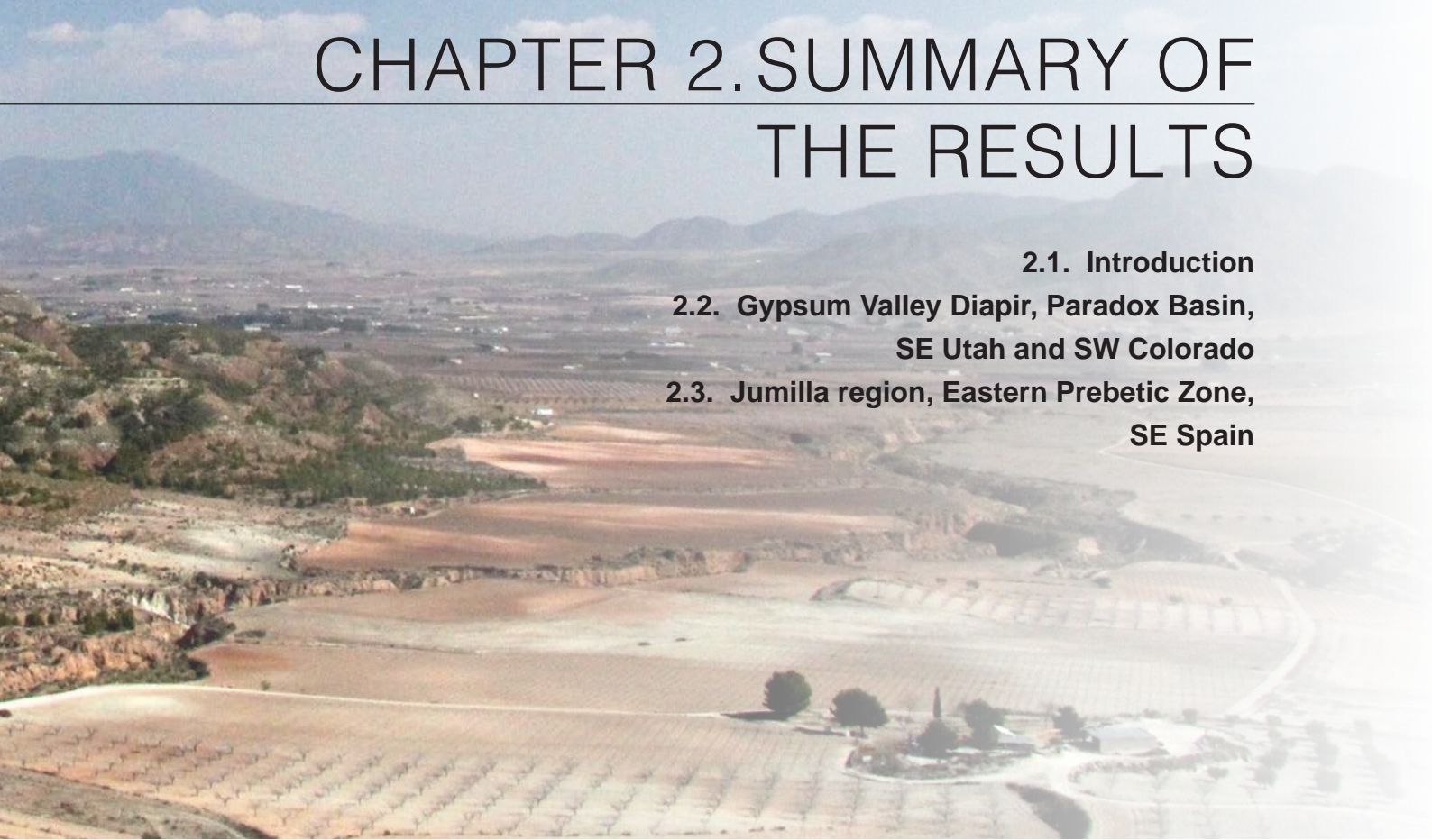
# CHAPTER 2. SUMMARY OF THE RESULTS

**2.1. Introduction**
**2.2. Gypsum Valley Diapir, Paradox Basin,**
**SE Utah and SW Colorado**
**2.3. Jumilla region, Eastern Prebetic Zone,**
**SE Spain**

*The cover of Chapter 2 is composed by two photos: an upper one depicting the southeastern termination of the Gypsum Valley salt wall (SW Colorado); and a lower one illustrating the Jumilla Diapir in the foreground and the characteristic "ridge and valley" landscape of the Eastern Prebetic Zone at the Jumilla region (SE Spain) in the background.*

## 2.1. Introduction

In order to accomplish the objectives outlined in the Preface of this thesis, a characterization of salt walls has been carried out in two distant field-work areas with distinct geological settings (**Fig. I.I**). Therefore, rather of presenting the study of both study areas in a single geological framework, the following summary of the results has been organized in two subchapters, in which the respective outcomes of the Paradox Basin (SW Colorado and SE Utah) and the Eastern Prebetic Zone (SE Spain) are presented separately. Besides this, the global results of the investigated areas are reflected in Chapter 4 which also lists the main concluding points of this thesis.

Accordingly, the results obtained from the study of salt walls and salt-related structures are introduced in the respective subchapters as follows: firstly, presenting a geological overview of each field-work area; secondly, indicating the articles enclosed in this memoir in which the major part of the corresponding results have been reflected; thirdly, enumerating the oral and poster presentations at international meetings that served to show either the results presented in this memoir as other ones not included in it; and finally, summarizing the main results and derived controlling factors on the development of salt walls in the respective tectonic settings.

**CHAPTER 2**

## 2.2. Gypsum Valley Diapir, Paradox Basin, SE Utah and SW Colorado.

### 2.2.1. Regional geological overview

The Paradox Basin, located in SE Utah and SW Colorado (USA), is a large and asymmetric intracratonic foreland basin defined by the depositional extent of the layered evaporites of the Paradox Fm. (**Fig. 2.1a**). Well and 2D seismic reflection data show that the Paradox Basin is located in the footwall of a 50° NE-dipping reverse fault bounding the southwestern flank of the basement-cored Uncompahgre Uplift (White & Jacobson, 1983; Moore et al., 2008; Timbel, 2015 (**Fig. 2.2a**). This uplift resulted from the Late Mississippian to Early Permian convergent tectonism that affected the western margin of North America coupled with the
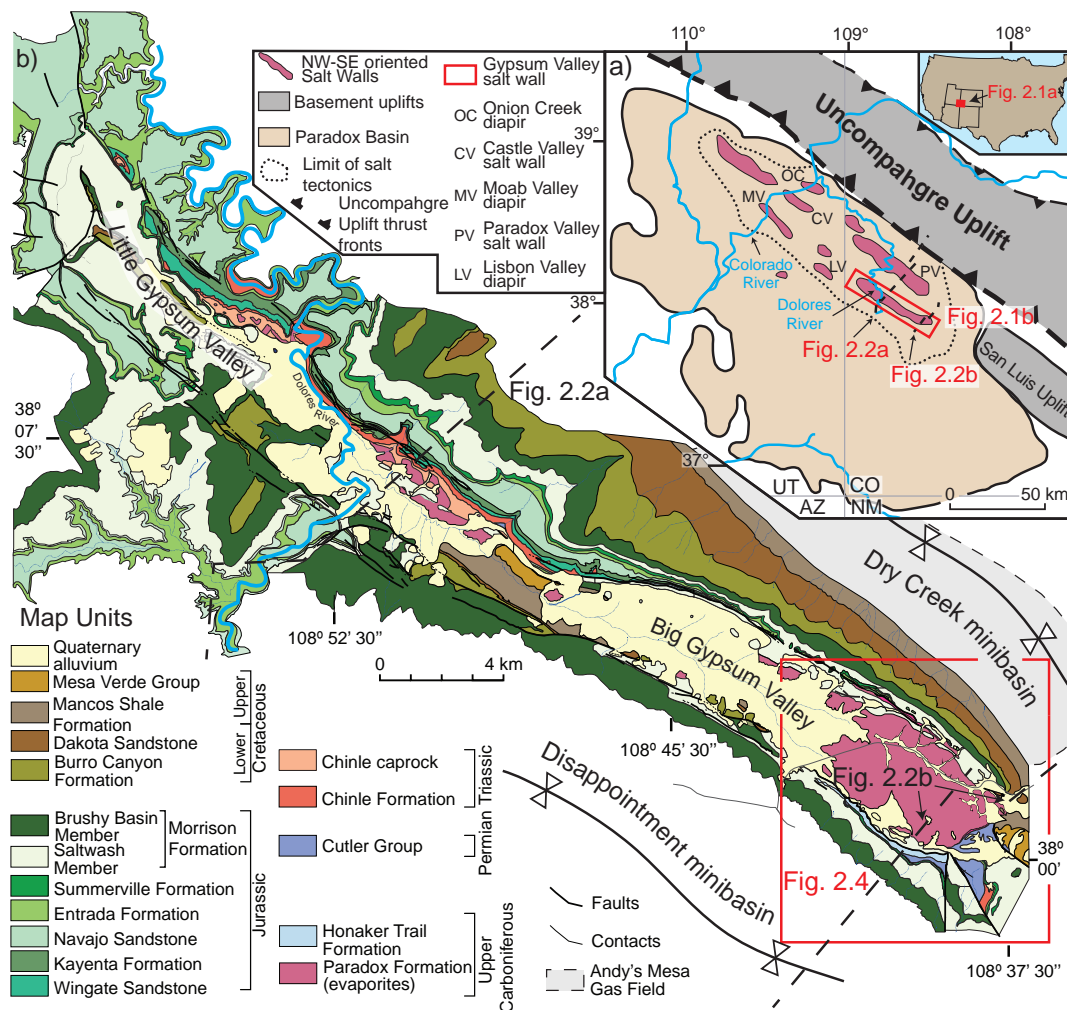


**Figure 2.1.** Location map: a) Paradox Basin and its major salt walls (after Shoemaker et al. 1958); UT: Utah, CO: Colorado, AZ: Arizona, NM: New Mexico; b) geologic map of Gypsum Valley salt wall. The red outlines indicate, in **Fig. 2.1a**, the location of **Fig. 2.1b**, and in **Fig. 2.1b**, the study area illustrated in **Fig. 2.4**.

collision of Gondwanaland to the south (Mallory, 1972; Kluth & Coney, 1981; Kluth, 1986; Barbeau, 2003). Maximum subsidence of the Paradox Basin coincided with the deposition of the Paradox Fm. evaporites (Barbeau, 2003; Blakey, 2009). Subsequent differential loading by prograding Upper Pennsylvanian to Permian fluvial sediment, shed from the Uncompahgre Uplift (**Fig. 2.1a**) caused salt inflation over subsalt extensional faults, thereby triggering a series of NW-SE trending salt walls (Elston et al., 1962; Baars & Stevenson, 1981; Ge et al., 1997; Lawton & Buck, 2006; Kluth & DuChene, 2009; Trudgill, 2011; e.g. see this process illustrated in **Fig. 1.10**). The onset of diapirism was earlier in the proximal (NE) than distal (SW) areas (Trudgill, 2011). Importantly, although contraction was involved in the emplacement of the Uncompahgre Uplift, there is no cited evidence for any contraction in the Paradox Basin, except for minor shortening during the Laramide Orogeny, postdating salt wall formation and diapir burial (Mankowski et al., 2002).

In this geological setting, the Gypsum Valley diapir is a NW-SE trending vertical salt wall located in the southeastern, distal part of the Paradox Basin in SW Colorado (**Fig. 2.1a**). It is almost 35 km long and from 2 to 3.5 km wide salt wall that is bounded on the northeastern side by the Dry Creek minibasin and on the southwestern side by the Disappointment minibasin (**Fig. 2.1b**). Seismic reflection, well, and field data depict an important asymmetry between the bounding minibasins (Amador et al., 2009; Rowan et al., 2016; **Fig. 2.2**). In the northeastern side, older strata are relatively thick and deeply buried. In contrast, the southwestern side is marked by the same older strata that gradually thin and upturn to near-vertical forming a megaflap adjacent to the diapir (Deatrick et al., 2015; Mast, 2016; Rowan et al., 2016; **Fig. 2.2b**).
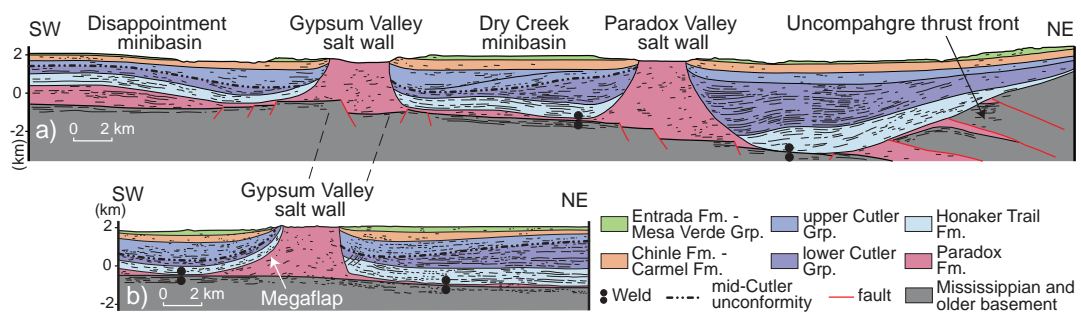


**Figure 2.2.** Line drawings of regional depth-converted seismic profiles in the southeastern Paradox Basin (see location in **Figs. 1.27** and **2.1**): a) across the center of Gypsum Valley diapir and the southeastern end of the Paradox Valley diapir; b) across the study area at the southeastern end of the Gypsum Valley salt wall modified from Rowan et al. (2016). Original data and depth conversions courtesy of ConocoPhillips.

65

The general evolution of the southeastern part of this salt wall, based on a 2-D analysis and restoration from Rowan et al., (2016) is depicted in **Figure 2.3**. Salt movement was triggered during the late Pennsylvanian by differential sedimentary loading, forming an early, asymmetric, single-flap active diapir (Schultz-Ela et al., 1993) with a thinned roof bounded by a suprasalt counterregional fault over the proximal (NE) edge of the diapir (**Fig. 2.3b** and **2.3c**). Lengthening and/or erosion of the thinned diapir roof (mid-Cutler unconformity) triggered salt breakthrough and the onset of passive diapirism (**Fig. 2.3d**). Subsequent evacuation of deep salt into the growing diapir generated diapir-flanking depocenters containing upper Cutler Grp. and younger strata, with progressive rotation of the southwestern flank into the megaflap geometry and consequent widening of the diapir (**Fig. 2.3e** and **2.3f**).
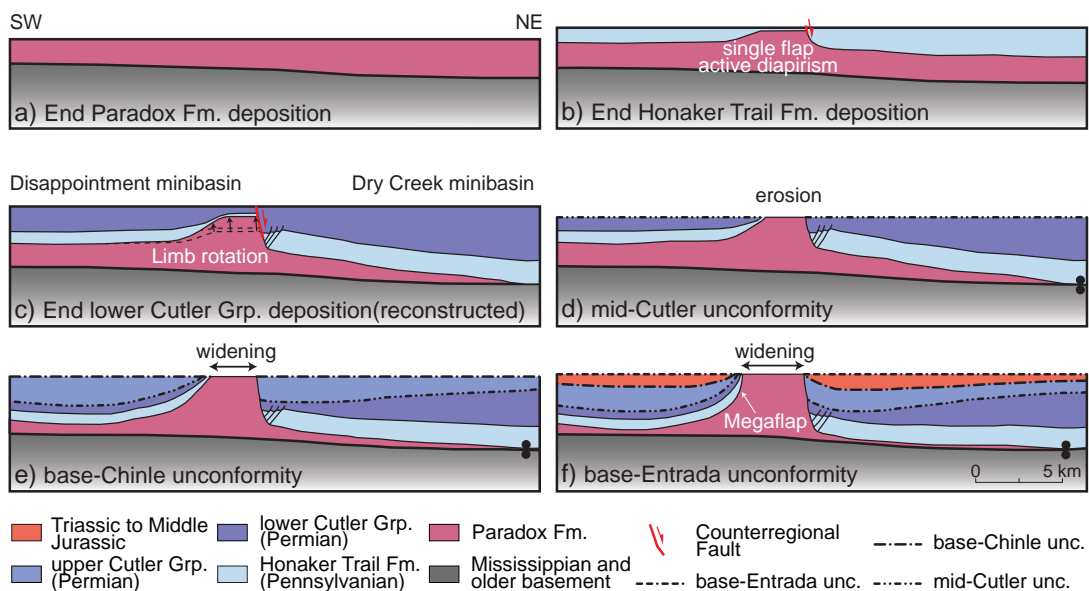


**Figure 2.3.** Sequential quantitative restoration of the Gypsum Valley salt wall (modified from Rowan et al. 2016) along the depth-converted seismic profile illustrated in **Fig. 2.2b**.

## 2.2.2. Results

The results obtained in the Gypsum Valley diapir are related to the structural and sedimentological characterization of the southeastern termination of the salt wall; and most of them are included in the following scientific article published in Basin Research:

- Escosa, F. O., Rowan, M. G., Giles, K. A., Deatrick, K. T., Mast, A. M., Langford, R. P., Hearon IV, T. E., & Roca, E. (2018). Lateral termination of salt walls and megaflaps: An example from Gypsum Valley diapir, Paradox Basin, Colorado, USA. *Basin Research*, *31*, 191–212. doi:10.1111/bre.12316 (**Annex 1**).

In addition to this article, the results have also been advertised at international conferences in posters and oral communications (see **Table 1**) in which other less significative outcomes were presented. These presentations and the above-mentioned article illustrate the main results and conclusions derived from the investigation in the Gypsum Valley diapir which are detailed in the following points:

| Authors | Year | Comunication title | Type of the comunication | Meeting name |
|---|---|---|---|---|
| Giles, K.A., Langford, R.P., Hearon IV, T.E., Brunner, M.G. Rowan, T.F. Lawton, Deatrick, K.A., F.O. Escosa, F.O., Foster, A., Heness, E.A., Lerer, K., Mast., A.M., McFarland, J.C., Shock, A.L. | 2016 | Emerging new paradigms in the Paradox salt Basin, Utah and Colorado | Conference paper | GSA Annual Meeting, Denver, Colorado, USA |
| Deatrick, K.T., Mast, A.M., Escosa, F.O. | 2016 | An integrated study of the structure and sedimentology of an exposed salt wall termination, Big Gypsum Valley, Colorado, USA | Poster | GSA Annual Meeting, Denver, Colorado, USA |
| Escosa, F.O., Rowan, M.G., Giles, K.A., Deatrick, K.T., Mast, A.M., Langford, R.P., Hearon IV, T.E. | 2016 | New mapping and cross-sections across the sourthern termination/megaflap of Gypsum Valley salt wall | Poster | S-SIRC Annual Sponsors Meeting, Cortez, Colorado |
| Escosa, F.O., Rowan, M.G., Giles, K.A., Deatrick, K.T., Mast, A.M., Langford, R.P., Roca, E., Hearon IV, T.E. | 2017 | Gypsum Valley megaflap and salt wall termination structures, Paradox Basin, Colorado | Poster | S-SIRC Annual Sponsors Meeting, Cortez, Colorado |
| Escosa, F.O., Rowan, M.G., Giles, K.A., Deatrick, K.T., Mast, A.M., Langford, R.P., Hearon IV, T.E., Roca, E. | 2018 | Lateral terminations of salt walls and megaflaps: An example from Gypsum Valley Diapir, Paradox Basin, Colorado | Conference paper | S-SIRC Annual Sponsors Meeting, Cortez, Colorado |

**Table 1.** Oral and poster communications at international meetings corresponding to the investigation carried out in the Paradox Basin (SE Utah and SW Colorado).

- The characterization of the three-dimensional architecture of the SE-termination of the Gypsum Valley diapir which is depicted in a new geological map (**Fig. 2.4**) and the corresponding cross-sections (**Fig. 2.5**). For a full explanation of the structure see **Annex 1**.

The geological map and the corresponding cross-sections recognize that:

- The southeastern end of the Gypsum Valley salt wall is asymmetric, with thicker, deeper, gently dipping strata in the proximal NE minibasin and thinned, rotated older strata forming a megaflap on the distal SW side. Its termination is characterized by a moderately plunging nose of salt overlain by SE-dipping strata with maximum 45° dips, a large counterregional fault that separates the nose of the deep proximal minibasin, and radial faults that accommodate concentric extension where the map-view curvature of the flanking strata is greatest.

**Legend:**

Qal — Quaternary alluvium — Cenozoic
Trg — Volcanic gravels — Cenozoic

Kmv — Mesa Verde Grp. — Upper Cretaceous
Km — Mancos Shale Fm. — Upper Cretaceous

Kd — Dakota Sandstone — Lower Cretaceous
Kbc — Burro Canyon Fm. — Lower Cretaceous

Jmb — Brushy Basin member — Morrison Fm. — Jurassic
Jms — Saltwash member — Morrison Fm. — Jurassic

Js — Summerville Fm. — Jurassic
Jce — Entrada Fm. — Jurassic
Jw — Wingate Fm. — Jurassic

TRcc — Chinle caprock — Triassic
TRc — Chinle Fm. — Triassic

Pcu — upper Cutler Grp. — Permian
Pcl — lower Cutler Grp. — Permian

IPh — Honaker Trail Fm. — Upper Carboniferous
IPn — Non evaporite Paradox Fm. — Upper Carboniferous
IPan — Anomalous Carbonates — Upper Carboniferous
IPp — Evaporite Paradox Fm. — Upper Carboniferous

syncline
anticline
extensional fault
topographic contours (20m)
unconformity
base-Entrada unc.
base-Chinle unc.
mid-Cutler unc.
roads
# well location
wells used on cross sections

**Figure 2.4.** Detailed geologic map of the southeastern termination of the Gypsum Valley salt wall (location in **Fig. 2.1b**), showing available well data, the trace of the cross sections (**Fig. 2.5**), and the trace of the seismic profile shown in **Fig. 2.2b** and restored in **Fig. 2.3**. Coordinates are in meters in Universal Transverse Mercator, zone 12 northern hemisphere and datum NAD83.

**Figure 2.5.** (**next page**) Geological cross sections constructed using surface and subsurface data (locations in **Fig. 2.4**). Vertical dashed lines marked by A-A', B-B', C-C', D-D' and X-X' indicate the limits of the geological map shown in **Fig. 2.4**, vertical solid lines denote the intersections with other cross sections, and vertical fine dashed lines indicate wells within 200 m of the cross sections. Stratigraphic colors, labels and unconformity styles as in **Figs. 2.4**. Coordinates are in meters in Universal Transverse Mercator, zone 12 northern hemisphere and datum NAD83.

Legend:

- **Trg** Volcanic gravels — Ceno.
- **Kmv** Mesa Verde Grp.
- **Km** Mancos Shale Fm.
- **Kd** Dakota Sandstone
- **Kbc** Burro Canyon Fm.

Lower/Upper Cretaceous

- **Jmb** Brushy Basin Member
- **Jms** Saltwash Member

Morrison Fm.

- **Js** Summerville Fm.
- **Jce** Entrada Fm.
- **Jlm** Lower San Rafael Grp. (Carmel) and Glen Canyon Grp.

Jurassic

- **TRc** Chinle Fm.
- **TRm** Moenkopi Fm.

Permian Triassic

- **Pcu** upper Cutler Grp.
- **Pcl** lower Cutler Grp.
- **IPh** Honaker Trail Fm. (including scattered bioherms)

- **IPn** Non-evaporite Paradox Fm.
- **IPp** Evaporite Paradox Fm.

Lower Upper Carboniferous

Mississippian Basement

normal fault

weld
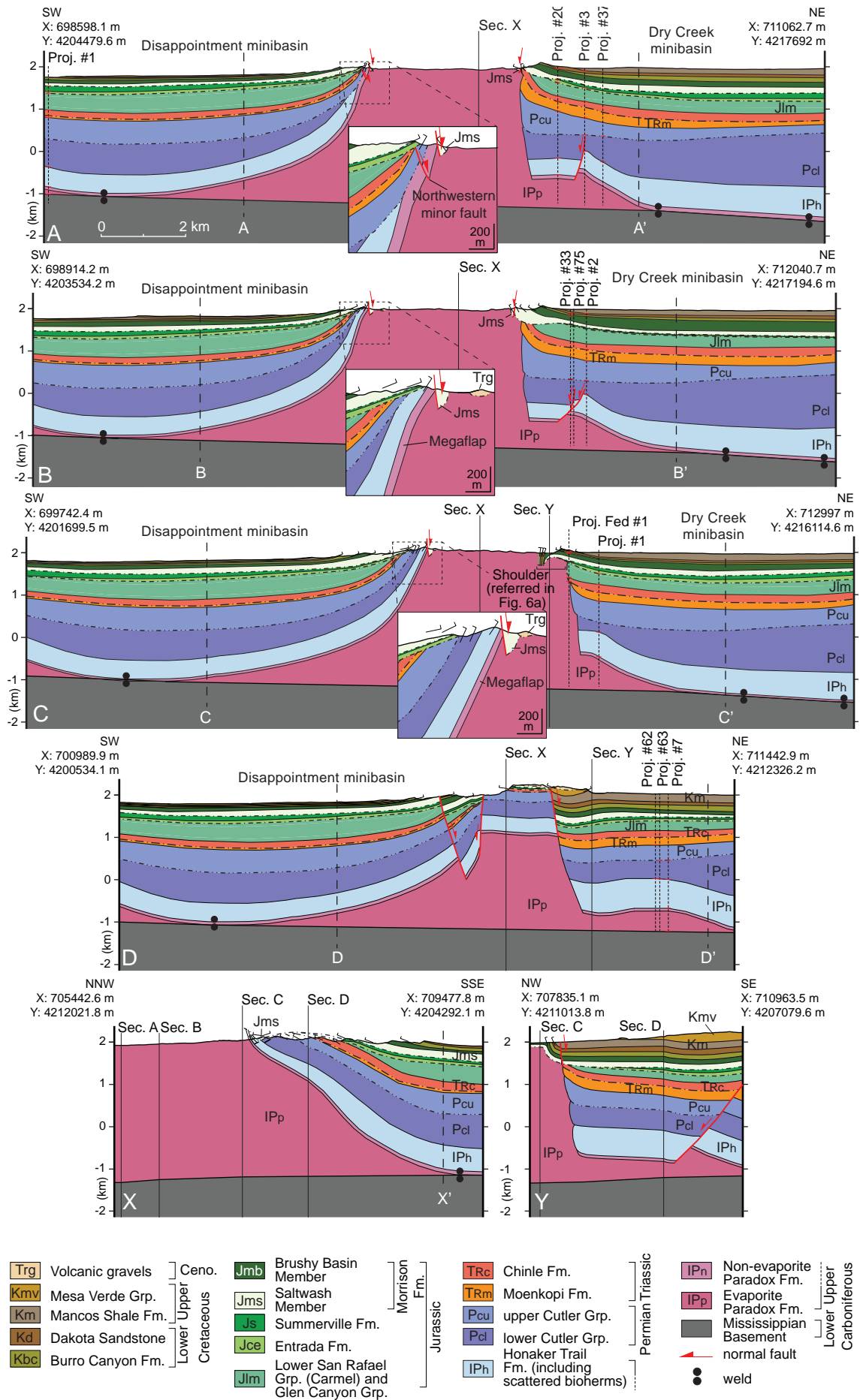
- The megaflap, which is characterized by near-vertical strata, terminates towards the southeastern end of the diapir by a decrease to ca. 60° dips over a distance of several hundred meters before being truncated by the western radial fault. The northwestern termination is buried by younger strata. The megaflap includes undeformed non-evaporite strata of the uppermost Paradox Fm. to the SE, but the same interval becomes increasingly deformed along strike to the NW. This deformation may represent early syn-sedimentary slumping or part of the intrasalt deformation; in the latter case, the base of the megaflap would change its stratigraphic position along strike.

- And finally, the gradual termination and decrease in dip of the megaflap may be related to the deep salt budget since limb rotation to vertical in halokinetic megaflap requires an adequate thickness of deep salt (Rowan et al., 2016). Thus, beneath the Gypsum Valley megaflap, the salt would have been thick enough for strata to rotate to vertical, but rotation was limited where the salt might have thinned southeastward towards the edge of the salt basin (see the extend of the Paradox Fm. evaporites in **Fig. 2.1a**).

From these results, and by comparison with analogue structures located elsewhere in the Paradox Basin and the northern Gulf of Mexico, a series of simple end-member models in which salt wall and megaflaps may terminate abruptly or gradually have been proposed (**Figs. 2.6**, **2.7** and **2.8**).
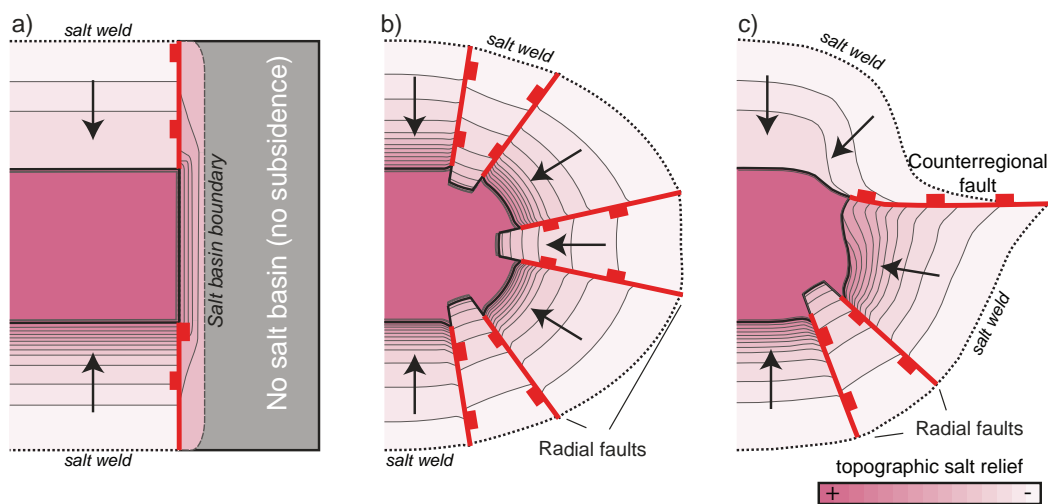


**Figure 2.6.** Schematic plan-view illustrations of end-member termination geometries of salt walls (red faults are all suprasalt, countour lines are on top salt): a) symmetric salt wall termination above a subsalt basement fault (not shown); b) symmetric salt wall termination where there is deep salt present off the end of the diapir; c) termination where the salt wall is asymmetric, with a counterregional fault off the end. Note that radial fault development depends on both map-view curvature and the degree of drape folding of flanking strata. Arrows indicate salt flow into diapir.

For example, the thickness and composition of salt as well as the location where the diapiric growth takes place in relation to the paleogeographic extend of a salt basin can control the shape of the salt wall termination (see **Figs. 2.6a** and **2.6b**). Additionally, the presence of nearby diapirs growing simultaneously, and thus the availability of deep salt budged to flow into the diapir may constrain the length of the salt wall termination and the presence of radial and/or counterregional faults (see **Figs. 2.6c**, **2.7a** and **2.7b**). Finally, the width of the early pillow or single-flap active diapir together with the along strike variation of the deep salt budged may control the lateral termination of a megaflap before reaching the end of a salt wall (see **Fig. 2.8**).
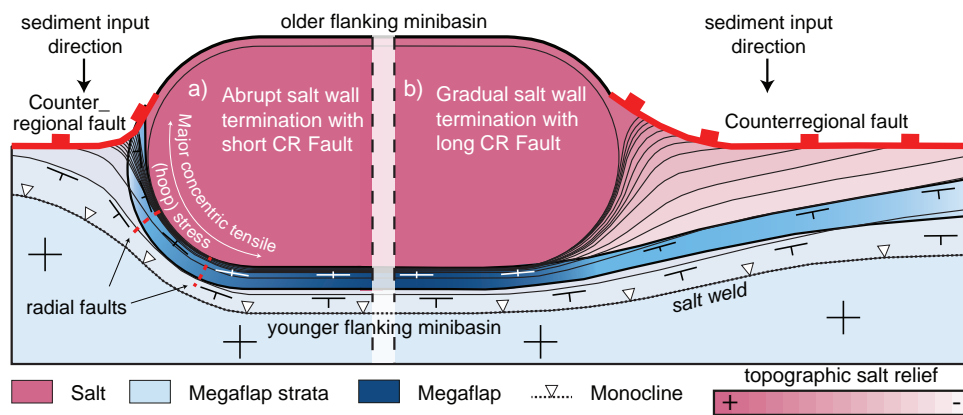


**Figure 2.7.** Schematic plan-view of varying terminations of salt walls with asymmetric minibasins and megaflaps. Red dashed lines indicate radial faults; red continuous lines indicate the counterregional fault at a) abrupt and b) gradual salt wall terminations; continuous black lines indicate topographic contours on the top salt.
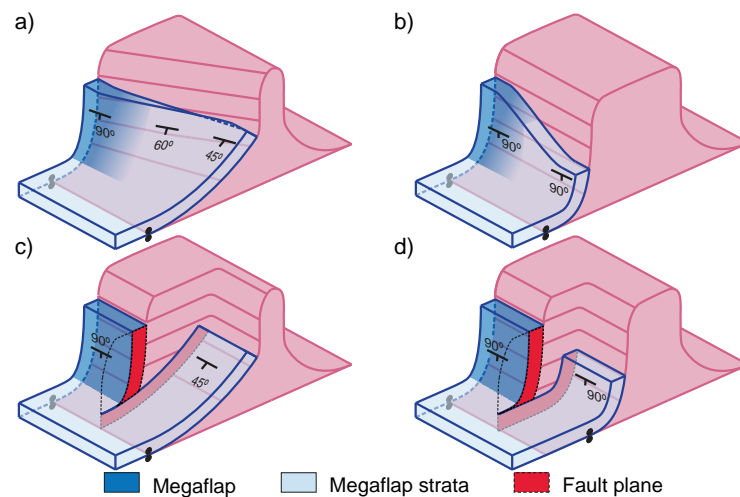


**Figure 2.8.** End-member styles of megaflap termination along the length of a salt wall: a) constant limb length with gradual decrease in dip along strike; b) gradual decrease of limb length with constant dip along strike; c) constant limb length with abrupt decrease of dip across a fault; d) abrupt decrease of limb length with constant dip across a fault. These are conceptual models of end-member geometries; most real examples combine elements of these.

71

Therefore, this investigation suggests that the controlling factors in determining these geometries include: the original thickness and spatial distribution of the deep salt, the presence of nearby diapirs (which determines the fetch area for salt flow into the diapir), spatial patterns of depositional sedimentary loading, and variations in the nature and location of salt breakout through the roof of the initial salt structure.

# 2.3. Jumilla region, Eastern Prebetic Zone, SE Spain

## 2.3.1. Regional geological overview

The Eastern Prebetic Zone is located in the southeastern Iberian Peninsula where the Betic Cordillera constitutes the main geographical feature (**Fig. 2.9a**). The Betic Cordillera together with the Rif (situated in the northwestern margin of Africa) compose the Gibraltar Arc (**Fig. 2.9a**), which is at the westernmost end of the Alpine Mediterranean belt (Dercourt et al., 1986; Dewey et al., 1989). The formation of this belt was driven by the N-S to NNW-SSE convergence between the major Eurasian and African plates, together with the westward displacement of the Alboran Domain, located in between (Spakman & Wortel, 2004; Crespo-Blanc & Frizon de Lamotte, 2006; Vergés & Fernàndez, 2012).
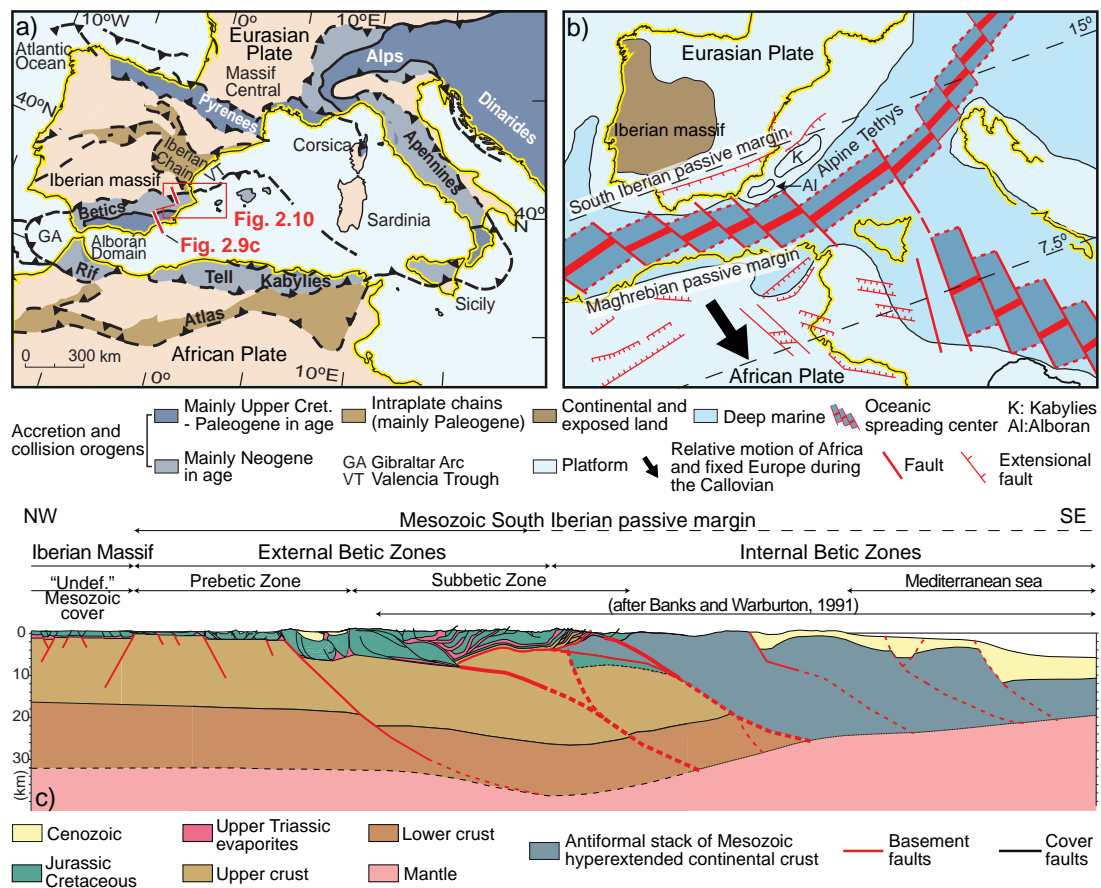


**Figure 2.9.** a) Present day tectonic map of the western Mediterranean depicting the southeastern termination of the Alpine fold-and-thrust belt. b) Paleotectonic map of North Africa and Iberia for Callovian times, modified from Frizon de Lamotte et al. (2011). c) Regional cross-section across the eastern Betic Cordillera illustrating the crustal geometry of the orogen (see location in **Fig. 2.9a**; the Internal Betic Zones and the Subbetic Zone are modified from Banks & Warburton, 1991).

The Betic Cordillera is generally subdivided from north to south into the External and Internal Betic Zones (Fallot, 1948; Balanyá & García-Dueñas, 1987; Vera, 2004). The Internal Betic Zones consist of an allochthonous stack of thrust sheets mainly made up of Triassic and older rocks metamorphosed during the Upper Cretaceous to Paleogene (Egeler & Simon, 1969; Torres-Roldán, 1979; De Jong, 1990). The External Betic Zones correspond to a broad orogenic wedge that is composed of a NW- to NNW-directed fold-and-thrust belt that is Campanian to middle Miocene in age and is detached from the Iberian subsalt basement along the Upper Triassic salt (Platt et al., 2003; **Fig. 2.10**). In general, the thrusted sheets are composed of an uppermost Triassic to Middle Jurassic unit characterized by a minor thickness increase towards the SE, and an Upper Jurassic to Santonian unit illustrating major thickening towards the SE (García-Hernández et al., 1980, 1989; De Ruig, 1992; Hanne et al., 2003). In addition, the thrust sheets are pierced by diapirs of Upper Triassic salt that were emplaced from Mesozoic to Quaternary times (Moseley, 1973; De Ruig, 1995; Escosa et al., 2018b).
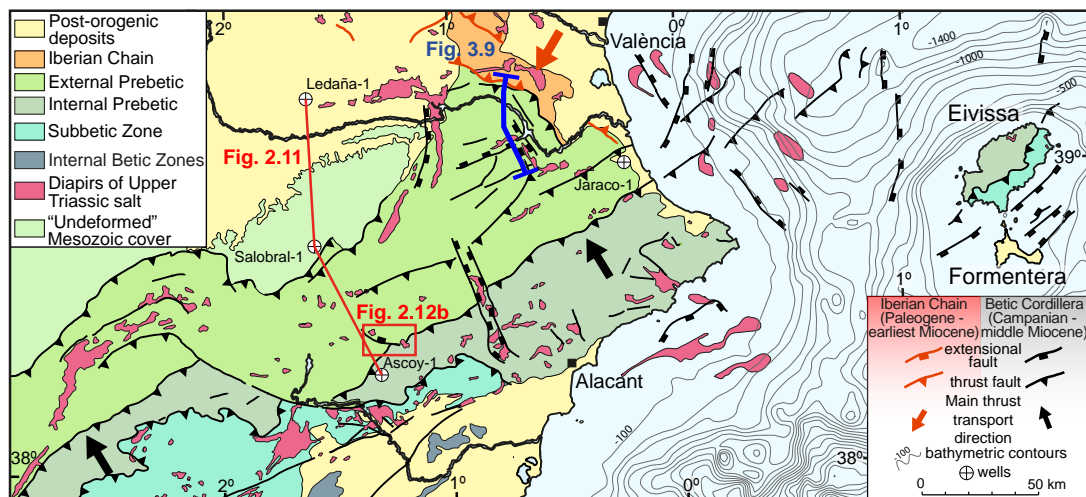


**Figure 2.10.** Tectonic map of the eastern Betic Cordillera, Eivissa and Formentera islands. Red line points out the stratigraphic well correlation shown in **Fig. 2.11**. Red square corresponds to the location of the studied area depicted in **Fig. 2.12b**. Blue line indicates the northern part of the cross-section shown in **Fig. 3.9**.

During the Mesozoic, the External Betic Zones represented the northern conjugate passive margin of the Alpine Tethys (i.e. South Iberian passive margin; **Fig. 2.9b**), which was located southeast of the Iberian Massif (Dewey et al., 1973; Bernoulli & Lemoine, 1980; Ziegler, 1982). The Alpine Tethys was the result of Lower and Middle Jurassic rifting followed by the Callovian oceanic flooring (**Fig. 2.9b**) that separated the Eurasian and African plates (Schettino & Turco, 2011). Oceanic flooring is evidenced by Middle Jurassic ophiolites currently outcropping in the Internal Betic Zones (Puga et al., 2011). This rifting episode is

clearly connected with the opening of the Central Atlantic Ocean to the west (Klitgord & Schouten, 1986; De Jong, 1990; Srivastava et al., 1990). However, a major Upper Jurassic to Santonian rift event affected the eastern External Betic Zones linked to a continued opening of the Central Atlantic Ocean combined with a synchronous development of extensional basins in the western Tethyan area (Ziegler, 1989; Hanne et al., 2003; Frizon de Lamotte et al., 2015).

In the Jumilla region, this rift allowed for the deposition of the Upper Jurassic to Santonian syn-extensional sediments unconformably overlying the uppermost Triassic to Middle Jurassic carbonates that show minor thickness variations (García-Hernández et al., 1980, 1989; De Ruig, 1992; Vera, 2004; Hanne et al., 2003; **Fig. 2.11**). During this time, based on both tectonic and stratigraphic criteria, the External Betic Zones were progressively subdivided into the northwestern Prebetic Zone and the southeastern Subbetic Zone (García-Hernández et al., 1980; **Fig. 2.10**).
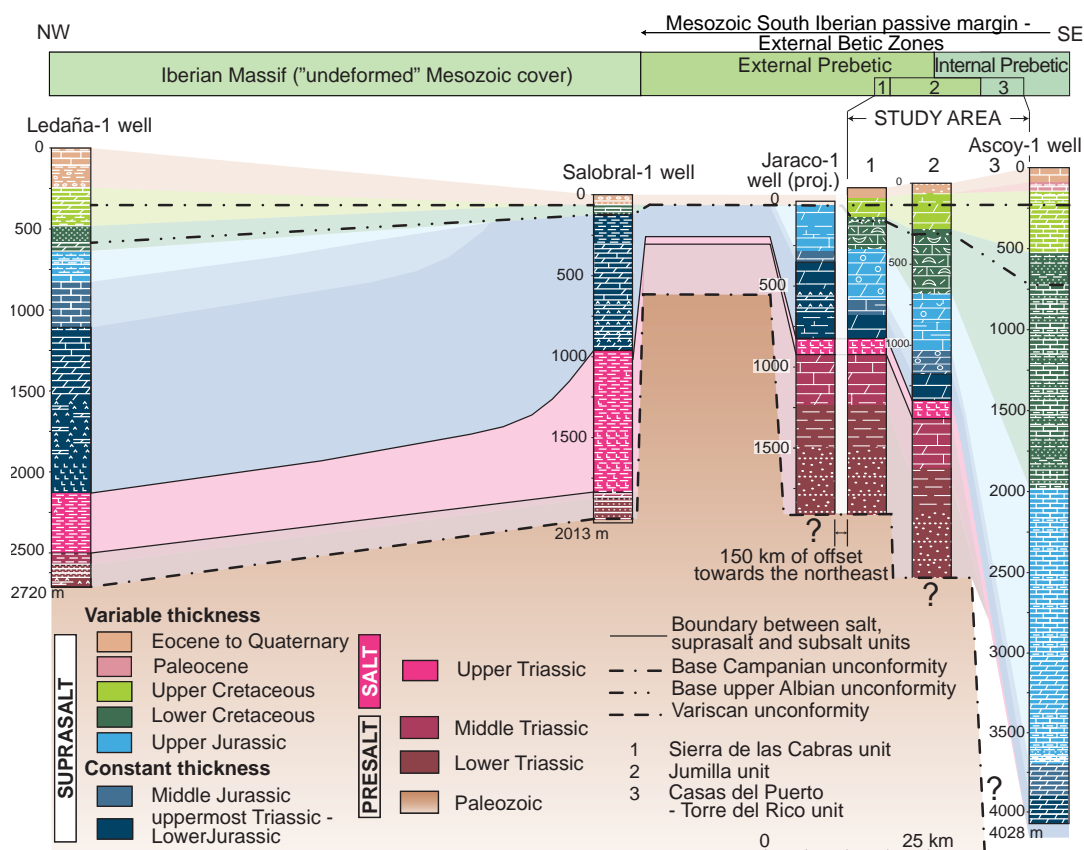


**Figure 2.11.** Well correlation throughout the undeformed Mesozoic cover, the External and Internal Prebetic (datum of the well correlation is defined at the base of the Campanian unconformity). Stratigraphic thickness of salt, supra- and subsalt units in the study area and the Salobral-1 obtained from field work and after García-Hernández et al. (1980) and Lanaja et al. (1987). Jaraco-1 well is located approximately 150 km towards the northeast from the study area (**Fig. 2.10**).

In particular, the Prebetic Zone is characterized by continental to shallow-platform deposits including inner and slope facies. The Subbetic Zone is formed by deep basinal and pelagic deposits (e.g. García-Hernández et al., 1980). According to the thickness and the stratigraphy of the Mesozoic units, the Prebetic Zone is subdivided (from NW to SE) into the External and Internal Prebetic (De Ruig, 1992; **Fig. 2.11**). In this geological setting, the Jumilla region is in the Eastern Prebetic Zone, comprising a portion of the External and Internal Prebetic paleogeographic domains (**Fig. 2.12a**). This is an area in which the Variscan basement to Middle Triassic autochthonous successions do not crop out and the overburden appears to be deformed by a system of ENE-trending, thin-skinned folds and thrusts detached in the Upper Triassic salt. Specifically, the lateral continuity of this fold-and-thrust belt is interrupted by the NW-trending Matamoros Basin located at the center of the study area (**Fig. 2.12b**). Despite this, the general structure of the area includes abundant salt diapirs made up of Upper Triassic evaporites displaying two main geometries: inactive and elongate salt walls that are parallel to the ENE-WSW trending folds (e.g. La Sarsa salt wall); and active sub-circular salt stocks situated in the lateral terminations of the Matamoros Basin (e.g. Jumilla and La Rosa diapirs; **Fig. 2.12b**).

## 2.3.2. Results

The main objective of the investigation in the Eastern Prebetic Zone, besides the understanding of the regional structure, was to characterize the geometric, kinematic and mechanical behavior of diapirs mainly driven by thick-skinned extension and affected by a subsequent thin-skinned contractional deformation. In this regard, the corresponding results have been presented in the following articles:

- ESCOSA, F. O., FERRER, O., & ROCA, E. (2018). Geology of the Eastern Prebetic Zone at the Jumilla region (SE Iberia). *Journal of Maps*, *14*, 77–86. doi:10.1080/17445647.2018. 1433562 (**Annex 2**).
- ESCOSA, F. O., ROCA, E., & FERRER, O. (2018). Testing thin-skinned inversion of a prerift salt-bearing passive margin (Eastern Prebetic Zone, SE Iberia). *Journal of Structural Geology*, *109*, 55–73. doi:10.1016/j.jsg.2018.01.004 (**Annex 3**).

Besides the two articles mentioned above, the outcomes of the investigation accomplished in the Jumilla region have also been presented in numerous international conferences including oral and poster communications (see **Table 2**).
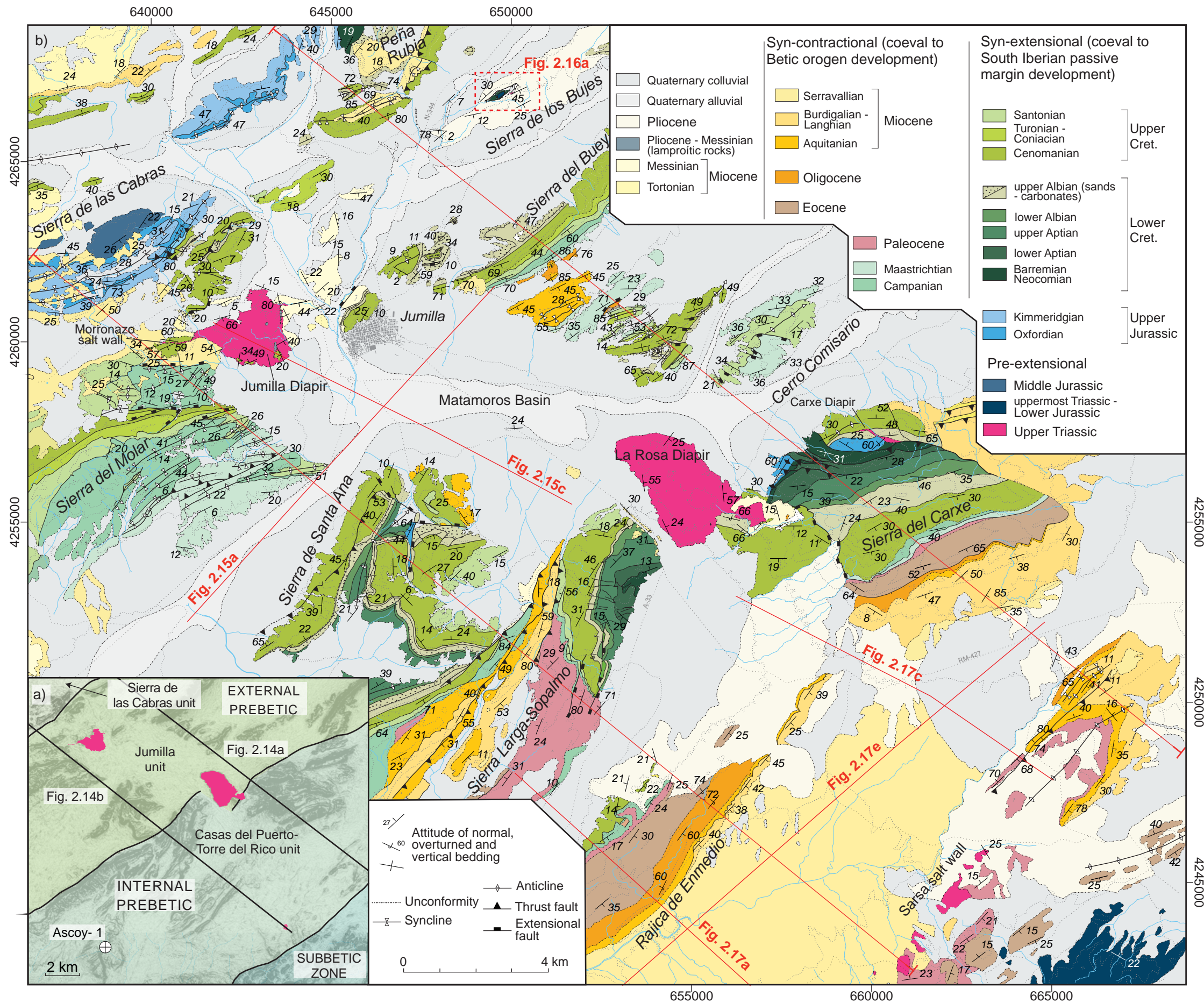
**Figure 2.12.** a) Relief map depicting the location of the main structural units along the Prebetic and Subbetic Zones in the Jumilla region as well as the Ascoy-1 well. b) Simplified geological map of the External and Internal Prebetic in the Jumilla region. The northernmost part integrates data from Baena (1979). Note the location of two cross-sections shown in Figs. **2.14a** and **2.14b**; a detailed geological map of the southwestern part of Sierra de los Bujes shown in **Fig. 2.16a**; and the location of the provided depth-converted seismic lines in **Fig. 2.17**. See **Annex 2** for more detail on the cartographic units. Coordinates are in meters in Universal Transverse Mercator, zone 30 northern hemisphere and datum ED50.

| Authors | Year | Comunication title | Type of the comunication | Meeting name |
|---|---|---|---|---|
| Escosa, F.O., Roca, E. | 2016 | The external eastern prebetics: paper of basement faults in an inverted salt-bearing passive margin | Poster | AAPG/SEG's International Conference and Exhibition, Barcelona |
| Escosa, F.O., Roca, E., Ferrer | 2016 | Thin- vs thick-skinned deformation in an inverted salt-bearing passive margin (the Eastern Prebetic) | Conference paper | Congreso Geológico de España, Huelva |
| Escosa, F.O., Roma, M., Roca, E., Butillé, M., Ferrer, O. | 2016 | The Mesozoic structure of the central part of the south-Iberian passive margin and its influence in the Cenozoic contractional deformation: comparison between the eastern Prebetic Zone (Betic Cordillera) and the Columbrets Basin (southwest Valencia Trough). | Conference paper | AAPG/SEG's International Conference and Exhibition, Barcelona |
| Escosa, F.O., Roca, E., Ferrer, O., Roma, M., Górriz, E. | 2018 | Subsalt extensional structure controls Mesozoic salt tectonics and the Betic inversion | Conference paper | AAPG/GTW Alpine Folded Belts and Extensional Basins, Granada |

**Table 2.** Oral and poster communications at international meetings corresponding to the investigation carried out in the Eastern Prebetic Zone.

The above outlined presentations include results obtained in adjacent studied areas that, also located in the eastern Betic Cordillera, have not materialized in articles yet, and therefore they are not included in this thesis. Nevertheless, focusing on the two enclosed articles (**Annex 2** and **3**), this investigation has shown that the Alpine structure and evolution of the Jumilla region is characterized by the following points:

- A Mesozoic to Cenozoic overburden that is decoupled above the Upper Triassic salt and is firstly displaced to the southeast and then to the northwest above a Paleozoic–Middle Triassic basement, which is affected by major southeast-dipping extensional subsalt faults (**Fig. 2.13**).

- The southern set of southeast-dipping subsalt faults (i.e. Carxe and Sopalmo faults) are the responsible for the thickness variations of the Mesozoic successions over the faulted blocks (**Fig. 2.14**).

- Above the footwall of this subsalt faults, the suprasalt structure is characterized by a thin overburden deformed by short-wavelength folds and thrust faults trending ENE-WSW (**Fig. 2.14**). This general architecture results from the Alpine contractional reactivation of a former extensional structure composed of salt walls and extensional faults, that having a listric geometry, are detached on the Upper Triassic salt.

- Conversely, in the hanging wall of the basement faults, a thicker and less deformed suprasalt strata displays a broad synclinal geometry, which resulted from the northwestwards contractional translation of the overburden above the hanging wall of the basement faults

and its intersection with the southeast-dipping subsalt faults (**Fig. 2.14**). Additionally, the thickened overburden is also deformed by the squeezed and NE-trending La Sarsa salt wall located in the southern limit of the Jumilla region (**Figs. 2.12b** and **2.13g**).
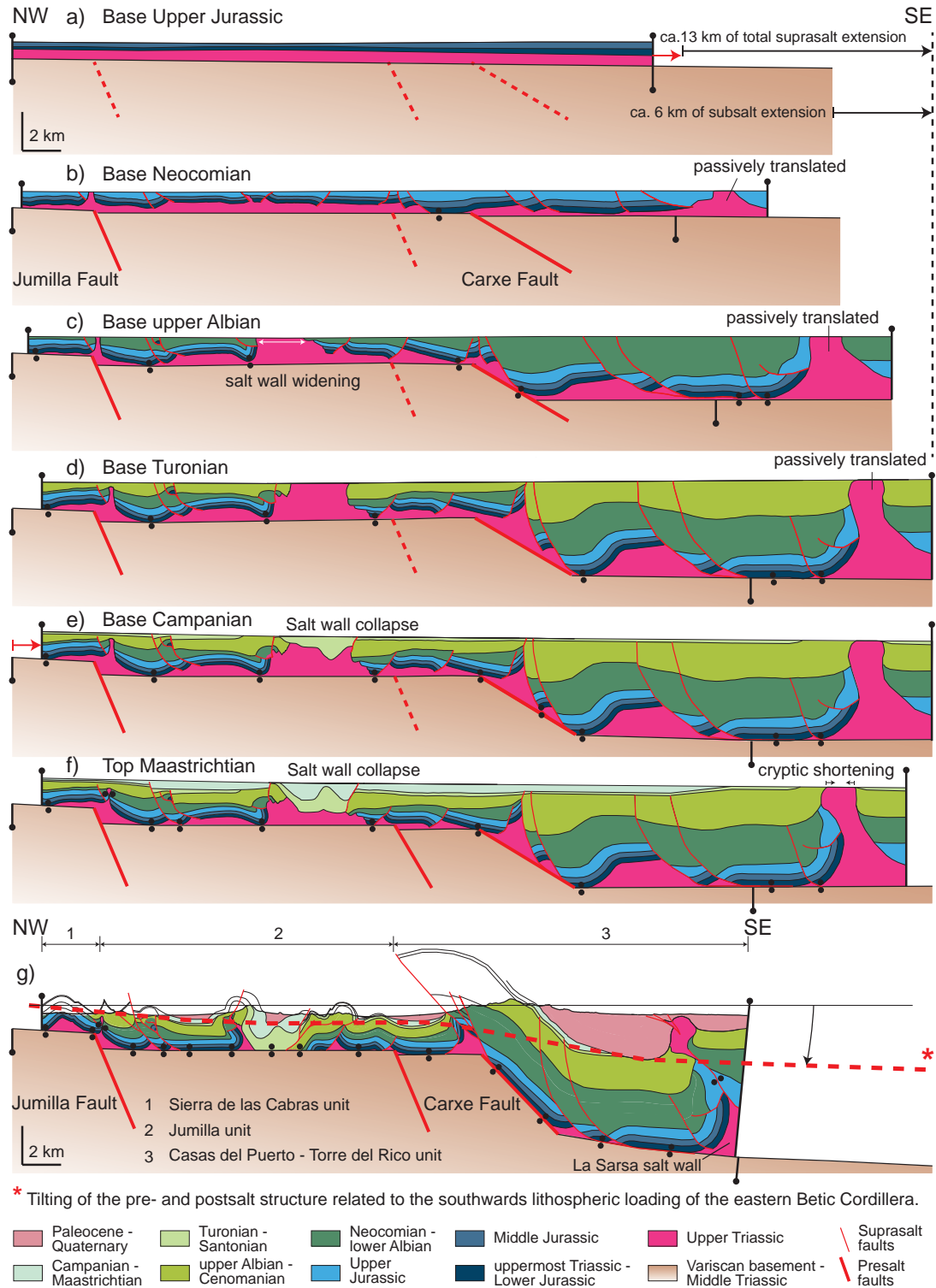


**Figure 2.13.** Qualitative sequential restoration for the Eastern Prebetic Zone at the Jumilla region. **Figure 2.13g** corresponds to the regional cross-section shown in **Fig. 2.14a**. The original thickness of the Upper Triassic salt is estimated according to Bartrina et al. (1990) and De Torres & Sánchez (1990).
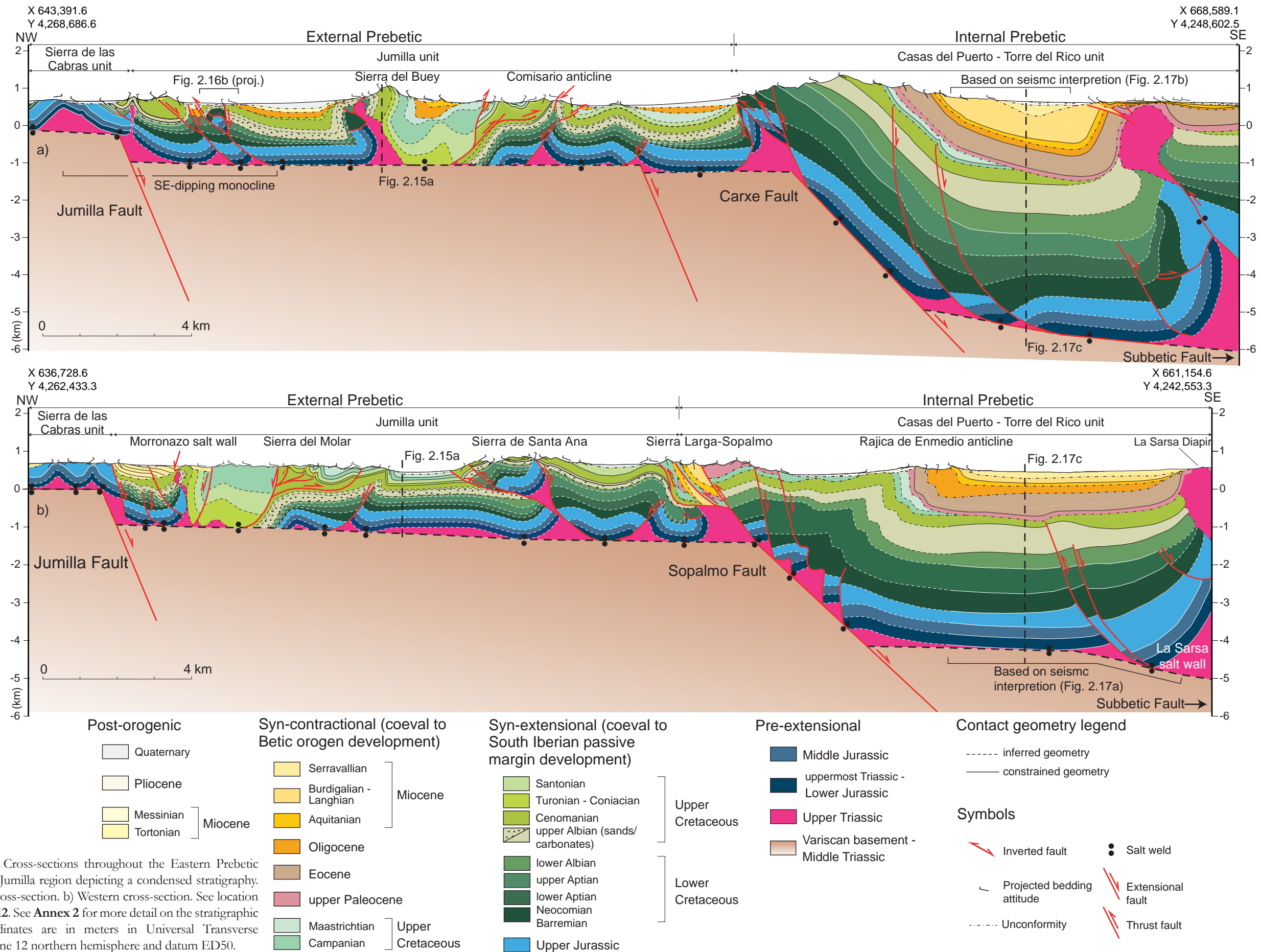
**Figure 2.14.** Cross-sections throughout the Eastern Prebetic Zone at the Jumilla region depicting a condensed stratigraphy. a) Eastern cross-section. b) Western cross-section. See location in **Figure 2.12**. See **Annex 2** for more detail on the stratigraphic units. Coordinates are in meters in Universal Transverse Mercator, zone 12 northern hemisphere and datum ED50.

- In the center of the study area, the lateral continuity of the ENE-trending structures is interrupted by an elongated NW-trending and 2–4 km wide Matamoros Basin (**Figs. 2.12b** and **2.15**). The geometrical analysis of the Mesozoic–Cenozoic sediments recognized in the seismic reflection profiles, show that the structure describes a drape syncline over a basement rollover in the hanging wall of a northeast-dipping basement fault (**Fig. 2.15**). In addition, located respectively at the tips of this subsalt fault, there are two active and sub-circular salt stocks (i.e. Jumilla and La Rosa diapirs).
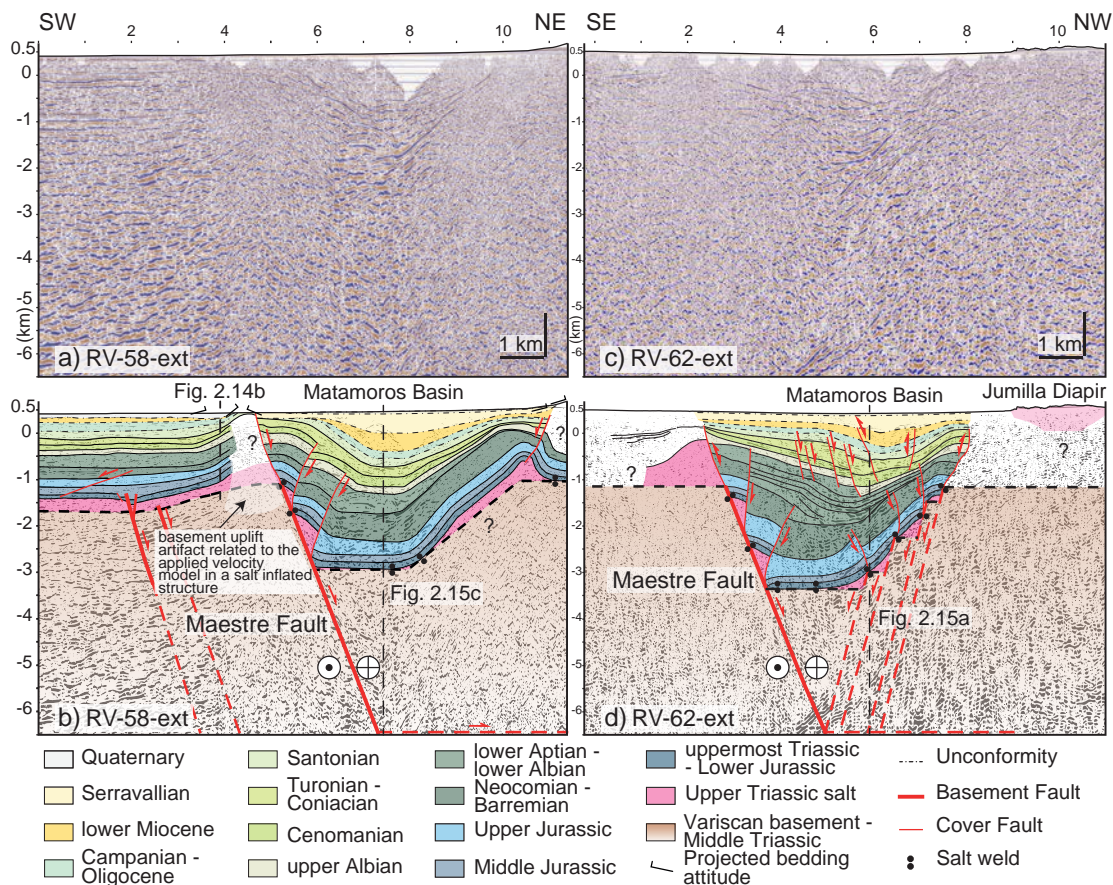


**Figure 2.15.** 2D seismic reflection profiles with their respective interpretations crossing the Maestre Fault and the Matamoros Basin (**Fig. 2.12b**). a) Seismic line RV-58-ext and b) its interpretation. c) Seismic line RV-62-ext and d) its interpretation.

- The structural analysis together with the sequential restoration have led to interpret the tectonic evolution of the overburden in relation to the subsalt rocks. This was conducted by a combination of thick- and thin-skinned styles of deformation (**Fig. 2.13**). Thick-skinned extension occurred mainly during Upper Jurassic to Santonian times deforming the Paleozoic to Middle Triassic autochthonous succession. Above the basement faults, the pre-kinematic units (i.e. uppermost Triassic to Middle Jurassic) mimicked

the resultant stepped subsalt geometry by using the Upper Triassic salt as an effective detachment. Thereby, the overburden was deformed by monoclinal drape folds and stretched by suprasalt faults and reactive diapirs (**Fig. 2.13b**). Locally, the offset of these suprasalt faults triggered the rise of salt walls on their footwalls, which progressively widened as the suprasalt strata was translated basinwards (**Fig. 2.13c** and **2.13d**). Passive diapirism ended due to the depletion of the salt source and the development of primary welds during upper Cenomanian to lower Turonian times (**Fig. 2.13e**). After extension, during the Campanian to Cenozoic times, the stepped subsalt geometry allowed for the NW-directed propagation of the thin-skinned contractional deformation, which was conducted by a thrust fault with a ramp-flat-ramp geometry rooted into the salt décollement (i.e. Upper Triassic salt; **Fig. 2.13f**). In this scenario, the precursor diapirs accommodated part of the contractional deformation by squeezing their stems and arching their roofs. As compression progressed, the compartmentalized overburden became reconnected by secondary welds, where further compression led the nucleation of thrust faults (**Fig. 2.13g**). Additionally, during the process, the thick-skinned faults were extensionally reactivated due to the flexural deformation that experienced the forebulge of the orogen because of the southwards lithospheric loading of the eastern Betic Cordillera (**Fig. 2.13g**).

In such a regional setting, the present investigation has also allowed to decipher the main geometric and kinematic features of the salt walls developed in the Jumilla region. In this regard, the following points detail the structure and kinematic evolution of four squeezed and/or collapsed salt walls and their adjacent overburden:

- The first example is found in the northwestern limit of the Jumilla region. Here, the structure is characterized by SE-dipping suprasalt extensional faults and thrusts, locally affected by short wavelength anticlines that deform Upper Cretaceous rocks detached from the underlying succession (**Fig. 2.14a**). The existence of a secondary décollement level right below the Upper Cretaceous rocks together with the presence of Upper Triassic evaporites cropping out at the fold hinges, suggests that these structures could correspond to folded roofs of pre-Albian salt walls that were shortened and squeezed during the Betic contractional deformation.

- A second example is observed in the Sierra de los Bujes anticline (see location in **Fig. 2.12b** and a detailed geological map in **Fig. 2.16a**). This fold is cut by a NW-directed

suprasalt thrust fault (Fault 4 in **Fig. 2.16a**), which displaces a minor scale ENE-trending double plunge anticline deforming an uppermost Triassic to Serravallian succession.
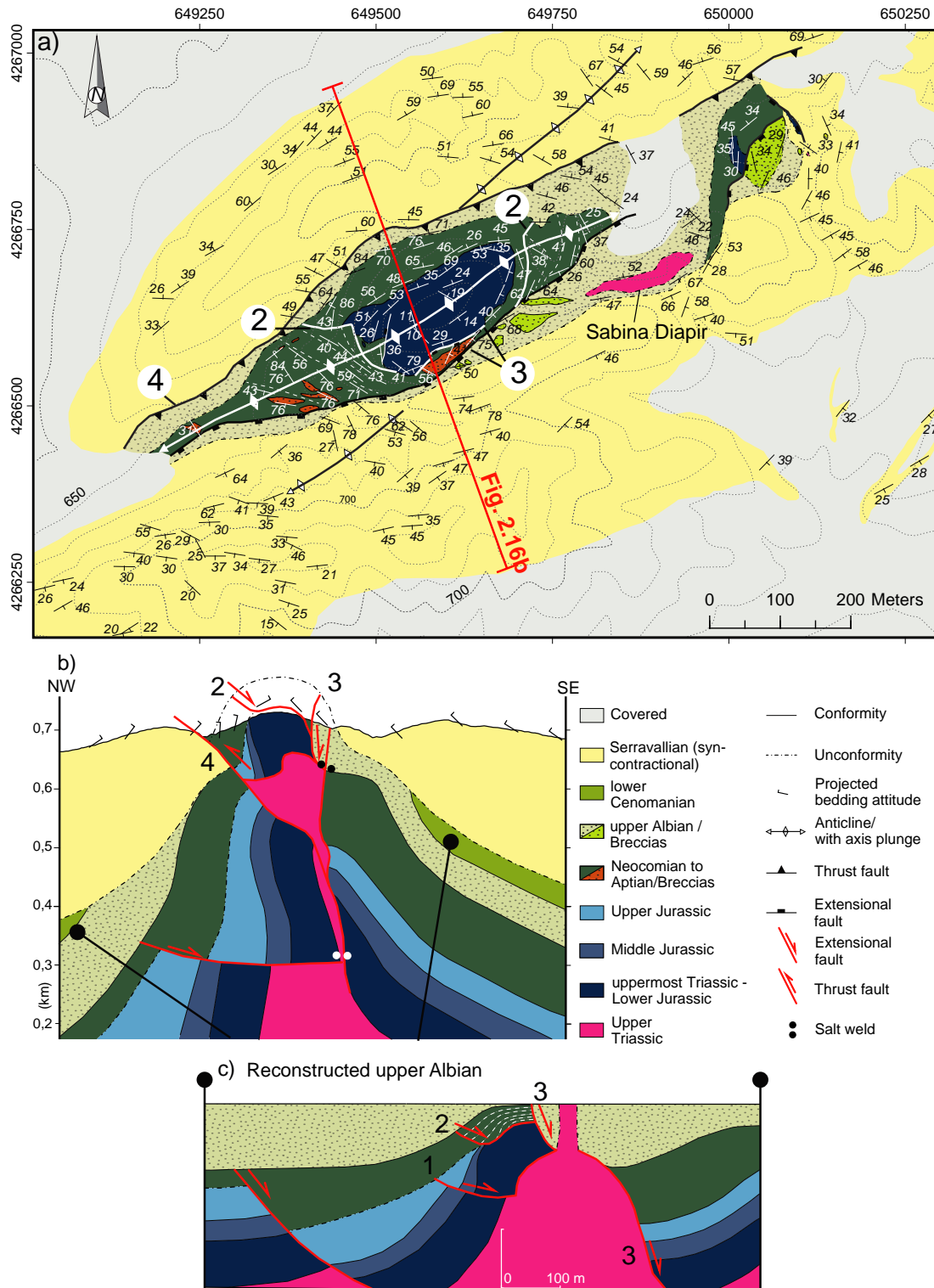


**Figure 2.16.** a) Detailed geological map of the Sierra de los Bujes anticline (see location in **Fig. 2.12b**). Numbers 1, 2, 3 and 4 indicate the relative age of each fault (i.e. 1 older than 4). b) Cross-section showing the internal geometry of the salt-cored anticline (see location in **Fig. 2.16a**). c) Qualitative restoration of cross-section depicted in **Fig. 2.16b** for the upper Albian. Fault 4 is a reverse fault resulting from the inversion of normal Fault 1. Coordinates are in meters in Universal Transverse Mercator, zone 12 northern hemisphere and datum ETRS89.

In the hanging wall of the thrust fault there is a minor fold that deforms uppermost Triassic to upper Albian rocks (**Fig. 2.16b**). The syn-extensional succession, Lower Cretaceous to upper Albian in age, display growth strata geometries in the core of the anticline (**Fig. 2.16a**). Locally, this sequence presents isolated carbonate breccias containing upper Albian rocks cropping out adjacent to the Sabina diapir (**Fig. 2.16a**). They are interpreted to be diapir-derived debris flows deposited as consequence of diapir rise and destabilization of the salt wall roof. The near-diapir abrupt facies change (<200 m) from carbonate breccias to massive sands attributed to the Utrillas sands Fm. (upper Albian in age) together with the presence of mass-wasting deposits are indicative of hook halokinetic sequences adjacent to the Sabina diapir (Giles & Rowan, 2012). Considering these observations and the general double-plunge folded structure, the core of the anticline shows evidences for a small-scale ramp-flat-ramp extensional fault (i.e. salt roller named Fault 2 in **Fig. 2.16**) soled above a NE-trending salt wall. According to the qualitative restoration depicted in **Figure 2.16c**, the salt roller developed due to the increase of the fault displacement (Fault 2 in **Fig. 2.16**) coeval to the growth of the underlying salt wall from Neocomian to upper Albian times. In this scenario, further extension promoted the piercement of the overburden and the subsequent passive salt extrusion of the Sabina diapir (**Fig. 2.16a**). Afterwards, during the inversion of the basin, the extensional faults were deformed by folding and thrusting –a process that also triggered the rejuvenation of the salt wall. In this scenario, the thin roof covering the diapir was arched and deformed by short wavelength contractional folds due to squeezing of the salt wall stem. Finally, further shortening might have led to the formation of secondary welds and the formation of thrust fault 4 (**Figs. 2.16a** and **2.16b**).

- The third example is found northwest of the Sierra del Molar and southeast of the Sierra del Buey (see location in **Fig. 2.12b**). These topographic reliefs are made up of folded and thickened Turonian to Maastrichtian successions unconformably lying above upper Cenomanian rocks. Turonian angular unconformities located at top of the upper Cenomanian succession in the Sierra del Buey are indicative of an uplifted area during the upper Cenomanian times. Despite the fact that diapirism occurred mostly during upper Cenomanian to lower Turonian, the Turonian to Maastrichtian thickened succession is interpreted to be the result of salt wall collapse as is proposed in the

constructed cross-sections (**Figs. 2.14a** and **2.14b**). Afterwards, upon inversion, the resulting Turonian to Maastrichtian basin was contractionally folded during the Betic contractional deformation as recorded in the Oligocene to lower Miocene growth-strata geometries, which unconformably overlap the Turonian to Maastrichtian folded strata (**Fig. 2.12b**).

- Finally, the fourth example is in the southeastern part of the study area (see location in **Fig. 2.12b**), where the seismic reflection data show a rapid steepening of the reflections followed by the presence of chaotic seismic facies (**Fig. 2.17d**). The seismic interpretation together with the existence of Upper Triassic evaporites outcropping at surface, suggest that this structure corresponds to the NE-SW trending and steep-sided La Sarsa salt wall (**Fig. 2.12b**). Above the diapir, a Paleocene to Quaternary succession is deformed by a pair of short wavelength syncline-anticline folds followed by a broader anticline cut by a NW-directed thrust fault (**Fig. 2.12b**). These contractional structures are more relevant adjacent to the salt wall termination and disappear in two kilometers away from the diapir. These documented evidences suggest that a Paleocene to Quaternary sedimentary roof covered the La Sarsa salt wall as consequence of the source layer depletion and ongoing sedimentation. This promoted the formation of primary welds, and the subsequent cessation of the salt wall growth (**Fig. 2.14a**). In addition to this, the NW-directed thrust fault could be indicative of secondary welding promoted by the contractional rejuvenation of the diapir and the depletion of the salt wall stem.

Therefore, the above explained results together with the mentioned regional outcomes, have contributed to a better understanding of the contractional reactivation of the proximal part of a passive margin containing pre-kinematic salt. In particular, our study has allowed to improve it by determining that:

- Thick-skinned extension controlled the rate of subsidence and hence the accumulation of sediment over mobile pre-kinematic salt. In this scenario, salt acted as a strain localizer by decoupling the overburden and subsalt deformation, thus generating two differentiated structural styles–above and below the salt layer. The subsalt extension controlled the suprasalt deformation and the "locus" for the development of piercing salt walls above the footwalls of the main basement faults.
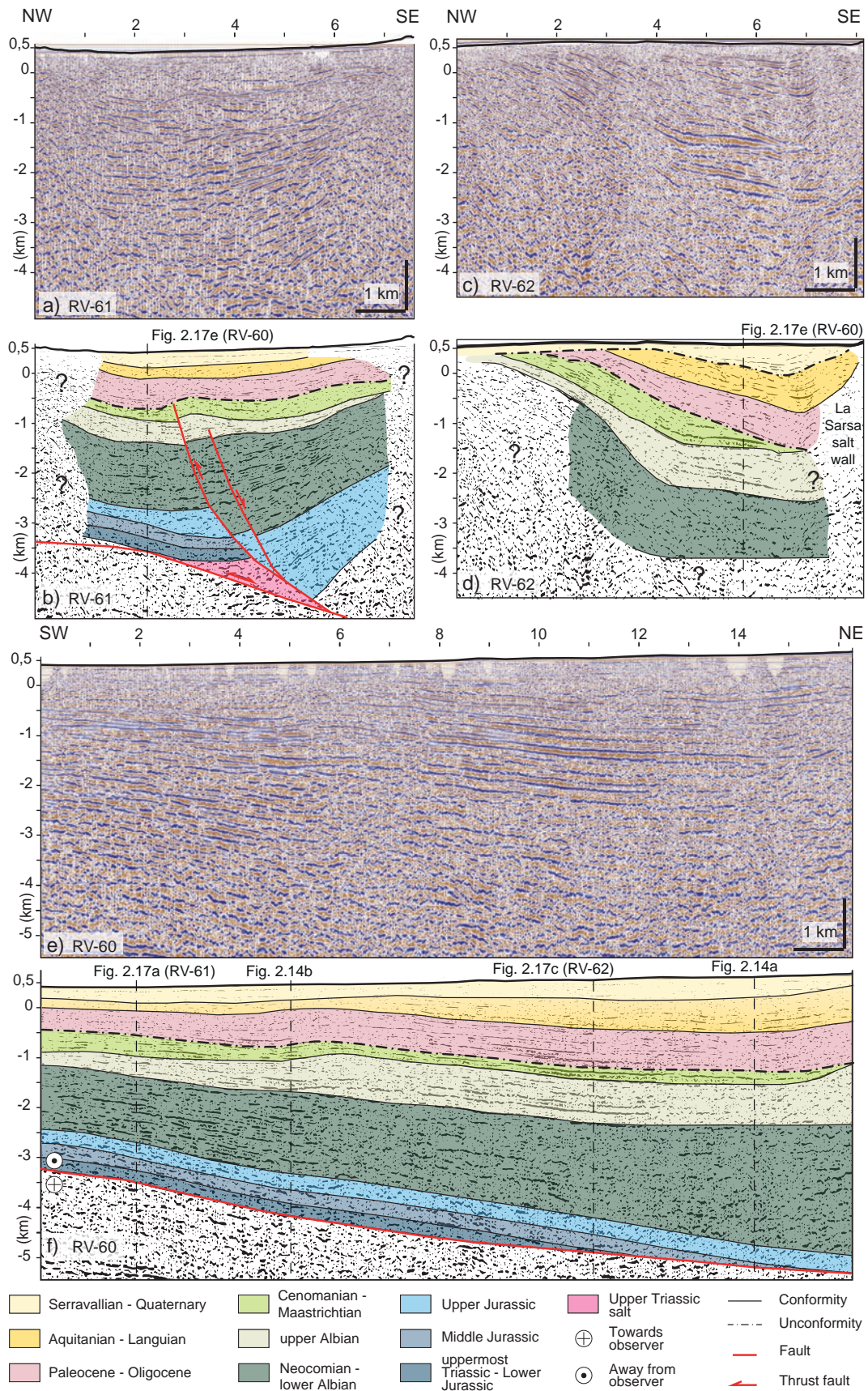
**Figure 2.17.** 2D seismic reflection profiles located in the Internal Prebetic (**Fig. 2.12b**). a) Seismic line RV-61 and b) its interpretation. c) Seismic line RV-62 and d) its interpretation. e) Seismic line RV-60 and f) its interpretation.

- Salt also localized strain during the incorporation of the passive margin into the external zones of a thin-skinned fold-and-thrust belt. Indeed, the preexisting salt walls, weaker than the adjacent overburden, preferentially absorbed the contractional deformation by nucleating folding and thrusting. Additionally, the stepped subsalt geometry which resulted from thick-skinned extension also controlled the shortening propagation. Therefore, the degree of strain localization of the salt walls was dependent on the thickness of the overburden and on the dip and dip direction of the subsalt faults relative to the thin-skinned shortening direction.

# CHAPTER 3. DISCUSSION

**3.1. Introduction**

**3.2. Controls on the geometry and kinematic evolution of salt walls driven by thick-skinned extension**

**3.3. Controls on the geometry and kinematic evolution of precursor salt walls affected by a subsequent thin-skinned contractional deformation**

*The cover of Chapter 3 depicts a close-up view of the vertical to overturned upper Miocene sandstones and marls outrcropping in the southern margin of the Jumilla Diapir.*

## 3.1. Introduction

The obtained results concerning the study of the salt walls in the Paradox Basin and the Eastern Prebetic Zone not only improve the regional knowledge of the respective areas (**Fig. I.I**), but also supply information that has permitted to deepen into the understanding of the controlling factors on the geometry and kinematic evolution of salt walls and adjacent strata in different tectonic settings. In particular, this investigation provides observations that significantly enrich the comprehension of two items that usually have received much less attention from a field-based approach. These are: firstly, the geometry and kinematics of salt walls developed above extensional subsalt faults whose movement occurs during or after the deposition of salt; and secondly, the behavior of these precursor salt structures when are involved in a subsequent thin-skinned contractional deformation.

Therefore, considering the advances detailed in the previous chapter, the following sections are devoted to stablishing new guidelines and/or to improve the existing ones about the geometric and kinematic evolution of salt walls in the above outlined tectonic settings. Specifically, this chapter firstly explores what are the main parameters controlling the geometry and kinematics of salt walls and adjacent strata during or after thick-skinned extension; and secondly, discusses the factors that define the geometry and kinematics of precursor salt walls and surrounding overburden when they are shortened during a latter thin-skinned contractional deformation. Importantly, the analysis presented in this chapter not only has considered the results obtained during the present investigation, but also has incorporated the information of previous studies carried out in this type of structures, both in nature examples and in scaled physical and numerical models.

**CHAPTER 3**

## 3.2. Controls on the geometry and kinematic evolution of salt walls driven by thick-skinned extension

Regional extension, whether thick- or thin-skinned, tends to attenuate the brittle overburden above mobile salt by forming grabens and/or half grabens flanked by suprasalt faults (Jackson & Vendeville, 1994). These suprasalt structures differentially load the salt by their surface relief and weaken the overburden by fracturing and thinning it, leading to salt upwelling forming first reactive and then active salt walls.

If extension affects both the supra- and subsalt strata (i.e. thick-skinned extension), salt tends to decouple the deformation, so distinct structural styles can coexist above and below it (e.g. Nalpas & Brun, 1993; Jackson & Vendeville, 1994; Stewart et al., 1996, 1997; Alves et al., 2002; Richardson et al., 2005; Marsh et al., 2010). In addition, the presence of a salt layer may limit the upward propagation of a subsalt fault tip, so the basement fault is mechanically decoupled from, but being responsible for, a drape fold deforming the suprasalt strata (Withjack et al., 1990; Hodgson et al., 1992; Koyi & Petersen, 1993; Stewart et al., 1996, 1997; Maurin & Niviere, 1999; Withjack & Callaway, 2000; Kane et al., 2010; Lewis et al., 2013). Accordingly, as the throw of the subsalt fault increases, the overburden is progressively draped over the subsalt faults, with salt accommodating the difference in geometry. In this regard, because the suprasalt strata must extend as much as the subsalt section, drape folding is accompanied by suprasalt extensional faulting, usually concentrated at the upper hinge of the monoclinal drape folds (Nalpas & Brun, 1993; Jackson & Vendeville, 1994; Stewart et al., 1997; Pascoe et al., 1999; **Fig. 3.1**).

With enough extension, reactive salt walls may initiate at the upper hinge of the monoclinal drape folds where suprasalt faulting is concentrated (Nalpas & Brun, 1993; Jackson and Vendeville, 1994; Vendeville et al., 1995; Withjack & Callaway, 2000). The location where diapirism takes place is also dependent on the capacity of a salt layer to decouple deformation above and below it (e.g. Nalpas & Brun, 1993; Jackson & Vendeville, 1994; Stewart et al., 1996, 1997; Alves et al., 2002; Richardson et al., 2005; Marsh et al., 2010). Furthermore, if decoupling between the basement and the overburden increases, the diapir will be located in a farther position in relation to the upper tip of the subsalt fault (Withjack & Callaway, 2000).

The degree of decoupling has been related to several factors, including the thickness and rheology of autochthonous salt and suprasalt strata, and slip rate and magnitude of the

subsalt fault (Withjack & Callaway, 2000). The previous factors not only determine the degree of decoupling between basement and overburden, but also control the distribution of the deformation as well as the geometry and number of the folds and faults affecting the suprasalt strata (see Fig. 14 in Withjack & Callaway, 2000). Therefore, they also constrain the geometry and kinematics of the suprasalt faults liable of generating future salt walls.

However, the geometry and kinematics of the suprasalt faults can be also governed by other factors that not necessarily depend on the decoupling degree. Thereby, the following subchapters are devoted to discussing the following controlling parameters: the geometry of the subsalt fault, the thickness variations of the suprasalt strata over time, the salt thickness variations (available salt budget), the syn-kinematic sedimentary loading pattern, and the early style of salt rise and position of the salt breakthrough.

## 3.2.1. Geometry of the subsalt fault

In decoupled scenarios, the deformation of the suprasalt strata takes place due to a combination of drape folding and coeval salt evacuation towards the upper tip of the subsalt fault (Withjack et al., 1989; Pascoe et al., 1999; Cosgrove & Ameen, 2000; Maurin & Niviere, 1999; Richardson et al., 2005; Kane et al., 2010; Duffy et al., 2012; **Fig. 3.1**). Accordingly, the geometry and kinematics of the folds and faults developed above salt are constrained by (Nalpas & Brun, 1993; Jackson et al., 1994; Withjack & Callaway, 2000; Lewis et al., 2013): a) the thicknesses of both salt and the overlying suprasalt strata; b) the inflation and/or depletion of salt induced by lateral changes of the pressure head (resulting from the differential accommodation space generated by the subsalt faults, which is filled by syn-kinematic sediments rather than by salt); c) the thick-skinned extensional rate; and finally, d) the total displacement of the subsalt fault.

Besides the above-mentioned controls, the suprasalt structures deforming the overburden are also controlled by the geometry of the subsalt fault. Considering field (e.g. Escosa et al., 2018b) and scaled physical model examples (e.g. Ferrer et al., 2016; Roma et al., 2018), aside from the thicknesses of salt and overburden and the displacement of the basement fault, the dip of the subsalt fault also exerts an important control on the wavelength of the resulting suprasalt drape monoclines. Considering the same amount of extension in each example, low-angle subsalt faults (e.g. Carxe Fault, dipping 30°-40°; **Fig. 3.1a**) tend to generate a smaller

**CHAPTER 3**

accommodation space above their hanging walls, and thus the overburden is deformed by long wavelength monoclines with gently dipping flanks. Conversely, high-angle subsalt faults (e.g. Maestre Fault, dipping 60º-70º; **Fig. 3.1b**), with the same amount of extension, tend to generate a greater accommodation space above their hanging walls and short wavelength monoclines depicting steep flanks. In this instance, there is a higher difference in the pressure head above salt between the faulted blocks, which enhances the migration of salt towards the upper tip of the basement fault. So, the resulting monoclinal drape fold has a major curvature in its upper hinge, contributing to a pronounced layer-parallel stretching in the outer arc of the hinge zone, and thus favoring the development of suprasalt faults and elongated reactive diapirs in their footwalls. In contrast, the upper hinge of the long-wavelength monoclines above low-angle subsalt faults are less affected by layer-parallel stretching, and thus tend to hamper the development of diapirism.



a) 30–40º dip subsalt fault (e.g. Carxe Fault)   b) 60–70º dip subsalt fault (e.g. Maestre Fault)

long wavelength drape fold   short wavelength drape fold

slower salt evacuation   faster salt evacuation

Thick-skinned extension   Thick-skinned extension

Thin-skinned extension   Thin-skinned extension

Syn-kinematic overburden 3 | Syn-kinematic overburden 1 | Pre-kinematic salt | rotation of the suprasalt faults (equal to the 30 - 40º dipping subsalt fault) | rotation of the suprasalt faults (equal to the 60 - 70º dipping subsalt fault)
Syn-kinematic overburden 2 | Pre-kinematic overburden | Basement

**Figure 3.1.** Time-serial cross-sections of a monoclinal drape fold developed over extensional planar subsalt faults: a) in the case of a 30–40º dipping fault similar to the Carxe Fault; and b) in the case of a 60–70º dipping fault similar to the Maestre Fault, in the Eastern Prebetic Zone (SE Spain). The sub- and suprasalt layers are bed length balanced.

In addition, the geometry of the subsalt faults also exerts a significant impact on the kinematics of the thin-skinned extensional deformation affecting the overburden. In this manner, the dip of the subsalt faults determines the dip of the pre-kinematic suprasalt strata as well as the dip of the suprasalt faults that, initially located above the footwall of the subsalt fault, are incorporated above its hanging wall as extension progresses (**Fig. 3.1**). So, the resultant dip of the suprasalt faults, once are incorporated into the hanging wall of the subsalt fault, will constrain their future extensional activity and kinematic evolution. For example, if the suprasalt faults are slightly rotated above the hanging wall of the basement fault (e.g. deforming a long wavelength monoclinal drape fold above a low-angle subsalt fault–the Carxe and/or Sopalmo faults; **Figs. 2.13b–2.13d**), they might remain active once are translated above the hanging wall of the subsalt fault. Conversely, if the suprasalt faults are highly rotated (e.g. deforming a short wavelength monoclinal drape fold above a high-angle subsalt fault), they may acquire a geometry similar to an inverse fault which will hamper their future extensional activity (e.g. see the rotated suprasalt faults above the Maestre Fault (**Figs. 2.15a and 2.15b**). Therefore, this implies that above low-angle basement faults, the suprasalt faults may have a longer extensional activity than in those areas deformed by high-angle basement faults. In addition, high-angle subsalt faults may tend to localize suprasalt deformation in a narrow and elongated zone of the overburden. Conversely, above low-angle subsalt faults, the suprasalt deformation may affect a broader area of the suprasalt strata.

Importantly, the previous assumptions are valid in situations where a salt layer has a homogeneous thickness and is deposited prior to thick-skinned extension (e.g. pre-kinematic). However, if salt is deposited synchronously to extension, then the previous assumptions may variate since suprasalt deformation may be mostly controlled by the salt thickness variations across the subsalt faults (e.g. see as an example the Sele High Fault System in the northern North Sea; Jackson & Lewis, 2016). In addition, if the sedimentation rate of salt is higher than the extensional rate of the subsalt fault, then the later may be negligible on contributing to the total suprasalt deformation affecting the overburden. In this scenario may be difficult or almost impossible to detect, from a field-based approach, the presence of such controlling subsalt fault as is the case at the termination of the Gypsum Valley salt wall. In this instance, a basement fault is well imaged in the center of the diapir (**Fig. 2.2a)** but not at the termination of the diapir (**Fig. 2.2b)**.

**CHAPTER 3**

## 3.2.2. Overburden thickness variations over time

During thick-skinned extension, the location and distribution of the deformation affecting the entire overburden changes over time (Escosa et al., 2018b). This is in part related to the thickness variations, and hence the strengthen that experience the overburden as syn-kinematic sedimentation occurs synchronously to thick-skinned extension.

At the beginning of their motion, the subsalt extensional faults are associated with small offsets, so they cannot control for suprasalt thickness which tend to remain almost constant. As a result, if salt decouples the deformation, similar thicknesses of the overburden favor a distributed suprasalt deformation because do not exist significantly differences in strength of the suprasalt strata over the faulted blocks (e.g. **Fig. 3.2b**).
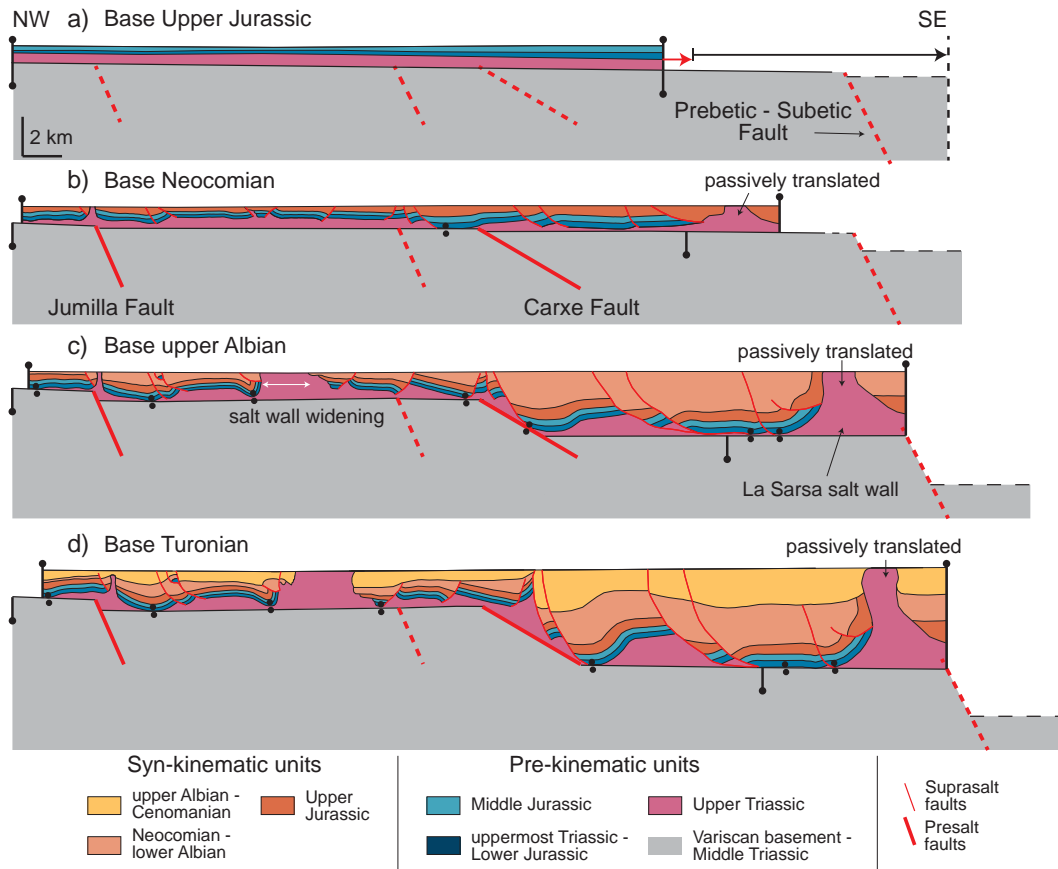


**Figure 3.2.** Upper Jurassic to Upper Cretaceous extension affecting the proximal part of the South Iberian passive margin at the Eastern Prebetic Zone (SE Iberia). Modified from Escosa et al. (2018b).

In this manner, if there is enough salt budged and the pre-kinematic strata is thin, diapirism might develop during the early stages of extension, and thus reactive diapirs might

be indistinctly formed over the extended area and/or incipient passive margin. For example, in the Eastern Prebetic Zone, during the Upper Jurassic to Lower Cretaceous extension, suprasalt extensional faults and reactive diapirs were developed above the footwalls of the main subsalt faults (i.e. Jumilla, Sopalmo and Carxe faults; **Fig. 3.2**).

As the offsets of the subsalt faults increase and syn-kinematic sedimentation continues, the thickness and thus the strength of the overburden experiments significant variations over the extended area (e.g. **Fig. 3.2c**). So, this is almost negligible at the margins of the basin and/ or passive margin where there is a lower syn-kinematic sedimentation, but the strength of the overburden increases considerably basinwards, where the syn-kinematic sedimentation rate is higher. In this scenario, faulting of the suprasalt strata tend to be concentrated above the footwall of those subsalt faults located in a marginal position (i.e. footwall of the Carxe and Sopalmo faults in the Eastern Prebetic Zone), where the overburden is thin and hence mechanically weak. In contrast, translation with minor folding is concentrated above the hanging walls where the overburden is thicker and thus mechanically resistant.

Accordingly, diapirs located above the hanging wall of the subsalt faults tend to be translated basinwards together with the thickened overburden, without concentrating a significant amount of strain (see translation of the La Sarsa salt wall over time on **Figs. 3.2b**, **3.2c**, and **3.2d**). Conversely, diapirs above the footwall of the subsalt faults located in a marginal position, where a thin overburden does not experiment significant thickness variations, are slightly displaced from their original location and tend to concentrate part of the suprasalt deformation. As a result, the stem of these diapirs may be progressively widened if there is enough salt supply from the source layer and primary welds are still not developed (e.g. **Figs. 3.2c** and **3.2d**).

Therefore, the capacity of a salt wall to concentrate future extensional deformation, besides its orientation respect to the regional stretching direction (see further details in Section 12.5 of Jackson & Hudec, 2017), will depend on the thickness/strength of the adjacent overburden (Vendeville & Jackson, 1992a; Escosa et al., 2018b). This will be maximum in a thin and weak overburden containing salt walls; and minimum in a thick, and hence stronger suprasalt strata.

**CHAPTER 3**

## 3.2.3. Salt thickness variations (available salt budget) in pre- and syn-kinematic salt basins

The local thickness and/or composition variations of salt in pre- and syn-kinematic evaporitic basins may constrain the available salt budget for salt walls to develop, and consequently control their geometric and kinematic evolution (Clausen & Korstgard, 1996; Jackson & Lewis, 2016; Escosa et al., 2018c).

In thick-skinned extensional settings with pre-kinematic salt, the thickness of the evaporitic sequence controls the degree of decoupling and the location where suprasalt deformation and diapirism are focused (i.e. Withjack & Callaway, 2000). Therefore, since suprasalt faults may trigger the development of salt walls (e.g. **Fig. 1.4b**), any variation on the pre-kinematic salt thickness will impact on their geometry and kinematic evolution. For example and assuming the same amount of suprasalt extension in each scenario, if subsalt extension occurs in a landward position with respect to the salt basin, a thinner salt layer will promote the early formation of primary welds, so coupling between subsalt and suprasalt units will occur earlier, and salt walls will have a short period of time to develop (e.g. see the pre-Albian salt wall developed above the Jumilla Fault; **Fig. 2.14a**). Conversely, if thick-skinned extension occurs in a basinward position with respect to the salt basin, the decoupling will be more widespread, and salt walls will develop in a longer period of time since primary welding might form later (e.g. see the long-lived La Sarsa salt wall formed in the Internal Prebetic; **Fig. 2.14a**). Furthermore, the salt thickness also controls the width of the diapir, so the thicker it is the wider is the resulting salt wall.

These variations in style and evolution of salt walls may occur across the faulted blocks of the thick-skinned extensional system with pre-kinematic salt (e.g. Eastern Prebetic Zone) or may also occur along strike the same salt wall developed in a syn-kinematic salt basin. In this manner, the structural characterization of the Gypsum Valley salt wall together with its comparison with analogue structures located elsewhere in the Paradox Basin (Table 1 in **Annex 1**) exemplify that, if for example there is no local variation in deep salt thickness, the salt wall is liable to plunge steeply to moderately along strike (**Fig. 2.6b**). So, its edge will have a curved map-view outline, with depocenters on all sides and radial faults best developed where curvature of drape-folded strata is greatest. But if the salt basin has an abrupt lateral boundary controlled by for example a subsalt fault, the developed salt wall abutting against the basin

edge will have an equally abrupt termination because of the restriction in deep salt budget (**Fig. 2.6a**). In this latter case, the salt wall is not able to grow laterally, so the depocenters flanking the diapir will be bounded by steep faults separating the subsiding minibasins from areas of no corresponding subsidence off the end of the salt wall.

Other case would be the situation in which the salt thickness decreases gradually along strike the growing salt wall (e.g. the syn-kinematic Paradox Fm. evaporites deposited in the Paradox foreland basin). The above explained geometric and kinematic models (**Fig. 2.6**) show symmetric diapir flanks, but diapirs may be slightly to highly asymmetric in plan- and cross-section view. If asymmetric, the salt wall may be associated with a counterregional fault at one corner, radial faults on the other corner, and a possible megaflap adjacent to the diapir (**Fig. 2.6c**), as is observed at Gypsum Valley. In these situations, the termination will be more abrupt with common radial faults if the salt budget decreases rapidly along strike; otherwise, the termination will be gradual and radial faults absent or minor. In the case in which the termination is relatively abrupt (**Fig. 2.7a**), differential subsidence would be high immediately adjacent to the end of the salt wall but decrease rapidly along strike away from the diapir, the top salt plunges relatively steep, radial faults are well developed due to high degrees of map-view curvature of the flanking strata, and counterregional faults or equivalent welds are relatively short. Instead, if the salt wall termination is more gradual (**Fig. 2.7b**), the differential subsidence would be diffused over a broader area, and it would have a gently plunging salt nose, less map-view curvature, and thus less common radial faults and a longer counterregional fault. For example, the SE termination of the Gypsum Valley diapir falls between these end-member geometries.

In addition to this, the adjacent overburden to a developing salt wall may also depict different geometries and underwent distinct kinematic evolutions depending on the available deep salt budget. For example, megaflaps adjacent to a diapir may also terminate before reaching the end of a salt wall. Because megaflaps are defined by the steepness and height of the stratal panel (Rowan et al., 2016), end-member styles of termination are a gradual decrease in elevation or maximum dip of the megaflap panel along strike or an abrupt drop or decrease in dip across one or more faults (**Fig. 2.8**). In this scenario, a common cause for lateral termination of megaflaps is a decrease in deep salt budget along strike, as suggested above for the Gypsum Valley case. As Rowan et al. (2016) noticed, a megaflap formed by limb rotation cannot reach vertical if the salt is too thin relative to the rotating roof panel.

**CHAPTER 3**

Therefore, considering a salt wall developed above a source layer with a variable thickness, an adjacent megaflap may not be homogenously developed since the salt thickness may decrease abruptly or gradually along strike, and thus the source layer has not longer the necessary critical thickness for a megaflap to form.

Finally, the critical thickness of salt for a megaflap to develop also cannot be achieved if a forming salt wall is located in a landwards position with respect to the pre-kinematic evaporitic basin. An example of this latter scenario would be the northeastern part of the Jumilla region (Eastern Prebetic Zone) where the salt walls located in a landward position with respect the Upper Triassic salt basin (Ortí, 1974; Ortí et al., 2017) do not have adjacent megaflaps. Conversely, the salt walls located in a basinward position (e.g. La Sarsa salt wall; **Figs. 2.14a** and **2.14b**), may have adjacent megaflaps since the source layer is thicker. However, in all scenarios mentioned above, it should be taken into account that the salt budget for flow into the diapir from beneath the sedimentary depocenters will be also controlled by the position of the nearby diapirs, and thus the fetch area for deep salt (Escosa et al., 2018c).

## 3.2.4. Syn-kinematic sedimentary loading patterns during thick-skinned extension

The geometry of the salt walls and surrounding strata as well as their lateral terminations are also constrained by the sedimentary loading patterns, and thus the spatial variations in salt evacuation and flow towards the diapir (Escosa et al., 2018c).

Therefore, during thick-skinned extension, the geometry and kinematics of the developing salt walls will be controlled by variations in the accommodation space, and thus the differences in the sedimentary load that generate the offset of the extensional subsalt faults. (e.g. see examples in the Lusitanian Basin (Portugal), Rasmussen et al., 1998; or in the Essaouira Basin, offshore Morocco, Tari & Jabour, 2013; **Fig. 3.3**).

In this manner, areas where subsalt extensional faulting generates a large accommodation space, a corresponding high syn-kinematic sedimentation rate will favor the development of salt walls having a tapered shape in cross-sectional view (McGuinness & Hossack, 1993; Talbot, 1995; Koyi, 1998; Karam & Mitra, 2016). So, an elevated pressure head above the source layer will foster a rapid salt depletion beneath the subsiding minibasins located above the hanging walls of the subsalt faults (**Fig. 3.1b**). Conversely, if subsalt extensional faulting

generates a small accommodation space and a corresponding low sedimentation rate above the pre-kinematic overburden (i.e. above the footwalls of the subsalt faults), salt walls with a flared shape in cross-sectional view will be liable to develop (McGuinness & Hossack, 1993; Talbot, 1995; Koyi, 1998; Karam & Mitra, 2016). In this latter case, a lower velocity on the salt source depletion will also favor a later formation of primary welds (**Fig. 3.1a**).
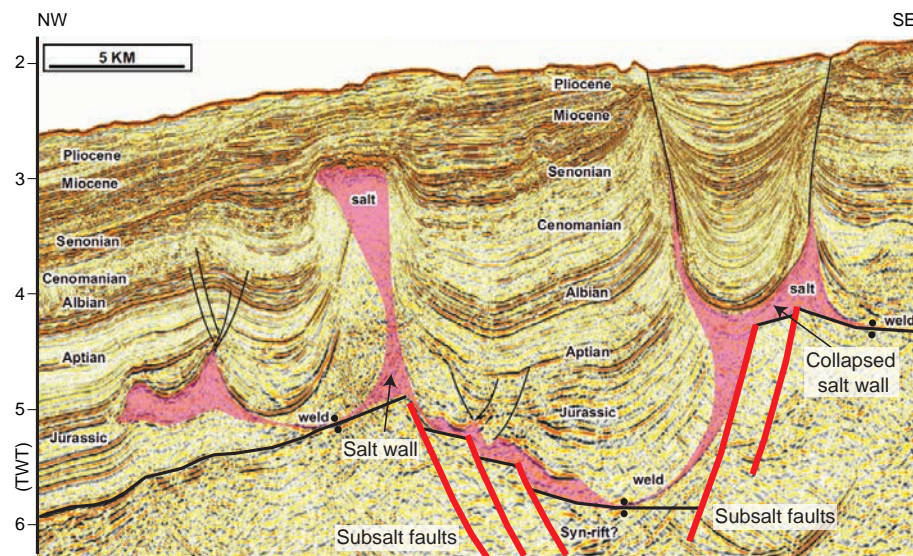


**Figure 3.3.** Three-dimensional seismic dip line in the Essaouira salt basin in the Atlantic margin of Morocco (modified from Tari & Jabour, 2013). The thickening of the Cretaceous strata is interpreted as the gradual depletion of the syn-extensional salt beneath the center of the subsiding basins and the development of salt walls in the upper tip of the subsalt faults.

The above explained different behaviors across the subsalt faults might explain the asymmetry of salt walls that are developed at the upper hinge of the monocline drape folds, where usually there is a megaflap on the landward side of the diapir (e.g. see the salt walls in the Sierra Larga-Sopalmo and Carxe in the Eastern Prebetic Zone, **Figs. 2.14a** and **2.14b**; and/ or the Gypsum Valley diapir, **Fig. 2.5 sections B–C**). Therefore, if subsalt faulting generates enough differential pressure head above salt across the faulted subsalt blocks, the formation of a megaflap in the overburden will take place if salt is thicker enough for a roof panel to rate and verticalize (see the salt walls and their adjacent megaflaps close to the upper tip of the Carxe and Sopalmo faults, in the Eastern Prebetic Zone; **Figs. 2.14a** and **2.14b**).

**CHAPTER 3**

## 3.2.5. Early style of salt rise and position of the salt breakout

The early style of salt rise and the position of diapir breakthrough may constrain the resulting geometry and kinematic evolution of diapirism and adjacent strata (Schultz-Ela et al., 1993; Rowan & Inman, 2011; Escosa et al., 2018c).

As it is explained above, the extensional movement of the basement faults triggers the salt migration towards the upper hinge of the overlying monoclinal drape fold and the subsequent layer-parallel stretching of the folded overburden located above the footwall of the subsalt fault (**Fig. 3.1**). This process promotes the development of salt inflated ridges and/or salt depleted areas. So, these salt-inflated structures are usually developed parallel to the trend of the subsalt faults where the overburden experiments a major thinning (e.g. at the upper hinges of the monoclinal drape folds and/or in extensionally faulted areas). In this scenario, different geometries of salt bodies can be developed: a) reactive salt walls with a triangular shape in cross-section view, when their formation is constrained by conjugated suprasalt extensional faults (Vendeville and Jackson, 1992a; **Fig. 1.4a**); b) salt rollers, when diapirism is constrained by a single suprasalt fault displaying a listric geometry (**Figs. 1.4b** and **3.1**); and c) salt inflated plateaus located above pre-existing subsalt faults (whose movement occurred during the deposition of salt) when the overburden is thinned over a broader zone (**Figs. 1.10** and **3.4**). Note that this latter model requires no regional extension to be accommodated by the faults, only differential sedimentary loading adjacent to the salt inflated plateau caused by a subsequent prograding wedge of sediment (Schuster, 1995).
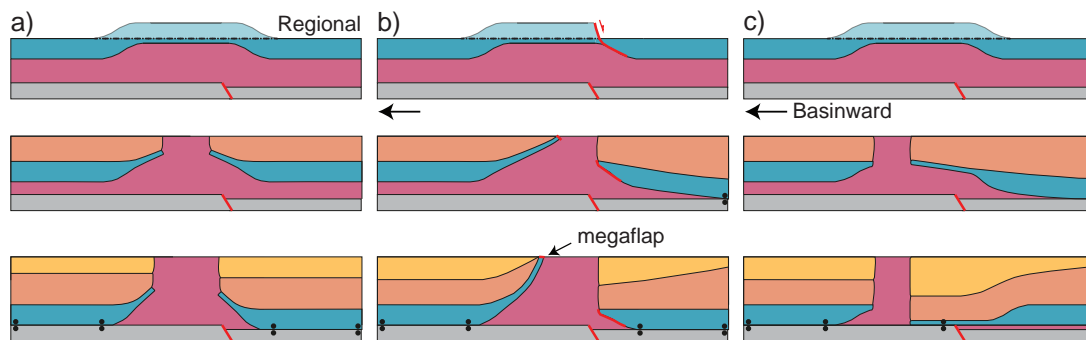


**Figure 3.4.** End-member scenarios for the evolution of salt inflated plateaus located above pre-existing basement faults (based in part on Rowan & Inman 2011; Rowan et al. 2016): a) early salt inflation due to equal and progressive depositional loading in both flanks of the diapir, with salt breakout at the center of the inflated salt; b) early single-flap active diapirism (Schultz-Ela et al. 1993), with salt breakout at the one edge of the salt inflated plateau and development of a megaflap along the basinward flank of the diapir. c) early salt inflation due to progressive depositional loading, with salt breakout at the basinward edge of the inflated salt.

In the first two cases, if a salt wall is formed, the salt breakthrough will likely be developed at the crest of those two types of salt structures, thus generating different geometries depending on the shape of the initial reactive diapir. So, for a symmetrical diapir, the active rise will promote the progressive folding of the pre-kinematic strata together with the rotation of the conjugate faults (**Fig. 1.11a**; see also examples either from scaled physical models in Vendeville & Jackson, 1992a; and from nature in Rowan, 1995). Conversely, the active rise of an asymmetrical diapir will promote folding of the pre-kinematic strata located in the footwall of the listric fault (**Fig. 1.11b**), so the fault plane will be also folded as the diapir progressively rises and breaks the thinned pre-kinematic strata (see an example in Sierra de los Bujes anticline in the Eastern Prebetic Zone, **Figs. 2.16b** and **2.16c**).

However, in a salt inflated plateau located above a pre-existing basement fault, the geometry of the resultant diapir will be controlled by the location of the salt breakthrough and the adjacent syn-kinematic patterns of depositional loading (Rowan & Inman, 2011; Rowan et al., 2016; Escosa et al., 2018c). For example, when salt breakout occurs in the middle of a salt inflated plateau (**Fig. 3.4a**), the pre-kinematic strata and the overlying syn-kinematic sediments will display a symmetric geometry adjacent to the resultant passive diapir. However, if salt breakthrough occurs at the edge of the roof, the subsequent diapir together with the flanking minibasin will display an asymmetrical geometry (**Fig. 3.4b**). In this case, the early history is that of single flap active diapirism (Schultz-Ela et al., 1993), with the fault and eventual diapir breakthrough located at the proximal end of the inflated salt, and the thinned roof (flap) ends up draped on the distal side of the diapir, potentially as a megaflap. Additionally, if the roof is not affected by faulting and salt simply inflates, progressive sedimentary loading on the proximal side leads to diapir breakout at the distal end of the inflated salt, with the thinned oldest strata (the roof of the early inflated salt) ending up at the base of the landward minibasin (**Fig. 3.4c**). Of course, the geometry may change from one style to the other along strike, possibly due to variations in roof thickness and strength, thereby providing one possible form of megaflap termination (Escosa et al., 2018c).

For example, the oldest strata on the proximal side at Gypsum Valley diapir are thicker than on the distal side. Similar relationships exist in the northern Gulf of Mexico (Schuster, 1995; Trudgill & Rowan, 2004; **Fig. 3.5**). In other cases, the opposite relationship also exists, with the oldest strata in the proximal minibasin being thinned and the younger section being thicker (Rowan & Inman, 2005, their figure 1). The same geometry is seen at Salt Valley diapir

**CHAPTER 3**

in the Paradox Basin (Trudgill, 2011; **Fig. 3.6**) indicating that both styles can exist in the two basins. Again, the difference in the resulting geometry of the salt wall and adjacent strata is related to the early style of salt rise and the position of diapir breakthrough (**Fig. 3.4**).
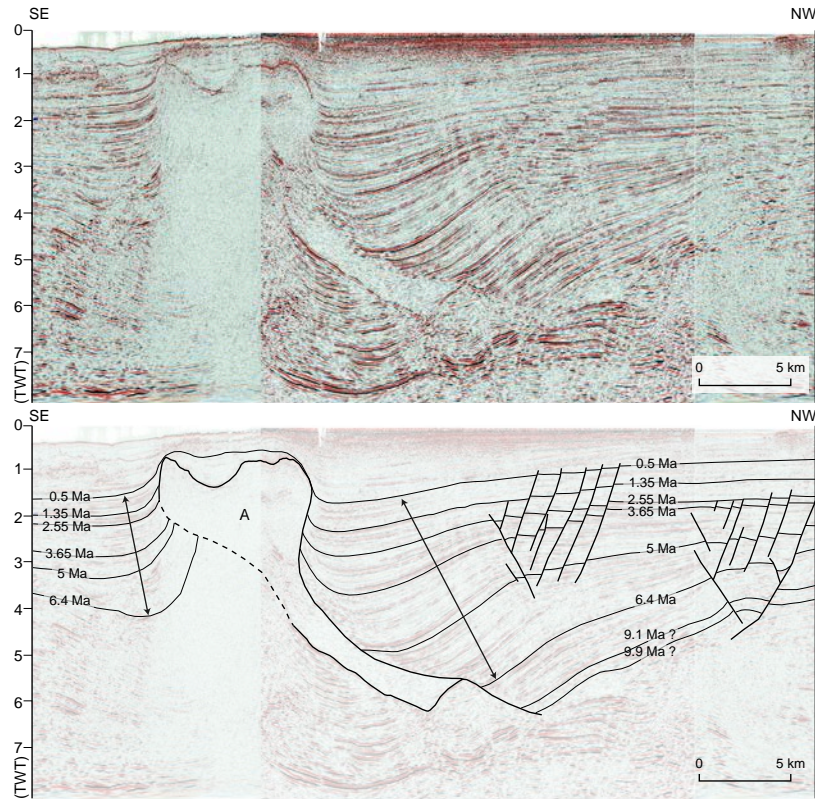


**Figure 3.5.** Dip-oriented, time-migrated seismic reflection profile crossing diapir A of Trudgill and Rowan (2004). Eight maximum flooding surfaces are illustrated and labelled. The ages of each horizon are constrained from biostratigraphic data obtained from wells. Note that the oldest strata on the downthrown side are thicker than on the upthrown side.
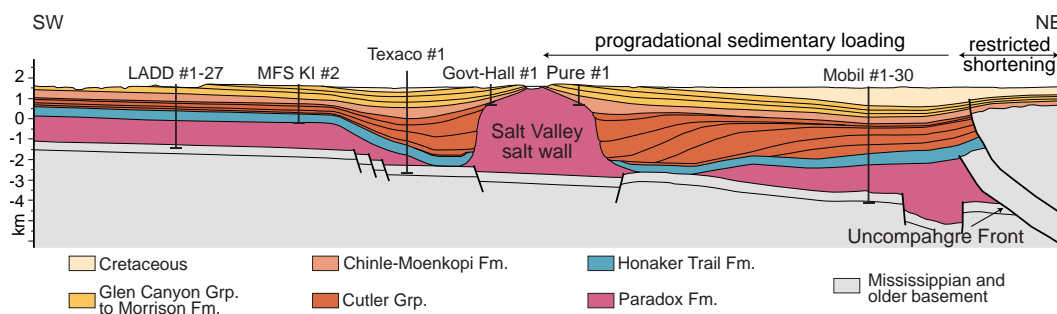


**Figure 3.6.** Regional cross-section across the Uncompahgre Front and the Salt Valley salt wall. After Doelling (1988) and Trudgill (2011).

Finally, in the case in which a salt wall is developed at the edge of a salt inflated plateau (e.g. **Fig. 3.4b**), the resultant geometry of an adjacent megaflap may be controlled by the width of the early salt anticline or single-flap active diapir and any lateral variation in where the roof pulls apart and salt breaks through (**Fig. 2.8**). Accordingly, as the width of the diapir's roof decreases, there is less length available to rotate into steep attitudes. If the early fault that separates the strata that end up on one or the other sides of the diapir is consistently along one edge of the early salt structure, then the geometry of a megaflap will change very little along strike (for a constant width early salt inflated plateau). If, however, the fault gradually or abruptly crosses the top of the diapir, the length of the roof panel that rotates into the megaflap is diminished and the rest of the roof ends up flanking the other side of the diapir (assuming none is removed by erosion).

CHAPTER 3

## 3.3. Controls on the geometry and kinematic evolution of precursor salt walls affected by a subsequent thin-skinned contractional deformation

Under regional shortening, the geometric and kinematic evolution of precursor salt walls is largely linked by the inherited subsalt structure, the difference in the mechanical strength between the relatively weak diapir and the adjacent suprasalt rocks, the structure and thickness of the adjacent overburden, the syn-orogenic sedimentation, and the flexural loading processes affecting the lithosphere during the orogenic building (e.g. Nilsen et al., 1995; Roca et al., 2006; Rowan & Vendeville, 2006; Callot et al., 2007; Izquierdo-Llavall et al., 2018; Pla et al., in review).

In the following sections, we address this connection by using the structural analysis of the Paradox Basin (SE Utah and SW Colorado) and the Eastern Prebetic Zone (SE Spain). Particularly, the investigation carried out in the Jumilla region (Eastern Prebetic Zone) allows to document the behavior of the above-mentioned factors in situations where the precursor salt walls are constituted of pre-kinematic salt, thick-skinned extension is their major drive, and have been affected by a subsequent thin-skinned contractional deformation detached on the salt layer. In this structural analysis, the geometry of the salt walls before being shortened is determined by documenting the structural and sedimentological features that depict the adjacent suprasalt sedimentary successions developed before and during the formation of the salt walls. Additionally, the following discussion is also complemented with bibliographic information and concepts of other studied zones (e.g. northern part of the Eastern Prebetic Zone, North Sea and/or the Atlantic margins of Iberia and east North America) where salt walls formed by thick-skinned extension and affected by differential sedimentary loading have been lately deformed by minor shortening. Among these, we could include the Gypsum Valley salt wall case study that, although was developed in a foreland basin and was constituted of syn-kinematic salt, was only affected by minor shortening during the Laramide Orogeny postading the salt wall formation and diapir burial (Mankowski et al., 2002; Escosa et al. 2018c).

Accordingly, the sections below address the controlling factors on the geometry and kinematic evolution of salt walls during thin-skinned contractional deformation by discussing the influence of: 1) the subsalt structure, 2) the precursor salt walls during the development of

a fold-and-thrust belt; 3) the structure of the suprasalt strata adjacent to the diapir; and finally, 4) the amount of shortening applied to the pre-existing salt wall. Note that the effects of thick-skinned inversion on precursor salt walls are beyond the scope of this analysis, and thus are not included in this discussion (for further information, see scaled physical models and field examples in Letouzey et al., 1995; Harrison & Jackson, 2014; Lickorish & Ford, 1998).

## 3.3.1. Influence of the pre-existing subsalt structure

The décollement level, where the thin-skinned contractional deformation is propagated, may depict a planar and continuous geometry (e.g. Appalachian Plateau and the Valley and Ridge province; Davis & Engelder, 1985) or may be folded and/or offset by subsalt faults (e.g. the western Alps; Butler, 1989; Deville & Chauviere, 2000). In the first scenario, shortening will result in a regularly spaced thin-skinned fold-and-thrust belt trending perpendicular to the propagation of the contractional deformation and having a cross-sectional tapper governed according to the critical wedge theory (e.g. Chapple, 1978; Davis et al., 1983; Suppe, 1983; Dahlen, 1984; Dahlen et al., 1984). In addition to these controlling factors, the thin-skinned fold-and-thrust belt developed over a folded and/or faulted décollement may result in a more complex structure; depicting an arcuate geometry deformed by directional faults, folds and thrusts with varying orientations and wavelengths (e.g. the Jura fold-and-thrust belt; Laubscher, 1986; Caër et al., 2015 and 2018).

In this regard, the study of the Eastern Prebetic Zone permits to determine the role of the thick-skinned extensional deformation offsetting a future décollement level and allows to decipher the influence that exerts this deformation on the subsequent formation of a thin-skinned fold-and-thrust belt with precursor salt structures. Our interpretations of the Eastern Prebetic Zone (see Chapter 2.3.2) and qualitative restoration (**Fig. 2.13**) together with the existing magnetoteluric and gravimetric data (Rubinat et al., 2010; Castaño, 1993) indicate that during the Mesozoic development of the South Iberian passive margin, the basement was deformed by planar subsalt faults offsetting the pre-kinematic Upper Triassic salt (e.g. Jumilla and Sopalmo-Carxe faults; **Fig. 2.13e**). These subsalt faults have in general an ENE-WSW orientation but locally they trend N-S, E-W and NW-SE (e.g. Maestre Fault; **Fig. 2.15**), depicting also opposite dipping directions.

Therefore, this is an ideal pre-contractional scenario that permits to address the influence of the orientation and dip direction of subsalt extensional faults offsetting a future contractional

décollement level. According to Rubinat et al. (2013) and Roca et al. (2013), this influence will depend on: 1) the subsalt fault orientation and 2) dip direction, in respect to the direction of the shortening propagation; 3) the dip of the subsalt fault; and 4) the displacement magnitude of the subsalt faults. Considering the field examples studied in this thesis, the following discussion will be mostly focused on the dip, dip direction and displacement magnitude of the subsalt faults.

First, depending on their dip, subsalt faults dipping towards the hinterland and cutting the continuity of the décollement level may difficult the propagation of the thin-skinned shortening (**Fig. 3.7**). So, if the subsalt fault dips nearly vertical, the overburden together with the salt structures might be deformed by buckling folds since the rigid basement may act as a buttress against the propagation of the thin-skinned thrust (**Fig. 3.7a**). In this scenario, the salt walls located in a hinterland position are highly deformed, and the ones located towards the foreland remain almost undeformed. Conversely, a low angle dipping subsalt fault may foster the activation of a thin-skinned thrust system, so the contractional deformation is easily propagated towards the foreland (e.g. Carxe Fault; **Fig. 2.13f**). In this case, the salt walls located in a hinterland position are squeezed but also translated towards the foreland (**Fig. 3.7b**).
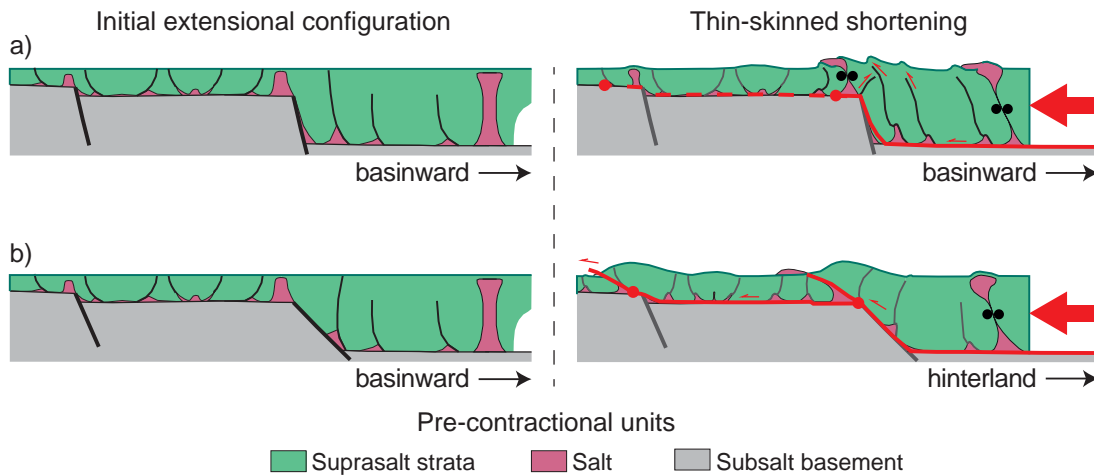


**Figure 3.7.** Schematic cross-sections depicting the propagation of thin-skinned shortening over a) high angle or b) low angle dipping subsalt faults.

Second, and related to the dip direction of the subsalt faults, two end-member scenarios are considered into this analysis (**Fig. 3.8**): subsalt faults dipping towards the foreland or towards the hinterland, with respect the main direction of the shortening propagation. In the

first case, when shortening propagates over the footwall of a subsalt fault dipping towards the foreland (**Fig. 3.8a**), its further advance may be hampered if the throw of the fault is larger than the thickness of the salt layer (e.g. see location of the Betic thrust front in **Fig. 3.9**; Roca et al., 2013). So, according to the critical Coulomb wedge theory (Dahlen, 1984), a downward offset of the décollement systematically generates an abandonment of the current décollement level and the activation of a thrust ramp where this level is disrupted. In other words, the thin-skinned thrust system does not step down into the hanging wall of the subsalt fault, contrarily the deformation ramps up at the upper hinge of the monoclinal drape fold and breaches the surface (**Fig. 3.8a**). In this scenario, the salt structures located above the footwall of the subsalt fault likely absorb part of the shortening, and therefore nucleate folding and thrusting. However, above the hanging wall of a subsalt fault dipping towards the foreland, a thicker overburden may also hamper the propagation of the contractional deformation, so the pre-existing salt structures located in this position are slightly affected by shortening (**Fig. 3.8a**).
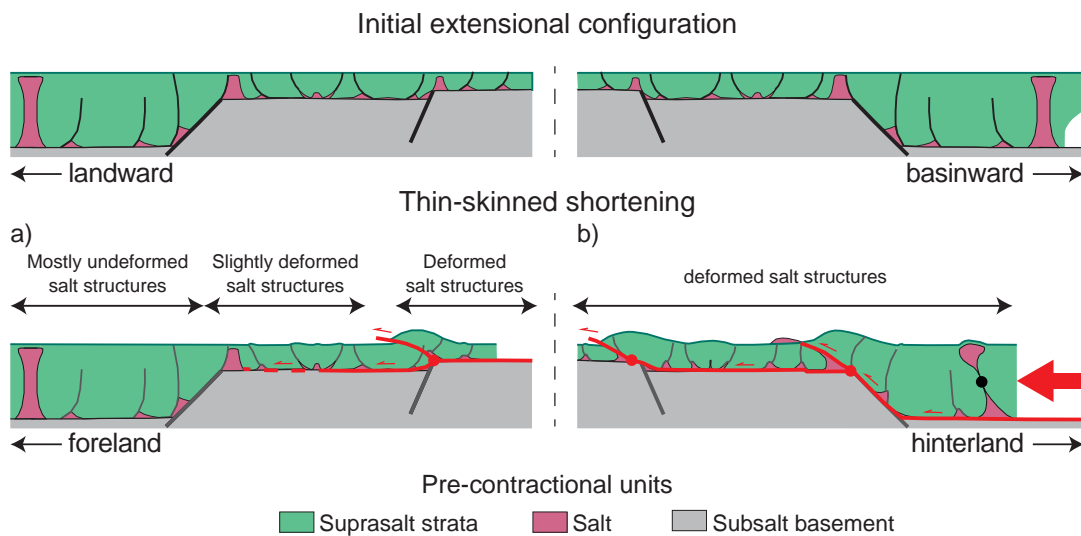


**Figure 3.8.** Schematic cross-sections depicting the propagation of thin-skinned shortening over a pre-existing extensional system with faults dipping towards the a) foreland and/or b) towards the hinterland.

Conversely, if subsalt faults dip towards the hinterland, the contractional deformation is conducted by a fold-and-thrust belt rooted into the décollement level with a flat-ramp-flat geometry (**Fig. 3.8b**). So, shortening is easily propagated over the hanging wall of a subsalt fault, forming a fault-bend fold with a suprasalt ramp anticline located over the upper tip of this fault (**Fig. 3.9**). This process is also facilitated by a decrease in thickness of the overburden

towards the foreland. In this scenario, the pre-existing salt walls located over the faulted subsalt blocks will cryptically accommodate shortening until secondary welds are developed at their stems (Vendeville & Nilsen, 1995; Gottschalk et al., 2004). At this stage, as shortening is easily propagated towards the foreland, thrust faults are rarely developed at the pedestals of the squeezed salt walls (e.g. **Figs. 2.13e** and **2.13f**). Only when shortening progresses, this type of contractional structures will be activated at and likely will decapitate the pre-existing diapirs (e.g. **Fig. 2.13g**).

In particular, when salt walls are developed above the upper hinge of the monoclinal drape fold, the presence of a thicker overburden in the hinterland side than in the foreland side of the diapir constitutes an important mechanical anisotropy for a future contractional deformation. So, under shortening, this inherited architecture may foster the squeezing of the uppermost part of the salt wall, the formation of secondary welds, and the activation of thrust faults in the hinterland side of the diapir and directed towards the foreland. As a result of this, suprasalt successions that were initially on the hanging wall of the subsalt fault will be thrusted and located on top of thinner successions with a similar age located above the footwall (e.g. Carxe Fault; **Fig. 2.13g**; or the southern margin of the Organyà Basin, Bóixols thrust sheet, Southern Central Pyrenees, Mencos et al., 2015).
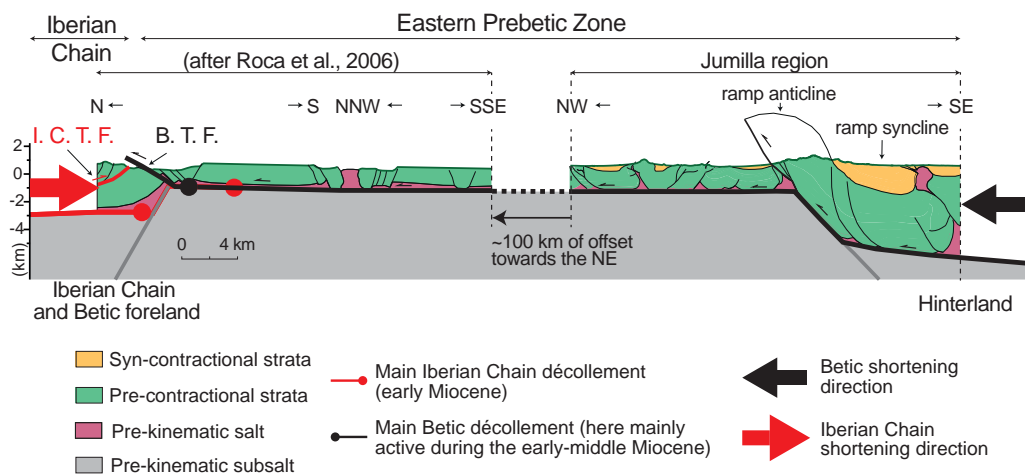


**Figure 3.9.** Simplified transect across the Eastern Prebetic Zone. B.T.F. and I.C.T.F., Betic and Iberian Chain thrust fronts, respectively. See the location of the northern segment in **Fig. 2.10**.

Finally, the throw magnitude of the subsalt fault also controls the propagation of the thin-skinned contractional deformation. For example, a small fault offset may not cut the continuity of the décollement level, so the contractional deformation is easily propagated towards the

foreland and the pre-existent salt walls are equally shortened over the faulted subsalt blocks. In this manner, the subsalt faults with small throws together with similar thicknesses of the suprasalt strata, will exert a little influence on the shortening propagation, independently of both their dip and dip direction.

## 3.3.2. Influence of the pre-existent salt structures

The existence of precursor salt structures also constrains the incorporation of extensional salt-bearing basins into foreland fold-and-thrust belts (e.g. Rowan & Vendeville, 2006; Escosa et al., 2018b; Granado et al., 2018). They are weaker than the adjacent overburden and thus tend to localize the contractional deformation as they are cryptically shortened (e.g. Nilsen et al., 1995; Vendeville & Nilsen, 1995; Gottschalk et al., 2004; Roca et al., 2006; Rowan & Vendeville, 2006; Callot et al., 2007; Dooley et al., 2009; Duffy et al., 2018).

During contraction, the narrowing process is principally concentrated at the central part of the salt wall where the difference between the flexure strength of the diapir and the contractional strength (i.e. $\sigma_1$) is maximum (Rowan & Vendeville, 2006; Dooley et al., 2015, see their figure 10). In this regard, the spatial and cross-sectional distribution of the strain gradient along the salt wall is ultimately constrained by the inherited geometry and/or length and width of the precursor diapir (Nilsen et al., 1995; Callot et al., 2007).

Furthermore, if the diapir is covered by a thin and weak roof or crops out at the topographic surface, the salt flow rate will increase and the diapir may disrupt the roof and flare upwards forming overhangs and/or salt sheets. However, if a buried diapir with a thicker roof is shortened, the salt body will be progressively narrowed and the diapir roof will be folded forming an anticline cored by the pressurized and displaced salt (Nilsen et al., 1995; Vendeville & Nilsen, 1995; Dooley et al., 2009, 2015). Scaled physical models conducted in Dooley et al. (2009, 2015) suggest that the diapir roof may deform in three different stages: firstly, far field shortening pressurizes salt promoting the arching of the diapir roof; secondly and as shortening progresses, the thin-skinned thrust front advances and reaches the narrowing diapir, forming then a thrust salient on its foreland side; and thirdly, the diapir roof is disrupted and one half might be translated and thrusted over the other half. At this stage, thrust faults and associated folds may extend off the end of the diapir. The geometry and kinematics of these contractional structures may be influenced in part by the shape of the lateral termination of the salt wall.

**CHAPTER 3**

Regardless the diapir situation (e.g. with or without a roof covering it), the upwards flow of pressurized salt along the stem of the diapir stops when a secondary weld develops connecting its pedestal to an upper teardrop diapir (Hudec & Jackson, 2007). If shortening continues, thrust faults are developed at the pedestal of the diapir and propagate off the end of the diapir to link other contractional structures deforming the adjacent overburden without diapirs (e.g. Callot et al., 2007, 2012; Jackson et al., 2008; Dooley et al., 2009).

Therefore, the geometric and kinematic evolution of a shortened salt wall is strongly influenced by the inherited width, shape and orientation of the precursor diapir, the possible linkage between adjacent diapiric structures, the lithological composition of the involved evaporitic sequence, the thickness of the diapir roof if any, and the shortening magnitude (Nilsen et al., 1995; Vendeville & Nilsen, 1995; Dooley et al., 2009, 2015). Among these, our analysis from the Paradox Basin and the Eastern Prebetic Zone enables to deepen the knowledge of the role played by the initial structure of the salt wall and adjacent overburden, its thickness and by the amount of shortening applied to the precursor diapir; key controlling factors that are discussed in the following sections.

### 3.3.3. Influence of the pre-existing overburden

In a thin-skinned contractional system detached into a regional salt décollement (e.g. Davis & Engelder, 1985; Letouzey et al., 1995; Hudec & Jackson, 2007), the spacing of a fold-and-thrust belt is controlled, among other factors, by the overburden and salt thicknesses, and the strength contrast between layers (e.g. formation of buckling folds; Biot, 1961; Ramberg, 1964). So, the thicker is the overburden, the major is the spacing between the resulting contractional structures.

According to Callot et al. (2012), the spacing or wavelength of the contractional structures in a fold-and-thrust belt is also controlled by the existence of precursor salt-stocks and thickened minibasins. If the spacing is small and hence the overburden is thin, all salt stocks will likely nucleate contractional structures (i.e. folds and thrust faults). Conversely, if the spacing is large (e.g. Zagros fold-and-thrust belt), not all salt stocks may nucleate contractional structures, so they will be located either in the limbs or in the hinges of the synclinal folds (see Callot et al., 2012; **Fig. 3.10**).

Therefore, the principal controlling factor is the mechanical strength of the entire overburden adjacent to the pre-existing salt structures. The thicker it is, the stronger behaves facing an ulterior contractional deformation; assuming that there is a fraction of the total shortening that is accommodated solely by lateral compaction of the adjacent suprasalt rocks (e.g. Koyi et al., 2004; Dooley et al., 2009). In this scenario, if there is an effective salt décollement, a squeezed diapir and a thicker overburden mostly experiment rigid body deformation (i.e. translation) over the main décollement. Alternatively, if the overburden is thin and thus mechanically weak, the pre-existing diapir together with the adjacent suprasalt strata accommodate both rigid and non-rigid body transformations. In this case, the diapir is narrowed until the formation of secondary welds, leading to the development of a fold-and-thrust belt connecting different isolated salt stocks.
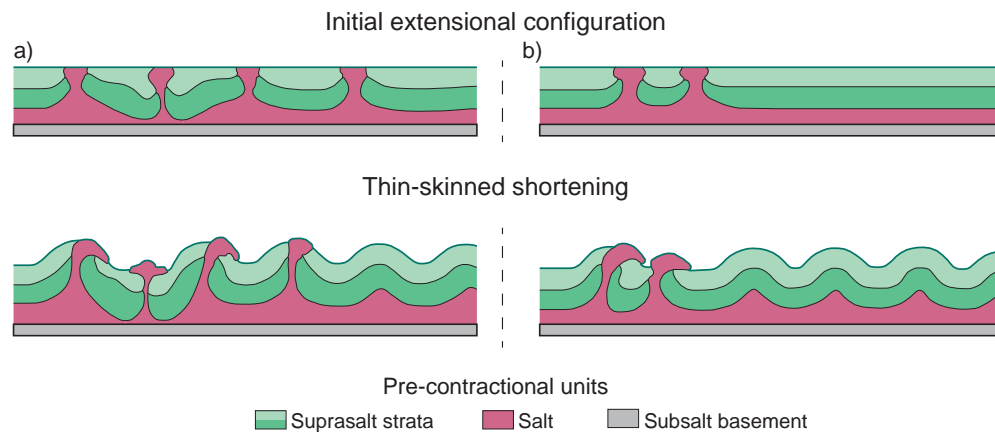


**Figure 3.10.** Simplified cross-sections obtained from scaled physical models that exemplify the interaction between the developing thin-skinned fold-and-thrust belt and the precursor diapirs and locally thickened minibasins: a) the wavelength of the contractional structures is disrupted by locally thickened overburden; b) the existence of precursor diapirs also modifies the wavelength of the contractional structures. Modified from Callot et al. (2012).

However, what if precursor salt walls instead of salt stocks are involved into the thin-skinned contractional deformation? The following subsections will address this question by discussing the studied examples in the Eastern Prebetic Zone, where salt walls formed in an overburden displaying thickness variations were subsequently affected by a thin-skinned contractional deformation. Particularly, we address the influence of the thickness and structure of the overburden adjacent to the contractionally reactivated salt walls.

**CHAPTER 3**

## 3.3.3.1. Thickness of the overburden

As it is explained above, the elliptical shape in plan-view of a salt wall (**Fig. 1.1**) constitutes a weakness point facing a contractional deformation that propagates perpendicular to it, since the salt wall offers less flexural strength in its elongated axis than in its shorter axis (e.g. see Dooley et al., 2015, their figure 10). Therefore, for a constant thickness overburden, pre-existing salt walls will narrow more readily than salt stocks as a result of perpendicular shortening.

However, the thickness of the overburden also exerts a significant influence once the salt wall has squeezed and secondary welds are developed. If for example the suprasalt strata adjacent to the diapir is thick and thus mechanically strong, the salt wall does not tend to accommodate further contractional deformation (e.g. La Sarsa salt wall; **Figs. 2.13f** and **2.13g**). Instead of this, the contractional deformation will result in: a) the formation of buckling folds affecting the entire overburden with a wavelength depending on the thickness of the suprasalt strata and the salt layer (Biot, 1961; Ramberg, 1964); and/or b) the propagation of the deformation towards regions where the thickness of the overburden decreases considerably (e.g. the External Prebetic; **Figs. 2.14a** and **2.14b**). In this latter case, the squeezed salt wall is passively translated over the décollement as the contractional deformation is propagated towards the foreland. Conversely, if the overburden is thin and thus mechanically weak, thrust faults will nucleate at the pedestal of the diapir once a secondary weld is formed. These thrust faults will decapitate the welded stem of the diapir and translate the upper teardrop diapir towards the foreland (e.g. Sierra de los Bujes; **Fig. 2.16b**), or towards the hinterland depending on the pre-existent structure of the overburden (see further details in the following subchapter 3.3.3.2).

Besides the thickness of the adjacent overburden, the resulting structure of a contractionally reactivated salt wall is also controlled by the thickness of a sedimentary roof covering the diapir. So, in absence of it, the narrowing of a salt wall increases the rate of the upwards flow of pressurized salt, which depending on the erosion and dissolution rates (Jackson & Vendeville, 1994), results on the formation of salt glaciers (e.g. Kuh-e-Namak salt extrusions, Talbot & Jarvis, 1984). However, if a sedimentary roof is covering the salt wall, meaning that the growth of the diapir is no longer active, the narrowing of the diapir may produce different situations depending on the thickness of the sedimentary roof (Duffy et al., 2018). Thereby, a thick roof will hamper the squeezing of the salt wall; and a thin roof may allow the narrowing

and hence foster the rejuvenation of the diapir. Nevertheless, in all scenarios, the resulting contractional structures deforming the diapir's roof will have a shorter wavelength compared with the regional style of the deformation, since the thickness of the folded roof is always thinner than the surrounding overburden (e.g. La Sarsa salt wall, **Fig. 2.14a**).

Furthermore, during the extensional development of a salt wall, the roof may collapse because of the formation of primary welds hampering the flux of salt into the diapir, resulting in the formation of a turtle structure if sedimentation continues (e.g. **Figs. 2.13e** and **2.13f**). In this case, the collapsed roof of the ancient diapir may depict a similar thickness than the adjacent suprasalt strata once the subsiding minibasin touches down and primary welds develop (see Chapter 1.5.1 for further details). During the subsequent thin-skinned contractional reactivation and after the formation of secondary welds at the respective salt horns, the turtle structure may be uplifted forming a symmetrical pop-up (see Jackson and Hudec, 2017, their figure 11.17b). Thereby, the thickened roof is thrusted above the flanks of the pre-existent salt wall using the secondary welded salt horns as décollements. A particular case is when the resulting salt wall is triggered by a single asymmetric extensional fault with a salt roller in its footwall (e.g. the Sierra del Buey and Sierra del Molar; **Figs. 1.4b**, **2.14a** and **2.14b**). In this scenario, upon inversion, strata in the footwall of the extensional fault is slightly folded, but strata in the hanging wall is highly deformed by thrust faults cross-cutting the overburden. Of course, thrust faults only develop if the overburden contains weak horizons susceptible of acting as décollement levels (e.g. Upper Cretaceous marls in the Eastern Prebetic Zone; **Fig. 2.11**).

### 3.3.3.2. Structure of the overburden

The example described above of a salt wall collapse in the Sierra del Buey and Sierra del Molar evidences the role of the adjacent suprasalt structure on the geometric and kinematic evolution of shortened salt walls. Thereby, if precursor salt walls with symmetrical flanks triggered by differential loading and/or contraction are shortened, a symmetrical pop-up structure may develop deforming the adjacent overburden (e.g. see natural examples of squeezed diapirs in the Nordkapp Basin, Nilsen et al., 1995; and in scaled physical models in Dooley et al., 2009). However, for salt walls formed by a single thin-skinned extensional fault, the resulting contractional structure will be more asymmetric (**Fig. 3.11**).

**CHAPTER 3**
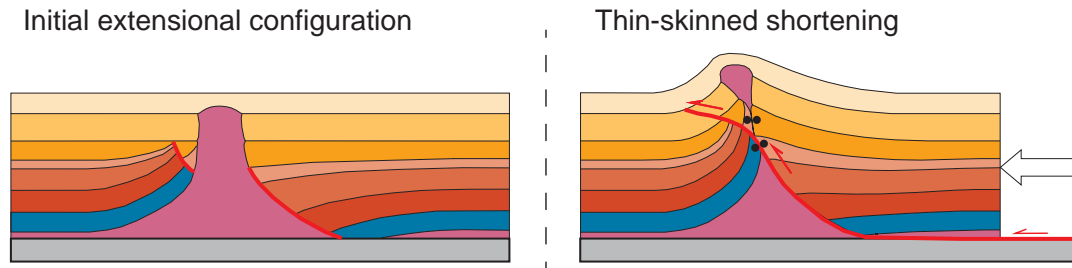
**Figure 3.11.** Geometric and kinematic model for the contractional reactivation of a salt wall triggered by a single asymmetric suprasalt fault. Upon inversion, the thin-skinned shortening uses part of the ancient extensional fault, decapitates the primary squeezed salt wall and translates the upper teardrop diapir over the ancient footwall of the suprasalt extensional fault.

As is depicted in the constructed cross-sections of the Eastern Prebetic Zone (e.g. **Figs. 2.14** and **2.14b**), shortening of an asymmetric salt wall may result in the formation of a thrust fault detached at the pedestal of the diapir and directed towards the ancient footwall of the extensional fault. This thrust fault decapitates the primary welded salt wall and translates the upper teardrop diapir over the footwall of the ancient extensional fault (see examples in Sierra de Santa Ana and Comisario anticline, **Figs. 2.14b** and **2.14b**; and Sierra de los Bujes, **Fig. 2.16b**). In this instance, the distinct mechanical behavior of the overburden in the flanks of the salt wall might be related to different dip attitudes of the salt-sediment interface in both sides of the diapir (**Fig. 3.11**). So, in the flank where the thrust fault is developed, this contractional structure may use part of the ancient extensional fault that, soled into the décollement, remained almost undeformed during the extensional growth of the salt wall.

Furthermore, the dip of the overburden adjacent to the precursor salt wall also influences its ulterior contractional deformation. Thereby, adjacent suprasalt strata dipping towards the diapir may facilitate the activation of bedding surfaces as folds and thrust faults once the diapir is secondary welded. Conversely, adjacent suprasalt strata dipping away from the diapir may hamper the activation of these contractional structures deforming the overburden.

## 3.3.4. Role of the amount of shortening

The amount of shortening applied to a precursor salt wall controls the resulting shape of the diapir, the type of contractional structures extending off its end, and the degree of salt extrusion of the reactivated diapir (e.g. Vendeville & Nilsen, 1995; Gottschalk et al., 2004; Rowan et al., 2004; Roca et al., 2006; Jackson et al, 2008; Dooley et al., 2009, 2015; Jackson

& Hudec, 2017). At the same time, the way how shortening affects precursor salt walls also depends on the direction, magnitude and rate of the contractional deformation as well as the initial width of the salt wall (e.g. Nilsen et al., 1995; Jackson & Hudec, 2017; Duffy et al., 2018). Thereby, if shortening occurs perpendicular to the long axis of a preexisting salt wall, the diapir will preferentially narrow and/or squeeze facilitating the nucleation of thrust faults at its pedestal (e.g. Rowan & Vendeville, 2006; Stefanescu et al., 2000). Conversely, if shortening is propagated parallel to the long axis of the salt wall, the diapir will be sheared and faults with a directional component will nucleate at its terminations but also along the salt wall sides (e.g. De Ruig, 1992; Sherkati et al., 2005; Dooley & Schreurs, 2012; Alsop et al., 2018). At the same time, the strain rate during the contractional deformation will control the mechanical behavior of the salt; thereby fast rates will promote a brittle response; and low stain rates will allow salt to flow in a ductile manner (Senseny et al., 1992; Wallner, 1983; Jackson & Hudec, 2017).

The sequence of structures that form during shortening of an isolated salt wall is strongly controlled by the strain magnitude in combination with the weakness of the salt in relation to the adjacent overburden (Duffy et al., 2018). So, at low strains, the diapir flanks begin to converge and therefore the diapir's roof arches as well (Nilsen et al., 1995). In this context the diapir accommodates the major part of the contractional deformation propagated from the hinterland (e.g. see the progressive cryptic shortening absorbed by la Sarsa salt wall in **Figs. 2.13e** and **2.13f**). The other part of the deformation is accommodated solely by lateral compaction of the adjacent sedimentary rocks (e.g. Koyi et al., 2004; Dooley et al., 2009).

As shortening strain increases, the salt wall continues accommodating deformation, thus pressurized salt rises allowing the diapir to narrow (Nilsen et al., 1995; Callot et al., 2007; Dooley et al., 2009). In map-view, thrusts and folds nucleate at the diapir and propagate out into the adjacent suprasalt strata to link up with other contractional structures deforming the overburden (Koyi, 1988; Nilsen et al., 1995; Gottschalk et al., 2004; Letouzey & Sherkati, 2004; Rowan et al., 2004; Callot et al., 2007; Jackson et al., 2008; Fernandez & Kaus, 2014). For example, the gentle folding of the Dakota Sst. and younger strata extending ca. 2 km from the edge of the Gypsum Valley salt wall (**Fig. 2.5, sections A–C**) cannot be explained by simple halokinetic drape-folding because this latter is restricted to 1 km away from the diapir margin (Giles & Rowan, 2012). In this case, we determined that the broader zone of gentle folding was generated by minor diapir rejuvenation during the subsequent Laramide Orogeny that affected the Paradox Basin (see Escosa et al., 2018c; **Annex 1**). Thereby, the total amount of

**CHAPTER 3**

shortening decreasing abruptly at the end of the salt wall, was accommodated in part by the formation of a lateral tear fault (see Fig. 6 in **Annex 1**).

At higher contractional strains, if salt disrupts the diapir's roof and extrudes passively, the stem of the salt wall is progressively depleted, and secondary welds are likely developed (e.g. **Fig. 2.14a**). For example, the presence of a NW-directed thrust affecting La Sarsa salt wall, the pronounced folding of its roof as well as the existence of isolated outcrops of Upper Triassic evaporites disrupting the diapir's roof (**Fig. 2.12**), indicate that this salt wall was contractionally deformed by moderate to high strains.

Finally, the results of the investigations conducted in this thesis also suggest that the strain magnitude affecting precursor salt walls is not only controlled by the initial width of the diapir but also by the location of the salt wall in respect to the subsalt structure. As it is observed in the Eastern Prebetic Zone, the salt walls located near the upper tip of the Carxe and Sopalmo subsalt faults (**Figs. 2.14a** and **2.14b**), are not totally squeezed during the thin-skinned contractional deformation. Instead of this, thrust faults are developed in the hinterland side of these slightly narrowed diapirs accommodating the major part of the shortening. Again, this might be related to a distinct mechanical behavior of the overburden adjacent to the salt wall, which is influenced by the dip attitude of the salt-sediment interface in both sides of the diapir and the existence of ancient extensional faults. Therefore, in this particular case, the salt-sediment interface in the hinterland side of the diapir may have a favorable dip for activating thrust faults instead of narrowing the whole diapir.

# CHAPTER 4. CONCLUSIONS

*The cover photo of Chapter 4 depicts a marvelous sunset with reddish and windy clouds over the base camp at the SE termination of the Gypsum Valley salt wall, after a long day of field-work.*

## 4.1. Introduction

This chapter is organized in two main parts in which the partial conclusions of the respective field-work areas are summarized before presenting, based on the previous partial conclusions, the global concluding points of this PhD thesis. Therefore, the last section of this chapter lists the factors that control the geometry and kinematics of salt walls developed above subsalt faults whose movement occurs during or after the deposition of salt. And finally, details the parameters that define a later thin-skinned contractional deformation of these precursor salt walls.

## 4.2. Conclusions regarding the study of the Gypsum Valley Diapir, Paradox Basin (SE Utah and SW Colorado)

The structural analysis of the southern end of the Gypsum Valley salt wall (SE Paradox Basin) compared with analogue structures located elsewhere in the Paradox Basin and in the northern Gulf of Mexico, have permitted to propose a series of simple end-member models for salt walls mostly driven by differential sedimentary loading without significant regional extension or contraction. This investigation evidences that controlling factors on determining the terminations of salt walls and adjacent megaflaps are:

- The original thickness and spatial distribution of the deep salt.
- The presence of nearby diapirs, which determines the fetch area for salt flow into the diapir.
- The spatial patterns of depositional sedimentary loading.
- And, variations in the nature and location of salt breakout through the roof of the initial salt structure.

## 4.3. Conclusions regarding the study of the Jumilla region, Eastern Prebetic Zone (SE Spain)

The investigation in the Eastern Prebetic Zone at the Jumilla region (SE Spain) has revealed that the observed structure corresponds to the proximal part of a passive margin containing prerift salt, that decouples a subsalt basement deformed by planar extensional faults from an overburden deformed by monoclinal drape folds, thin-skinned extensional faults and diapirs; an overburden that has been contractionally reactivated during the Betic

orogeny with the subsequent development of the thin-skinned fold-and-thrust belt.

This structural analysis has contributed to a better understanding of the development of salt walls and salt-related structures triggered by thick-skinned extension during the formation of a passive margin; and their reaction to a thin-skinned contractional deformation during the incorporation of a passive margin into a foreland fold-and-thrust belt. In particular, this study has allowed to improve this understanding by determining that:

- Thick-skinned extension controls the rate of subsidence over faulted subsalt blocks, creates accommodation space, and thus constrains the accumulation of syn-kinematic sediments above pre-kinematic salt. Therefore, this stablishes a differential sedimentary load over mobile salt that promotes the salt migration towards the upper tip or towards the hangingwall of the subsalt faults, respectively. In this scenario, the subsalt extension controls suprasalt deformation, which its location and distribution changes over time. In the early stages of extension, the suprasalt deformation is accommodated by the development of monoclinal drape folds, suprasalt faults and diapirs. As extension progresses folding and faulting is concentrated above the footwall of the main subsalt faults where the cover is thin and mechanically weak. In spite of this, translation with minor folding is concentrated above their hanging walls where the cover is thick and mechanically resistant.

- Upon inversion, salt also localizes strain during the incorporation of the passive margin into the external zones of a thin-skinned fold-and-thrust belt. In this scenario, the preexisting salt walls, weaker than the adjacent overburden, preferentially absorb part of the contractional deformation until secondary welds are developed at their narrowed stems. Afterwards, further shortening is accommodated by the formation of folds and thrusts that nucleate at the pedestals of the squeezed diapiric structures. In addition to this, the stepped subsalt geometry, inherited from the previous thick-skinned extension, also influences the propagation and localization of the thin-skinned contractional deformation. Therefore, the degree of shortening localization of the squeezed salt walls is dependent on the thickness of the adjacent overburden and on the dip and dip direction of the subsalt faults relative to the thin-skinned contractional propagation.

## 4.4. General conclusions

The previous studies and the respective partial conclusions together with the discussion conducted in this PhD thesis have permitted to highlight a series of global factors controlling the geometry and kinematics of salt walls developed in the above outlined tectonic settings. Accordingly, salt walls formed above subsalt faults whose movement occurs during or after the deposition of salt are constrained by:

- The lateral changes in the syn-kinematic sedimentary loading induced by the subsalt fault motion. During thick-skinned extension, the geometry and kinematics of the developing salt walls are controlled by variations in the accommodation space, and thus the differences in the sedimentary loading that generate the offset of the extensional subsalt faults. Thereby, a large accommodation space and corresponding high syn-kinematic sedimentation rate might favor an elevated pressure head above the source layer and a rapid migration of salt above the footwall of the subsalt faults. Conversely, a small accommodation space and corresponding low sedimentation rate might favor a lower velocity on the salt source depletion. In this regard, the different behaviors of salt migration over the subsalt faulted blocks might explain the asymmetry of salt walls that are developed at the upper hinge of the monocline drape folds; where usually there is a megaflap and a thinner suprasalt succession at the landward side of the diapir and a deeper and thicker succession at the basinward side.

- The geometry of the subsalt faults. Indeed, in an equal amount and direction of regional extension, high-angle dipping (e.g. 60–70º) subsalt faults tend to generate a greater accommodation space above their hanging walls than low-angle dipping (e.g. 30–40º) basement faults. In this regard, a higher accommodation space and a thicker syn-kinematic succession above the hanging wall of the subsalt fault promotes a greater differential pressure head above mobile salt between the faulted subsalt blocks. Thereby, thick-skinned extension conducted by high-angle subsalt faults favors the migration of salt towards the upper tip of the subsalt fault, contributes to a major outer arc stretching at the upper hinge of the overlying monocline drape fold, and fosters the development of suprasalt faults and reactive salt walls above their footwalls. Conversely, the upper hinge of the monoclinal drape folds over low-angle subsalt faults are less affected by outer arc stretching, therefore there is a major decoupling and suprasalt extension is distributed over a wider zone of the overburden.

- The lateral thickness variations of the overburden over time, which is directly linked to the strengthen that experience the suprasalt strata adjacent to the developing salt walls as syn-kinematic sedimentation occurs synchronously to thick-skinned extension. Thus, at the beginning of extension, when the subsalt faults have not generated significant lateral variations of accommodation space filled by syn-kinematic sediments, the overburden does not show noticeable thickness difference favoring a distributed suprasalt deformation. Therefore, diapirism might be indistinctly developed over the entire extended area. However, as extension progresses and the subsalt faults produce major differences in the thickness of the syn-kinematic sediments, suprasalt faulting and diapirism tend to be concentrated above the footwalls of the subsalt faults where the overburden is thin and mechanically weak. Conversely, on the hanging walls, where the overburden is thicker and hence mechanically resistant, there is almost no suprasalt deformation and the previous structures are essentially translated basinwards above the decoupling salt. Therefore, the capacity of a salt wall to concentrate future extension, besides its orientation respect to the regional stretching direction, appears strongly dependent on the lateral mechanical strength/thickness variations of the adjacent overburden driven by the underlying subsalt faults.

- The salt thickness variations and the available deep salt budget for a salt wall to form. In pre-kinematic salt basins, if subsalt extension occurs in a landward position respect to the evaporitic basin, a thinner salt layer will promote the early formation of primary welds, so coupling between subsalt and suprasalt units will occur earlier, and salt walls will have a short period of time to develop. Conversely, if thick-skinned extension occurs in a basinward position with respect to the salt basin, the decoupling will be more widespread because of a thicker salt unit, and salt walls will develop in a longer period of time since primary welding might form later. Furthermore, the thickness of the salt also controls the width of the diapir, so the thicker it is the wider is the resulting salt wall. Variations in salt thickness may also occur along strike the same diapir developed in for example syn-kinematic salt basins. In this scenario, the available salt budget for a salt wall to form is also controlled by 1) the presence of subsalt faults offsetting the source layer, and thus controlling the deposition and the spatial distribution of the evaporites; and 2), the variations in the lithological composition of the evaporites, which constrains the mobility of the salt.

- The location of the salt breakout through the roof of the initial salt structure which is ultimately controlled by the early style of diapirism and the pre-kinematic salt wall piercement geometry. In regional extension with pre-kinematic salt, the active rise of a symmetrical reactive salt wall may promote the progressive folding of the pre- and syn-kinematic suprasalt strata together with the conjugate suprasalt faults. Instead of this, the active rise of an asymmetrical salt wall will promote folding of the pre-kinematic strata located in the footwall of the listric fault. Thereby, the fault plane will be also folded as the diapir progressively rises and breaks the thinned roof. Finally, salt walls may also develop in absence of regional extension above pre-existent subsalt faults whose movement occurred during the deposition of salt. So, the position of the salt breakout in a salt inflated plateau may be led only by progressive differential sedimentary loading adjacent to the diapir. In this instance, the resultant geometry of the salt wall and adjacent overburden might be symmetric or asymmetric depending on the position of the salt breakthrough. Of course, the geometry may change from one style to the other along strike the salt wall, possibly due to variations in roof thickness and mechanical strength.

- Finally, it is worth noting that all the above-mentioned factors may variate over time but also along the elongated axis of the developing salt wall, thus leading to distinct geometries and kinematics along strike the same diapir.

As the weaker part of the overburden, precursor salt walls are readily deformed by any subsequent deformational event. In this regard, the investigation conducted in this thesis suggests that the structure resulting from the thin-skinned contractional reactivation of pre-existent salt walls is largely determined by:

- The subsalt structure, which controlled the extensional development of salt walls, and is defined by the dip, dip direction and the displacement magnitude of the subsalt extensional faults:

    - So, high angle dipping subsalt faults may act as a buttress against the propagation of the thin-skinned shortening. In other words, the highly dipping salt panels resulting from drape folding over this type of subsalt faults may difficult the contractional activation of a thrust system, and thus may hamper the propagation of the deformation towards the foreland. In this instance, the overburden and precursor diapirs above the hanging walls may be highly

deformed, meanwhile the suprasalt strata and salt walls above the footwalls may remain slightly deformed. Conversely, low angle dipping subsalt faults may foster the activation of a thin-skinned thrust system that propagates over the faulted blocks along the salt décollement. In this latter case, the thin-skinned shortening affects the precursor salt walls and adjacent overburden regardless their position with respect to the subsalt structure.

- Subsalt faults dipping towards the foreland with respect to the main direction of shortening may hamper the propagation of the contractional deformation if the vertical fault offset is greater than the thickness of the salt layer acting as a décollement level. In this scenario, precursor salt walls located above the footwall of the subsalt fault may likely absorb part of the shortening and therefore nucleate folding and thrusting once they are squeezed. However, above the hanging wall, a thicker overburden together with a bigger fault offset may difficult the shortening propagation, so the pre-existing salt structures are slightly affected by the contractional deformation. Alternatively, thin-skinned shortening is easily propagated towards the foreland over subsalt faults dipping to the hinterland –a process that is also facilitated by a decrease in thickness of the overburden towards the foreland and by a favorable flat-ramp-flat geometry of the salt décollement. In this scenario, shortening affects the precursor salt walls and adjacent overburden regardless their position with respect to the subsalt structure.

• The thickness and strength of the pre-contractional overburden adjacent to the contractionally reactivated salt wall, once the diapir has squeezed and secondary welds are developed. If shortening continues, the squeezed salt walls may nucleate thrust faults at their pedestals that decapitate the welded stems. These contractional structures are formed when the differential contractional strengths are greater than the rupture strength of the overburden which depends among other factors on its lithology and thickness. Therefore, the activation of these contractional structures is facilitated in thin and weak overburdens rather than in thicker and hence mechanically stronger ones. In this regard, a thick overburden impedes the localization of further contractional deformation into the squeezed salt wall. So, the diapir is passively translated over the décollement level as the contractional deformation is propagated towards the foreland

–a process that is also facilitated by a decrease in thickness of the overburden towards the external parts of the fold-and-thrust belt. Conversely, a thinner and mechanically weak overburden may facilitate the nucleation of thrust faults at the pedestal of the salt wall, thus decapitating the welded stem of the diapir and translating the detached teardrop diapir towards the foreland or the hinterland. Furthermore, in the case of previous inactive salt walls, the thickness of the diapiric roof also controls the resulting structure of the reactivated diapir structure. So, a thin and mechanically weak roof may foster the squeezing and thus the rejuvenation of the salt wall; and a thick and mechanically strong roof may hamper their squeezing and narrowing.

- The structure of the overburden adjacent to the precursor salt wall which is directly linked to the early style of diapirism stablished during extension. Thus, the contractional reactivation of a salt wall triggered by symmetrical extensional faults may result in a symmetrical pop-up structure; and in a more asymmetrical one if the salt wall is triggered by a single listric suprasalt fault. In this last scenario, the distinct mechanical behavior of the overburden at the flanks of the salt wall might be related to different dip attitudes of the salt-sediment interface in both sides of the diapir. In addition to this, the dip of the adjacent overburden also influences the ulterior contractional deformation of the precursor diapir. Thereby, suprasalt strata dipping towards the salt wall (e.g. a turtle structure) may facilitate the activation of bedding surfaces as thrust faults once the diapir is secondary welded. Alternatively, adjacent suprasalt strata dipping away from the diapir may hamper the activation of these contractional structures deforming both the overburden and the diapir.

- The ratio between the amount of shortening and the initial width of the precursor salt wall. If the ratio is <1, the salt wall is cryptically shortened by pressurizing the salt which enhances its upwards flow and promotes the arching of the diapiric roof. In this case, far field shortening is mainly accommodated by the salt wall and in a less proportion by lateral compaction of the adjacent sedimentary rocks. If the ratio is ~1, shortening in a precursor salt wall may result in the development of a thrust salient on its foreland side and the possible disruption of the arched diapiric roof. Here, the pressurized salt may extrude passively at the surface, with the consequent progressive depletion of the salt wall stem. And finally, if the ratio is >1, that means the flanks of the salt wall have converged, the stem has been depleted and therefore secondary welds may be developed. In this latter

case, a thrust fault can be nucleated at the pedestal of the shortened salt wall, decapitating the welded stem of the diapir and translating a possible detached teardrop diapir.

- Finally, besides all the above-mentioned factors, the resulting contractional structure of preexisting salt walls and adjacent overburden is also controlled by the length, shape and orientation of the precursor diapir, the possible linkage between adjacent diapiric structures, and the lithological composition of the evaporitic sequence.

# LIST OF REFERENCES

Alsharhan, A. S., & Nairn, A. E. M. (1997). *Sedimentary Basins and Petroleum Geology of the Middle East.* Amsterdam, The Netherlands: Elsevier Science.

Alsop, G. I., Weinberger, R., Marco, S., & Levi, T. (2018). Fault and fracture patterns around a strike-slip influenced salt wall. *Journal of Structural Geology*, *106*, 103–124. doi:10.1016/j.jsg.2017.10.010

Alves, T. M., Gawthorpe, R. L., Hunt, D. W., & Monteiro, J. H. (2002). Jurassic tectono-sedimentary evolution of the Northern Lusitanian Basin (offshore Portugal). *Marine and Petroleum Geology*, *19*, 727–754. doi:10.1016/S0264-8172(02)00036-3

Amador, C. M., Schurger, S. G., & Miller, B. L. (2009). Andy's Mesa Unit, San Miguel County, Colorado. In W. S. Houston, L. L. Wray & P. G. Moreland (Eds.), *The Paradox Basin revisited – New developments in petroleum systems and basin analysis* (pp. 497–518). Denver, Colorado: Rocky Mountain Association of Geologists, Special Publication.

Andrie, J. R., Giles, K. A., Lawton, T. F., & Rowan, M. G. (2012). Halokinetic-sequence stratigraphy, fluvial sedimentology and structural geometry of the Eocene Carroza Formation along La Popa salt weld, La Popa Basin, Mexico. *Geological Society, London, Special Publications*, *363*, 59–79. doi:10.1144/sp363.4

Baars, D. L., & Stevenson, G. M. (1981). Tectonic evolution of the Paradox basin, Utah & Colorado. In D. L. Wiegand (Ed.), *Geology of the Paradox basin* (pp. 23–31). Denver, Colorado: Rocky Mountain Association of Geologists.

Baena, J. (1979). Mapa Geológico y Memoria explicativa de la Hoja Jumilla (n° 869) del Mapa geológico Nacional a escala 1:50.000. Madrid, Spain: Instituto Geológico y Minero de España.

Balanyá, J. C., & García-Dueñas, V. (1987). Les directions structurales dans le Domaine d'Alborán de part et d'autre du Détroit de Gibraltar. *Comptes Rendus de l'Académie des Sciences de Paris, 304,* 929–932.

Balkwill, H. R., & Legall, F. D. (1989). Whale Basin, offshore Newfoundland: Extension and salt diapirism. In A. J. Tankard & H. R Balkwill (Eds.), *Extension tectonics and stratigraphy of the North Atlantic margins. American Association of Petroleum Geologists Memoir*, *46*, 233–245.

Banks, C. J., & Warburton, J. (1991). Mid-crustal detachment in the Betic system of southeast Spain. *Tectonophysics*, *191*, 275–289. doi:10.1016/0040-1951(91)90062-W

Barbeau, D. L. (2003). A flexural model for the Paradox basin: Implications for the tectonics of the Ancestral Rocky Mountains. *Basin Research*, *15*, 97–115. doi:10.1046/j.1365-2117.2003.00194.x

Barton, D. C. (1933). Mechanics of formation of salt domes with special reference to Gulf Coast salt domes of Texas and Louisiana. *American Association of Petroleum Geologists Bulletin*, *17*, 1025–1083.

Bartrina, T., Hernández, E., & Serrano, A. (1990). Estudio de subsuelo del Trías salino en la Depresión Intermedia. In F. Ortí & J. M. Salvany (Eds.), *Formaciones evaporíticas de la Cuenca del Ebro y cadenas periféricas y de la zona de Levante* (pp. 232–238). Barcelona, Spain: Universitat de Barcelona and ENRESA.

Bengston, C. A. (1980). Structural uses of tangent diagrams. *Geology*, *8*, 599–602.

Bernoulli, D., & Lemoine, M. (1980). Birth and early evolution of the Tethys: the overall situation. Paper presented at the 26th International Geological Congress, Paris.

Biot, M. A. (1961). Theory of folding of stratified viscoelastic media and its implications in tectonics and orogenesis. *Geological Society of America Bulletin*, *72*, 1595–1620.

**REFERENCES**

BLAKEY, R. C. (2009). Paleogeography and Geologic History of the Western Ancestral Rocky Mountains, Pennsylvanian-Permian, southern Rocky Mountains and Colorado Plateau. In W. S. Houston, L. L. Wray & P. G. Moreland (Eds.), *The Paradox Basin revisited – New developments in petroleum systems and basin analysis* (pp. 222–264). Denver, Colorado: Rocky Mountain Association of Geologists, Special Publication.

BLOCH, R. B., VON HUENE, R., HART, P. E., & WENTWORTH, C. M. (1993). Style and magnitude of tectonic shortening normal to the San Andreas fault across Pyramid Hills and Kettleman Hills South Dome, California. *Geological Society of America Bulletin*, *105*, 464–478.

BOSÁK, P., JAROŠ, J., SPUDIL, J., SULOVSKÝ, P., & VÁCLAVEK, V. (1998). Salt plugs in the eastern Zagros, Iran: Results of regional geological reconnaissance. *Geolines, Praha, GlÚ AV ČR Praha*, *7*, 3–180.

BUTLER, R. W. H. (1989). The influence of pre-existing basin structure on thrust system evolution in the Western Alps. *Geological Society, London, Special Publications*, *44*, 105–122. doi:10.1144/GSL.SP.1989.044.01.07

Caër, T., MAILLOT, B., SOULOUMIAC, P., LETURMY, P., FRIZON DE LAMOTTE, D., & NUSSBAUM, C. (2015). Mechanical validation of balanced cross-sections: The case of the Mont Terri anticline at the Jura front (NW Switzerland). *Journal of Structural Geology*, *75*, 32–48. doi:10.1016/j.jsg.2015.03.009

CAËR, T., SOULOUMIAC, P., MAILLOT, B., LETURMY, P., & NUSSBAUM, C. (2018). Propagation of a fold-and-thrust belt over a basement graben. *Journal of Structural Geology*, *115*, 121–131. doi:10.1016/j.jsg.2018.07.007

CALLOT, J. P., JAHANI, S., & LETOUZEY, J. (2007). The role of pre-existing diapirs in fold and thrust belt development. In O. Lacombe, J. Lavé, F. Roure & J. Vergés (Eds.), *Thrust Belts and Foreland Basins from Fold Kinematics to*

*Hydrocarbon Systems: Frontiers in Earth Sciences, Part V*, 309–325. doi:10.1007/978-3-540–69426-7_16

CALLOT, J. -P., TROCME, V., LETOUZEY, J., ALBOUY, E., JAHANI, S., & SHERKATI, S. (2012). Pre-existing salt structures and the folding of the Zagros Mountains. *Geological Society, London, Special Publications*, *363*, 545–561. doi:10.1144/SP363.27

CASTAÑO-FERNÁNDEZ, S. (1993). *La estructura cortical del área de unión de las cordilleras ibérica y béticas*. PhD Thesis, Universidad Complutense de Madrid, Madrid, España.

CHAPPLE, W. M. (1978). Mechanics of thin-skinned fold-and-thrust belts. *Geological Society of America Bulletin*, *89*, 1189–1198.

CLAUSEN, O. R., & KORSTGÅRD, J.A. (1996). Planar detaching faults in the southern Horn Graben, Danish North Sea. *Marine and Petroleum Geology*, *13*, 537–548. doi:10.1016/0264-8172(96)00001-3

COLEMAN, A. J., JACKSON, C. A. -L, DUFFY, O. B., & MARIA, A. (2018). How, where and when do radial faults grow near salt diapirs? Implications for paleo-stress analysis in sedimentary basins. *Geology*, *46*, 655–658.

COSGROVE, J. W., & AMEEN, M. S. (2000). A comparison of the geometry, spatial organization and fracture patterns associated with forced folds and buckle folds. *Geological Society, London, Special Publications*, *169*, 7–21. doi:10.1144/GSL.SP.2000.169.01.02

COWARD, M., & STEWART, S. (1995). Salt-influenced structures in the Mesozoic–Tertiary cover of the southern North Sea, U.K. In M. P. A. Jackson, D. G. Roberts & S. Snelson (Eds.), *Salt tectonics: A global perspective. American Association of Petroleum Geologists Memoir*, *65*, 229–250.

CRESPO-BLANC, A., & DE LAMOTTE, D. F. (2006). Structural evolution of the external zones derived from the Flysch trough and the South Iberian and Maghrebian paleomargins around the Gibraltar arc: A comparative study. *Bulletin*

*de La Societé Géologique de France, 177*, 267–282. doi:10.2113/gssgfbull.177.5.267

DAVIS, D. M., & ENGELDER, T. (1985). The role of salt in fold-and-thrust belts. *Tectonophysics, 119*, 67–88.

DAVIS, D., SUPPE, J., DAHLEN, F. A. (1983). Mechanics of fold-and-thrust belts and accretionary wedges. *Journal of Geophysical Research, 88*, 1153–1172.

DAVISON, I., ALSOP, I., BIRCH, P., ELDERS, C., EVANS, N., NICHOLSON, H., RORISON, P., WADE, D., WOODWARD, J., & YOUNG, M. (2000). Geometry and late-stage structural evolution of Central Graben salt diapirs, North Sea. *Marine and Petroleum Geology, 17*, 499–522. doi:10.1016/S0264-8172(99)00068-9

DAHLEN, F. A. (1984). Noncohesive critical Coulomb wedges: an exact solution. *Journal of Geophysical Research, Solid Earth (1978–2012), 89*, 10125–10133.

DAHLEN, F., SUPPE, J., & DAVIS, D. (1984). Mechanics of fold-and-thrust belts and accretionary wedges: Cohesive Coulomb theory. *Journal of Geophysical Research, Solid Earth (1978–2012), 89*, 10087–10101.

DAHLSTROM, C. D. A. (1969). Balanced cross sections. *Canadian Journal of Earth Sciences, 6*, 743–757.

DEATRICK, K. T., GILES, K., LANGFORD, R., ROWAN, M. G., & HEARON IV, T. E. (2015). Geometry and depositional facies of an exposed mega- flap: Pennsylvanian Honaker Trail Formation, Gypsum Valley salt wall, Paradox Basin, Colorado. Oral communication presented at the American Association of Petroleum Geologists Annual Convention and Exhibition, Denver, Colorado, May 31–June 3.

DECELLES, P. G., GRAY, M. B., RIDGWAY, K. D., COLE, R. B., SRIVASTAVA, P., PEQUERA, N., & PIVNIK, D. A. (1991). Kinematic history of a foreland uplift from Paleocene synorogenic conglomerate, Beartooth Range, Wyoming and Montana. *Geological Society of America Bulletin, 103*, 1458–75.

DEGOLYER, E. (1925). Origin of North American salt domes. In R. C. Moore (Ed.), *Geology of salt dome oil fields* (pp. 1–44). Tulsa, Oklahoma: American Association of Petroleum Geologists.

DE JONG, K. (1990). Alpine tectonics and rotation pole evolution of Iberia. *Tectonophysics, 184*, 279–296. doi:10.1016/0040-1951(90)90444-D

DEPAOR, D. G. (1988). Balanced section in thrust belts. Part 1: construction. *American Association of Petroleum Geologists Bulletin, 72*, 73–90.

DERCOURT, J., ZONENSHAIN, L. P., RICOU, L. E., KAZMIN, V. G., LE PICHON, X., KNIPPER, A.L., … BIJU-DUVAL, B. (1986). Geological evolution of the tethys belt from the atlantic to the pamirs since the lias. *Tectonophysics, 123*, 241–315. doi:10.1016/0040-1951(86)90199-X

DE RUIG, M. J. (1992). *Tectono-sedimentary evolution of the Prebetic Fold Belt of Alicante (SE Spain)-a study of stress fluctuations and foreland basin deformation*. Ph.D. Thesis, Vrije Universiteit, Amsterdam, The Netherlands.

DE RUIG, M. J. (1995). Extensional Diapirism in the Eastern Prebetic Foldbelt, Southeastern Spain. In M. P. A. Jackson, D. G. Roberts & S. Snelson (Eds.), *Salt tectonics: A global perspective. American Association of Petroleum Geologists Memoir, 65*, 353–367.

DE TORRES, T., & SÁNCHEZ, A. (1990). Espesores de las facies keuper en la rama castellana de la Cordillera Ibérica y en el dominio Prebético. In: F. Ortí & J. M. Salvany (Eds.), *Formaciones evaporíticas de la Cuenca del Ebro y cadenas periféricas, y de la zona de Levante* (pp. 212–218). Barcelona, Spain: Universitat de Barcelona and ENRESA.

DEVILLE, É., & CHAUVIÈRE, A. (2000). Thrust tectonics at the front of the western Alps: constraints provided by the processing of seismic reflection data along the Chambéry transect. *Comptes Rendus de l'Académie Des*

*Sciences-Series IIA*, *331*, 725–732. doi:10.1016/ s1251-8050(00)01463-4

Dewey, J. F., Helman, M. L., Knott, S. D., Turco, E., & Hutton, D. H. W. (1989). Kinematics of the western Mediterranean. *Geological Society, London, Special Publications*, *45*, 265–283. doi:10.1144/GSL.SP.1989.045.01.15

Dewey, J. F., Pitman, W. C., Ryan, W. B. F., Bonnin, J. (1973). Plate tectonics and the evolution of the Alpine system. *Geological Society of America Bulletin*, *84*, 3137–3180. doi:10.1130/0016-7606(1973) 84b3137. PTATEO>2.0.CO;2

Diegel, F. A., Schuster, D. C., Karlo, J. F., Shoup, R. C., & Tauvers, P. R. (1995). Cenozoic Structural Evolution and Tectono-Stratigraphic Framework of the Northern Gulf Coast Continental Margin. *American Association of Petroleum Geologists Memoir*, *65*, 109–151.

Doelling, H. H. (1988). Geology of Salt Valley Anticline and Arches National Park, Grand County, Utah. In H. H. Doelling, C. G. Oviatt & P. W. Huntoon (Eds.), *Salt deformation in the Paradox Region. Utah Geological and Mineral Survey Bulletin*, *122*, 7–58.

Dooley, T. P., & Schreurs, G. (2012). Analogue modelling of intraplate strike–slip tectonics: A review and new experimental results. *Tectonophysics*, *574–575*, 1–71. doi:10.1016/j. tecto.2012.05.030

Dooley, T. P., Jackson, M. P. A, & Hudec, M. R. (2009). Inflation and deflation of deeply buried salt stocks during lateral shortening. *Journal of Structural Geology*, *31*, 582–600. doi:10.1016/j.jsg.2009.03.013

Dooley, T. P., Jackson, M. P. A., Jackson, C. A. -L., Hudec, M. R., & Rodriguez, C. R. (2015). Enigmatic structures within salt walls of the Santos Basin—Part 2: Mechanical explanation from physical modeling. *Journal of Structural Geology*, *75*, 163–187. doi:10.1016/j. jsg.2015.01.009

Duerto, L., & McClay, K. (2009). The role of syntectonic sedimentation in the evolution of doubly vergent thrust wedges and foreland folds. *Marine and Petroleum Geology*, *26*, 1051–1069. doi:10.1016/j.marpetgeo.2008.07.004

Duffy, O. B., Dooley, T. P., Hudec, M. R., Jackson, M. P. A., Fernandez, N., Jackson, C. A. -L., & Soto, J. I. (2018). Structural evolution of salt-influenced fold-and-thrust belts: A synthesis and new insights from basins containing isolated salt diapirs. *Journal of Structural Geology*, *114*, 206–221. doi:10.1016/j. jsg.2018.06.024

Duffy, O. B., Gawthorpe, R. L., Docherty, M., & Brocklehurst, S. H. (2012). Mobile evaporite controls on the structural style and evolution of rift basins: Danish Central Graben, North Sea. *Basin Research*, *24*, 310–330. doi:10.1111/ bre.12000

Egeler, C. G., & Simon, O. J. (1969). Orogenic evolution of the betic zone (betic cordilleras, Spain), with emphasis on the nappe structures. *Geologie en Mijnbouw*, *48*, 296–205.

Elliott, D. (1976). Energy balance in thrust and deformation mechanisms of thrust sheets. *Proceedings of the Royal Society, London*, *A283*, 289–312.

Elston, D. P., Shoemaker, E. M., & Landis, E. R. (1962). Uncompahgre front and salt anticline region of Paradox Basin, Colorado and Utah. *American Association of Petroleum Geologists Bulletin*, *46*, 1857–1878.

Escosa, F. O., Ferrer, O., & Roca, E. (2018a). Geology of the Eastern Prebetic Zone at the Jumilla region (SE Iberia). *Journal of Maps*, *14*, 77–86. doi:10.1080/17445647.2018.1433562

Escosa, F. O., Roca, E., & Ferrer, O. (2018b). Testing thin-skinned inversion of a prerift salt-bearing passive margin (Eastern Prebetic Zone, SE Iberia). *Journal of Structural Geology*, *109*, 55–73. doi:10.1016/j.jsg.2018.01.004

ESCOSA, F. O., ROWAN, M. G., GILES, K. A., DEATRICK, K. T., MAST, A. M., LANGFORD, R. P., HEARON IV, T. E., & ROCA, E. (2018c). Lateral terminations of salt walls and megaflaps: An example from Gypsum Valley Diapir, Paradox Basin, Colorado, USA. *Basin Research*, *31*, 191–212. doi:10.1111/bre.12316

FALLOT, P. (1948). Les Cordillères Bétiques. *Estudios Geológicos*, *8*, 83–172.

FARRAN, M. (2008). IMAGE2SEGY: Una aplicación informática para la conversión de imágenes de perfiles sísmicos a ficheros en formato SEG Y. In F. J. Pérez & M. C. Cabrera (Eds.), *Geo-Temas*, *10*, 1215–1218.

FERNANDEZ, N., & KAUS, B. J. P. (2014). Influence of pre-existing salt diapirs on 3D folding patterns. *Tectonophysics*, *637*, 354–369. doi:10.1016/j.tecto.2014.10.021

FERNÁNDEZ, O. (2005). Obtaining a best fitting plane through 3D georeferenced data. *Journal of Structural Geology*, *27*, 855–858. doi:10.1016/j.jsg.2004.12.004

FERNÁNDEZ, O., ROCA, E., & MUNOZ, J. A. (2003). Projection of dip data in conical folds onto a cross-section plane. *Journal of Structural Geology*, *25*, 1875–1882. doi:10.1016/S0191-8141(03)00034-8

FERRER, O. (2012). S*alt tectonics in the Parentis Basin (eastern Bay of Biscay): Origin and kinematics of salt structures in a hyperextended margin affected by subsequent contractional deformation*. Ph.D. Thesis, Universitat de Barcelona, Barcelona, Spain.

FERRER, O., McCLAY, K., & SELLIER, N. C. (2016). Influence of fault geometries and mechanical anisotropies on the growth and inversion of hanging-wall synclinal basins: insights from sandbox models and natural examples. *Geological Society, London, Special Publications*, *439*, 487–509. doi:10.1144/SP439.8

FIDUK, J. C., CLIPPARD, M., POWER, S., ROBERTSON, V., RODRIGUEZ, L., AJOSE, O., FERNANDEZ, D., & SMITH, D. (2014). Origin, Transportation and deformation of Mesozoic carbonate rafts in the northern Gulf of Mexico. Gulf *Coast Association of Geological Societies Journal*, *3*, 20–32.

FLETCHER, R. C., HUDEC, M. R., & WATSON, I. A., (1995). Salt glacier and composite salt-sediment models for the emplacement and early burial of allochthonous salt sheets. In M. P. A. Jackson, D. G. Roberts & S. Snelson (Eds.), *Salt tectonics: A global perspective. American Association of Petroleum Geologists Memoir*, *65*, 77–108.

FRIZON DE LAMOTTE, D., RAULIN, C., MOUCHOT, N., WROBEL-DAVEAU, J. -C., BLANPIED, C., & RINGENBACH, J. -C. (2011). The southernmost margin of the Tethys realm during the Mesozoic and Cenozoic: Initial geometry and timing of the inversion processes. *Tectonics*, *30*, 1–22. doi:10.1029/2010TC002691

FRIZON DE LAMOTTE, D., FOURDAN, B., LELEU, S., LEPARMENTIER, F., & DE CLARENS, P. (2015). Style of rifting and the stages of Pangea breakup. *Tectonics*, *34*. doi:10.1002/2014TC003760

GARCÍA-HERNÁNDEZ, M., LÓPEZ GARRIDO, A. C., MARTÍN ALGARRA, A., MOLINA CÁMARA, J. M., RUIZ-ORTIZ, P. A., & VERA FERRÁNDIZ, J. A. (1989). Las discontinuidades mayores del Jurásico de las Zonas Externas de las Cordilleras Béticas: análisis e interpretación de los ciclos sedimentarios. *Cuadernos de Geología Ibérica*, *13*, 35–52.

GARCÍA-HERNÁNDEZ, M., LOPEZ GARRIDO, A. C., RIVAS, P., SANZ DE GALDEANO, C., & VERA, J. A. (1980). Mesozoic palaeogeographic evolution of the external zones of the Betic Cordillera. *Geologie en Mijnbouw*, *59*, 155–168.

GE, H., & JACKSON, M. P. A. (1998). Physical modeling of structures formed by salt withdrawal: Implications for deformation caused by salt dissolution. *American Association of Petroleum Geologists Bulletin*, *82*, 228–250.

GE, H., JACKSON, M. P. A., & VENDEVILLE, B. C. (1997). Kinematics and Dynamics of Salt

**REFERENCES**

Tectonics Driven by Progradation. *American Association of Petroleum Geologists Bulletin, 81*, 398–423.

Giles, K. A., & Lawton, T. F. (2002). Halokinetic sequence stratigraphy adjacent to the El Papalote diapir, northeastern Mexico. *American Association of Petroleum Geologists Bulletin, 86*, 823–840.

Giles, K. A., & Rowan, M. G. (2012). Concepts in halokinetic-sequence deformation and stratigraphy. In G. I. Alsop, S. G. Archer, A. J. Hartley, N. T. Grant & R. Hodgkinson (Eds.), *Salt Tectonics, sediments and prospectivity. Geological Society, Special Publication, 363*, 7–31. doi: 10.1144/SP363.2

Giles, K. A., Rowan, M. G., Langford, R. P., McFarland, J., & Hearon IV, T. E. (2017). Salt shoulders. Oral communication presented at the AAPG/SEG International Conference and Exhibition, London, England, October 15-18.

Gottschalk, R. R., Anderson, A. V., Walker, J. D. & Da Xilva, J. C., (2004). Modes of contractional salt tectonics in Angola Block 33, Lower Congo basin, West Africa. In P. J. Post, D. L. Olson, K. T. Lyons, S. L. Palmes, P. F. Harrison & N. C. Rosen (Eds.), *Salt-sediment interactions and hydrocarbon prospectivity: concepts, applications, and case studies for the 21st century* (pp. 705–734). Houston, Texas: 24th Annual Research Conference, Gulf Coast Section of the SEPM Foundation.

Graham, R., Jackson, M., Pilcher, R., & Kilsdonk, B. (2012). Allochthonous salt in the sub-Alpine fold-thrust belt of Haute Provence, France. In G. I. Alsop, S. G. Archer, A. J. Hartley, N. T. Grant & R. Hodgkinson (Eds.), *Salt Tectonics, sediments and prospectivity. Geological Society, Special Publication, 363*, 595–615. doi:10.1144/SP363.30

Granado, P., Roca, E., Strauss, P., Pelz, K., & Muñoz, J. A. (2018). Structural styles in fold-and-thrust belts involving early salt structures: The Northern Calcareous Alps (Austria). *Geology, 47*, 51–54. doi:10.1130/G45281.1

Groshong, R. H. Jr. (2006). *3-D structural geology*, 2d ed. Heidelberg, Germany: Springer-Verlag.

Hanne, D., White, N., & Lonergan, L. (2003). Subsidence analysis from the Betic Cordillera, Southeast Spain. *Basin Research, 15*, 1–21. doi:10.1046/j.1365-2117.2003.00192.x

Hardy, S., & Poblet, J. (1994). Geometric and numerical model of progressive limb rotation in detachment folds. *Geology, 22*, 371–374. doi:10.1130/0091-7613(1994)022<0371:GANMOP>2.3.CO;2

Harrison, J. C., & Jackson, M. P. A. (2014). Exposed evaporite diapirs and minibasins above a canopy in central Sverdrup Basin, Axel Heiberg Island, Arctic Canada. *Basin Research, 26*, 567–596. doi:10.1111/bre.12037

Hearon IV, T. E., Rowan, M. G., Giles, K. A., & Hart, W. H. (2014). Halokinetic deformation adjacent to the deepwater Auger diapir, Garden Banks 470, northern Gulf of Mexico: Testing the applicability of an outcrop-based model using subsurface data. *Interpretation, 2*, SM57–SM76.

Hearon IV, T. E., Rowan, M. G., Giles, K. A., Kernen, R. A., Gannaway, C. E., Lawton, T. F., & Fiduk, J. C. (2015). Allochthonous salt initiation and advance in the northern Flinders and eastern Willouran ranges, South Australia: Using outcrops to test subsurface-based models from the northern Gulf of Mexico. *American Association of Petroleum Geologists Bulletin, 99*, 293–331. doi:10.1306/08111414022

Hodgson, N. A., Farnsworth, J., & Fraser, A. J. (1992). Salt-related tectonics, sedimentation and hydrocarbon plays in the Central Graben, North Sea, UKCS. In R. F. P. Hardman (Ed.), *Exploration Britain: Geological insights for the next decade, London, Geological Society, Special Publication, 67*, 31–63.

Hossack, J. R. (1983). A cross-section through the Scandinavian Caledonides constructed with the aid of branch-line maps. *Journal of Structural Geology, 5*, 103–111. doi:10.1016/0191-8141(83)90036-6

HOSSACK, J.R. (1995). Geometric rules of section balancing for salt structures. In M.P.A. Jackson, D.G. Roberts, S. Snelson (Eds.), *Salt Tectonics: A Global Perspective. American Association of Petroleum Geologists Memoir*, *65*, 29–40.

HUDEC, M. R., & JACKSON, M. P. A. (2004). Regional restoration across the Kwanza Basin, Angola: Salt tectonics triggered by repeated uplift of a metastable passive margin. *American Association of Petroleum Geologists Bulletin*, *88*, 971–990. doi:10.1306/02050403061

HUDEC, M. R., & JACKSON, M. P. A. (2007). Terra infirma: Understanding salt tectonics. *Earth-Science Reviews*, *82*, 1–28. doi:10.1016/j.earscirev.2007.01.001

HUDEC, M. R., & JACKSON, M. P. A. (2011). *The salt mine: a digital atlas of salt tectonics.* Austin, Texas: The University of Texas at Austin, Bureau of Economic Geology, Udden Book Series 5; Tulsa, Oklahoma: American Association of Petroleum Geologists Memoir, 99.

IZQUIERDO-LLAVALL, E., ROCA, E., XIE, H., PLA, O., MUÑOZ, J. A., ROWAN, M. G., YUAN, N., & HUANG, S. (2018). Influence of Overlapping décollements, Syntectonic Sedimentation, and Structural Inheritance in the Evolution of a Contractional System: The Central Kuqa Fold-and-Thrust Belt (Tian Shan Mountains, NW China). *Tectonics*, *37*, 2608–2632. doi:10.1029/2017TC004928

JACKSON, C. A. -L., & LEWIS, M. M. (2012). Origin of an anhydrite sheath encircling a salt diapir and implications for the seismic imaging of steep-sided salt structures, Egersund Basin, Northern North Sea. *Journal of the Geological Society*, *169*, 593–599, doi:10.1144/0016-76492011-126.

JACKSON, C. A.-L., & LEWIS, M. M. (2016). Structural style and evolution of a salt-influenced rift basin margin; the impact of variations in salt composition and the role of polyphase extension. *Basin Research*, *28*, 81–102. doi:10.1111/bre.12099

JACKSON, C. A.-L., JACKSON, M. P. A., HUDEC, M. R., & RODRIGUEZ, C. (2014). Internal structure, kinematics, and growth of a salt wall: Insights from 3-D seismic data. *Geology*, *42*, 307–310. doi:10.1130/G34865.1

JACKSON, M. P. A., & HUDEC, M. R. (2017). *Salt tectonics – Principles and practice.* Cambridge, England: Cambridge University Press.

JACKSON, M. P. A., & TALBOT, C. J. (1991). *Glossary of salt tectonics. Geological Circular 91-4.* Austin, Texas: Bureau of Economic Geology, University of Texas at Austin.

JACKSON, M. P. A., & VENDEVILLE, B. C. (1994). Regional extension as a geologic trigger for diapirism. *Geological Society of America Bulletin*, *106*, 57–73. doi:10.1130/0016-7606(1994)106<0057:REAAGT>2.3.CO;2

JACKSON, M. P. A., CORNELIUS, R. R., CRAIG, C. H., GANSSER, A., STOCKLIN, J., & TALBOT, C. J. (1990). Salt diapirs of the Great Kavir, central Iran. *Geological Society of America Memoirs*, *177*, 1–150. doi:10.1130/MEM177-p1

JACKSON, M. P. A., HUDEC, M. R., JENNETTE, D. C., & KILBY, R. E. (2008). Evolution of the Cretaceous Astrid thrust belt in the ultradeep-water Lower Congo Basin, Gabon. *American Association of Petroleum Geologists Bulletin*, *92*, 487–511. doi:10.1306/12030707074

JACKSON, M. P. A., VENDEVILLE, B. C., & SCHULTZ-ELA, D. D. (1994). Structural dynamics of salt systems. *Annual Review of Earth and Planetary Sciences*, *22*, 93–117.

JAHANI, S., CALLOT, J. P., LETOUZEY, J., & FRIZON DE LAMOTTE, D. (2009). The eastern termination of the Zagros fold and thrust belt (Iran): relationship between salt plugs, folding and faulting. *Tectonics*, *28*, 1–22, doi:10.1029/2008TC002418

JAMISON, W. R. (1987). Geometric analysis of fold development in overthrust terranes. *Journal of Structural Geology*, *9*, 207–219. doi:10.1016/0191-8141(87)90026-5

KANE, K. E., JACKSON, C. A. -L., & LARSEN, E. (2010). Normal fault growth and fault-related folding in a salt-influenced rift basin: South viking graben, offshore Norway. *Journal of Structural Geology*, *32*, 490–506.

KARAM, P., & MITRA, S. (2016). Experimental studies of the controls of the geometry and evolution of salt diapirs. *Marine and Petroleum Geology*, *77*, 1309–1322. doi:10.1016/j.marpetgeo.2016.05.010

KERGARAVAT, C., RIBES, C., LEGEAY, E., CALLOT, J. P., KAVAK, K. S., & RINGENBACH, J. -C. (2016). Minibasins and salt canopy in foreland fold-and-thrust belts: The central Sivas Basin, Turkey. *Tectonics*, *35*, 1342–1366. doi:10.1002/2016TC004186

KERNEN, R. A., GILES, K. A., ROWAN, M. G., LAWTON, T. F., & HEARON IV, T. E. (2012). Depositional and halokinetic-sequence stratigraphy of the Neoproterozoic Wonoka Formation adjacent to Patawarta allochthonous salt sheet, Central Flinders Ranges, South Australia. In G. I. Alsop, S. G. Archer, A. J. Hartley, N. T. Grant & R. Hodgkinson (Eds.), *Salt Tectonics, sediments and prospectivity. Geological Society, Special Publication*, *363*, 81–105. doi:10.1144/SP363.5

KIRKLAND, D. W., & EVANS, R. (1981). Source-rock potential of evaporitic environment. *American Association of Petroleum Geologists Bulletin*, *65*, 181–190.

KLITGORD, K. D., & SCHOUTEN, H. (1986). Plate kinematics of the central Atlantic. In P. R. Vogt & B. E. Tucholke (Eds.), *The Geology of North America*, *M*, *The western north Atlantic Region* (pp. 351–378). Boulder, Colorado: Geological Society of America.

KLUTH, C. F. (1986). Plate tectonics of the Ancestral Rocky Mountains. In J. A. Peterson (Ed.), *Paleotectonics and sedimentation in the Rocky Mountain Region, United Sates. American Association of Petroleum Geologists Memoir*, *41*, 353–369.

KLUTH, C. F., & CONEY, P. J. (1981). Plate tectonics of the Ancestral Rocky Mountains. *Geology*, *9*, 10–15. doi:10.1130/0091-7613(1981)9<10:ptotar>2.0.co;2

KLUTH, C. F., & DuCHENE, H. R. (2009). Late Pennsylvanian and early Permian structural geology and tectonic history of the Paradox Basin and Uncompahgre uplift, Colorado and Utah. In W. S. Houston, L. L. Wray & P. G. Moreland (Eds.), *The Paradox Basin revisited – New developments in petroleum systems and basin analysis* (pp. 178–197). Denver, Colorado: Rocky Mountain Association of Geologists, Special Publication.

KOYI, H. (1998). The shaping of salt diapirs. *Journal of Structural Geology*, *20*, 321–338. doi:10.1016/S0191-8141(97)00092-8

KOYI, H., & PETERSEN, K. (1993). Influence of basement faults on the development of salt structures in the Danish Basin. *Marine and Petroleum Geology*, *10*, 83–94.

Koyi, H. A., Sans, M., Teixell, A., Cotton, J., Zeyen, H. (2004). The significance of penetrative strain in the restoration of shortened layers – insights from sand models and the Spanish Pyrenees. In K. R. McClay (Ed.), *Thrust Tectonics and hydrocarbon systems. American Association of Petroleum Geologits Memoir, 82*, 211-226.

KRZYWIEC, P. (2006). Structural inversion of the Pomeranian and Kuiavian segments of the Mid-Polish Trough-Lateral variations in timing and structural style. *Geological Quarterly*, *50*, 151–168.

LANAJA, J. M., QUEROL, R., & NAVARRO, A. (1987). *Contribución de la exploración petrolífera al conocimiento de la geología de España*. Madrid, Spain: Instituto Geológico y Minero de España.

LANGENBERG, W., CHARLESWOTH, H., & LA RIVIERE, A. (1987). Computer-constructed cross-sections of the Morcles nappe. *Eclogae Geologica Helvetica*, *80*, 655–667.

LAUBSCHER, H. P. (1986). The eastern jura: relations between thin-skinned and basement tectonics, local and regional. *Geologische Rundschau*, *75*, 535–553.

LAWTON, T. F., & BUCK, B. J. (2006). Implications of diapir-derived detritus and gypsic paleosols in Lower Triassic strata near the Castle Valley salt wall, Paradox Basin, Utah. *Geology*, *34*, 885–888. doi:10.1130/G22574.1

LETOUZEY, J., & SHERKATI, S. (2004). Salt movement, tectonic events, and structural style in the central Zagros fold and thrust belt (Iran). In P. J. Post, D. L. Olson, K. T. Lyons, S. L. Palmes, P. F. Harrison & N. C. Rosen (Eds.), S*alt-sediment interactions and hydrocarbon prospectivity: concepts, applications, and case studies for the 21st century* (pp. 444–462). Houston, Texas: 24th Annual Research Conference, Gulf Coast Section of the SEPM Foundation.

LETOUZEY, J., COLLETA, B., VIALLY, R., & CHERMETTE, J. C. (1995). Evolution of salt-related structures in compressional settings. In M. P. A. Jackson, D. G. Roberts & S. Snelson (Eds.), *Salt Tectonics: A Global Perspective. American Association of Petroleum Geologists Memoir*, *65*, 41–60.

LEWIS, M. M., JACKSON, C. A.-L., & GAWTHORPE, R. L. (2013). Salt-influenced normal fault growth and forced folding: The Stavanger Fault System, North Sea. *Journal of Structural Geology*, *54*, 156–173. doi:10.1016/j.jsg.2013.07.015

LICKORISH, W. H., & FORD, M. (1998). Sequential restoration of the external Alpine Digne thrust system, SE France, constrained by kinematic data and synorogenic sediments. In A. Mascle, C. Puigdefabregas, H. P. Luterbacker & M. Fernandez (Eds.), *Cenozoic foreland basins of western Europe, London, Geological Society, Special Publication,* 134, 189–211.

LINK, T. A. (1930). Experiments relating to salt-dome structures. *American Association of Petroleum Geologists Bulletin*, *14*, 483–508.

MALLORY, W. W. (1972). Pennsylvanian system: Regional synthesis. In W. W. Mallory (Ed.), *Geologic Atlas of the Rocky Mountain Region* (pp. 111–128). Denver, CO: Rocky Mountain Association of Geologists.

MANKOWSKI, L. C., CAMPBELL, T. R., HUNTOON, J. E., GREGG, W. J., & LINARI, D. J. (2002). Structural mapping of the Uncompahgre front near Gateway, Colorado, with emphasis on Ancestral Rocky Mountain fabrics. Oral communication presented at the American Association of Petroleum Geologists Hedberg Conference, Vail, Colorado, July 21–26.

MARSH, N., IMBER, J., HOLDSWORTH, R. E., BROCKBANK, P., & RINGROSE, P. (2010). The structural evolution of the Halten Terrace, offshore Mid-Norway: extensional fault growth and strain localization in a multi-layer brittle–ductile system. *Basin Research*, *22*, 195–214. doi:10.1111/j.1365-2117.2009.00404.x

MARTÍN-MARTÍN, J. D., VERGÉS, J., SAURA, E., MORAGAS, M., MESSAGER, G., BAQUÉS, V., RAZIN, P., GRÉLAUD, C., MALAVAL, M., JOUSSIAUME, R., CASCIELLO, E., CRUZ-OROSA, I., & HUNT, D. W. (2016). Diapiric growth within an Early Jurassic rift basin: The Tazoult salt wall (central High Atlas, Morocco). *Tectonics*, *35*,1–31. doi:0.1002/ 2016TC004300

MAST, A. M. (2016). *The origin of anomalous carbonate units outcropping at the salt-sediment interface of the southern end of Gypsum Valley salt wall, Paradox Basin, Colorado*. MSc. Thesis, University of Texas at El Paso, El Paso, TX.

MAURIN, J. -C., & NIVIERE, B. (1999). Extensional forced folding and décollement of the pre-rift series along the Rhine graben and their influence on the geometry of the syn-rift sequences. *Geological Society, London, Special Publications*, *169*, 73–86. doi:10.1144/GSL. SP.2000.169.01.06

MCFARLAND, J., GILES, K. A., LANGFORD, R. P., & ROWAN, M. G. (2015). Structural and stratigraphic development of a salt diapir shoulder, Gypsum Valley Salt Wall, Paradox Basin, Colorado. Oral communication

**REFERENCES**

presented at the Gulf Coast Association of Geological Societies Convention, Houston, Texas, September 20–22.

McGee, D. T., Bilinski, P. W., Gary, P. S., Pfeiffer, D. S., & Sheiman, J. L. (1994). Geologic models and geometries of Auger field, deep-water Gulf of Mexico. In P. W. Weimer, A. H. Bouma & B. F. Perkins (Eds.), *Submarine fans and turbidite systems-sequence stratigraphy, reservoir architecture, and production characteristics* (pp. 245–256). Houston, Texas: 15th Annual Research Conference, Gulf Coast Section, SEPM Foundation.

McGuinness, D. B, & Hossack, J. R. (1993). The development of allochthonous salt sheets as controlled by the rates of extension, sedimentation, and salt supply. Society of Economic Paleontologists and Mineralogists Gulf Coast Section, 14th annual research conference, 127–139.

Medwedeff, D. A. (1989). Growth fault-bend folding at Southeast Lost Hills, San Joaquin Valley, California. *American Association of Petroleum Geologists Bulletin, 73*, 54–67.

Medwedeff, D. A. (1992). Geometry and kinematics of an active, laterally propagating wedge thrust, Wheeler Ridge, California. In S. Mitra & G. W. Fisher (Eds.), *Structural geology of fold and thrust belts* (pp. 3–28). Baltimore, Maryland: The Johns Hopkins University Press.

Mencos, J., Carrera, N., & Muñoz, J. A. (2015). Influence of rift basin geometry on the subsequent postrift sedimentation and basin inversion: The Organyà Basin and the Bóixols thrust sheet (south central Pyrenees). *Tectonics, 34*, 1452–1474. doi:10.1002/2014TC003692

Mohr, M., Kukla, P. A., Urai, J. L., & Bresser, G. (2005). Multiphase salt tectonic evolution in NW Germany: Seismic interpretation and retro-deformation. *International Journal of Earth Sciences, 94*, 917–940. doi:10.1007/s00531-005-0039-5

Moore, K. D., Soreghan, G. S., & Sweet, D. E. (2008). Stratigraphic and structural relations in the proximal Cutler Formation of the Paradox Basin: Implications for timing of movement on the Uncompahgre front. *The Mountain Geologist, 45*, 49–68.

Moseley, F. (1973). Diapiric and gravity tectonics in the Pre-Betic, (Sierra Bernia) of south-east Spain. *Boletin Geológico y Minero, LXXXIV.-III*, 114–126.

Mount, V. S., Suppe, J., & Hook, S. (1990). A forward modeling strategy for balancing cross sections. *American Association of Petroleum Geologists Bulletin, 74*, 521–531.

Mrazec, L. (1907). Despre cute cu simbure de străpungere [On folds with piercing cores]. *Buletinul Societăţii de Ştiinţe din Bucureşci, 16*, 6–8.

Nalpas, T., & Brun, J. P. (1993). Salt flow and diapirism related to extension at crustal scale. *Tectonophysics, 228*, 349–362.

Nelson, T. H. (1989). Style of salt diapirs as a function of the stage of evolution and the nature of the encasing sediments. Oral communication presented at the 10th Annual Research Conference Gulf Coast Section SEPM Foundation.

Nicol, A. (1993). Conical folds produced by dome and basin fold interference and their application to determining strain: examples from North Canterbury, New Zealand. J*ournal of Structural Geology, 15*, 785–792.

Nilsen, K. T., Vendeville, B. C., & Johansen, J. -T. (1995). Influence of regional tectonics on halokinesis in the Nordkapp Basin, Barents Sea. In M. P. A. Jackson, D. G. Roberts, S. Snelson (Eds.), *Salt Tectonics: A Global Perspective. American Association of Petroleum Geologists Memoir, 65*, 413–436.

Norris, D. K. (1958). Structural conditions in Canadian Coal Mines. *Bulleting of the Geological Survey of Canada, 44*, 1–53.

Oʀᴛí, F. (1974). El Keuper del Levante español. *Estudios Geológicos, 30*, 7-46.

Oʀᴛí, F., Péʀᴇᴢ-López, A., & Sᴀʟᴠᴀɴʏ, J. M. (2017). Triassic evaporites of Iberia: Sedimentological and palaeogeographical implications for the western Neotethys evolution during the Middle Triassic–Earliest Jurassic. *Palaeogeography, Palaeoclimatology, Palaeoecology, 471*, 157–180. doi:10.1016/j.palaeo.2017.01.025

Pᴀʀᴋᴇʀ, T. J., & McDowᴇʟʟ, A. N. (1955). Model studies of salt-dome tectonics. *American Association of Petroleum Geologists Bulletin, 39*, 2384–2470.

Pᴀꜱᴄᴏᴇ, R., Hooᴘᴇʀ, R. J., Sᴛᴏʀʜᴀᴜɢ, K., & Hᴀʀᴘᴇʀ, H. (1999). Evolution of extensional styles at the southern termination of the Nordland Ridge, Mid-Norway: a response to variations in coupling above Triassic salt. In A. J. Fleet & S. A. R. Boldy (Eds.), *Petroleum Geology of Northwest Europe: Proceedings of the 5th Conference*, 83–90. doi:10.1144/0050083

Pɪᴄʜoᴛ, T., & Nᴀʟᴘᴀꜱ, T. (2009). Influence of synkinematic sedimentation in a thrust system with two decollement levels; analogue modelling. *Tectonophysics, 473*, 466–475. doi:10.1016/j.tecto.2009.04.003

Pʟᴀ, O., Muñoᴢ, J. A., Fᴇʀʀᴇʀ, O., Rocᴀ, E., Gʀᴀᴛᴀᴄós, O., & Rᴀᴍíʀᴇᴢ, B. (2015). Halokinetic deformations during the development of detachment folds on multilayered syn-orogenic evaporitic sequences. results from analogue modeling and comparison with the Sanaüja anticline (Ebro foreland basin, Iberian Peninsula). Oral communication presented at the American Association of Petroleum Geologists International Conference & Exhibition 2015, Melbourne, Australia.

Pʟᴀ, O., Rocᴀ, E., Xɪᴇ, H., IᴢQᴜɪᴇʀᴅo-Lʟᴀᴠᴀʟʟ, E., Muñoᴢ, J. A., Rowᴀɴ, M. G., Fᴇʀʀᴇʀ, O., Gʀᴀᴛᴀᴄós, O., Yuᴀɴ, N., & Huᴀɴɢ, S. (in review). Influence of syntectonic sedimentation and décollement rheology on the geometry and evolution of orogenic

wedges: analogue modeling of the Kuqa fold-and-thrust belt (NW China). *Tectonics, XX*, XXX–XXX.

Pʟᴀᴛᴛ, J. P., Aʟʟᴇʀᴛoɴ, S., Kɪʀᴋᴇʀ, A., Mᴀɴᴅᴇᴠɪʟʟᴇ, C., Mᴀʏғɪᴇʟᴅ, A., Pʟᴀᴛᴢᴍᴀɴ, E. S., & Rɪᴍɪ, A. (2003). The ultimate arc: Differential displacement, oroclinal bending, and vertical axis rotation in the External Betic-Rif arc. *Tectonics, 22*. doi:10.1029/2001TC001321

Poʙʟᴇᴛ, J., & Hᴀʀᴅʏ, S. (1995). Reverse modelling of detachment folds; application to the Pico del Aguila anticline in the South Central Pyrenees (Spain). *Journal of Structural Geology, 17*. doi:10.1016/0191-8141(95)00059-M

Poʙʟᴇᴛ, J., & McCʟᴀʏ, K. (1996). Geometry and kinematics of single-layer detachment folds. *American Association of Petroleum Geologists Bulletin, 80*, 1085–1109. doi:10.1306/64ED8CA0-1724-11D7-8645000102C1865D

Poʙʟᴇᴛ, J., McCʟᴀʏ, K., Sᴛoʀᴛɪ, F., & Muñoᴢ, J. A. (1997). Geometries of syntectonic sediments associated with single-layer detachment folds. *Journal of Structural Geology, 19*, 369–381. doi:10.1016/S0191-8141(96)00113-7

Puɢᴀ, E., Fᴀɴɴɪɴɢ, M., Díᴀᴢ ᴅᴇ Fᴇᴅᴇʀɪᴄo, A., Nɪᴇᴛo, J. M., Bᴇᴄᴄᴀʟᴜᴠᴀ, L., Bɪᴀɴᴄʜɪɴɪ, G., & Díᴀᴢ Puɢᴀ, M. A. (2011). Petrology, geochemistry and U-Pb geochronology of the Betic Ophiolites: Inferences for Pangaea break-up and birth of the westernmost Tethys Ocean. *Lithos, 124*, 255–272. doi:10.1016/j.lithos.2011.01.002

Rᴀᴍʙᴇʀɢ, H. (1960). Relationships between length of arc and thickness of ptygmatically folded veins. *American Journal of Science, 258*, 36–46.

Rᴀᴍʙᴇʀɢ, H. (1964). Selective buckling of composite layers with contrasted rheological properties, a theory for simultaneous formation of several orders of folds. *Tectonophysics, 1*, 307–341.

**REFERENCES**

Ramsay, R. G. (1967). *Folding and Fracturing of Rocks*. London, England: McGraw-Hill.

Rasmussen, E. S., Lomholt, S., Andersen, C., & Vejbæk, O. V. (1998). Aspects of the structural evolution of the Lusitanian Basin in Portugal and the shelf and slope area offshore Portugal. *Tectonophysics*, *300*, 199–225. doi:10.1016/S0040-1951(98)00241-8

Richardson, N. J., Underhill, J. R., & Lewis, G. (2005). The role of evaporite mobility in modifying subsidence patterns during normal fault growth and linkage, Halten Terrace, Mid-Norway. *Basin Research*, *17*, 203–223. doi:10.1111/j.1365-2117.2005.00250.x

Roca, E., Anadón, P., Utrilla, R., & Vázquez, A. (1996). Rise, closure and reactivation of the Bicorb-Quesa evaporite diapir, eastern Prebetics, Spain. *Journal of the Geological Society*, *153*, 311–321.

Roca, E., Beamud, E., Rubinat, M., Soto, R., & Ferrer, O. (2013). Paleomagnetic and inner diapiric structural constraints on the kinematic evolution of a salt-wall: The Bicorb-Quesa and northern Navarrés salt-wall segments case (Prebetic Zone, SE Iberia). *Journal of Structural Geology*, *52*, 80–95. doi:10.1016/j.jsg.2013.04.003

Roca, E., Sans, M., & Koyi, H. A. (2006). Polyphase deformation of diapiric areas in models and in the eastern Prebetics (Spain). *American Association of Petroleum Geologists Bulletin*, *90*, 115–136. doi:10.1306/07260504096

Rojo, L. A., & Escalona, A. (2018). Controls on minibasin infill in the Nordkapp Basin: Evidence of complex Triassic synsedimentary deposition influenced by salt tectonics. *American Association of Petroleum Geologists Bulletin*, *102*, 1239–1272. doi:10.1306/0926171524316523

Roma, M., Ferrer, O., Roca, E., Pla, O., Escosa, F. O., & Butillé, M. (2018). Formation and inversion of salt-detached ramp-syncline basins. Results from analog modeling and application to the Columbrets Basin (Western Mediterranean). *Tectonophysics*, *745*, 214–228. doi:10.1016/j.tecto.2018.08.012

Rowan, M. G. (1993). A systematic technique for the sequential restoration of salt structures. *Tectonophysics*, *228*, 331–348. doi:10.1016/0040-1951(93)90347-M

Rowan, M. G. (1995). Structural styles and evolution of allochthonous salt, central Louisiana outer shelf and upper slope. In M. P. A. Jackson, D. G. Roberts & S. Snelson (Eds.), *Salt tectonics: A global perspective*, *American Association of Petroleum Geologists, Memoir 65*, 199–228.

Rowan, M. G., & Inman, K. F. (2005). Counterregional-Style deformation in the deep ahelf of the northern Gulf of Mexico. *Gulf Coast Association of Geological Societies Transactions*, *55*, 947–969.

Rowan, M. G., & Inman, K. F. (2011). Salt-related deformation recorded by allochthonous salt rather than growth strata. *Gulf Coast Association of Geological Societies Transactions*, *61*, 379–390.

Rowan, M. G., & Kligfield, R. (1989). Cross section restoration and balancing as an aid to seismic interpretation in extensional terranes. *American Association of Petroleum Geologists Bulletin*, *73*, 955–966.

Rowan, M. G., & Lindsø, S. (2017). Salt tectonics of the Norwegian Barents Sea and Northeast Greenland Shelf. In J. I. Soto, J. F. Flinch & G. Tari (Eds.), *Permo-Triassic Salt Provinces of Europe, North Africa and the Atlantic Margins* (pp. 265–286). Amsterdam, the Netherlands: Elsevier.

Rowan, M. G., & Ratliff, R. A. (2012). Cross-section restoration of salt-related deformation: Best practices and potential pitfalls. *Journal of Structural Geology*, *41*, 24–37. doi:10.1016/j.jsg.2011.12.012

Rowan, M. G., & Vendeville, B. C. (2006). Foldbelts with early salt withdrawal and diapirism: Physical model and examples from the northern Gulf of Mexico and the Flinders Ranges, Australia. *Marine and Petroleum Geology*, *23*, 871–891. doi:10.1016/j.marpetgeo.2006.08.003

Rowan, M. G., Giles, K. A., Hearon IV, T. E., & Fiduk, J. C. (2016). Megaflaps adjacent to salt diapirs. *American Association of Petroleum Geologists Bulletin*, *11*, 1723–1747. doi:10.1306/05241616009

Rowan, M. G., Jackson, M. P. A., & Trudgill, B. D. (1999). Salt-Related Fault Families and Fault Welds in the Northern Gulf of Mexico. *American Association of Petroleum Geologists Bulletin*, *9*, 1454–1484.

Rowan, M. G., Lawton, T. F., Giles, K. A., & Ratliff, R. A. (2003). Near-salt deformation in La Popa basin, Mexico, and the northern Gulf of Mexico: A general model for passive diapirism. *American Association of Petroleum Geologists Bulletin*, *87*, 733–756. doi:10.1306/01150302012

Rowan, M. G., Peel, F. J., & Vendeville, B. C. (2004). Gravity-driven Fold Belts on Passive Margins. *American Association of Petroleum Geologists Memoir*, *82*, 157–182.

Rowan, M. G., Villamil, T., Flemings, P. B., & Weimer, P. (1996). Use of cross-section restoration to determine paleobathymetry and sea-floor paleotopography in the Gulf of Mexico basin. *Geology*, *24*, 299–302. doi:10.1130/0091-7613(1996)024<0299:UO CSRT>2.3.CO;2

Rubinat, M., Ledo, J., Roca, E., Rosell, O., & Queralt, P. (2010). Magnetotelluric characterization of a salt diapir: a case study on Bicorb-Quesa Diapir (Prebetic Zone, SE Spain). *Journal of the Geological Society*, *167*, 145–153. doi:10.1144/0016-76492009-029

Rubinat, M., Roca, E., Escalas, M., Queralt, P., Ferrer, O., & Ledo, J.J. (2013). The influence of basement structure on the evolution of the Bicorb-Quesa Diapir (eastern Betics, Iberian Peninsula): contractive thin-skinned deformation above a pre-existing extensional basement fault. *International Journal of Earth Sciences*, *102*, 25–41. doi:10.1007/s00531-012-0789-9

Sans, M. (2003). From thrust tectonics to diapirism. The role of evaporites in the kinematic evolution of the eastern South Pyrenean front. *Geologica Acta*, *1*, 239–259.

Sans, M., & Koyi, H. A. (2001). Modeling the role of erosion in diapir development in contractional settings. In H. A. Koyi & N. S. Mancktelow (Eds.), *Tectonic modeling: a volume in honor of Hans Ramberg, Geological Society of America Memoir*, *193*, 111–122.

Saura, E., Vergés, J., Martín-Martín, J. D., Messager, G., Moragas, M., Razin, P., Grélaud, C., Joussiaume, R., Malaval, M., Homke, S., & Hunt, D. W. (2014). Syn- to post-rift diapirism and minibasins of the Central High Atlas (Morocco): the changing face of a mountain belt. *Journal of the Geological Society*, *171*, 97–105.

Schettino, A., & Turco, E. (2011). Tectonic history of the western Tethys since the Late Triassic. *Geological Society of America Bulletin*, *123*, 89–105. doi:10.1130/B30064.1

Schultz-Ela, D. D. (1992). Restoration of cross-sections to constrain deformation processes of extensional terranes. *Marine and Petroleum Geology*, *9*, 372–388. doi:10.1016/0264-8172(92)90049-K

Schultz-Ela, D. D., Jackson, M. P. A., & Vendeville, B. C. (1993). Mechanics of active salt diapirism. *Tectonophysics*, *228*, 275–312. doi:10.1016/0040-1951(93)90345-K

Schuster, D. C. (1995). Deformation of allochthonous salt and evolution of related salt – structural systems, Eastern Louisiana Gulf Coast. *American Association of Petroleum Geologists Memoir*, *65*, 177–198. doi:10.1306/D9CB6371-1715-11D7-8645000102C1865D

Senseny, P. E., Hansen, F. D., Russell, J. E., Carter, N. L., & Handin, J. W. (1992). Mechanical behaviour of rock salt: Phenomenology and micromechanisms. International *Journal of Rock Mechanics, Mining Sciences and Geomechanics*, *29*, 363–378. doi:10.1016/0148-9062(92)90513-Y

**REFERENCES**

SHAW J. H., & SUPPE J. (1994). Active faulting and growth folding in the eastern Santa Barbara Channel, California. *Geological Society of America Bulletin*, *106*, 607–626.

SHERKATI, S., MOLINARO, M., FRIZON DE LAMOTTE, D., & LETOUZEY, J. (2005). Detachment folding in the Central and Eastern Zagros fold belt (Iran). *Journal of Structural Geology*, *27*, 1680–1696. doi:10.1016/j.jsg.2005.05.010

SHOEMAKER, E. M., CASE, J. E., & ELSTON, D. P. (1958). *Salt anticlines of the Paradox Basin. Guidebook 9th Annual Field Conference* (pp. 39–59). Salt Lake City, Utah: Intermountain Association of Petroleum Geologists.

SIMS, D. W., MORRIS, A. P., WYRICK, D. Y., FERRILL, D. A., WAITING, D. J., FRANKLIN, N. M., COLTON, S. L., UMEZAWA, Y. T., TAKANASHI, M., & BEVERLY, E. J. (2013). Analog modeling of normal faulting above Middle East domes during regional extension. *American Association of Petroleum Geologists Bulletin*, *97*, 877–898. doi:10.1306/02101209136

SPAKMAN, W., & WORTEL, R. (2004). A tomographic view on western Mediterranean geodynamics. In W. Cavazza, F. Roure, W. Spakman, G. M. Stampfli & P. Ziegler (Eds.), *The TRANSMED Atlas: The Mediterranean Region from Crust to Mantle* (pp. 31–52). Berlin, Germany: Springer Heidelberg.

SRIVASTAVA, S. P., SCHOUTEN, H., ROEST, W. R., KLITGORD, K. D., KOVACS, L. C., VERHOEF, J., MACNAB, R. (1990). Iberian plate kinematic: a jumping between Eurasia and Africa. *Nature, 344*, 756–759.

STAUFFER, M. R. (1964). The geometry of conical folds. *New Zealand Journal of Geology and Geophysics*, *7*, 340–347.

STEFANESCU, M., DICEA, O., & TARI, G. (2000). Influence of extension and compression on salt diapirism in its type area, East Carpathians Bend area, Romania. In B. Vendeville, Y. Mart & J. -L. Vigneresse (Eds.), *Salt, Shale and Igneous Diapirs in and around Europe. Geological Society, London, Special Publications*, *174*, 131–

147. doi:10.1144/gsl.sp.1999.174.01.08

STEWART, S.A. (1999). Geometry of thin-skinned tectonic systems in relation to detachment layer thickness in sedimentary basins. *Tectonics*, *18*, 719–732. doi:10.1029/1999TC900018

STEWART, S. A. (2006). Implications of passive salt diapir kinematics for reservoir segmentation by radial and concentric faults. *Marine and Petroleum Geology*, *23*, 843–853. doi:10.1016/j.marpetgeo.2006.04.001

STEWART, S. A. (2007). Salt tectonics in the North Sea Basin: a structural style template for seismic interpreters. In A. C. Ries, R. W. H. Butler, & R. H. Graham (Eds.), *Geological Society, London, Special Publications*, *272*, 361–396. doi:10.1144/GSL.SP.2007.272.01.19

SUPPE, J. (1983). Geometry and Kinematics of fault-bend folding. A*merican Journal of Science*, *283*, 684- 721.

SUPPE, J. (1985). *Principles of Structural Geology*. Englewood Cliffs, New Jersey: Prentice-Hall.

SUPPE, J., SÀBAT, F., MUÑOZ, J. A., POBLET, J., ROCA, E., & VERGÉS, J. (1997). Bed-by-bed fold growth by kink-band migration: Sant llorenç de Morunys, eastern Pyrenees. *Journal of Structural Geology*, *19*, 443–461. doi:10.1016/S0191-8141(96)00103-4

TALBOT, C. J. (1995). Molding of salt diapirs by stiff overburden. In M. P. A. Jackson, D. G. Roberts & S. Snelson (Eds.), *Salt tectonics: A global perspective, American Association of Petroleum Geologists, Memoir, 65*, 61–75.

TALBOT, C. J. (1998). Extrusions of Hormuz Salt in Iran. In D. J. Blundell & A. C. Scott (Eds.), *Lyell: The past is the key to the present. Geological Society, Special Publication*, *143*, 315–334.

TALBOT, C. J., & JARVIS, R. J. (1984). Age, budget and dynamics of an active salt extrusion in Iran. *Journal of Structural Geology*, 6, 521–533. doi:10.1016/0191-8141(84)90062-2

TARI, G., & JABOUR, H. (2013). Salt tectonics along the Atlantic margin of Morocco. In W. U. Mohriak, A. Danforth, P. J. Post, D. E. Brown, G. C. Tari, M. Nemcok & S. T. Sinha (Eds.), *Conjugate Divergent Margins. Geological Society, London, Special Publications*, *369*, 337–353. doi:10.1144/sp369.23

TIMBEL, C. B. (2015). *Uncompahgre fault geometry: a seismic, field, and gravity study near nucla, Colorado, Paradox Basin, USA*. MSc. Thesis, Colorado School of Mines, Golden, Colorado.

TORRES-ROLDÁN, R. L. (1979). The tectonic subdivision of the Betic Zone (Betic Cordilleras, southern Spain): its significance and one possible geotectonic scenario for the westernmost Alpine belt. *American Journal of Science*, *279*, 19–51.

TRUDGILL, B. D. (2011). Evolution of salt structures in the northern Paradox Basin: controls on evaporite deposition, salt wall growth and supra-salt stratigraphic architecture. *Basin Research*, *23*, 208–238. doi:10.1111/j.1365-2117.2010.00478.x

TRUDGILL, B. D., & ROWAN, M. G. (2004). Integrating 3D seismic data with structural restorations to elucidate the evolution of a stepped counter-regional salt system, Eastern Louisiana Shelf, Northern Gulf of Mexico. In R. J. Davies, J. A. Cartwright, S. A. Stewart, M. Lappin & J. R. Underhill (Eds.), *3D Seismic Technology: Application to the Exploration of Sedimentary Basins*, *29*, 165–176. doi:10.1144/GSL.MEM.2004.029.01.16

TRUSHEIM, F. (1960). Mechanism of Salt Migration in Northern Germany. *American Association of Petroleum Geologists Bulletin*, *44*, 1519–1540. doi:10.1306/0BDA61CA-16BD-11D7-8645000102C1865D

VENDEVILLE, B. C., & JACKSON, M. P. A. (1992a). The rise of diapirs during thin-skinned extension. *Marine and Petroleum Geology*, *9*, 331–354. doi:10.1016/0264-8172(92)90047-I

VENDEVILLE, B. C., & JACKSON, M. P. A. (1992b). The fall of diapirs during thin-skinned extension*. *Marine and Petroleum Geology*, *9*, 354–371.

VENDEVILLE, B. C., & NILSEN, K. T. (1995). Episodic growth of salt diapirs driven by horizontal shortening. In C. J. Travis, H. Harrison, M. R. Hudec, B. C. Vendeville, F. J. Peel & B. F. Perkins (Eds.), *Salt, Sediment and Hydrocarbons* (pp. 285–295). Houston, Texas: 10th Annual Research Conference, Gulf Coast Section, SEPM Foundation.

VENDEVILLE, B., GE, H., & JACKSON, M. P. A. (1995). Scale models of salt tectonics during basement-involved extension. *Petroleum Geoscience*, *1*, 179–183.

VERA, J. A. (2004). *Geología de España*. Madrid, Spain: Sociedad Geológica de España and Instituto Geológico y Minero de España.

VERGÉS, J., & FERNÀNDEZ, M. (2012). Tethys–Atlantic interaction along the Iberia–Africa plate boundary: The Betic–Rif orogenic system. *Tectonophysics*, *579*, 144–172. doi:10.1016/j.tecto.2012.08.032

VOLOZH, Y., TALBOT, C., & ISMAIL-ZADEH, A. (2003). Salt structures and hydrocarbons in the Precaspian basin. *American Association of Petroleum Geologists Bulletin*, *87*, 313–334. doi:10.1306/09060200896

WALLNER, M. (1983). Stability calculations concerning a room pillar design in rock salt. Paper presented at the 5th Congress, International Society for Rock Mechanics, Mebourne, Australia.

WAGNER III, B. H. (2010). *An analysis of salt welding*. Ph.D. Thesis, The University of Texas at Austin, Austin, Texas.

WARREN, J. K. (2006). *Evaporites: sediments, resources and hydrocarbons*. Berlin, Germany: Springer.

Webb, B. C., Lawrence, D. J. D. (1986). Conical fold terminations in the Bannisdale Slates of the English Lake District. *Journal of Structural Geology*, *8*, 79–86.

White, M. A., & Jacobson, M. I. (1983). Structures associated with the southwest margin of the ancestral Uncompahgre Uplift. In W. R. Averett (Ed.), *Northern Paradox Basin – Uncompahgre uplift* (pp. 33–39). Grand Junction, Colorado: Grand Junction Geological Society.

Wilson, G. (1967). The geometry of cylindrical and conical folds. *Proceedings of the Geological Association*, *18*, 179–210.

Withjack, M. O., & Callaway, S. (2000). Active normal faulting beneath a salt layer: An experimental study of deformation patterns in the cover sequence. *American Association of Petroleum Geologists Bulletin*, *84*, 627–651. doi:10.1306/c9ebce73-1735-11d7-8645000102c1865d

Withjack, M. O., & Scheiner, C. (1982). Fault patterns associated with domes-an experimental and analytical study. *American Association of Petroleum Geologists Bulletin*, *66*, 302–316. doi:10.1016/0148-9062(82)90318-7

Withjack, M.O., Meisling, K.E. & Russell, L.R. (1989). Forced folding and basement detached normal faulting in the Haltenbanken area, offshore Norway. In A. J. Tankard & H. R. Balkwill (Eds.), *Extensional Tectonics and Stratigraphy of the North Atlantic Margins, American Association of Petroleum Geololgist Memoir*, *46*, 567–575.

Withjack, M. O., Olson, J., & Peterson, E. (1990). Experimental models of extensional forced folds. *American Association of Petroleum Geologists Bulletin*, *74*, 1038–1054.

Woodward, N. B., Boyer, S. E., & Suppe, J. (1985). *An outline of balanced cross-sections (2nd edition)*. Knoxville, Tennesse: Department of Geological Sciences, University of Tennessee.

Yin, H., & Groshong, R. H. (2007). A three-dimensional kinematic model for the deformation above an active diapir. *American Association of Petroleum Geologists Bulletin*, *91*, 343–363. doi:10.1306/10240606034

Ziegler, P. A. (1982). *Geological Atlas of Western and Central Europe*. Amsterdam, The Netherlands: Elsevier.

Ziegler, P. A. (1989). Evolution of the north Atlantic–an overview. In A. J. Tankard & H .R. Balkwell (Eds.), *Extensional Tectonics and Stratigraphy of the North Atlantic Margins. American Association of Petroleum Geologists Memoir*, *46*, 111–129.

ANNEXES

**Annex 1: "Lateral Terminations of salt walls and megaflaps: An example from Gypsum Valley Diapir, Paradox Basin, Colorado, USA".**

**ORIGINAL ARTICLE**

WILEY · Basin Research · IAS EAGE

# Lateral terminations of salt walls and megaflaps: An example from Gypsum Valley Diapir, Paradox Basin, Colorado, USA

Frederic O. Escosa[1] (iD) | Mark G. Rowan[2] | Katherine A. Giles[3] | Kyle T. Deatrick[3] | Allison M. Mast[3] | Richard P. Langford[3] | Thomas E. Hearon IV[4] | Eduard Roca[1]

[1]Institut de Recerca Geomodels, Departament de Dinàmica de la Terra i de l'Oceà, Facultat de Ciències de la Terra, Universitat de Barcelona, Barcelona, Spain

[2]Rowan Consulting, Inc., Boulder, Colorado

[3]Institute of Tectonic Studies, Department of Geological Sciences, The University of Texas at El Paso, El Paso, Texas

[4]EOG Resources, Inc., Houston, Texas

**Correspondence**
Frederic O. Escosa, Institut de Recerca Geomodels, Departament de Dinàmica de la Terra i de l'Oceà, Facultat de Ciències de la Terra, Universitat de Barcelona, Barcelona, c/Martí i Franquès s/n, 08028, Spain.
Email: fredescosa@ub.edu

**Funding information**
Universitat de Barcelona, Grant/Award Number: SALTECRES (CGL2014-54118-C2-1-R); The University of Texas at El Paso; BHP; ExxonMobil; Hess; Kosmos; Repsol; BP; Chevron; ConocoPhillips; Shell

**Abstract**

Descriptions of exposed salt structures help improve the ability to interpret the geometry and evolution of similar structures imaged in seismic reflection data from salt-bearing sedimentary basins. This study uses detailed geologic mapping combined with well and seismic data from the southeastern end of the Gypsum Valley diapir (Paradox Basin, Colorado), to investigate the three-dimensional geometry of the terminations of both the salt wall and its associated megaflap. The salt wall trends NW-SE and is characterized by highly asymmetric stratal architecture on its northeastern and southwestern flanks, with thicker, deeper, gently dipping strata in the depositionally proximal (NE) minibasin and thinned older strata rotated to near-vertical in a megaflap on the distal (SW) side. The megaflap terminates to the SE through a decrease in maximum dip and ultimately truncation by a pair of radial faults bounding a down-dropped block with lower dips. East of these faults, the salt wall termination is a moderately plunging nose of salt overlain by gently southeast-dipping strata, separated from the down-dropped NE minibasin by a counterregional fault. From this analysis, and by comparison with analogue structures located elsewhere in the Paradox Basin and in the northern Gulf of Mexico, we propose a series of simple end-member models in which salt walls and megaflaps may terminate abruptly or gradually. We suggest that controlling factors in determining these geometries include the original thickness and spatial distribution of the deep salt, the presence of nearby diapirs (which determines the fetch area for salt flow into the diapir), spatial patterns of depositional loading, and variations in the nature and location of salt breakout through the roof of the initial salt structure.

**KEYWORDS**
megaflaps, Paradox Basin, radial faults and counterregional faults, salt diapirs, salt walls

## 1 | INTRODUCTION

Steep-sided salt diapirs can have variable map-view shapes. They are termed salt stocks when the planform axial ratio is <2, and salt walls when it is >2 (Hudec & Jackson, 2011; Trusheim, 1960). Salt walls may form in a variety of tectonic settings. For example, they may result from extension (e.g. Zechstein Basin, Krzywiec, 2006; Mohr, Kukla,

Urai, & Bresser, 2005; Atlas Mountains, Martín-Martín et al., 2016; Saura et al., 2013; Newfoundland, Balkwill & Legall, 1989). When the thick-skinned extension is decoupled by the presence of autochthonous salt, the walls typically develop above or slightly on the footwalls of the main presalt faults (Jackson & Vendeville, 1994). Conversely, salt walls may form during contraction (e.g. Sverdrup Basin, Harrison & Jackson, 2014; Sivas Basin, Kergaravat et al., 2016). For example, a salt-cored contractional anticline may be eroded, so that salt breaks through to form elongate diapirs (Stewart, 2007). Salt walls may also form by differential loading in the absence of extension or contraction (e.g. Paradox Basin, Trudgill, 2011; La Popa Basin, Rowan, Lawton, Giles, & Ratliff, 2003; Nordkapp Basin, Rowan & Lindsø, 2017), when progradational loading causes inflation above or immediately updip of the pre-existing presalt faults (Ge, Jackson, & Vendeville, 1997). In most cases, regardless of the triggering mechanism, they grow as passive diapirs once the salt has pierced its initial roof.

Stratal geometries flanking salt walls typically range from halokinetic sequences to megaflaps, depending on the scale of near-diapir deformation. Halokinetic sequences are localized (<1 km wide), unconformity-bound successions of growth strata that form as drape folds due to the interplay between the salt-rise rate and the sediment-accumulation rate (Giles & Lawton, 2002; Rowan et al., 2003). Stacked halokinetic sequences form tabular and tapered composite halokinetic sequences, which have relatively narrow and broad zones of thinning, respectively (Giles & Rowan, 2012). Megaflaps are panels of deep minibasin strata that extend far up the sides of steep diapirs or their equivalent welds (Giles & Rowan, 2012; Graham, Jackson, Pilcher, & Kilsdonk, 2012; Rowan, Giles, Hearon, & Fiduk, 2016). The width of folding and vertical relief of megaflaps span multiple kilometres, with the maximum bedding attitude ranging from near-vertical to completely overturned beneath an allochthonous salt sheet.

Many studies have focused on cross-sectional views of near-diapir deformation and thus are primarily two dimensional; three-dimensional analyses are relatively rare. Rowan, Lawton, and Giles (2012) showed along-strike variations in minibasin-scale folding, local halokinetic drape folding, and small-scale deformation of a welded salt wall in La Popa Basin. Similarly, Martín-Martín et al. (2016) determined the 3D geometry of the Tazoult salt wall in Morocco (including megaflaps), showing along-strike variations of flanking stratal geometries. In both cases the variations in stratal geometries were explained as being caused, in part by changes in the style and/or amount of shortening along the lengths of the walls. In contrast, Hearon, Rowan, Giles, and Hart (2014) tracked composite halokinetic sequences around the Auger salt

**Highlights**

- The Gypsum Valley salt wall is characterized by highly asymmetric stratal architecture on its NE and SW flanks.
- The SW flank comprises thinned, rotated strata in a megaflap that terminates to the SE by a decrease in dip and truncation by a radial fault.
- Strata on the NE flank are thicker, deeper, and only gently folded.
- The salt wall terminates to the SE in a moderately plunging nose of salt in the footwall of a NE-dipping counterregional fault.
- We propose end-member models in which salt walls and megaflaps may terminate abruptly or gradually.
- Controlling factors include the deep salt budget, the depositional loading pattern, and the position where the salts breaks through its early roof.

stock in the northern Gulf of Mexico, demonstrating that composite halokinetic sequences progressively change in geometry around the margin of the diapir and suggesting this was caused by local variations in diapir-roof thickness. Despite these studies, very little is known about strike-parallel changes in structural and stratigraphic architecture at the terminations of salt walls or megaflaps. Investigating this variability is important for a better understanding of salt-sediment interaction in three dimensions, as well as for aiding interpretations of poorly imaged seismic reflection data and thus risk assessment in hydrocarbon exploration.

The purpose of this paper is to present new data from the southeastern end of the Gypsum Valley salt wall, in the Paradox Basin of SW Colorado, in order to evaluate the structural styles and associated controls on lateral terminations of salt walls and megaflaps. The main goals are three-fold: (a) to build on the brief two-dimensional analysis of the Gypsum Valley megaflap in Rowan et al. (2016) and characterize the 3D structure and kinematic evolution of both the megaflap and southeastern end of the salt wall; (b) to compare our findings with other salt walls in the Paradox Basin, and analogous to counterregional systems in the northern Gulf of Mexico; and (c) to establish simple models for the lateral terminations of salt walls and megaflaps. We suggest that factors controlling the nature and geometry of these lateral terminations include the type and location of bounding structures, the salt budget for flow into the diapir, the spatial patterns of depositional loading, and variations in the style and location of salt breakout through the roof of the initial salt structure.

## 2 | GEOLOGICAL SETTING AND PREVIOUS WORK

### 2.1 | Paradox Basin

The Paradox Basin (SE Utah and SW Colorado, USA), is a large, asymmetric, intracratonic foreland basin defined by the depositional extent of the layered evaporites of the Pennsylvanian Paradox Formation (Figure 1a). The basin measures ca. 300 km in length (NW-SE) and ca. 150 km in width (Condon, 1997; Trudgill, 2011; Whidden, Lillis, Anna, Pearson, & Dubiel, 2013). During the Late Mississippian to Early Permian time, convergent tectonism along the western margin of North America, coupled with the collision of Gondwanaland to the south, generated intraplate deformation in the form of a series of thick-skinned, basement-cored uplifts, extending from Canada to Mexico, known as the Ancestral Rocky Mountains (Barbeau, 2003; Kluth, 1986; Kluth & Coney, 1981; Mallory, 1972). Borehole and 2D seismic reflection data show the Paradox Basin (Figure 1a) is located in the footwall of a 50° NE-dipping reverse fault, with ca. 10 km of slip, bounding the southwestern flank of the basement-cored Uncompahgre Uplift (Moore, Soreghan, & Sweet, 2008;
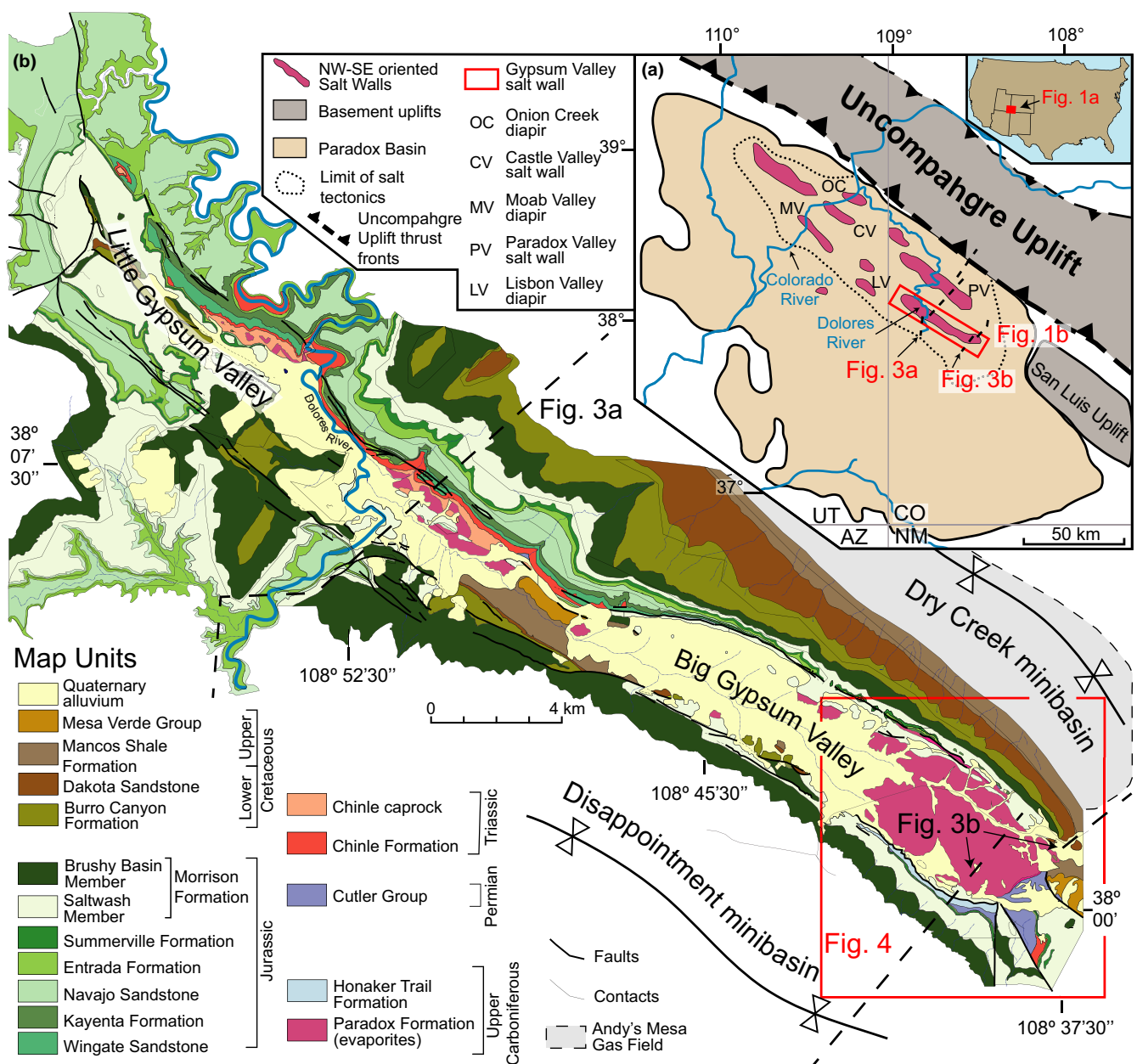


**FIGURE 1** Location map: (a) Paradox Basin and its major salt walls (after Shoemaker, Case, & Elston, 1958); UT: Utah, CO: Colorado, AZ: Arizona, NM: New Mexico; (b) geologic map of Gypsum Valley salt wall. The red outlines indicate, in (a), the location of Fig. 1b, and in (b), the study area illustrated in Figure 4

Timbel, 2015; White & Jacobson, 1983). The emplacement of the Uncompahgre Uplift and concurrent flexural loading of the crust in its foreland created accommodation for sediment infill (Barbeau, 2003; Condon, 1997; DeCelles & Giles, 1996; Trudgill, 2011).

The Paradox Basin contains as much as ca. 7 km of Pennsylvanian to Cretaceous basin fill (Figure 2) adjacent to the Uncompahgre Uplift (Barbeau, 2003; Goldhammer, Oswald, & Dunn, 1994; Trudgill & Paz, 2009). The upper Paleozoic to Mesozoic section comprises four lithostratigraphic units separated by three regional unconformities (Figure 2). At the base is the Middle Pennsylvanian (Desmoinesian) Paradox Fm., a layered evaporite sequence that passes upward to mixed marine carbonates (Honaker Trail Fm.) and marine to nonmarine siliciclastics (lower Cutler Grp.). The mid-Cutler unconformity (which is readily imaged on seismic data; Figure 3a,b) separates this basal unit from those above, which comprise upper Cutler Grp. to Mesozoic alluvial, fluvial and eolian strata. These in turn are separated by two regional unconformities at the bases of the Chinle Fm. (Molenaar, 1981) and Entrada Sst. (Figure 2).

According to Barbeau (2003) and Blakey (2009), maximum subsidence of the Paradox Basin coincided with deposition of the Paradox Fm. evaporites. Subsequent differential loading by prograding Upper Pennsylvanian to Permian fluvial sediment, shed from the Uncompahgre Uplift (Figure 1a), caused salt inflation over presalt normal faults, thereby triggering a series of NW-SE trending salt walls (Baars & Stevenson, 1981; Elston, Shoemaker, & Landis, 1962; Ge et al., 1997; Kluth & DuChene, 2009; Lawton & Buck, 2006; Trudgill, 2011). The onset of diapirism was earlier in proximal (NE) than distal (SW) areas (Trudgill, 2011).

Throughout the basin, passive diapirism was a dominantly Permian event, with activity decreasing during the Triassic (Barbeau, 2003; Elston et al., 1962; Lawton & Buck, 2006; Trudgill, 2011). According to Rasmussen and Rasmussen (2009), diapirism across the deepest part of the basin ended in the Early Triassic. However, Vogel (1960) and later Rowan et al. (2016) interpret diapirism at Gypsum Valley, which is located in a distal position, to have ended by the mid-Jurassic. Importantly, although contraction was involved in the emplacement of the Uncompahgre Uplift, there is no cited evidence for any contraction in the Paradox Basin, except for minor shortening during the

**FIGURE 2** Stratigraphic column of the southern Paradox Basin including: the colours used in the geological map, cross sections and restoration; thickness variations; and simplified lithology with the three main unconformities (after Doelling, 2001; Trudgill, 2011). Salt tectonics phases are specific to the Gypsum Valley diapir and are not necessarily appropriate for other Paradox Basin salt walls
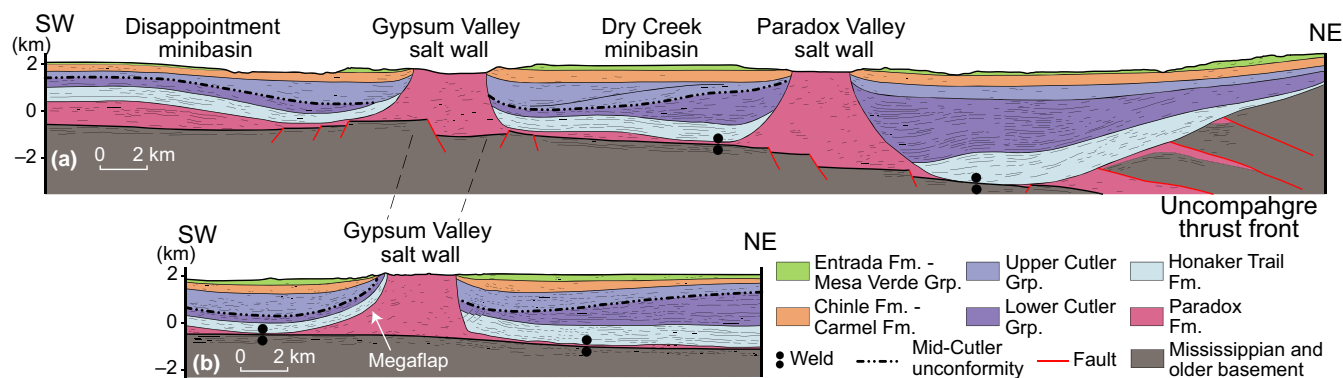
**FIGURE 3** Line drawings of regional depth-converted seismic profiles in the southeastern Paradox Basin (see location in Figure 1): (a) across the centre of Gypsum Valley diapir and the southeastern end of the Paradox Valley diapir; (b) across the study area at the southeastern end of the Gypsum Valley salt wall modified from Rowan et al. (2016). Original data and depth conversions courtesy of ConocoPhillips

Laramide Orogeny, postdating salt wall formation and diapir burial (Mankowski, Campbell, Huntoon, Gregg, & Linari, 2002).

## 2.2 | Gypsum Valley salt wall

The Gypsum Valley diapir is a NW-SE trending vertical salt wall located in the southeastern, distal part of the Paradox Basin in SW Colorado (Figure 1). The salt wall is bounded on the northeastern side by the Dry Creek minibasin and on the southwestern side by the Disappointment minibasin, forming a breached anticline geometry almost 35 km long and from 2 to 3.5 km wide. The core of the structure has been eroded to form the Gypsum Valley physiographic feature, which is divided into a northern, narrower part referred to as Little Gypsum Valley, and a broader, southern part referred to as Big Gypsum Valley. The southeastern termination of the salt wall, at the southern end of the Big Gypsum Valley, is the focus of this study (Figures 1b and 4).

Seismic reflection, well, and field data depict an important asymmetry (Figure 3b) between the bounding minibasins of the study area (Amador, Schurger, & Miller, 2009; Rowan et al., 2016). On the northeastern side (Dry Creek minibasin), older (Upper Pennsylvanian to Permian) strata are relatively thick and deeply buried, with only minor upturn near the diapir. On a broad scale, Cutler Grp. strata form basinward (SW) shifting depocentres (Figure 3a,b) characteristic of expulsion–rollover structures (Ge et al., 1997; Trudgill, 2011). In contrast, the southwestern side (Disappointment minibasin, Figure 3b) is marked by Pennsylvanian strata that gradually becomes thin and upturns to the near-vertical adjacent to the diapir, forming a megaflap (Deatrick, Giles, Langford, Rowan, & Hearon, 2015; Mast, 2016; Rowan et al., 2016).

The general evolution of the southeastern part of this salt wall, based on a 2-D analysis and restoration (Rowan

et al., 2016), is depicted in Figure 5. Salt movement was triggered during the Late Pennsylvanian by differential sedimentary loading, forming an early, asymmetric, single-flap active diapir (Schultz-Ela, Jackson, & Vendeville, 1993) with a thinned roof bounded by a suprasalt counterregional fault over the proximal (NE) edge of the diapir (Figure 5b, c). Erosion of the thinned diapir roof (mid-Cutler unconformity) triggered salt breakthrough and the onset of passive diapirism (Figure 5d). Subsequent evacuation of deep salt into the growing diapir generated diapir-flanking depocentres containing upper Cutler Grp. and younger strata, with progressive rotation of the southwestern flank into the megaflap geometry and consequent widening of the diapir (Figure 5e,f).

## 3 | OBSERVATIONS

### 3.1 | Methods

To achieve the goals outlined for this study, both subsurface and field data were incorporated into the analysis. Subsurface data include one regional 2D depth-converted seismic reflection profile across the southeastern end of the Gypsum Valley salt wall (Figure 3b; Rowan et al., 2016). The interpretation in depth was constrained by horizon tops from 13 wells (see well locations in Figure 4). Field data include more than 1,200 stations with structural and stratigraphic data.

### 3.2 | Stratigraphy

According to field and well data (Baars, 1965; Hite & Buckner, 1981; Mahrer, Ake, O'Connell, & Block, 2012; Timbel, 2015; Weimer 1982), the nonoutcropping presalt units are Cambrian to lowermost Pennsylvanian carbonate and siliciclastic rocks (Figure 2). Overlying this, the thick Paradox Fm. contains 29 cycles of primarily halite,
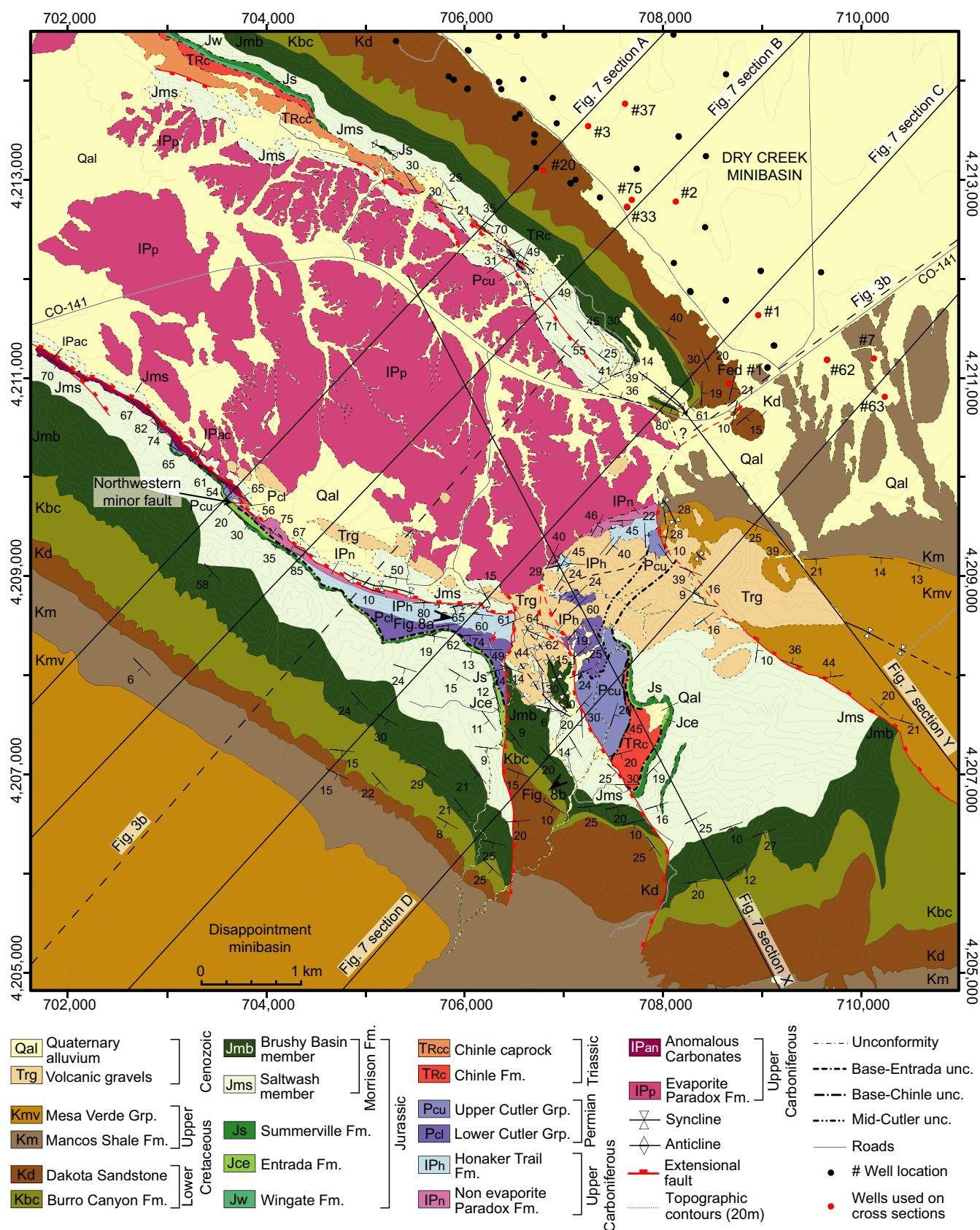
**FIGURE 4** Detailed geologic map of the southeastern termination of the Gypsum Valley salt wall (location in Figure 1b), showing available well data, the trace of the cross sections (Figure 7), and the trace of the seismic profile shown in Figure 3b and restored in Figure 5. Stratigraphic colours and labels as in Figure 2. Coordinates are in metres in Universal Transverse Mercator, zone 12 northern hemisphere and datum NAD83
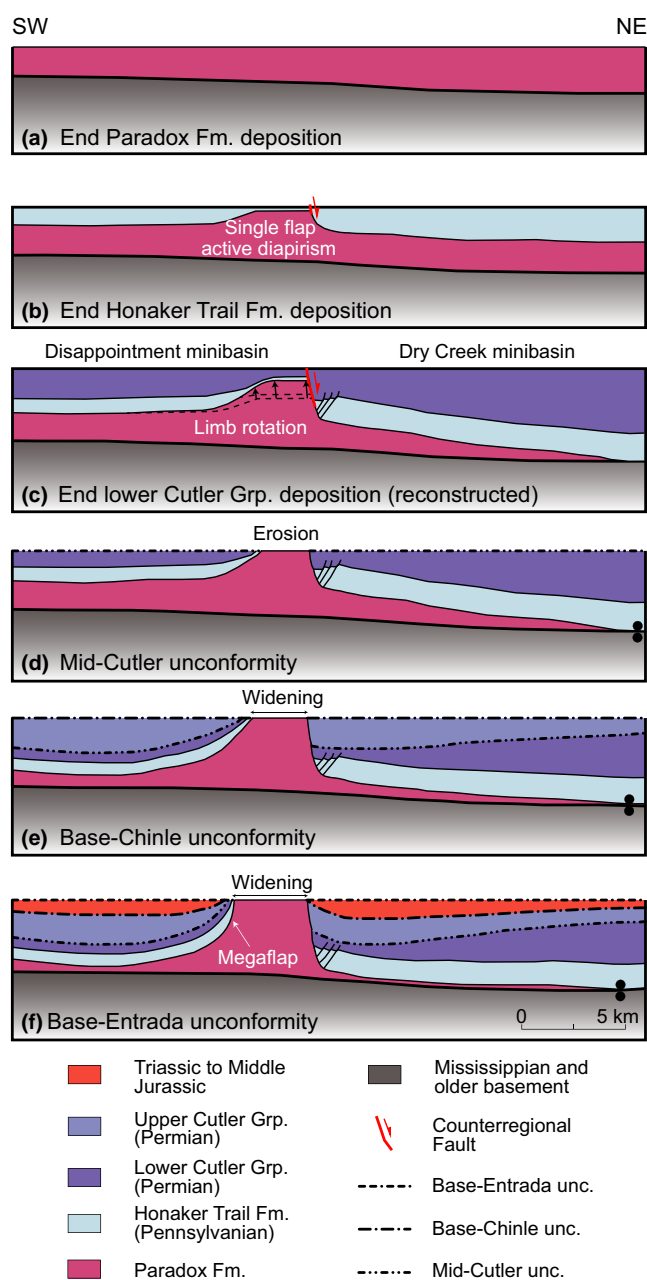
**FIGURE 5** Sequential quantitative restoration of the Gypsum Valley salt wall (modified from Rowan et al., 2016) along the depth-converted seismic profile of Figure 3b

anhydrite, and organic mudstones (Figure 2) that are interbedded with coarse-grained siliciclastics in the fore-deep near the Uncompahgre Uplift and carbonates in the distal margins of the Paradox Basin, which includes Gypsum Valley (Franczyk, 1992; Goldhammer et al., 1994; Hite & Buckner, 1981; Lawton, Buller, & Parr, 2015; Nuccio & Condon, 1996). The Paradox Fm. serves as the salt source for the Gypsum Valley diapir.

Stratal units influenced by concurrent salt tectonics range from the uppermost Ismay member, an informal rock unit of the Upper Pennsylvanian Paradox Fm., through the

Lower Cretaceous Dakota Sst. (Figure 2). On the southwestern flank of the diapir, the thinned package of the megaflap comprises: the uppermost Paradox Fm. shales and carbonates (Mast, 2016), the cyclic carbonate and siliciclastics of the Honaker Trail Fm., and the lower Cutler Grp. carbonates interbedded with shales (Deatrick et al., 2015). Growth strata recording passive diapirism are composed of the following: the upper Cutler Grp., the Moenkopi and Chinle formations, the Glen Canyon Grp. and the San Rafael Grp. (Figure 2). The lower Cutler fossiliferous carbonates and upper Cutler nonmarine red arkosic conglomerates and sandstones are separated by the mid-Cutler unconformity (Barbeau, 2003), and the base-Chinle unconformity divides marine fine-grained sediment of the Moenkopi Fm. from continental red sandstones and conglomerates of the Chinle Fm. (Doelling, 1988; Hazel, 1994; Molenaar, 1981; O'Sullivan & MacLachlan, 1975; Stewart, Poole, & Wilson, 1972). Above the base-Entrada unconformity, eolian and fluvial strata of the San Rafael Grp. (and younger units) have a different relationship to the diapir, overlapping the salt wall, thickening into synclines located over the top of the diapir in the Little Gypsum Valley, or exposed as blocks that have been faulted down onto the top of salt. Finally, the Mancos Shale and Mesa Verde Grp. (Figure 2) were deposited in the Sevier Foreland Basin (Lawton et al., 1997), by which time the salt wall was no longer active and was buried beneath at least a kilometre of sediment.

## 3.3 | Structural geometry

The southeastern end of the Gypsum Valley salt wall is subdivided into five structural domains (SD) that are bounded by different types of faults (Figure 6a). In the sections below, we describe first the faults and then the defining attributes of structural domains and sub-domains, generally moving from the megaflap counter-clockwise around the end of the diapir to the northeastern flank.

### 3.3.1 | Faults

**Northwestern minor fault**

A minor WNW-ESE trending fault on the SW flank of the Gypsum Valley salt wall divides structural domain I into two sub-domains, I′ and I″ (Figure 6a). Although mostly covered by Quaternary sediment, the fault is inferred from the ca. 80 m offset of the Paradox-Cutler contact and associated different attitudes in strata on either side (Figure 4). Although the origin of the fault is unknown, the geometry is compatible with a down-to-the-N normal fault (Figure 7, section A inset). Moreover, it was active relatively early since it terminates at the base-Entrada unconformity (Figures 4 and 6a).
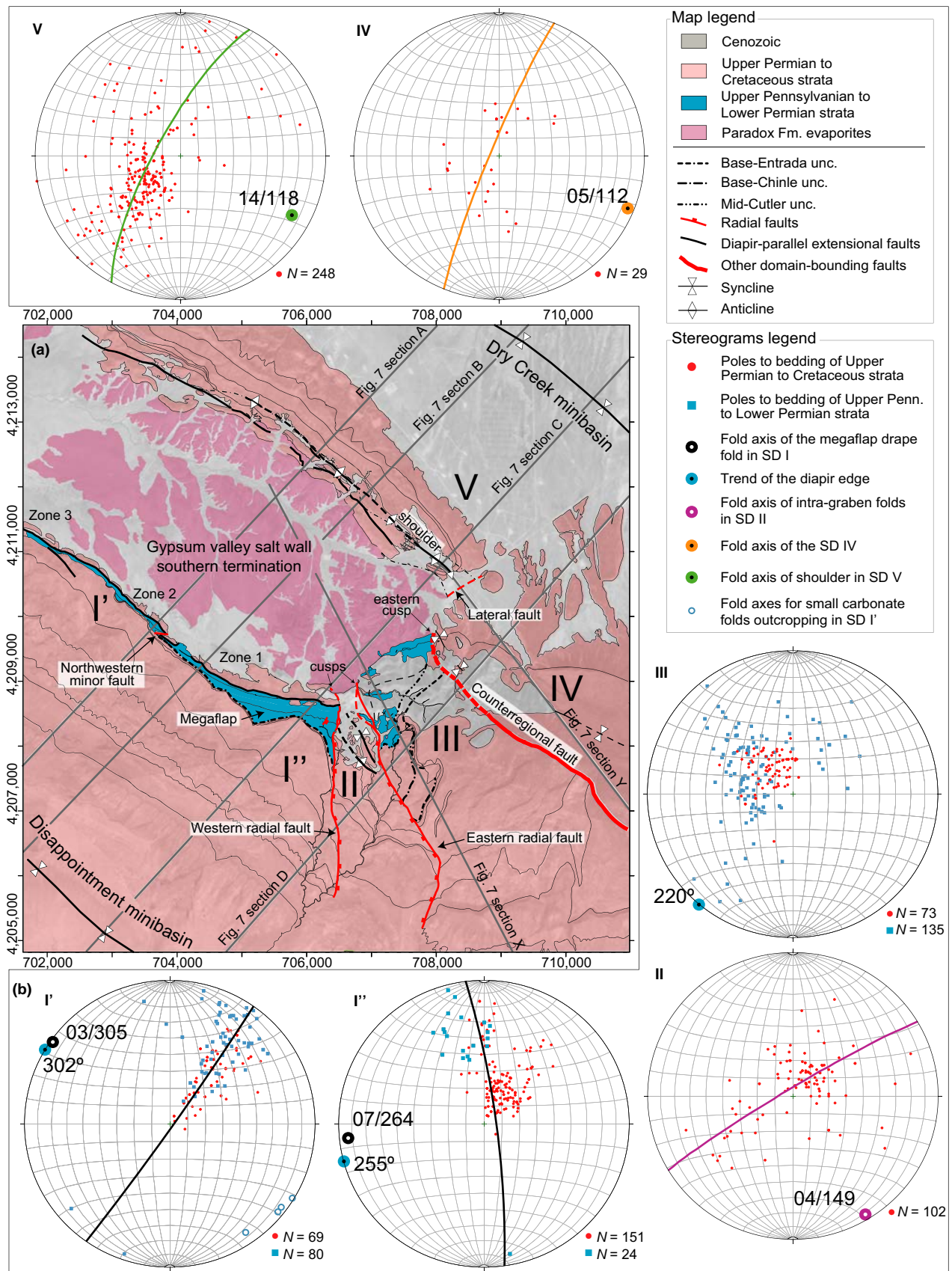
**FIGURE 6** Structural domains: (a) black and white orthophoto overlain by the structural map of the study area and showing the division of the study area into five structural domains (Roman numerals); (b) lower-hemisphere equal-area (Schmidt) stereographic projections of structural data for each domain. Zones 1–3 along megaflap are those of Mast (2016)

**FIGURE 7** Geologic cross sections constructed using surface and sub-surface data (locations in Figures 4 and 6). Vertical dashed lines marked by A–A′, B–B′, C–C′, D–D′ and X–X′ indicate the limits of the geological map shown in Figure 4, vertical solid lines denote the intersections with other cross sections and vertical fine dashed lines indicate wells within 200 m of the cross sections. Stratigraphic colours, labels and unconformity styles as in Figures 2 and 4

**FIGURE 8** (a) Interpreted photo panorama of the megaflap (nonevaporite Paradox Fm., Honaker Trail Fm. and lower Cutler Grp.) and strata above the capping base-Entrada unconformity (Entrada Fm., Summerville Fm. and Morrison Fm.) in SD I″. (b) Interpreted photo panorama of the strata overlying the southeastern termination of the salt wall (SD III). See the location of the photo panoramas in Figure 4. Stratigraphic colours and labels as in Figures 2 and 4. Thin black continuous lines – bedding traces; dot-dashed lines – main unconformities; thick black continuous lines – concordant contacts; red lines – faults; grey lines – topographic mountain profile

## Radial faults

Strata flanking the diapir at its southern corner are cut by the western and eastern radial faults (2.9 and 3.5 km long respectively). They are approximately orthogonal to the diapir edge, diverge away from the diapir, and bound a down-dropped block (Figure 4 and 6a). The N-S trending western fault dips towards the NE and has an estimated throw of *ca*. 480 m on section D (Figure 7) and the NW-SE to NNE-SSW trending eastern fault dips towards the SW and has an estimated throw of *ca*. 400 m (Figure 4 and 7, section D). Both radial faults decrease in throws southwards away from the diapir until they terminate within the Mancos Shale.

## Counterregional fault

A large, NW-SE trending, down-to-the-NE normal fault extends away from the southeastern termination of the Gypsum Valley salt wall (Figure 4 and 7, section D). Because its geometry is analogous to that of counterregional (landward-dipping) faults in the northern Gulf of Mexico, in that it dips towards the source of prograding sediment and curves into the proximal edge of the diapir (Diegel, Karlo, Schuster, Shoup, & Tauvers, 1995; Schuster, 1995), we apply the same terminology. The counterregional fault accommodates more than 1.5 km of throw close to the salt wall, with Honaker Trail Fm. in the footwall and a thickened Upper Pennsylvanian to Cretaceous sequence in its hanging wall (Figure 7, section D). Displacement decreases away from the diapir to the SE (Figure 4).

## Lateral fault

Northeast of where the counterregional fault merges with the diapir is a small, NE-SW trending, down-to-the-SE normal fault (Figure 6a) within the Dakota Sst. Slickenlines plunge 24° and 40° towards 150 and 171, respectively (i.e. NNW-SSE-oriented oblique slip). We do not term this a radial fault because radial faults merely segment drape-folded strata, whereas this fault separates two very different structural domains (see below).

## Diapir-parallel faults

Along both outer edges of the diapir are steep normal faults oriented parallel to the salt wall margin (Figures 4 and 6a). The hanging walls have Morrison Fm. strata down-dropped directly onto the Paradox Fm. evaporites (Figure 7, sections A–C insets).

## 3.3.2 | Structural domains

Diapir-flanking strata around the southeastern termination of the Gypsum Valley salt wall are divided into five SD separated by some of the faults described above (Figure 6a).

## SD I

The southwestern flank of the Gypsum Valley salt wall (SD I) is dominated by the megaflap (Figures 6a and 8a). It is subdivided into two sub-domains (SD I′ and SD I″), separated by the northwestern minor fault (Figures 4 and 6a), according to the character and amount of internal deformation observed within the megaflap, as described below. In addition to the megaflap, another common element is the diapir-parallel normal faults that juxtapose low-dipping Morrison Fm. above the diapir against vertical megaflap strata adjacent to the diapir (Figures 4 and 7, sections A–C).

Although SD I″ is southeast of SD I′, it is described first because it has a simpler character. It is equivalent to Zone 1 of Mast (2016), where the megaflap is composed of two mechanically differentiated but concordant units: (a) an upper unit formed by the Honaker Trail Fm. carbonates and siliciclastics and the lowermost part of the lower Cutler Grp. carbonates; and (b) a lower unit made up of carbonates interbedded with mudstones of the Paradox Fm. (probably corresponding to the uppermost Ismay informal Mbr., Deatrick et al., 2015; Mast, 2016). In other words, the nonevaporite uppermost part of the salt diapir is part of the megaflap.

The megaflap decreases in dip south-eastward, from near-vertical to overturned in the northwestern part of SD I″ to about 60° close to the western radial fault (Figure 4). Above the mid-Cutler unconformity, the upper Cutler Grp. through Lower Jurassic strata form a growth wedge that is truncated beneath the 30–35° dipping base-Entrada unconformity (Figures 4, 7 sections B and C, and 8a). The entire structure (megaflap and capping unconformity) deepens along strike to the northwest so that only the nonevaporite member of the Paradox Fm. is exposed between the unconformity and diapir near the boundary with SD I′ (Figure 4). The fold axis of the megaflap drape fold plunges 7° towards 264°, slightly oblique to the 255° trend of the diapir edge (Figure 6b).

SD I′, like the northwestern part of SD I″, exposes only the uppermost Ismay Mbr. of the Paradox Fm. between the diapir and the mid-Cutler unconformity (Figures 4 and 7, section A). Just NW of the northwestern minor fault (Zone 2 of Mast, 2016; Figure 6a), however, it is characterized by discontinuous dolomite ridges that form short-wavelength, low-amplitude asymmetric folds interbedded with black shales. Fold axes are sub-horizontal (ca. 3°–15° plunge) and roughly parallel to the edge of the diapir and the fold axis of the megaflap panel (Figure 6b). Longer fold limbs are near vertical and shorter limbs dip ca. 70° to the SW, suggesting a NE-side-up sense of shear.

The uppermost Ismay Mbr. in Zone 3 of Mast (2016), at the northwestern end of the megaflap in SD I′ (Figure 6a), contains discordant dolomite blocks. The lithology

is similar to Zone 2 of Mast (2016) and folds are still recognized, but the dolomite blocks appear to be isolated and encased in black shales and marls. Thus, the oldest strata in the megaflap become increasingly deformed towards the NW: they are conformable, without significant internal deformation, in SD I″; they include coherent asymmetric folds in southeastern SD I′; and they are disrupted in northwestern SD I′.

There is no evidence for any structural thinning of the Honaker Trail Fm. and the lowermost part of the lower Cutler Grp. during stratal rotation (Rowan et al., 2016). In addition, well control shows that the Honaker Trail Fm. at the base of the Disappointment minibasin has a thickness intermediate between that within the megaflap and that at the base of the Dry Creek minibasin.

### SD II

SD II is the graben bounded by the two large radial faults at the southern corner of the diapir (Figure 6a). Bedding dips are a maximum of ca. 65° to the SSW near the diapir and gradually decrease southward. Jurassic strata in the northern part of the graben (Figure 4) are folded into a low-amplitude anticline-syncline pair with sub-horizontal fold axes trending roughly parallel to the eastern bounding fault (Figure 6b). The Brushy Basin Mbr. to Dakota Sst. are ca. 150 m thicker within the graben (Figure 7, section D); older strata are not exposed.

### SD III

SD III, located off the southeastern termination of the salt wall, is bounded by the eastern radial fault to the W and the counterregional fault to the NE (Figures 6a and 8b). Strata in SD III form a moderately to gently dipping panel over the plunging nose of the diapir (Figure 7, section X), with maximum dips (45°) close to the diapir (Figures 4 and 6b). Within SD III, the mid-Cutler unconformity progressively cuts out more strata closer to the counterregional fault and the base-Entrada unconformity cuts out more section approaching the diapir (Figures 7, section X and 8b).

### SD IV

SD IV forms the hanging wall of the counterregional fault (Figure 6a). Strata are generally sub-horizontal (Figure 7, sections D and Y), but a broad, gentle syncline with a fold axis plunging 5° towards 112° probably intersects the counterregional fault near its termination against the diapir (Figures 4 and 6b). SD IV is bounded to the NW by SE-dipping strata cut by the lateral fault (Figure 7, section Y).

### SD V

SD V is located along the northeastern flank of the salt wall (Figure 6a). Strata in the Dry Creek minibasin are folded within 2 km of the diapir, with dips as steep as 80°

immediately adjacent to the salt structure (Figure 7, sections A–C). Along most of its length, SD V is bound to the SW by a SW-dipping normal fault with Morrison Fm. strata in its hanging wall adjacent to exposed diapir caprock (Figure 4). The fault dies out towards the SE and is replaced by a SE-plunging asymmetric anticline with a gently-dipping (ca. 20°) NE limb and a steep (ca. 80°) SW limb (Figures 4 and 6b). The fold-axis plunge increases to ca. 60° near the termination of the salt wall, with the SE-dipping strata offset slightly by the lateral fault (Figures 4 and 7, section Y).

## 4 | SUMMARY AND INTERPRETATION

The stratal geometry flanking Gypsum Valley diapir is asymmetric, whereas strata on the SW flank are depositionally thinned and folded to near-vertical in the megaflap, strata on the NE side are thicker, deeper and mostly gently dipping. The asymmetry continues off the southeastern end of the diapir, where the counterregional fault separates SDs III and IV. This style is typical of counterregional systems (Rowan & Inman, 2005; Schuster, 1995), where differential minibasin subsidence is accommodated by a combination of the diapir (Figure 7, sections A–C) and counterregional faults extending off its ends (Figure 7, section D). At the diapir, slip is likely to have been accommodated by shear within the salt, not by a discrete fault at its edge. Because the Honaker Trail Fm. is thin in the footwall of the counterregional fault and along the southwestern flank of the diapir, and thicker in the hanging wall and along the northeastern flank, the asymmetry and counter-regional-style relationship were established from the onset of salt movement (Figure 5). The style of diapirism was that of single-flap active diapirism (Schultz-Ela et al., 1993), not reactive rise.

### 4.1 | Southwest (high) side

There are significant along-strike changes in geometry on the southwestern, upthrown side of the diapir and counterregional fault. The most prominent is the existence of the radial faults and intervening graben (Figures 4 and 6a). These were probably caused by drape folding around a curved edge of salt and the resultant concentric tensile (hoop) stress regime (Coleman, Jackson, Duffy, & Nikolinakou, 2018; Rowan et al., 2003; Stewart, 2006; Figure 9). Indeed, the radial faults are located exactly where the strike direction of the diapir edge and adjacent Honaker Trail Fm. strata changes most abruptly (Figures 4 and 6a). The concentration of radial faults at the ends of the salt wall is compatible with observations from the North Sea (Davison

et al., 2000; Stewart, 2006). The minor folds within the graben are more enigmatic. They may have formed due to crowding as the wider younger section was dropped down into a narrower space (Figure 9); alternatively, they may have formed during late (Laramide) contraction. The onset and duration of radial faulting is unknown, except that the faults were active as late as during deposition of the Mancos Shale Fm. Because they presumably formed due to drape folding, they were probably long-lived since differential salt evacuation/diapirism began during Honaker Trail deposition (Figure 5). They would have grown in displacement with increased folding and would gradually have propagated away from the diapir (Figure 9). The fault lengths and net displacement may have increased due to late reactivation during the Laramide contraction.

The geometry of the Honaker Trail Fm., and thus probably the salt–sediment interface, changes as the termination of the diapir is approached. The strata are steep, approaching vertical, along the elongate SW side (Figures 3 and 7, sections A–B), but gradually decrease towards the SE (Figure 7, section C), so that the diapir termination forms a plunging nose over a distance of about 4 km (Figure 7, section X). Because megaflaps are defined as having near-vertical to overturned dips (Rowan et al., 2016), the Gypsum Valley megaflap terminates gradually to the SE as the dips decrease near the western radial fault (Figure 4), and there is no megaflap at the structural nose of the salt wall termination. This gradual termination and decrease in dip may be related to the deep salt budget since limb rotation to vertical in halokinetic megaflaps requires an adequate thickness of deep salt (Rowan et al., 2016). Thus, beneath the Gypsum Valley megaflap, the salt would have been thick enough for strata to rotate to vertical, but rotation was limited where the salt might have thinned southeastward towards the edge of the basin (Figure 1a).

The style of megaflap termination to the NW is uncertain. Maximum dips of the megaflap strata are slightly decreased in SD I′ (65–80°) and the strata are buried beneath the Morrison Fm. farther NW. Seismic data show that the megaflap is absent 13 km to the NW, with the Honaker Trail Fm. truncated at depth beneath the mid-Cutler unconformity (Figure 3a). Whether the megaflap gradually decreases in dip and elevation, or is truncated abruptly by one or more faults, is unknown.

As described above, the uppermost Paradox Fm. black shales and interbedded carbonates are parallel to the Honaker Trail Fm. in SD I′, but the latter are folded in the southeastern part of SD I′, and completely disrupted to the NW. The asymmetric fold geometries suggest formation during roughly diapir-parallel shear, with a sense of motion of the inside of the diapir up relative to flanking strata in the minibasin. Two possible origins for this deformation are considered. First, the deformation might have occurred
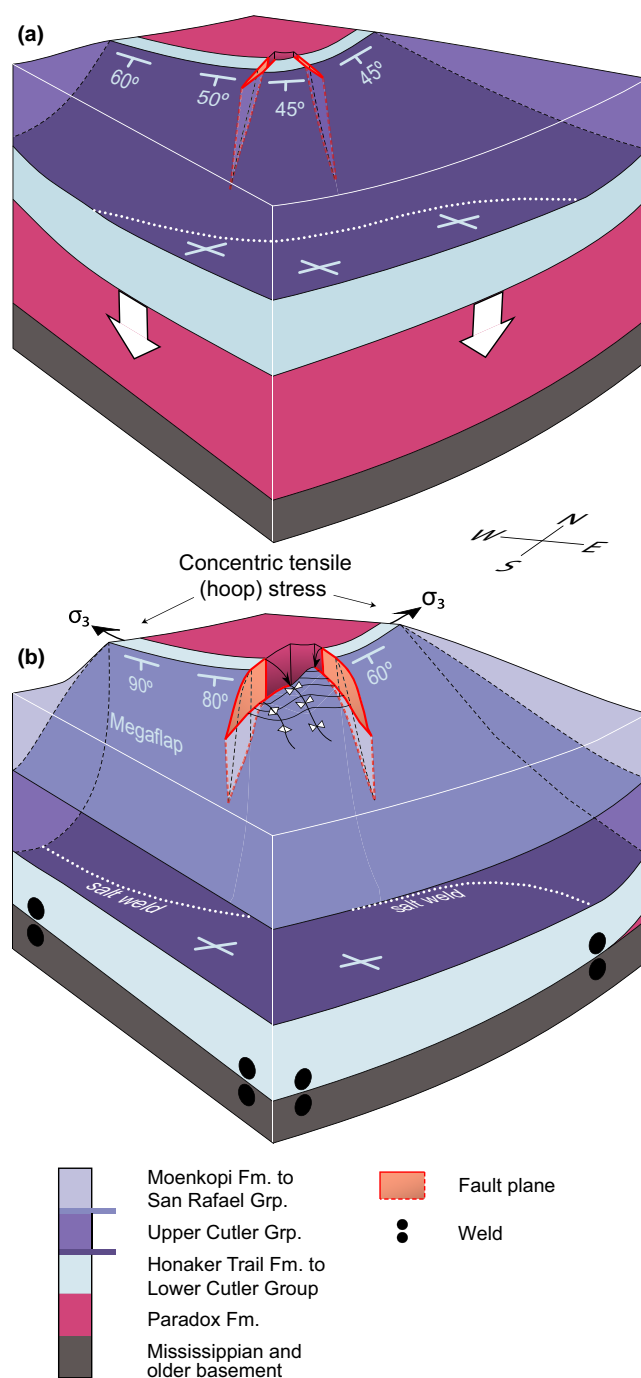


**FIGURE 9** Block diagrams showing the evolution of the radial faults at the termination of Gypsum Valley salt wall: (a) earlier drape fold stage; and (b) later stage with strata rotated to vertical in megaflap

early as soft-sediment deformation during the earliest inflation of the diapir just to the NE. In this case, the deformed and disrupted strata would still be considered part of the megaflap, simply rotated during drape folding. Alternatively, the deformation could have been caused at any time by ductile flow of the salt and associated weak shales, in which case the uppermost Paradox in this area acted as part

of the diapir, not the megaflap. One implication of this latter interpretation is that the base of the megaflap can shift stratigraphically along the edge of the diapir.

## 4.2 | Northeast (low) side

There is relatively minor along-strike variation in the large-scale geometry of the northeastern, downthrown flank of the diapir (Figures 4 and 7). One difference is that the Mesozoic strata climb gently towards the diapir over a zone about 1.5–2 km wide within SD V (Figure 7, sections A–C), the same strata in the hanging wall of the counter-regional fault (SD IV) are sub-horizontal (Figure 7, section D). The required change in elevation occurs right at the SE termination of the diapir, manifested by the local SE-dipping Dakota Fm. strata, the minor lateral fault, and the presence of the Mesa Verde Grp. only to the SE (Figures 4 and 7, section Y).

Is this change in elevation due to ongoing drape folding adjacent to the diapir during the Late Cretaceous or to some other factor, and is the lateral fault separating SD IV and V just a radial fault due to drape folding? We have already pointed out that there is no drape fold to the SE of the fault, so that it is unlikely to be a radial fault. To the NW of the fault, there are two scales of folding: gentle folding of the Dakota Sst. and younger strata extending close to 2 km from the salt (Figure 7, sections A–C); and a narrower zone of folding within the underlying Morrison Fm., as indicated by a sudden increase in dip, within about 300 m of the diapir on section B (Figure 7). The latter is compatible with halokinetic folding, which occurs within 1 km of a passive diapir (Giles & Rowan, 2012). Moreover, the regional level of the top Dakota Sst. (defined as the level where the strata have not gone up or down due to local deformation; Hossack, 1995) is consistent over a broad area along the eastern portions of sections A–D and most of section Y (Figure 7). In contrast, the Dakota Sst. within the 1.5–2 km wide zone of folding is above regional. Thus, we attribute the near-diapir folding to a combination of two processes. The more pronounced folding occurring within 300–500 m of the diapir likely represents halokinetic drape folding during ongoing passive diapirism in the Jurassic. However, we infer that the broader zone of gentler folding, recorded by the Burro Canyon Fm. and Dakota Sst., was generated by minor diapir rejuvenation during the subsequent Laramide Orogeny. The amount of shortening decreasing abruptly at the end of the salt wall, accommodated in part by a lateral tear fault.

Another change in near-diapir deformation on the NE flank of the diapir is that a normal fault dipping towards the diapir transitions to the SE to an anticline with a steeper limb on the diapir side (Figure 4). The tightness of the fold cannot be explained by deformation above the deep

salt level and thus suggests the presence of an inward stepping of the diapir edge (i.e. salt shoulder) that was progressively overlapped by Morrison Fm. strata (Figure 7, sections C and Y). Both the diapir-parallel normal fault and the fold are interpreted as different manifestations of shoulder collapse due to halite dissolution and the formation of caprock (see McFarland, Giles, Langford, & Rowan, 2015).

## 5 | DISCUSSION

In the following sections, we compare the southeastern termination of Gypsum Valley salt wall, with its counter-regional fault, firstly to other diapir terminations in the Paradox Basin and secondly to similar features in the northern Gulf of Mexico. We then discuss general aspects of salt wall and megaflap terminations.

## 5.1 | Paradox Basin salt wall terminations

Four other diapirs (shown in Figure 1a) have known similarities to the Gypsum Valley diapir (Table 1). First, the Onion Creek diapir has a megaflap on the distal (SW) side (Hudec, 1995; Trudgill, 2011), but no counterregional faults are mapped. Second, the Castle Valley diapir has no megaflap, although a 300 m long and N-S trending counterregional (E-dipping) structure extending away from its NW end has been identified as a salt weld, not a fault (Lawton et al., 2015). Welding was presumably caused by some combination of NE side subsidence, dissolution, and late contraction. Third, the nearby Moab Valley diapir extends in the subsurface for over 20 km NW from the surface termination as a salt roller in the footwall of the NE-dipping Moab fault. This fault was active during late (Cenozoic) extension and/or salt dissolution (Pevear, Vrolijk, & Longstaffe, 1997; Solum, van der Pluijm, & Peacor, 2005; Trudgill, 2011; Trudgill, Banbury, & Underhill, 2004), but an early origin as a counterregional fault is uncertain. Finally, the Lisbon Valley diapir is an inflated salt roller in the footwall of a 20-km long counterregional fault (Morrison & Parry, 1986; Parker, 1981). The slightly asymmetric geometry of its flanking minibasins demonstrates that fault activation occurred early (Fleming, 2015); it may have been analogous to the early single-flap active diapir phase at Gypsum Valley diapir (Figure 5b). However, the Lisbon Valley salt never broke through to grow as a passive diapir, but was simply reactivated during late contraction and extension (Fleming, 2015).

We highlight these aspects of other salt walls to show that there are both similarities and differences between their geometries and those described here for the Gypsum Valley salt wall. The comparison is intriguing, and suggests that

**TABLE 1** Selected attributes of different salt walls within the Paradox Basin derived from the literature (information for salt walls other than Gypsum Valley taken from Banbury, 2005; Fleming, 2015; Hudec, 1995; Lawton & Buck, 2006; Lawton et al., 2015; Morrison & Parry, 1986; Parker, 1981; Trudgill, 2011)

|  | SE Gypsum Valley | SW Onion Creek | NW Castle Valley | NW Moab Valley | Lisbon Valley |
|---|---|---|---|---|---|
| Type | Salt wall | Salt wall (Fisher Valley) | Salt wall | Salt wall | Salt roller |
| Structural relief (m) | 2,300 | 3,800 | 3,000 | 2,500 | 2,700 |
| Timing of diapirism | Pennsylvanian to Jurassic | Pennsylvanian to Permian | Pennsylvanian to Early Triassic | Pennsylvanian to Triassic | Pennsylvanian, Cenozoic |
| Major bounding structure | Counterregional fault | Is not mapped | Counterregional weld | Late extensional fault | Late extensional fault |
| Geometry of flanking minibasins | Asymmetric | Asymmetric | Asymmetric | Slightly asymmetric | Slightly asymmetric |
| Salt wall termination geometry | Steep plunging nose | Steep plunging nose | Steep plunging nose | Gradual plunging salt roller | Gradual plunging salt roller |
| Salt wall attenuation distance (km) | Short (4) | Short (3.1) | Short (1.6) | Long (20) | Short to moderate (8) |
| Megaflap | Yes | Yes | No | Yes | No |
| Radial faults | Yes | Are not mapped | Yes | No | No |

further work is warranted in order to understand better the styles and processes of diapirism and salt–sediment interaction in the Paradox Basin.

## 5.2 | Counterregional systems in the northern Gulf of Mexico

Counterregional faults extending away from diapir terminations are also known from the northern Gulf of Mexico (Diegel et al., 1995; Rowan & Inman, 2005; Rowan, Jackson, & Trudgill, 1999; Schuster, 1995; Trudgill & Rowan, 2004). They are found above both the autochthonous and allochthonous salt levels, the diapirs are often basinward-leaning rather than vertical, sub-circular stocks are more common than salt walls, and megaflaps have not been reported.

The oldest strata on the downthrown side at Gypsum Valley diapir are thicker than on the upthrown side. Similar relationships exist in the northern Gulf of Mexico (Schuster, 1995, figures 10 and 11; Trudgill & Rowan, 2004, figure 7b). In other cases, the opposite relationship exists, with the oldest strata in the proximal minibasin being thinned and the younger section being thicker (Rowan & Inman, 2005, their figure 1). The same geometry is seen at Salt Valley diapir in the Paradox Basin (Trudgill, 2011, figure 5a) indicating both styles can exist in the two basins. The difference in style is related to the early style of salt rise and the position of diapir breakthrough. If the roof is unfaulted and the salt simply inflates, progressive loading on the proximal side leads to diapir breakout at the distal end of the inflated salt, with the thinned oldest strata (the roof of the early inflated salt) ending up at the base of the landward minibasin (Figure 10a). If, in contrast, the early history is that of single-flap active diapirism, with the fault and eventual diapir breakthrough located at the proximal end of the inflated salt, the thinned roof (flap) ends up draped on the distal side of the diapir, potentially as a megaflap (Figure 10b). Of course, the geometry may change from one style to the other along strike, possibly due to variations in roof thickness and strength, thereby providing one possible form of megaflap termination.

In counterregional-style systems of the northern Gulf of Mexico, the largest differential subsidence is centred adjacent to the diapirs (Rowan & Inman, 2005). Differential subsidence may still be significant along strike from the diapirs, where it is taken up by slip on counterregional faults that merge into the proximal edges of the diapirs (Rowan & Inman, 2005; Rowan et al., 1999; Trudgill & Rowan, 2004). Note that this model requires no regional extension to be accommodated by the faults (Schuster, 1995). The deeper portions of the faults are actually welds since the salt evolves from linear, low-relief walls to high-relief stocks (Trudgill & Rowan, 2004). As fault displacement decreases along strike, the differential subsidence is increasingly accommodated by folding, until only monoclinal folding records the deformation around the landward and lateral margins of the minibasin. This is similar to the geometry observed at the southeastern termination of the Gypsum Valley salt wall, where the counterregional fault emanates from the proximal edge of the diapir,
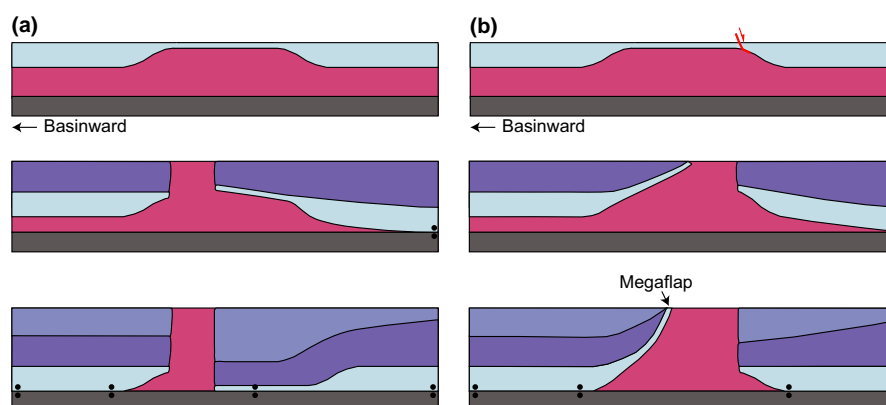
**FIGURE 10** End-member scenarios for the evolution of counterregional-style diapirs (based in part on Rowan & Inman, 2011; Rowan et al., 2016): (a) early salt inflation due to progressive depositional loading, with salt breakout at the basinward edge of the inflated salt; (b) early single-flap active diapirism (Schultz-Ela et al., 1993), with salt breakout at the proximal edge of the diapir and development of a megaflap along the basinward flank of the diapir

accommodates differential subsidence of the two mini-basins, and decreases in displacement away from the diapir.

## 5.3 | Salt wall and megaflap terminations

In general, structures extending off the terminations of salt walls differ depending on the local tectonic setting. They may be contractional salt-cored anticlines, thrust faults, extensional faults, strike-slip faults, or counterregional faults related to differential salt evacuation. However, we focus here only on passive diapirism driven by differential loading, without significant regional extension or contraction, and specifically on the final geometry after the flanking minibasins have touched down to form welds. We first address the termination geometry of the diapir itself (with or without a megaflap, Figure 11), then cases in which the salt wall and megaflap terminations are coincident (Figure 12), and finally cases in which a halokinetic (noncontractional) megaflap terminates away from the end of the salt wall (Figure 13).

The geometry of the termination of a passive salt wall is ultimately controlled by the available salt budget and the patterns of sedimentary loading, and thus the spatial variations in salt evacuation and flow towards the diapir. If, for example, the autochthonous salt basin has an abrupt lateral boundary (such as a basement-involved fault), a salt wall formed near the basin edge will have an equally abrupt termination, with flanking depocentres bounded by steep faults separating the subsiding minibasins from areas of no corresponding subsidence off the end of the diapir (Figure 11a). If there is no local variation in deep salt thickness to begin with, the salt wall is liable to plunge along strike and its edge will have a curved map-view outline, with depocentres on all sides and radial faults best developed

where curvature of drape-folded strata is greatest (Figure 11b). The salt budget for flow into the diapir from beneath the depocentres will be controlled in part by the position of nearby diapirs and thus the fetch area for deep salt.

The cartoons in Figure 11a, b show symmetric diapir flanks, but diapirs may be slightly to highly asymmetric. If asymmetric, the diapir may be associated with a counterregional fault at one corner, radial faults on the other corner, and a possible megaflap (Figure 11c), as observed at Gypsum Valley. Note that although the corner where the counterregional fault intersects the diapir is broadly curved, no significant radial faults form because there is no curved drape fold. The diapir termination may be relatively abrupt, in which case differential subsidence is high immediately adjacent to the end of the salt wall but decreases rapidly along strike away from the diapir, the top salt correspondingly plunges relatively steeply, radial faults are well developed due to high degrees of map-view curvature of the flanking strata, and the counterregional fault or equivalent weld is relatively short (Figure 12a). Alternatively, the salt wall termination may be gradual, with differential subsidence diffused over a broader area, a gently plunging salt nose, less map–view curvature and thus less common radial faults and a longer counterregional fault (Figure 12b). The difference might again be explained by the deep salt budget: if it decreases rapidly along strike, the termination will be more abrupt and radial faults will be common (Figure 12a); otherwise, the termination will be gradual and radial faults absent or minor (Figure 12b). The SE termination of the Gypsum Valley diapir falls between these end-member geometries.

Megaflaps may also terminate before reaching the end of a salt wall. Because megaflaps are defined by the
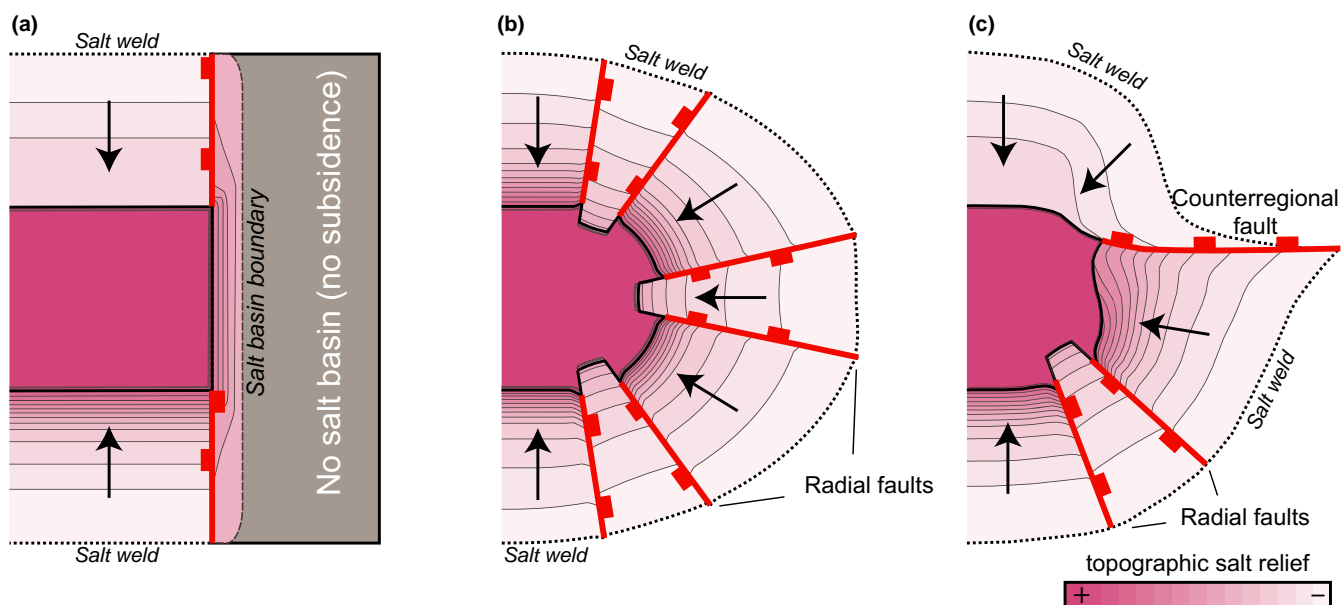
**FIGURE 11** Schematic illustrations of end-member termination geometries of salt walls (red faults are all suprasalt, countour lines are on top salt): (a) symmetric salt wall termination above a presalt basement fault (not shown); (b) symmetric salt wall termination where there is deep salt present off the end of the diapir; (c) termination where the salt wall is asymmetric, with a counterregional fault off the end. Note that radial fault development depends on both map–view curvature and the degree of drape folding of flanking strata. Arrows indicate salt flow into diapir

**FIGURE 12** Schematic plan view of varying terminations of salt walls with asymmetric minibasins and megaflaps. Red dashed lines indicate radial faults; red continuous lines indicate the counter-regional fault at (a) abrupt and (b) gradual salt wall terminations; continuous black lines indicate topographic contours on the top salt
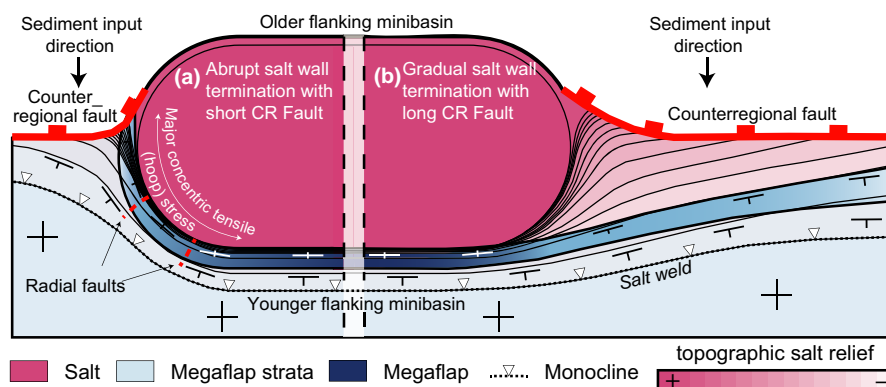


steepness and height of the stratal panel, end-member styles of termination are a gradual decrease in elevation or maximum dip of the megaflap panel along strike or an abrupt drop or decrease in dip across one or more faults (Figure 13). Combinations of any of these are possible and likely in natural examples. One possible cause for lateral termination is a decrease in deep salt budget along strike, as suggested above for the Gypsum Valley megaflap; again, a megaflap forming by limb rotation cannot reach vertical if the salt is too thin relative to the rotating roof panel (Rowan et al., 2016). A second factor is the width of the early pillow or single-flap active diapir; as the width decreases, there is less roof length available to rotate into steep attitudes. Similarly, a third factor is any lateral variation in where the roof pulls apart and salt breaks through. If the early fault that separates the strata that end up on

one or the other sides of the diapir is consistently along one edge of the early salt structure, then the geometry of a megaflap will change very little along strike (for a constant width early pillow). If, however, the fault gradually or abruptly crosses the top of the pillow, the length of the roof panel that rotates into the megaflap is diminished and the rest of the roof ends up flanking the other side of the diapir (assuming none is removed by erosion).

## 6 | CONCLUSIONS

The Gypsum Valley diapir is an outstanding natural laboratory for studying the three-dimensional architecture of the terminations of both a salt wall and a megaflap. From this example, and from comparison to analogous structures in
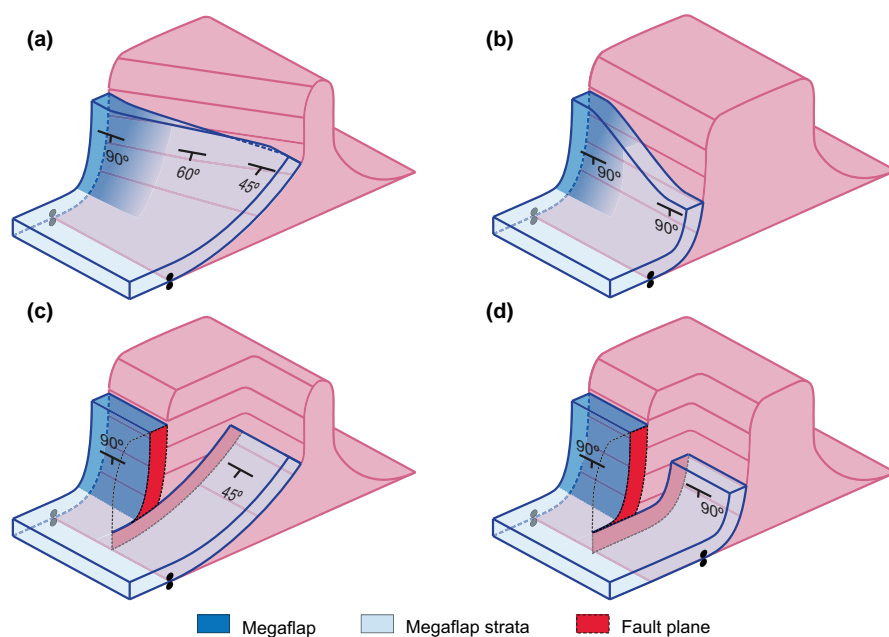
**FIGURE 13** End-member styles of megaflap termination along the length of a salt wall: (a) constant limb length with gradual decrease in dip along strike; (b) gradual decrease in limb length with constant dip along strike; (c) constant limb length with abrupt decrease in dip across a fault; (d) abrupt decrease in limb length with constant dip across a fault. These are conceptual models of end-member geometries; most real examples combine elements of these

the Paradox Basin and the northern Gulf of Mexico, we have demonstrated or suggested the following:

1. The southeastern end of the Gypsum Valley salt wall is asymmetric, with thicker, deeper, gently dipping strata in the proximal NE minibasin and thinned, rotated older strata forming a megaflap on the distal SW side. Its termination is characterized by a moderately plunging nose of salt overlain by SE-dipping strata with maximum 45° dips, a large counterregional fault that separates the nose from the deep proximal minibasin, and radial faults that accommodate concentric extension where the map-view curvature of the flanking strata is greatest.

2. The megaflap, which is characterized by near-vertical strata, terminates towards the southeastern end of the diapir by a decrease to ca. 60° dips over a distance of several hundred metres before being truncated by the western radial fault. The northwestern termination is buried by younger strata. The megaflap includes undeformed nonevaporite strata of the uppermost Paradox Fm. to the SE, but this same interval becomes increasingly deformed along strike to the NW. This deformation may represent early syn-sedimentary slumping or part of the intrasalt deformation; in the latter case, the base of the megaflap would change stratigraphic position along strike.

3. In counterregional systems like the Gypsum Valley diapir and possibly analogous structures in the northern Gulf of Mexico, megaflap formation on the distal flank is favoured when the salt breaks out on the proximal side of the initial salt pillow or diapir.

4. In general, salt wall terminations may be abrupt or gradual. Controlling factors probably include the spatial and thickness variation in the deep salt, the presence of

nearby diapirs and thus the fetch area for salt feeding the wall, and the pattern of depositional loading and associated flow of salt into the diapir.

5. For a salt wall without significant extension or contraction, if the two flanking minibasins are highly asymmetric, a counterregional fault extends off the end of the wall. The length of the counterregional fault away from the diapir depends in part on the degree of plunge of the salt wall nose.

6. Megaflaps may terminate at any position along the salt wall. Termination is accommodated by decreased length and/or dip of the megaflap strata that occurs either gradually or abruptly at one or more faults. Controlling factors include the deep salt budget, the width of the initial salt pillow or single-flap active diapir and variations in the position on the early salt structure at which the roof separates and the salt breaks out.

7. In all cases, radial faults will be most prevalent where there is the maximum map–view curvature of drape-folded strata. They tend to have more offset and extend farther from the diapir with wider zones and higher degrees of stratal upturn, as found in megaflaps.

acknowledge Cynthia Ebinger, Chris Talbot, and Chris Jackson for their helpful reviews which greatly contributed to improving the final product. We thank Mark Fischer and Gary Gianniny for helpful discussions on salt–sediment interaction and all the people who helped the first author in numerous field campaigns. We also acknowledge Midland Valley for providing the Move™ software.

## ORCID

*Frederic O. Escosa* iD http://orcid.org/0000-0002-1908-1037

## REFERENCES

Amador, C. M., Schurger, S. G., & Miller, B. L. (2009). Andy's Mesa Unit, San Miguel County, Colorado. In W. S. Houston, L. L. Wray & P. G. Moreland (Eds), *The Paradox Basin revisited-New developments in petroleum systems and basin analysis: Denver, Colorado* (pp. 497–518). Denver, CO: Rocky Mountain Association of Geologists, 2009 Special Publication.

Baars, D. L. (1965). *Pre-Pennsylvanian paleotectonics of southwestern Colorado (San Juan County and vicinity) and east-central Utah.* PhD Thesis, University of Colorado, Boulder, CO.

Baars, D. L., & Stevenson, G. M. (1981). Tectonic evolution of the Paradox basin, Utah & Colorado. In D. L. Wiegand (Ed.), *Geology of the Paradox basin: Denver Colorado* (pp. 23–31). Denver, CO: Rocky Mountain Association of Geologists.

Balkwill, H. R., & Legall, F. D. (1989). Whale Basin, offshore Newfoundland: Extension and salt diapirism. In A. J. Tankard & H. R Balkwill (Eds), *Extension tectonics and stratigraphy of the North Atlantic margins. American Association of Petroleum Geologists Memoir 46*, 233–245.

Banbury, N. J. (2005). *The role of salt mobility in the development of supra-salt sedimentary depocentres and structural style.* PhD Thesis, University of Edinburgh, Edinburgh, UK.

Barbeau, D. L. (2003). A flexural model for the Paradox basin: Implications for the tectonics of the Ancestral Rocky Mountains. *Basin Research*, *15*, 97–115. https://doi.org/10.1046/j.1365-2117.2003.00194.x

Blakey, R. C. (2009). Paleogeography and Geologic History of the Western Ancestral Rocky Mountains, Pennsylvanian-Permian, southern Rocky Mountains and Colorado Plateau. In W. S. Houston, L. L. Wray & P. G. Moreland (Eds), *The Paradox Basin revisited – New developments in petroleum systems and basin analysis: Denver, Colorado* (pp. 222–264). Denver, CO: Rocky Mountain Association of Geologists, Special Publication.

Coleman, A., Jackson, C. A.-L., Duffy, O. B., & Nikolinakou, M. A. (2018). How, where, and when do radial faults grow near salt diapirs? *Geology*, *48*, 655–658. https://doi.org/10.1130/G40338.1

Condon, S. M. (1997). Geology of the Pennsylvanian and Permian Cutler Group and Permian Kaibab Limestone in the Paradox Basin, southeastern Utah and southwestern Colorado. US Department of the Interior, US Geological Survey Bulletin 2000-P.

Davison, I., Alsop, I., Birch, P., Elders, C., Evans, N., Nicholson, H., … Young, M. (2000). Geometry and late-stage structural evolution of Central Graben salt diapirs, North Sea. *Marine and Petroleum Geology*, *17*, 499–522. https://doi.org/10.1016/S0264-8172(99)00068-9

Deatrick, K. T., Giles, K., Langford, R., Rowan, M. G., & Hearon, T. E. (2015). Geometry and depositional facies of an exposed mega-flap: Pennsylvanian Honaker Trail Formation, Gypsum Valley salt wall, Paradox Basin, Colorado (abstract). AAPG Annual Convention and Exhibition, Denver, CO, May 31–June 3.

DeCelles, P. G., & Giles, K. A. (1996). Foreland basin systems. *Basin Research*, *8*, 105–123. https://doi.org/10.1046/j.1365-2117.1996.01491.x

Diegel, F. A., Karlo, J. F., Schuster, D. C., Shoup, R. C., & Tauvers, P. R. (1995). Cenozoic structural evolution and tectono-stratigraphic framework of the Northern Gulf Coast continental margin. In M. P. A. Jackson, D. G. Roberts & S. Snelson (Eds), *Salt tectonics a global perspective.* AAPG Memoir, 65, 109–151.

Doelling, H. H. (1988). Geology of Salt Valley Anticline and Arches National Park, Grand County, Utah. In H. H. Doelling, C. G. Oviatt & P. W. Huntoon (Eds), *Salt deformation in the Paradox Region. Utah Geological and Mineral Survey Bulletin*, 122, 7–58.

Doelling, H. H. (2001). Geologic map of the Moab and eastern part of the San Rafael Desert 30′x 60′ Quadrangles, Grand and Emery Counties, Utah and Mesa County, Colorado. Utah Geological Survey Map 180.

Elston, D. P., Shoemaker, E. M., & Landis, E. R. (1962). Uncompahgre front and salt anticline region of Paradox Basin, Colorado and Utah. *AAPG Bulletin*, *46*, 1857–1878.

Fleming, M. W. (2015). *Integrated structural and fracture analysis of Lisbon Valley salt anticline, Utah.* MSc. Thesis, Northern Illinois University, DeKalb, IL.

Franczyk, K. J. (1992). Measured section of the Pennsylvanian Hermosa Group near Hermosa, Colorado (pp. 5). US Department of the Interior, US Geological Survey Open-File Report, 92-689.

Ge, H., Jackson, M. P. A., & Vendeville, B. C. (1997). Kinematics and dynamics of salt tectonics driven by propagation. *AAPG Bulletin*, *81*, 398–423.

Giles, K. A., & Lawton, T. F. (2002). Halokinetic sequence stratigraphy adjacent to the El Papalote diapir, northeastern Mexico. *AAPG Bulletin*, *86*, 823–840.

Giles, K. A., & Rowan, M. G. (2012). Concepts in halokinetic-sequence deformation and stratigraphy. In G. I. Alsop, S. G. Archer, A. J. Hartley, N. T. Grant & R. Hodgkinson (Eds), *Salt tectonics, sediments and prospectivity. Geological Society, London, Special Publications*, 363, 7–31, https://doi.org/10.1144/sp363.2

Goldhammer, R. K., Oswald, E. J., & Dunn, P. A. (1994). High-frequency, glacio-eustatic cyclicity in the Middle Pennsylvanian of the Paradox Basin – an evaluation of Milankovitch forcing. In deBoer P. L. & D. G. Smith (Eds), *Orbital forcing and cyclic sequences.* Special publication of International Association of Sedimentologists, 19, 243–283.

Graham, R., Jackson, M., Pilcher, R., & Kilsdonk, B. (2012). Allochthonous salt in the sub-Alpine fold-thrust belt of Haute Provence, France. In G. I. Alsop, S. G. Archer, A. J. Hartley, N. T. Grant & R. Hodgkinson (Eds), *Salt tectonics, sediments and prospectivity. Geological Society, London, Special Publications*, 363, 595–615, https://doi.org/10.1144/sp363.30

Harrison, J. C., & Jackson, M. P. A. (2014). Exposed evaporite diapirs and minibasins above a canopy in central Sverdrup Basin,

Axel Heiberg Island, Arctic Canada. *Basin Research*, 26, 567–596. https://doi.org/10.1111/bre.12037

Hazel, J. E. (1994). Sedimentary response to intrabasinal salt tectonism in the Upper Triassic Chinle Formation, Paradox basin, Utah. US Department of the Interior, US Geological Survey Bulletin, 2000-F, 34.

Hearon, T. E. IV, Rowan, M. G., Giles, K. A., & Hart, W. H. (2014). Halokinetic deformation adjacent to the deep-water Auger diapir, Garden Banks 470, northern Gulf of Mexico: Testing the applicability of an outcrop-based model using subsurface data. *Interpretation*, 2, SM57–SM76. https://doi.org/10.1190/int-2014-0053.1

Hite, R. J., & Buckner, D. H. (1981). Stratigraphic correlations, facies concepts, and cyclicity in Pennsylvanian rocks of the Paradox Basin. In D. L. Wiegand (Ed.), *Geology of the Paradox Basin* (pp. 147–159). Denver, CO: Rocky Mountain Association of Geologist.

Hudec, M. R. (1995). The Onion Creek salt diapir: An exposed diapir fall structure in the Paradox basin, Utah. In C. J. Travis, H. Harrison, M. R. Hudec, B. C. Vendeville, F. J. Peel & B. E. Perkins (Eds.), Salt, sediment and hydrocarbons (pp. 125–134). SEPM Foundation, Gulf Coast Section, 16th Annual Research Conference Program with Papers.

Hudec, M. R., & Jackson, M. P. A. (2011). The salt mine: A digital atlas of salt tectonics: The University of Texas at Austin, Bureau of Economic Geology, Udden Book Series No. 5. *AAPG Memoir*, 99, 305.

Hossack, J. (1995). Geometric rules of section balancing for salt structures. In M. P. A. Jackson, D. G. Roberts & S. Snelson (Eds.), *Salt tectonics: A global perspective. American Association of Petroleum Geologists Memoir*, vol. 65, 29–40.

Jackson, M. P. A., & Vendeville, B. C. (1994). Regional extension as a geologic trigger for diapirism. *GSA Bulletin*, 106, 57–73. https://doi.org/10.1130/0016-7606(1994)106&lt;0057:REAAGT&gt;2.3.CO;2

Kergaravat, C., Ribes, C., Legeay, E., Callot, J.-P., Kavak, K. S., & Ringenbach, J.-C. (2016). Minibasins and salt canopy in foreland fold-and-thrust belts: The central Sivas Basin, Turkey. *Tectonics*, 35, 1342–1366. https://doi.org/10.1002/2016TC004186

Kluth, C. F. (1986). Plate tectonics of the Ancestral Rocky Mountains. In J. A. Peterson (Ed.), *Paleotectonics and sedimentation in the Rocky Mountain Region, United Sates. AAPG Memoir*, 41, 353–369.

Kluth, C. F., & Coney, P. J. (1981). Plate tectonics of the Ancestral Rocky Mountains. *Geology*, 9, 10–15. https://doi.org/10.1130/0091-7613(1981)9<10:ptotar>2.0.co;2

Kluth, C. F., & DuChene, H. R. (2009). Late Pennsylvanian and early Permian structural geology and tectonic history of the Paradox Basin and Uncompahgre uplift, Colorado and Utah. In W. S. Houston, L. L. Wray & P. G. Moreland (Eds). *The Paradox Basin revisited—New developments in petroleum systems and basin analysis* (pp. 178–197). Denver, CO: Rocky Mountain Association of Geologists, Special Paper (CD-ROM).

Krzywiec, P. (2006). Structural inversion of the Pomeranian and Kuiavian segments of the Mid-Polish Trough – lateral variations in timing and structural style. *Geological Quarterly*, 50, 151–168.

Lawton, T. F., & Buck, B. J. (2006). Implications of diapir-derived detritus and gypsic paleosols in Lower Triassic strata near the Castle Valley salt wall, Paradox Basin, Utah. *Geology*, 34, 885–888. https://doi.org/10.1130/G22574.1

Lawton, T. F., Buller, C. D., & Parr, T. R. (2015). Provenance of a Permian erg on the western margin of Pangea: Depositional system of the Kungurian (late Leonardian) Castle Valley and White Rim sandstones and subjacent Cutler Group, Paradox Basin, Utah, USA. *Geosphere*, 11, 1475–1506. https://doi.org/10.1130/GES01174.1

Lawton, T. F., Sprinkel, D. A., Decelles, P. G., Mitra, G., Sussman, A. J., & Weiss, M. P. (1997). Stratigraphy and structure of the Sevier thrust belt and proximal foreland-basin system in central Utah: A transect from the Sevier Desert to the Wasatch Plateau. *Brigham Young University Geology Studies*, 42, 33–67.

Mahrer, K., Ake, J., O'Connell, D., & Block, L. (2012). 2002 Status report-paradox valley seismic network. Paradox Valley Project, Southwestern Colorado, U.S. Department of the Interior, Seismotectonics and Geophysics Group. Technical Memorandum No. D8330- 2003-009, Bureau of Reclamation.

Mallory, W. W. (1972). Pennsylvanian system: Regional synthesis. In: W. W. Mallory (Ed.), *Geologic Atlas of the Rocky Mountain Region* (pp. 111–128). Denver, CO: Rocky Mountain Association of Geologists.

Mankowski, L. C., Campbell, T. R., Huntoon, J. E., Gregg, W. J., & Linari, D. J. (2002, July 21–26). Structural mapping of the Uncompahgre front near Gateway, Colorado, with emphasis on Ancestral Rocky Mountain fabrics. AAPG Hedberg Conference, Vail, CO.

Martín-Martín, J. D., Vergés, J., Saura, E., Moragas, M., Messager, G., Baqués, V., … Hunt, D. W. (2016). Diapiric growth within an Early Jurassic rift basin: The Tazoult salt wall (central High Atlas, Morocco). *Tectonics*, 35, 1–31. https://doi.org/0.1002/2016TC004300

Mast, A. M. (2016). *The origin of anomalous carbonate units outcropping at the salt-sediment interface of the southern end of Gypsum Valley salt wall, Paradox Basin, Colorado*. MSc. Thesis, University of Texas at El Paso, El Paso, TX.

McFarland, J., Giles, K. A., Langford, R., & Rowan, M. G. (2015, September 20–22). Structural and stratigraphic development of a salt diapir shoulder, Gypsum Valley Salt Wall, Paradox Basin, Colorado (abstract). Gulf Coast Association of Geological Societies Convention, Houston, TX.

Mohr, M., Kukla, P. A., Urai, J. L., & Bresser, G. (2005). Multiphase salt tectonic evolution in NW Germany: Seismic interpretation and retro-deformation. *International Journal of Earth Sciences*, 94, 917–940. https://doi.org/10.1007/s00531-005-0039-5

Molenaar, C. M. (1981). Mesozoic stratigraphy of the Paradox basin: An overview. In D. L. Wiegand (Ed.), *Geology of the Paradox basin* (pp. 119–127). Rocky Mountain Association of Geologists Field Conference.

Moore, K. D., Soreghan, G. S., & Sweet, D. E. (2008). Stratigraphic and structural relations in the proximal Cutler Formation of the Paradox Basin: Implications for timing of movement on the Uncompahgre front. *The Mountain Geologist*, 45, 49–68.

Morrison, S. J., & Parry, W. T. (1986). Deposits from Saline Basin Brines, Lisbon Valley, Utah. *Economic Geology*, 81, 1853–1866. https://doi.org/10.2113/gsecongeo.81.8.1853

Nuccio, V. F., & Condon, M. (1996). Burial and thermal history of the Paradox basin, Utah and Colorado, and petroleum potential of the Middle Pennsylvanian Paradox Formation, US Department of the Interior. US Geological Survey Bulletin, 2000-O, 41.-->

O'Sullivan, R. B., & MacLachlan, M. E. (1975). Triassic rocks of the Moab-White Canyon area, southeastern Utah. In Canyonlands Country: Four Corners Geological Society, Eighth Field Conference, Guidebook (pp. 129–142).

Parker, J. M. (1981). Lisbon Field Area, San Juan County, Utah. In: D. L. Wiegand (Ed.), *Geology of the Paradox Basin field conference*, Rocky Mountain Association of Geologists, AAPG Memoir 9 Natural Gases of North America, 5, 2009.

Pevear, D. R., Vrolijk, P. J., & Longstaffe, F. J. (1997). Timing of Moab Fault displacement and fluid movement integrated with burial history using radiogenic and stable isotopes. In J. P. Hendry (Ed.), *Geofluids II – Extended abstracts* (pp. 42–45). Belfast, UK: Geofluids Research.

Rasmussen, L., & Rasmussen, D. L. (2009). Burial history analysis of the pennsylvanian petroleum system in the Deep Paradox Basin Fold and Fault Belt, Colorado and Utah. In: W. S. Houston, L. L. Wray & P. G. Moreland (Eds), *The Paradox Basin revisited: New developments in petroleum systems and basin analysis* (pp. 24–94). Rocky Mountain Association Geologist Special Publication.

Rowan, M. G., Giles, K. A., Hearon, T. E. IV, & Fiduk, J. C. (2016). Megaflaps adjacent to salt diapirs. *AAPG Bulletin*, 11, 1723–1747. https://doi.org/10.1306/05241616009

Rowan, M. G., & Inman, K. F. (2005). Counterregional-style deformation in the Deep Shelf of the Northern Gulf of Mexico. *Gulf Coast Association of Geological Societies Transactions*, 55, 947–969.

Rowan, M. G., & Inman, K. F. (2011). Salt-related deformation recorded by allochthonous salt rather than growth strata. *Gulf Coast Association of Geological Societies Transactions*, 61, 379–390.

Rowan, M. G., Jackson, M. P. A., & Trudgill, B. D. (1999). Salt-related fault families and fault welds in the northern Gulf of Mexico. *AAPG Bulletin*, 9, 1454–1484.

Rowan, M. G., Lawton, T. F., & Giles, K. A. (2012). Anatomy of an exposed vertical salt weld and flanking strata, La Popa Basin, Mexico. In G. I. Alsop, S. G. Archer, A. J. Hartley, N. T. Grant & R. Hodgkinson (Eds), *Salt tectonics, sediments and prospectivity* (pp. 33–57). Geological Society, London, Special Publications, 363. https://doi.org/10.1144/sp363.3

Rowan, M. G., Lawton, T. F., Giles, K. A., & Ratliff, R. A. (2003). Near-salt deformation in La Popa basin, Mexico, and the northern Gulf of Mexico: A general model for passive diapirism. *AAPG Bulletin*, 87, 733–756. https://doi.org/10.1306/01150302012

Rowan, M. G., & Lindsø, S. (2017). Salt tectonics of the Norwegian Barents Sea and Northeast Greenland Shelf. In J. I. Soto, J. F. Flinch, & G. Tari (Eds), *Permo-Triassic Salt Provinces of Europe, North Africa and the Atlantic Margins* (pp. 265–286). Amsterdam, the Netherlands: Elsevier.

Saura, E., Vergés, J., Martín-Martín, J. D., Messager, G., Moragas, M., Razin, P., … Hunt, D. W. (2013). Syn- to post-rift diapirism and minibasins of the Central High Atlas (Morocco): The changing face of a mountain belt. *Journal of the Geological Society*, 171, 97–105. https://doi.org/10.1144/jgs2013-079

Schultz-Ela, D. D., Jackson, M. P. A., & Vendeville, B. C. (1993). Mechanics of active salt diapirism. *Tectonophysics*, 228, 275–312. https://doi.org/10.1016/0040-1951(93)90345-K

Schuster, D. C. (1995). Deformation of Allochthonous Salt and Evolution of Related Salt–structural Systems, Eastern Louisiana Gulf Coast. In M. P. A. Jackson, D. G. Roberts & S. Snelson (Eds), *Salt tectonics a global perspective*. AAPG Memoir, 65, 177–198.

Shoemaker, E. M., Case, J. E., & Elston, D. P. (1958). Salt anticlines of the Paradox Basin. *Guidebook 9th Annual Field Conference* (pp. 39–59). Intermountain Association of Petroleum Geologists: Salt Lake City, IT.

Solum, J. G., van der Pluijm, B. A., & Peacor, D. R. (2005). Neocrystallization, fabrics and age of clay minerals from an exposure of the Moab Fault, Utah. *Journal of Structural Geology*, 27, 1563–1576. https://doi.org/10.1016/j.jsg.2005.05.002

Stewart, S. A. (2006). Implications of passive salt diapir kinematics for reservoir segmentation by radial and concentric faults. *Marine and Petroleum Geology*, 23, 843–853. https://doi.org/10.1016/j.marpetgeo.2006.04.001

Stewart, S. A. (2007). Salt tectonics in the North Sea Basin: A structural style template for seismic interpreters. In A. C. Ries, R. W. H. Butler & R. H. Graham (Eds), *Deformation of the continental crust: The Legacy of Mike Coward* (pp. 361–396). Geological Society, London, Special Publications, 272.

Stewart, J. H., Poole, F. G., & Wilson, R. F. (1972). Stratigraphy and origin of the Triassic Moenkopi Formation and related strata in the Colorado Plateau region. US Department of the Interior. *US Geological Survey Professional Paper*, 691, 195.

Timbel, C. B. (2015). *Uncompahgre Fault Geometry: a Seismic, Field, and Gravity Study Near Nucla, Colorado, Paradox Basin, USA*. MSc. Thesis, Colorado School of Mines, Golden, CO.

Trudgill, B. (2011). Evolution of salt structures in the northern Paradox Basin: Controls on evaporite deposition, salt wall growth and supra-salt stratigraphic architecture. *Basin Research*, 23, 208–238. https://doi.org/10.1111/j.1365-2117.2010.00478.x

Trudgill, B., Banbury, N., & Underhill, J. (2004). Salt evolution as a control on structural and stratigraphic systems: Northern Paradox foreland basin, SE Utah, USA. In P. J. Post (Ed.), Salt-Sediment Interactions and Hydrocarbon Prospectivity: Concepts, Applications and Case Studies for the 21st Century. Gulf Coast Society of Economic Paleontologists and Mineralogists Foundation, 24th Bob F. Perkins Research Conference Proceedings (CD-ROM) (pp. 669–700). Houston, TX: Gulf Coast Section SEPM Foundation.

Trudgill, B. D., & Paz, M. (2009). Restoration of Mountain Front and salt structures in the Northern Paradox Basin, SE Utah. In W. S. Houston, L. L. Wray & P. G. Moreland (Eds), *The Paradox Basin revisited: New developments in Petroleum systems and basin analysis* (pp. 132–177). Rocky Mountain Association of Geologist Special Publication.

Trudgill, B. D., & Rowan, M. G. (2004). Integrating 3D seismic data with structural restorations to elucidate the evolution of a stepped counter-regional salt system, Eastern Louisiana Shelf, Northern Gulf of Mexico. In R. J. Davies, J. A. Cartwright, S. A. Stewart, M. Lappin & J. R. Underhill (Eds), *3D Seismic technology: Application to the exploration of sedimentary basins* (pp. 165–176). *Geological Society, London, Memoirs 29*.

Trusheim, F. (1960). Mechanism of Salt Migration in Northern Germany. *AAPG Bulletin*, 44, 1519–1540.

Vogel, J. D. (1960). Geology and ore deposits of the Klondike Ridge Area, CO: U.S. Geological Survey, Open-File Report USGS Numbered Series 60–145.

Weimer, P. C. (1982). Upper Cretaceous stratigraphy and tectonic history of the Ridgway area, northwestern San Juan Mountains. *Colorado. The Mountain Geologist*, 19(4), 91–104.

Whidden, K. J., Lillis, P. G., Anna, L. A., Pearson, K. M., & Dubiel, R. F. (2013). Geology and total petroleum systems of the Paradox Basin, Utah, Colorado, New Mexico, and Arizona. *The Mountain Geologist*, *51*, 119–138.

White, M. A., & Jacobson, M. I. (1983). Structures associated with the southwest margin of the ancestral Uncompahgre Uplift. In W. R. Averett (Ed.), *Northern Paradox Basin – Uncompahgre uplift* (pp. 33–39). Grand Junction, CO: Grand Junction Geological Society.

**Annex 2: "Geology of the Eastern Prebetic Zone at the Jumilla region (SE Iberia)".**

Science

# Geology of the Eastern Prebetic Zone at the Jumilla region (SE Iberia)

Frederic O. Escosa ⓘ, O. Ferrer ⓘ and E. Roca ⓘ

Institut de Recerca Geomodels, Departament de Dinàmica de la Terra i de l'Oceà, Facultat de Ciències de la Terra, Universitat de Barcelona, Barcelona, Spain

**ABSTRACT**

This article presents a geological map and cross-sections at 1:50,000 scale covering an area of 609 km$^2$ of the Eastern Prebetic Zone (SE Iberia). The structure of the studied area is characterized by an NW-directed fold-and-thrust belt and inactive salt diapirs that are parallel to the ENE- to NE-regional trend of the eastern Betic Cordillera. This regional trend is locally disrupted by the NW-trending Matamoros Basin, which is flanked by the active Jumilla and La Rosa diapirs. The geological map, the cross-sections and the outcrop observations support the hypothesis that the major Mesozoic rifting phase affecting the Eastern Prebetic Zone occurred during the Upper Jurassic to Santonian times coeval to the development of extensional basins in the Western Tethyan area. The proximal part of this passive margin was subsequently incorporated into the external part of the Betic thin-skinned fold-and-thrust belt. The Upper Cretaceous to Cenozoic tectonic evolution of the study area encompassed the following stages: a Campanian to Aquitanian NW-directed contraction; a Burdigalian to upper Miocene extensional reactivation of the main subsalt faults; and a Serravallian NW-directed contractional reactivation. In this scenario, the combined effect of the previous contractional reactivation of pre-existing salt structures together with the Miocene subsalt extension triggered passive salt extrusion of the La Rosa and Jumilla diapirs.

## 1. Introduction

The Betic Cordillera, located in the southwestern part of the Alpine fold-and-thrust belt (Figure 1), is the result of the N–S to NNW–SSE convergence between the major Eurasian and African plates during the Upper Cretaceous to Present times (De Galdeano, 1990; Dercourt et al., 1986; Dewey, Helman, Knott, Turco, & Hutton &, 1989). The eastern part of this cordillera (Figure 2) is subdivided from north to south into the External and Internal Betic Zones (Balanyá & García-Dueñas, 1987; Fallot, 1948). The Internal Betic Zones (e.g. the Malaguide Complex outcropping in Sierra Espuña, Murcia) consist of an allochthonous stack of thrust sheets composed mainly of a thick succession of Triassic to Early Miocene sedimentary rocks (De Jong, 1990; Egeler & Simon, 1969; Martín-Martín et al., 2006; Torres-Roldán, 1979). The External Betic Zones correspond to an orogenic wedge composed by an NW- to NNW-directed fold-and-thrust belt that is detached from the Iberian basement along the Upper Triassic evaporites (Platt et al., 2003). Locally, diapirs made up by these evaporites pierce the thin-skinned thrusted sheets that constitute the fold-and-thrust belt (De Ruig, 1995; Martínez del Olmo, Motis, & Martín, 2015; Moseley, 1973).

During the Mesozoic, the External Betic Zones were represented by the proximal part of the NE-trending South Iberian passive margin (i.e. northern conjugate passive margin of the Alpine Tethys, Bernoulli & Lemoine, 1980; Dewey, Pitman, Ryan, & Bonnin, 1973; Ziegler, 1982). The Alpine Tethys resulted from the Lower to Middle Jurassic rifting followed by the Callovian oceanic flooring that separated the Eurasian and African plates (Schettino & Turco, 2011). However, in the External Betic Zones, the most important rifting phase occurred later allowing the deposition of the Upper Jurassic to Santonian syn-extensional sediments unconformably above the pre-extensional Lower and Middle Jurassic carbonates (De Ruig, 1992; García-Hernández, López-Garrido, Rivas, Sanz de Galdeano, & Vera, 1980; Hanne, White, & Lonergan, 2003; Vera, 2001). During the Upper Jurassic to Santonian, the External Betic Zones (Figure 2) were subdivided into the northwestern Prebetic Zone and the southeastern Subbetic Zone (García-Hernández et al., 1980). According to the thickness and the stratigraphy of the Mesozoic units, the Prebetic Zone is divided, from NW to SE, into the External and Internal Prebetic (De Ruig, 1992; García-Hernández et al., 1980).

**Figure 1.** Geologic map of the Southern termination of the Alpine fold-and-thrust belt in the Western Mediterranean (modified from Vera, 2004).

This study presents a detailed geological map of the Jumilla region, comprising part of the External and Internal Prebetic (see the red square in Figure 2). The structure of the studied area is characterized by an NW-directed fold-and-thrust belt and inactive salt diapirs that are parallel to the ENE- to NE-regional trend of the Betic Cordillera and the Mesozoic South Iberian passive margin. However, the ENE- to NE-regional trend is locally disrupted by the NW-trending Mesozoic to Cenozoic Matamoros Basin, which is flanked by the active Jumilla and La Rosa diapirs.
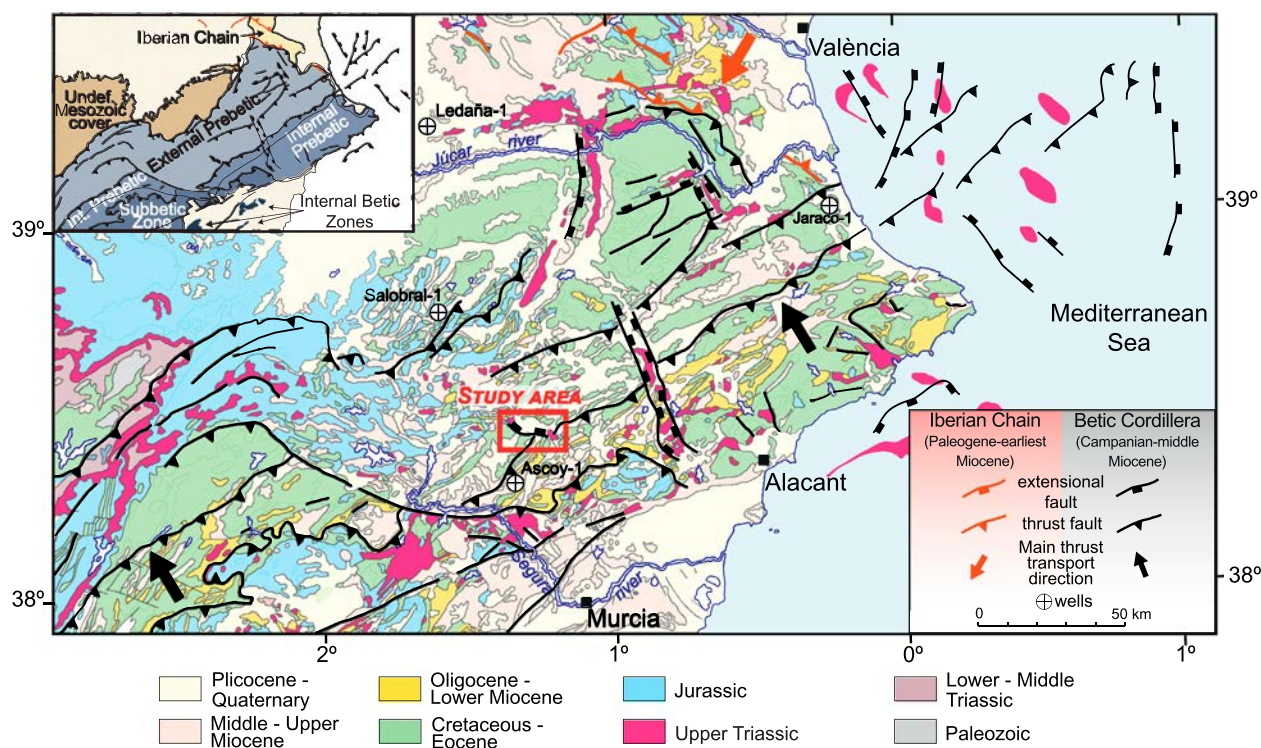


**Figure 2.** Geologic and tectonic maps of the Eastern Betic Cordillera (modified from IGME 1M scale Geological map).

## 2. Methods

The geological map of the Eastern Prebetic Zone at the Jumilla region covers 609 km². The map was constructed as part of a PhD dissertation, with more than six months of fieldwork distributed in three years. The cartographic base consists of 1:50,000 topographic maps, digital terrain models (DTM's at 5 m cell size) and orthophotographs (with 0.25 m pixel resolution) provided by the *Centro Nacional de Información Geográfica* (C.N.I.G.) of the Spanish Government. Geological mapping was performed at 1:5000 scale. Traces of the outcropping geological surfaces (mostly bedding and faults) were mapped in the field using the orthophotographs and up to 6000 dip data were collected using a compass-clinometer. The field data were geo-referenced and transferred into a three-dimensional digital environment (Move™ software from Midland Valley). In this scenario, the digital outcrop characterization using the methodology developed by Fernández (2005) allowed us to complete the mapping of the geological surfaces. The northernmost part of the geological map (i.e. northern part of Sierra de las Cabras unit) is also represented on the map, but it was mapped at less detail than the rest of the area. The mapping of this part benefited from previous works of Baena (1979) and Gallego Coíduras, García Domingo, López Olmedo, and Baena Pepez (1981). The fault symbols depicted on the Main Map reflect the stratigraphical relationship of hanging wall to footwall (i.e. thrust fault: older over younger; extensional fault: younger over older).

The Main Map is accompanied by three cross-sections at 1:50,000 scale. Their orientation was chosen to depict the main structural features of the studied area. Using Move™ software, dip data were projected into the cross-section lines according to the projection vectors calculated by the definition of cylindrical dip-domains. Interpolation and extrapolation of data were also performed using Move™ software. The geometry of the faults was interpreted according to the stratal architecture located in its hanging wall.

## 3. Results

### 3.1. Stratigraphy

The stratigraphic units depicted on the map are classified into four well-differentiated main groups of rocks according to the tectonic events that controlled their deposition (Figure 3).

The pre-extensional succession is subdivided into three main groups of rocks Paleozoic to Middle Triassic, Upper Triassic and uppermost Triassic to Middle Jurassic in age, respectively. The Paleozoic to Middle Triassic unit, which does not crop out in the study area, is located underneath the main detachment (Upper Triassic salt) and is therefore considered mechanical basement. Despite this, the analysis of the stratigraphy based on the Salobral-1 and Jaraco-1 wells (see wells location in Figure 2) reveals Middle Triassic marine carbonates (∼300 m thick) and Lower Triassic detrital continental rocks (∼670 m thick) unconformably overlaying meta-sedimentary quartzites Silurian in age (Lanaja et al., 1987). The Upper Triassic unit is mostly characterized by halite with minor intercalations of volcanic, carbonate and detrital rocks (Ortí, 1974). In the study area (Main Map), this unit acts as the principal detachment decoupling the suprasalt cover from the subsalt basement. Its preserved normal stratigraphy and original thickness are difficult to reconstruct because it is highly deformed by diapiric structures (e.g. La Rosa, Jumilla and Carxe diapirs). Nevertheless, based on well data and composite outcrop sections along the Eastern External Betic Zones, the original Upper Triassic salt thickness is estimated to be ca. 600–700 m (Bartrina et al., 1990; De Torres & Sánchez, 1990). The uppermost Triassic to Middle Jurassic rocks consist of two cartographic units conformable lying above the Upper Triassic salt: the uppermost Triassic – Lower Jurassic mudstones and dolostones and the Middle Jurassic dolostones and oolithic limestones. This unit crops out only in the Sierra de las Cabras, partially in the northern part of Sierra del Carche and in the southeastern part of the study area (Main Map). According to outcrop scale observations and the stratigraphy based on the Ascoy-1 well (see its location in Figure 2), this unit thickens towards the SE: ∼240 m in this part of the External Prebetic to ∼370 m in the Internal Prebetic. In the northwestern part of the study area (Sierra de las Cabras), a low angle unconformity and hard grounds Callovian – Oxfordian in age are located above the Middle Jurassic rocks. This unconformity (Figure 3) is interpreted as the onset of the major extension that affected this segment of the South Iberian margin (García-Hernández et al., 1989).

The syn-extensional succession consists of three main groups of rocks: Upper Jurassic, Neocomian to lower Albian and upper Albian to Santonian in age, respectively. The Upper Jurassic group consists of marine marly limestones, mudstones and oolithic dolostones unconformable lying above the uppermost Triassic to Middle Jurassic unit. It is subdivided into two cartographic units Oxfordian and Kimmeridgian – Tithonian in age (Vilas et al., 1982). This unit crops out in the northern part of the study area (i.e. Sierra de las Cabras) and in the northern part of the Sierra del Carche (Main Map) showing a thickness increase from ∼300 m in the External Prebetic to ∼1700 m in the Internal Prebetic (Azéma, 1977; García-Hernández et al., 1980). The second group of rocks (Neocomian to lower Albian in age) is mainly composed by shallow water limestones, calcarenites, bioclastic calcarenites
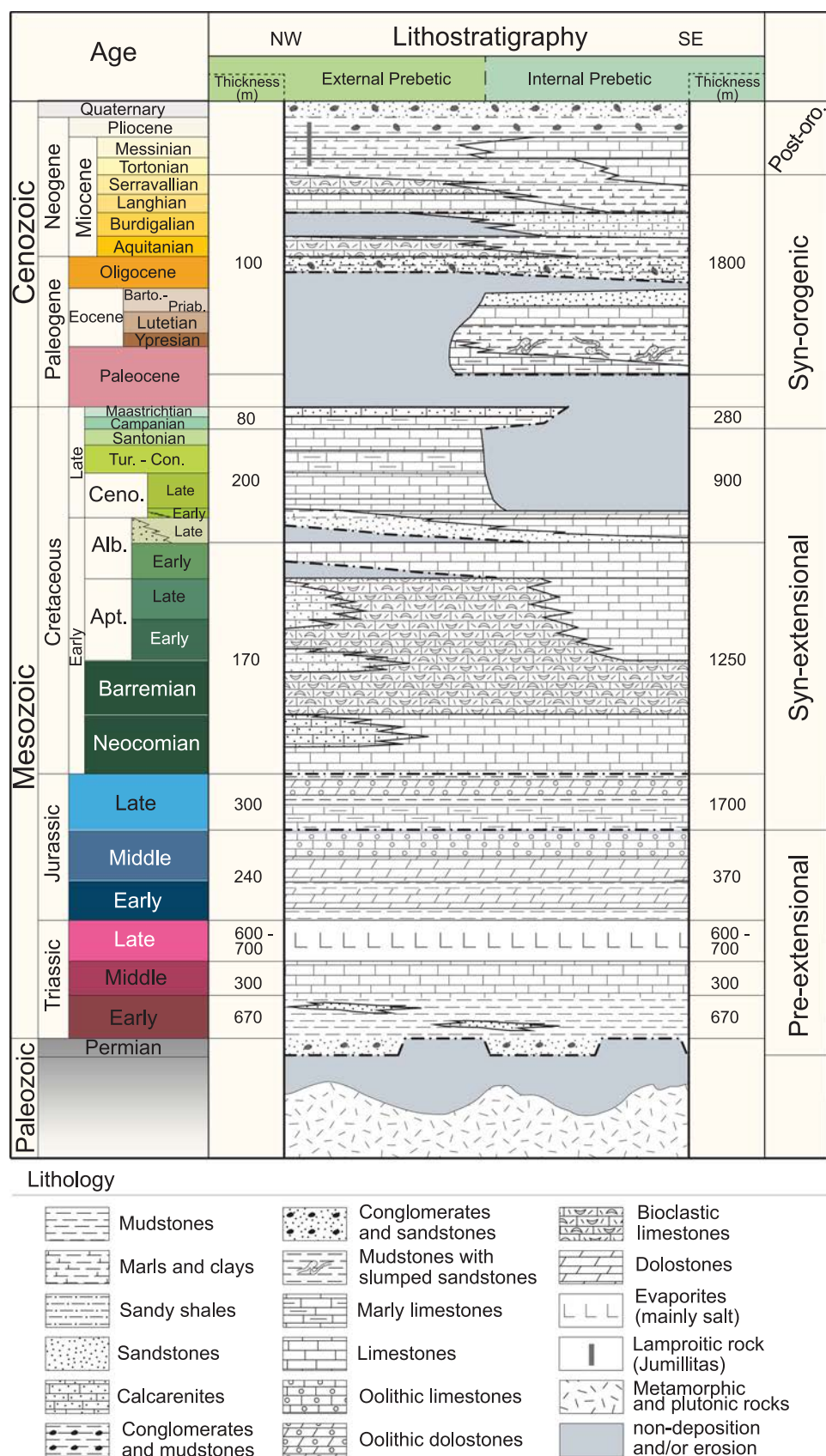
**Figure 3.** Lithostratigraphic chart of the sedimentary facies variation across the External and Internal Prebetic in the Jumilla region. After López-Garrido, 1971; Moseley, 1973; von Hillebrandt, 1974; Ortí, 1974; Martínez del Olmo, Benzaquen, Cabañas, & Uralde, 1975; Azéma, 1977; Rodríguez-Estrella, 1977; García-Hernández et al., 1980; Vera et al., 1982; Vilas, Arias, Elizaga, García de Domingo, & López-Olmedo, 1982; Lanaja, Querol, & Navarro, 1987; Bartrina, Hernández, & Serrano, 1990; Arias, Masse, & Vilas, 1993; Vilas, Martin-Chivelet, & Arias, 2003; Guerrera et al., 2014.

and siliciclastics lying unconformably above the Upper Jurassic unit (Arias et al., 1993; Vilas et al., 1982). This group has been subdivided into four cartographic units (Neocomian – Barremian, lower Aptian, upper Aptian and lower Albian in age) cropping out in the northern part of the Sierras Larga-Sopalmo and Carche and also in Sierra de Santa Ana and Peña Rubia (Main Map). In general, this group thickens towards the SE being ~170 m thick in the External Prebetic and ~1250 m thick in the Internal Prebetic. The third group, upper Albian to Santonian in age, lays unconformable above the previous units and has a more homogeneous carbonate facies association. It has been subdivided into seven cartographic units corresponding to the sedimentary formations defined by Martín-Chivelet (1992): the upper Albian sands (Utrillas sands Fm.), the upper Albian limestones (Jumilla Fm.), the lower Cenomanian marls (Villa de Ves Fm.), the lower Cenomanian dolostones (Alatoz Fm.), the upper Cenomanian limestones (Moratillas Fm.), the Turonian – Coniacian marly limestones (Alarcón Fm.) and the Santonian massive limestones (Sierra de Utiel Fm.). According to outcrop scale observations and well data, the upper Albian to Santonian group thickens towards the SE having an average thickness of ~200 m in the External Prebetic and ~900 m in the Internal Prebetic (Vilas et al., 2003). Locally in the External Prebetic, the Turonian to Santonian succession thickens suddenly related to halokinetic processes (e.g. Sierra del Molar and Buey). In the southern part of the Sierra del Carche, the presence of an erosive unconformity at the base of the Campanian rocks and a regressive general trend from hemipelagic to continental facies is interpreted as the onset of the contractional deformation probably related to the Pyrenean Orogeny and the incipient Betic compression (Andeweg, 2002; Guerrera et al., 2014; Martín-Chivelet, Giménez, & Luperto Sinni, 1997; Rodríguez-Estrella, 1977; Vilas et al., 2003).

The syn-orogenic succession consists of two main groups of rocks: Campanian – Maastrichtian and upper Paleocene – Serravallian. The first group is subdivided into two cartographic units corresponding to the sedimentary formations defined by Martín-Chivelet (1994): the Campanian marly limestones (Carche Fm.) and the Maastrichtian sandy limestones (Molar Fm.). This group displays a moderate thickening trend to the SE being ~80 m thick in the External Prebetic and ~280 m thick in the Internal Prebetic. Locally in the External Prebetic, this unit thickens related to halokinetic processes (e.g. Sierras del Molar and Buey). The Cenozoic succession is well developed in the Internal Prebetic (Main Map) and involves nine cartographic units made up of: upper Paleocene marly limestones and slumped sandstones; Ypresian green clays and marls; Lutetian nummulitic limestones; Bartonian – Priabonian sands and clays; Oligocene

conglomerates, sandstones and marls; Aquitanian bioclastic limestones and marls; Burdigalian calcarenites; Langhian limestones and marls; and Serravallian bioclastic calcarenites and marls. South of the Sierras Larga-Sopalmo and Carche, the Burdigalian to Langhian succession thicken towards the SE and display growth strata geometries related to the subsalt extensional reactivation of the same age. The complete syn-orogenic succession is up to ~100 m thick in the External Prebetic increasing to more than ~1800 m in the Internal Prebetic.

Finally, the post-orogenic succession consists of Tortonian to Quaternary rocks. This succession is subdivided into six cartographic units made up of: Tortonian white marls and limestones; Messinian limestones and marls; Pliocene red conglomerates, sandstones and sands; Pliocene lamproitic rocks; Quaternary alluvial; and Quaternary colluvial (von Hillebrandt, 1974; Guerrera et al., 2014). The deposition of this succession was mainly controlled by extension accommodated by the NE-dipping Maestre subsalt fault (Figure 4(a)). In addition, upper Miocene to Quaternary growth stratal geometries adjacent to the La Rosa and Jumilla diapirs suggest passive diapirism coeval to the deposition of these sediments (Figure 4(b–e)).

### 3.2. Structure

Based on the stratigraphic thickness of the sedimentary succession and the wavelength of the ENE-trending folds, the study area can be subdivided from NW to SE into three different units: Sierra de las Cabras, Jumilla and the Casas del Puerto-Torre del Rico units. The first two units are located in the External Prebetic, and the third one is located in the Internal Prebetic (Escosa, Roca, & Ferrer 2018).

The Sierra de las Cabras unit is characterized by short wavelength and symmetric NE-trending folds involving a thin Jurassic to upper Cenomanian succession unconformably overlain by Serravallian and Tortonian deposits. According to the fold geometry and the thickness of the involved sedimentary successions, it is interpreted that these are detachment folds cored by Upper Triassic salt. Considering the position of the fold hinges, the detachment is interpreted to be horizontal being located between the 0 and 100 m below the sea level. Southeast from this area, the Jumilla unit includes a Lower to Middle Jurassic succession with an assumed constant thickness (García-Hernández et al., 1980) overlain by the Upper Jurassic to Quaternary rocks displaying thickness changes across the area. This sedimentary succession is deformed by NE-trending narrow anticlines and broad synclines and by suprasalt faults dipping in general towards the northwest and southeast. According to the stratigraphic thickness, the wavelength of the folds and the position of the fold hinges, it is interpreted that

**Figure 4.** (a) Oblique Google Earth® image of the Jumilla Region with the location of the main structural and geomorphological features, the Matamoros Basin and La Rosa and Jumilla Diapirs. (b) Vertical to overturned upper Miocene sandstones and marls in the southern margin of the Jumilla Diapir (see location in Figure 4(a). (c) Panoramic view of the La Rosa Diapir from Sierra del Carche (see location in Figure 4(a). (d) Edge of La Rosa Diapir where Upper Triassic clays and gypsum are in contact with highly deformed Quaternary sediments. (e) E-dipping white marls and sandstones probably Tortonian – Messinian in age adjacent to the Jumilla Diapir.

the main detachment is horizontal being located at 800–1000 m below the sea level. In this unit, the lateral continuity of the NE-trending structures is interrupted by the Matamoros Basin (Figure 4(a)) which occupies an elongated NW-trending area extending from the Jumilla Diapir to the La Rosa Diapir (Figure 4(b,c)).

South of the previous unit, the Casas del Puerto – Torre del Rico unit is characterized by a thicker Upper Jurassic to Campanian succession and a complete Paleogene to Miocene sequence that is not present in the northern units. At the northwestern limit of the Sierras Larga-Sopalmo and Carche, there is a system of NW-directed thrust faults affecting a thinned succession of Upper Jurassic to middle Miocene rocks. From here to the south and according to the stratigraphic thickness and the dip attitudes, the general structure of this unit can be interpreted as a broad monoclinal followed by a nearly horizontal panel. The base of the horizontal panel of this monocline could be located between −3200 and −5000 m below the sea level slightly dipping towards the southeast.

## 4. Discussion

The Eastern Prebetic Zone at the Jumilla region is characterized by a well exposed uppermost Triassic to Quaternary sedimentary succession. The geometrical analysis of the Mesozoic to Cenozoic structures in these units allows inferring a progressive SE-deepening of the Upper Triassic regional detachment associated with NE-trending basement steps. From NW to SE, these basement steps are interpreted to be controlled by the SE-dipping Jumilla and Sopalmo-Carxe subsalt faults. In the NW-trending Matamoros Basin, the analysis of surficial dip attitudes allows inferring that this basin is controlled by the NE-dipping Maestre Fault. The age of the associated growth stratal geometries of the suprasalt cover along the faulted blocks allows constraining the age of the faulting. Considering this, the Jumilla, Sopalmo-Carxe and the Maestre subsalt extensional faults were active during the Upper Jurassic to Santonian and were later extensionally reactivated during the Burdigalian to Langhian. The base of the syn-contractional sediments (i.e. Campanian unconformity) over the hanging wall of the subsalt faults show similar or less topographic elevation compared with the same syn-contractional sequence over their footwalls. Therefore, these evidences suggest that basement faults were not positive inverted, and thus in the study area, a thin-skinned inversion model needs to be assumed during the Betic compression.

These observations together with the sequential restoration of the extensional structures led to interpret that in the Eastern Prebetic Zone, the Upper Jurassic to Santonian extensional deformation affecting the subsalt basement and the suprasalt cover was decoupled by the Upper Triassic salt. This implied that extension within the sedimentary cover was partially controlled by subsalt faults and partially by thin-skinned tectonics represented by listric suprasalt faults and piercing diapirs. This agrees with regional stratigraphic and structural evidences along the Eastern Prebetic Zone supporting the existence of a Mesozoic phase of extension (De Ruig, 1995; García-Hernández et al., 1989; Pedrera, Marín-Lechado, Galindo-Zaldívar, & García-Lobón, 2014; Vilas et al., 2003). However, ophiolites Middle Jurassic in age outcropping in the Internal Betic Zone demonstrates that the Southern Iberian margin was already a passive margin with the oceanic crust at this time (Puga et al., 2011). Extension in the South Iberian margin which took place between the Lower and Middle Jurassic was clearly connected with the opening of the Central Atlantic Ocean to the west (De Jong, 1990; Srivastava et al., 1990). Therefore, the following Upper Jurassic to Santonian extension could be related to the continued opening of the Central Atlantic and synchronous development of extensional basins in the Western Tethyan area (Hanne et al., 2003; Ziegler, 1989). Examples of Mesozoic extension (i.e. post Alpine Tethys rifting) are also documented in the Eastern Iberia (e.g. Columbrets Basin, Roca, Salas, & Guimerà, 1994), in the Organyà Basin (García-Senz, 2002) or along the Maghrebian margin represented by E–W rifting in Tunisia (Guiraud, 1998) and the Riffian – Tellian troughs (Wildi, 1983). Therefore, we interpret that the Upper Jurassic to Santonian extension is limited to the eastern parts of the South Iberian margin, and this process is independent from the formation of the Alpine Tethys.

The subsequent Betic compression was governed by thin-skinned shortening detached along the Upper Triassic salt which deformed the sedimentary cover and diapirs. In the study area, two major contractional events Campanian – Aquitanian and Serravallian in age are identified. The Campanian – Aquitanian contractional deformation appeared to be absorbed by diapir squeezing. Afterwards, in the Serravallian stage, the suprasalt cover together with the squeezed salt structures was contractionally translated towards the NW. However, the study area was affected by a Burdigalian to upper Miocene extensional reactivation of the main subsalt faults (i.e. Jumilla, Sopalmo – Carxe and Maestre faults). In the Eastern Prebetic Zone, this extension was mainly SW–NE and in the study area was conducted by the NE-dipping Maestre Fault. As a result, a thickened Miocene succession was deposited in the Matamoros Basin. This late extension could be related to the late Oligocene to Miocene extension that took place in the western Mediterranean region, in the Alboran Sea and in the Valencia Trough (Hanne et al., 2003; Maillard & Mauffret, 1999; Roca & Guimerà, 1992; Torné & Banda, 1992). In addition, the

combined effect of the Campanian to Aquitanian contractional reactivation of pre-existing salt structures and the Miocene extensional reactivation conducted by the NE-dipping Maestre Fault, triggered passive salt extrusion of La Rosa and Jumilla diapirs (Figure 4(b,c)). In this scenario, according to the Tortonian to Quaternary growth strata located adjacent to these diapirs (Figure 4(d,e)), salt was evacuated from beneath the Matamoros Basin to the rising diapirs creating sedimentary space for the deposition of the Miocene to Quaternary units.

## 5. Conclusions

This work presents a new detailed geological map of the Eastern Prebetic Zone at the Jumilla region that has facilitated the construction of cross-sections and a sequential restoration illustrating the interpretation of the tectonic evolution of the area. The geological map, the cross-sections and the outcrop observations support the hypothesis that the major Mesozoic rifting phase affecting the Eastern Prebetic Zone occurred during the Upper Jurassic to Santonian times coeval to the development of extensional basins in the Western Tethyan area. The proximal part of this passive margin was subsequently incorporated into the external part of the Betic thin-skinned fold-and-thrust belt. The Upper Cretaceous to Cenozoic tectonic evolution of the study area was characterized by: a Campanian to Aquitanian NW-directed contraction; a mainly Burdigalian to upper Miocene extensional reactivation of the main subsalt faults; and a Serravallian NW-directed contractional reactivation of the thin-skinned thrust faults. In addition, the Campanian to Aquitanian contractional reactivation of pre-existing salt structures together with the Miocene subsalt extension triggered passive salt extrusion of the La Rosa and Jumilla diapirs coeval to the deposition of the Miocene to Quaternary units.

## Software

The Main Map was produced using Move™ software from Midland Valley which was used to ensemble the digital terrain models (DTM), the orthophotographs and to digitize the lithological contacts and the main structures mapped in the field. The cross-sections were also constructed and restored using Move™ from Midland Valley. Final editing and PDF construction were made using Adobe Illustrator™.

## Acknowledgements

## Disclosure statement

## Funding

## ORCID

*Frederic O. Escosa* http://orcid.org/0000-0002-1908-1037
*O. Ferrer* http://orcid.org/0000-0001-5545-9992
*E. Roca* http://orcid.org/0000-0002-0827-4175

## References

Andeweg, B. (2002). *Cenozoic tectonic evolution of the Iberian Peninsula: Causes and effects of changing stress fields* (PhD dissertation). Vrije Universiteit, Amsterdam, 178 p.

Arias, C., Masse, J. P., & Vilas, L. (1993). Caracterización secuencial y bioestratigráfica del Aptiense-Albiense p.p. en la Sierra de Sopalmo, Prebético Interno (Prov. de Murcia). *Boletín del Instituto Geológico y Minero de España*, *104–106*, 603–612.

Azéma, J. (1977). *Étude géologique des zones externes des cordillères bétiques aux confins des provinces d'Alicante et de Murcie (Espagne)* (PhD dissertation). Université Pierre et Marie Curie, Paris, 393 p.

Baena, J. (1979). Mapa Geológico y Memoria explicativa de la Hoja Jumilla (nº 869) del Mapa geológico Nacional a escala 1:50.000. Instituto Geológico y Minero de España, Madrid, 49.

Balanyá, J. C., & García-Dueñas, V. (1987). Les directions structurales dans le Domaine d'Alborán de part et d'autre du Détroit de Gibraltar. *Comptes Rendus de l'Académie des Sciences de Paris*, *304*, 929–932.

Bartrina, T., Hernández, E., & Serrano, A. (1990). Estudio de subsuelo del Trías salino en la Depresión Intermedia. In F. Ortí & J. M. Salvany (Eds.), *Formaciones evaporíticas de la Cuenca del Ebro y cadenas periféricas y de la zona de Levante* (pp. 232–238). Barcelona: ENRESA – Universitat de Barcelona.

Bernoulli, D., & Lemoine, M. (1980). *Birth and early evolution of the Tethys: The overall situation*. Paper presented at the 26th International Geological Congress (pp. 59–96), Paris.

De Galdeano, C. S. (1990). Geologic evolution of the Betic Cordilleras in the Western Mediterranean, Miocene to the present. *Tectonophysics*, *172*, 107–119. doi:10.1016/0040-1951(90)90062-D

De Jong, K. (1990). Alpine tectonics and rotation pole evolution of Iberia. *Tectonophysics*, *184*, 279–296. doi:10.1016/0040-1951(90)90444-D

De Ruig, M. J. (1992). *Tectono-sedimentary evolution of the Prebetic fold belt of Alicante (SE Spain). A study of stress fluctuations and foreland basin deformation* (PhD dissertation). Vrije Universiteit, Amsterdam, 277 p.

De Ruig, M. J. (1995). Extensional diapirism in the Eastern Prebetic Foldbelt, southeastern Spain. In M. P. A. Jackson, D. G. Roberts, & S. Snelson (Eds.), *Salt tectonics: A global perspective* (pp. 353–367). AAPG Memoir 65.

De Torres, T., & Sánchez, A. (1990). Espesores de las Facies Keuper en la Rama Castellana de la Cordillera Ibérica y en el Dominio Prebético. In F. Ortí & J. M. Salvany (Eds.), *Formaciones evaporíticas de la Cuenca del Ebro y cadenas periféricas, y de la zona de Levante* (pp. 212–218). Barcelona: ENRESA – Universitat de Barcelona.

Dercourt, J., Zonenshain, L. P., Ricou, L. E., Kazmin, V. G., Le Pichon, X., Knipper, A. L., … Biju-Duval, B. (1986). Geological evolution of the Tethys belt from the Atlantic to the Pamirs since the Lias. *Tectonophysics*, *123*, 241–315. doi:10.1016/0040-1951(86)90199-X

Dewey, J. F., Helman, M. L., Knott, S. D., Turco, E., & Hutton &, D. H. W. (1989). Kinematics of the western Mediterranean. In M. P. Coward, D. Dietrich, & R. G. Park (Eds.), *Alpine tectonics. Geological society of London special publications* (pp. 45, 265–283). doi:10.1144/GSL.SP.1989.045.01.15

Dewey, J. F., Pitman III, W. C., Ryan, W. B. F., & Bonnin, J. (1973). Plate tectonics and the evolution of the Alpine System. *Geological Society of America Bulletin*, *84*, 3137–3180. doi:10.1130/0016-7606(1973)84<3137:PTATEO>2.0.CO;2

Egeler, C. G., & Simon, O. J. (1969). Orogenic evolution of the Betic Zone (Betic Cordilleras, Spain), with emphasis on the nappe structures. *Geologie en Mijnbouw*, *48*, 296–205.

Escosa, F. O., Roca, E., & Ferrer. O. (2018). Testing thin-skinned inversion of a prerift salt-bearing passive margin (Eastern Prebetic Zone, SE Iberia). *Journal of Structural Geology*, *109*, 55–73.

Fallot, P. (1948). Les Cordillères Bétiques. *Estudios Geológicos*, *8*, 83–172.

Fernández, O. (2005). Obtaining a best fitting plane through 3D georeferenced data. *Journal of Structural Geology*, *27*, 855–858. doi:S0191814105000143

Gallego Coíduras, I., García Domingo, A., López Olmedo, F., & Baena Pepez, J. (1981). Mapa Geológico y Memoria explicativa de la Hoja Ontur (n° 844) del Mapa geológico Nacional a escala 1:50.000. Instituto Geológico y Minero de España, Madrid, 49.

García-Hernández, M., López Garrido, A. C., Martín Algarra, A., Molina Cámara, J. M., Ruiz-Ortiz, P. A., & Vera, J. A. (1989). Las discontinuidades mayores del Jurásico de las Zonas Externas de las Cordilleras Béticas: análisis e interpretación de los ciclos sedimentarios. *Cuadernos de Geología Ibérica*, *13*, 35–52.

García-Hernández, M., López-Garrido, A. C., Rivas, P., Sanz de Galdeano, C., & Vera, J. A. (1980). Mesozoic palaeogeographic evolution of the external zones of the Betic Cordillera. *Geologie en Mijnbouw*, *59*, 155–168.

García-Senz, J. M. (2002). *Cuencas extensivas del Cretácico Inferior en los Pirineos centrales, formación y subsecuente inversión* (PhD dissertation). University of Barcelona, Barcelona, 310 pp.

Guerrera, F., Mancheño, M. A., Martín-Martín, M., Raffaelli, G., Rodríguez-Estrella, T., & Serrano, F. (2014). Paleogene evolution of the External Betic Zone and geodynamic implications. *Geologica Acta*, *12*, 170–192. doi:10.1344/GeologicaActa2014.12.3.1

Guiraud, R. (1998). Mesozoic rifting and basin inversion along the northern African Tethyan margin: An overview. In D. S. MacGregor, R. T. J. Moody, & D. D. Clark-Lowes (Eds.), *Petroleum geology of North Africa. Geological society, London, special publication* (Vol. 133, pp. 217–229). London: Geological Society.

Hanne, D., White, N., & Lonergan, L. (2003). Subsidence analyses from the Betic Cordillera, southeast Spain. *Basin Research*, *15*, 1–21.

von Hillebrandt, A. (1974). Bioestratigrafía del Paleógeno en el sureste de España (Provincias de Murcia y Alicante). *Cuadernos de Geología Ibérica*, *5*, 135–153.

Lanaja, J. M., Querol, R., & Navarro, A. (1987). Contribución de la exploración petrolífera al conocimiento de la geología de España. Instituto Geológico y Minero de España, Madrid, 465.

López-Garrido, A. C. (1971). *Geología de la Zona Prebética al NE de la provincia de Jaén* (PhD dissertation). Universidad de Granada, 317 p.

Maillard, A., & Mauffret, A. (1999). Crustal structure and riftogenesis of the Valencia trough (northwestern Mediterranean Sea). *Basin Research*, *11*, 357–379.

Martín-Chivelet, J. (1992). *Las plataformas carbonatadas del Cretácico Superio de la Margen Bética (altiplano de Jumilla – Yecla, Murcia)* (PhD dissertation). Universidad Complutense de Madrid, 899 p.

Martín-Chivelet, J. (1994). Litoestratigrafia del Cretácico superior del Altiplano de Jumilla-Yecla (Zone Prebética). *Cuadernos de Geología Ibérica*, *18*, 117–173.

Martín-Chivelet, J., Giménez, R., & Luperto Sinni, E. (1997). La discontinuidad del Campaniense basal en el Prebético: ¿Inicio de la convergencia alpina en el Margen Bética? *Geogaceta*, *22*, 121–124.

Martín-Martín, M., Martín-Rojas, I., Caracuel, J. E., Estévez-Rubio, A., Algarra, A. M., & Sandoval, J. (2006). Tectonic framework and extensional pattern of the Malaguide Complex from Sierra Espuña (Internal Betic Zone) during Jurassic–Cretaceous: Implications for the Westernmost Tethys geodynamic evolution. *International Journal of Earth Sciences*, *95*, 815–826.

Martínez del Olmo, W., Benzaquen, M., Cabañas, I., & Uralde, M. A. (1975). Mapa y memoria explicativa de la Hoja Onteniente (n° 820) del Mapa geológico Nacional a escala 1:50.000. Instituto Geologico y Minero de España, Madrid, 49.

Martínez del Olmo, W., Motis, K., & Martín, D. (2015). El papel del diapirismo de la sal Triásica en la estructuración del Prebético (SE de España). *Revista de la Sociedad Geológica de España*, *28*, 3–24.

Moseley, F. (1973). Diapiric and gravity tectonics in the Pre-Betic, (Sierra Bernia) of south-east Spain. *Boletín del Instituto Geológico y Minero de España*, *84*, 114–126.

Ortí, F. (1974). El Keuper del Levante español. *Estudios Geológicos*, *30*, 7–46.

Pedrera, A., Marín-Lechado, C., Galindo-Zaldívar, J., & García-Lobón, J. L. (2014). Control of preexisting faults and near-surface diapirs on geometry and kinematics of fold-and-thrust belts (Internal Prebetic, Eastern Betic Cordillera). *Journal of Geodynamics*, *77*, 135–148.

Platt, J. P., Allerton, S., Kirker, A., Mandeville, C., Mayfield, A., Platzman, E. S., & Rimi, A. (2003). The ultimate arc: Differential displacement, oroclinal bending, and vertical axis rotation in the external Betic-Rif arc. *Tectonics*, *22*, 1017–1048. doi:10.1029/2001TC001321

Puga, E., Fanning, M., Díaz de Federico, A., Nieto, J. M., Beccaluva, L., Bianchini, G., & Díaz Puga, M. A. (2011). Petrology, geochemistry and U-Pb geochronology of the Betic Ophiolites: Inferences for Pangaea break-up and birth of the westernmost Tethys Ocean. *Lithos*, *124*, 255–272.

Roca, E., & Guimerà, J. (1992). The neogene structure of the eastern Iberian margin: Structural constraints on the crustal evolution of the Valencia trough (western Mediterranean). *Tectonophysics*, *203*, 203–218.

Roca, E., Salas, R., & Guimerà, J. (1994). Mesozoic extensional tectonics in the southeast Iberian Chain. *Geological Magazine*, *131*, 155–168.

Rodríguez-Estrella, T. (1977). Síntesis geológica del Prebético de la provincia de Alicante. *Boletín del Instituto Geológico y Minero de España*, *88*, 183–214 and 88, 273–299.

Schettino, A., & Turco, E. (2011). Tectonic history of the western Tethys since the Late Triassic. *Geological Society of America Bulletin*, *123*, 89–105.

Srivastava, S. P., Schouten, H., Roest, W. R., Klitgord, K. D., Kovacs, L. C., Verhoef, J., & Macnab, R. (1990). Iberian plate kinematics: A jumping plate boundary between Eurasia and Africa. *Nature*, *344*, 756–759.

Torné, M., & Banda, E. (1992). Crustal thinning from the Betic Cordillera to the Alboran Sea. *Geo-Marine Letters*, *12*, 76–81.

Torres-Roldán, R. L. (1979). The tectonic subdivision of the Betic Zone (Betic Cordilleras, southern Spain): Its significance and one possible geotectonic scenario for the westernmost Alpine belt. *American Journal of Sciences*, *279*, 19–51.

Vera, J. A. (2001). Evolution of the south Iberian continental margin. In P. A. Ziegler, W. Cavazza, A. H. F. Roberston, & S. Crasquin-Soleau (Eds.), *Peri-Tethys Memoir 6: Peri-Tethyan Rift/Wrench Basins and passive margins* (pp. 186, 109–143). Madrid: SGE and IGME.

Vera, J. A. (2004). *Geología de España*. Madrid: SGE-IGME.

Vera, J. A., García-Hernández, M., López-Garrido, A. C., Comas, M. C., Ruíz-Ortíz, P. A., & Martín-Algarra, A. (1982). El Cretácico de las Cordilleras Béticas. In A. García (Ed.), *El Cretácico de España* (pp. 515–632). Madrid: Universidad Complutense de Madrid.

Vilas, L., Arias, C., Elizaga, E., García de Domingo, A., & López-Olmedo, F. (1982). Consideraciones sobre el Cretácico inferior de la zona de Jumilla-Yecla. *Cuadernos Geología Ibérica*, *8*, 635–649.

Vilas, L., Martin-Chivelet, J., & Arias, C. (2003). Integration of subsidence and sequence stratigraphic analyses in the Cretaceous carbonate platforms of the Prebetic (Jumilla–Yecla Region), Spain. *Palaeogeography, Palaeoclimatology, Palaeoecology*, *200*, 107–129. doi:10.1016/S0031-0182(03)00447-4

Wildi, W. (1983). La chaîne tello-rifaine (Algérie, Maroc, Tunisie): Structure, stratigraphie et évolution du Trias au Miocène. *Rev. Géol. Dyn. Géogr. Phys.*, *24*, 201–297.

Ziegler, P. A. (1982). *Geological atlas of Western and Central Europe*. Amsterdam: Elsevier.

Ziegler, P. A. (1989). Evolution of the North Atlantic – An overview. In A. J. Tankard & H. R. Balkwill (Eds.), *Extensional tectonics and stratigraphy of the North Atlantic margins* (pp. 111–129). AAPG Memoir, 46.

**Annex 3: "Testing thin-skinned inversion of a prerift salt-bearing passive margin (Eastern Prebetic Zone, SE Iberia)".**

# Testing thin-skinned inversion of a prerift salt-bearing passive margin (Eastern Prebetic Zone, SE Iberia)

Frederic O. Escosa*, Eduard Roca, Oriol Ferrer

*Institut de Recerca Geomodels, Departament de Dinàmica de la Terra i de l'Oceà, Facultat de Ciències de la Terra, Universitat de Barcelona, Barcelona, c/ Martí i Franquès s/n., 08028, Spain*

## ARTICLE INFO

## ABSTRACT

Detailed geologic mapping combined with well and seismic data from the Eastern Prebetic Zone (SE Iberia) reveal extensional and contractional structures that permit characterization of passive margin development and its incorporation into a thin-skinned fold-and-thrust belt. The study area is represented by NW-directed, ENE-trending folds and thrusts faults locally disrupted by the NW-trending Matamoros Basin and the active Jumilla and La Rosa diapirs. These structures resulted from the thin-skinned inversion of the proximal part of the Eastern South Iberian passive margin containing prerift salt. Here, Upper Jurassic to Santonian thick-skinned extension controlled the accumulation of sediment over mobile prerift salt. This in turn defined the style of salt tectonics characterized by monoclinal drape folds, suprasalt extensional faults and diapirs. The structural and sedimentological analysis suggests that during extension, salt localizes strain thus decoupling sub- and suprasalt deformation. Thick-skinned extension controls suprasalt deformation as well as its location and distribution which changes over time. Salt also localizes strain during inversion. The preexisting salt structures, weaker than adjacent areas, preferentially absorb the contractional deformation. In addition, the stepped subsalt geometry that results from thick-skinned extension also controls the shortening propagation. Therefore, the degree of strain localization depends on the thickness of the suprasalt cover and on the dip of subsalt faults relative to the thin-skinned transport direction.

## 1. Introduction

Salt is common in passive-margin basins such as in the central Atlantic or the Tethyan margins (e.g. Rowan et al., 2004; Roca et al., 2006; Saura et al., 2013; Jackson et al., 2015). As a function of the relationship between evaporite deposition and passive margin development, salt can be classified as prerift, syn-stretching, syn-thinning and syn-exhumation (e.g. Jackson and Vendeville, 1994; Tari et al., 2003; Rowan, 2014). Of these, prerift salt decouples supra- and subsalt deformation during early extension thereby inhibiting the upwards propagation of subsalt faults into the cover and favoring the development of monoclinal drape folds and suprasalt faults (Withjack and Callaway, 2000; Jackson and Vendeville, 1994). As extension progresses, active suprasalt faults soled into the salt detachment can trigger diapirism. Deformation gradually becomes more coupled as the offset of the subsalt faults increases and the salt layer is depleted. This disrupts the salt continuity allowing the upwards propagation of the subsalt faults into the suprasalt cover.

The role of the prerift salt during the tectonic evolution of the central Atlantic margins is well known because the extensional architecture has not been subsequently affected by inversion (Favre and Stampfli, 1992; Cramez and Jackson, 2000; Tari et al., 2003; Rowan et al., 2004). However, most of the Tethyan passive margins have been incorporated into orogenic edifices like the Pyrenees – Bay of Biscay system or the Alps (e.g. Lemoine et al., 1986; Serrano et al., 1994; Muñoz, 2002; Canérot et al., 2005; Roca et al., 2011; Decarlis et al., 2014; Tavani and Granado, 2014). In this case, their structural style depends on many factors such as the strain rate, the inherited architecture or the distribution and position of mechanically weak horizons (e.g. salt detachments) resulting in two deformation styles end-members: thick- and/or thin-skinned tectonic models (Ellis et al., 1998; Beaumont et al., 2000; Jammes and Huismans, 2012). In orogens where thick-skinned inversion dominates, the reconstruction of the tectonic evolution of the salt-bearing passive margin is obscured by large thrust faults and folds involving the sub- and suprasalt rocks (e.g. Cantabrian Mountains, Western Pyrenees, Carola et al., 2015).

What is the response of the extensional structure ahead of a contractional reactivation? Does the inherited extensional structure control

---

the inversion of passive-margin basins that contain prerift salt? The present study aims to answer these questions by providing new data from the Eastern Prebetic Zone (SE Iberia) that resulted from the moderate inversion of the Eastern South Iberian passive margin. In this scenario, thick-skinned extension controlled the accumulation of sediment over mobile prerift salt. This in turn defined the style of salt tectonics that developed during extension. The contractional structure is characterized by a thin-skinned deformation style restricted to the suprasalt cover with moderate folding and thrusting (Platt et al., 2003; Ter Borgh et al., 2011). The cover was slightly translated in relation to its original location with respect to the undeformed subsalt basement. This general configuration allows for an accurate kinematic and architectural reconstruction of the salt-bearing passive margin and the subsequent fold-and-thrust belt development.

The case study presented here provides key insights into the understanding of the role of the prerift salt during passive margin development and its subsequent incorporation into a fold-and-thrust belt. We suggest that salt localizes strain during extension thereby decoupling supra- and subsalt deformation. Thick-skinned extension controls the suprasalt deformation, and its location and distribution changes over time. In the early stages, deformation is equally distributed over the faulted blocks. Despite this, as extension progresses, folding and faulting is mostly localized above the footwall of the main subsalt faults; and translation with minor folding is concentrated above the hanging walls. During inversion, the interplay between shortening, the inherited subsalt structure and the preexisting salt diapirs plays an important role in forming the deformation structures of the cover, which is influenced by an effective salt detachment, the dip and dip direction of the subsalt faults, and the presence of mechanically weak salt bodies that compartmentalize mechanically resistant cover blocks.

## 2. Regional geologic overview

The Betic Cordillera and the Rif constitute the Gibraltar Arc (Fig. 1a), which is situated at the westernmost end of the Alpine Mediterranean belt (Dercourt et al., 1986; Dewey et al., 1989). Its formation was driven by the N-S to NNW-SSE convergence between the major Eurasian and African plates, together with the westward displacement of the Alboran Domain, located in between (e.g. De Galdeano, 1990).

The Betic Cordillera is generally subdivided from north to south into the External and Internal Betic Zones (Fallot, 1948; Balanyá and García-Dueñas, 1987; Vera, 2004). The Internal Betic Zones consist of an allochthonous stack of thrust sheets composed mainly of Triassic and older rocks metamorphosed during the Upper Cretaceous to Paleogene (Egeler and Simon, 1969; Torres-Roldán, 1979; De Jong, 1990). The External Betic Zones correspond to a broad orogenic wedge that is composed of a NW- to NNW-directed fold-and-thrust belt that is Campanian to middle Miocene in age and is detached from the Iberian basement along the Upper Triassic salt (Platt et al., 2003). In general, the thrusted sheets are composed of an uppermost Triassic to Middle Jurassic unit characterized by a minor thickness increase towards the SE, and an Upper Jurassic to Santonian unit illustrating major thickening towards the SE (García-Hernández et al., 1980, 1989; De Ruig, 1992; Hanne et al., 2003). In addition, the thrusted sheets are pierced by diapirs of Upper Triassic salt that were emplaced from Mesozoic to Quaternary times (Moseley, 1973; De Ruig, 1995).

During the Mesozoic, the External Betic Zones represented the proximal part of the NE-trending South Iberian passive margin (i.e. northern conjugate passive margin of the Alpine Tethys, Fig. 1b) located southeast of the Iberian Massif (Dewey et al., 1973; Bernoulli and Lemoine, 1980; Ziegler, 1982). The Alpine Tethys was the result of Lower and Middle Jurassic rifting followed by the Callovian oceanic flooring (Fig. 1b) that separated the Eurasian and African plates (Schettino and Turco, 2010). Oceanic flooring is evidenced by Middle Jurassic ophiolites currently outcropping in the Internal Betic Zones
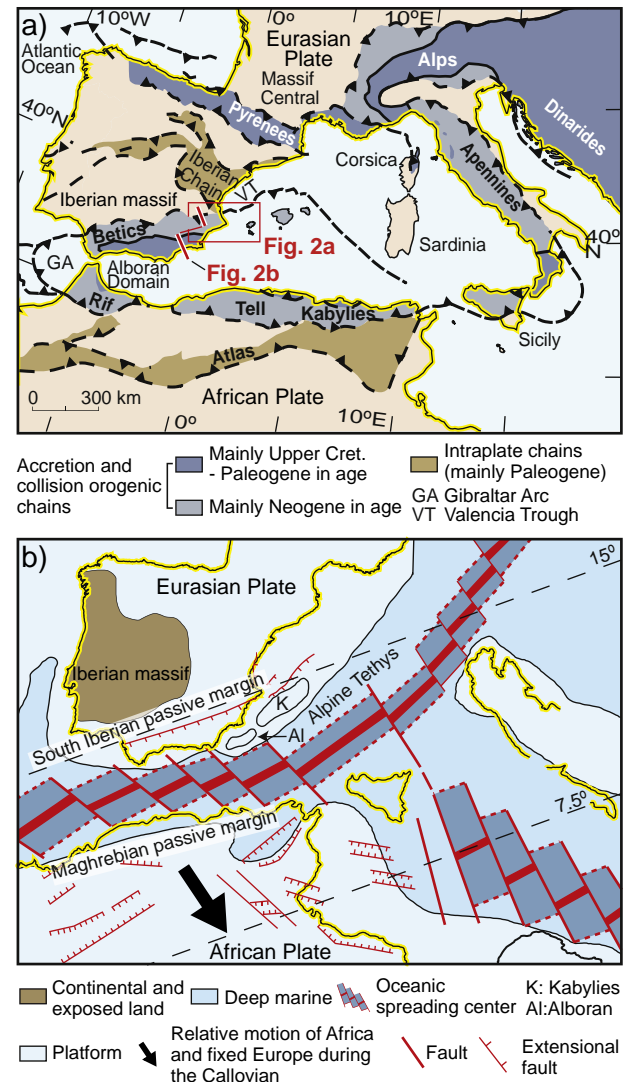


**Fig. 1.** a). Present day tectonic map of the eastern Mediterranean depicting the southeastern termination of the Alpine fold-and-thrust belt. b) Paleotectonic map of North Africa and Iberia for Callovian times, modified from Frizon de Lamotte et al. (2011).

(Puga et al., 2011). This rifting episode is clearly connected with the opening of the Central Atlantic Ocean to the west (Klitgord and Schouten, 1986; De Jong, 1990; Srivastava et al., 1990). However, a major Upper Jurassic to Santonian rift event affected the Eastern External Betic Zones related to a combination of continued opening of the Central Atlantic and synchronous development of extensional basins in the western Tethyan area (Ziegler, 1989; Hanne et al., 2003). In the study area, this rift allowed for the deposition of the Upper Jurassic to Santonian syn-extensional sediments unconformably overlying the uppermost Triassic to Middle Jurassic carbonates that show minor thickness changes (García-Hernández et al., 1980, 1989; De Ruig, 1992; Vera, 2004; Hanne et al., 2003). During this time, on the basis of both tectonic and stratigraphic criteria, the External Betic Zones (Fig. 2a) were subdivided into the northwestern Prebetic Zone and the southeastern Subbetic Zone (García-Hernández et al., 1980). The Prebetic Zone is characterized by continental to shallow-platform deposits including inner and slope facies. The Subbetic Zone is formed by deep basinal and pelagic deposits (e.g. García-Hernández et al., 1980). According to the thickness and the stratigraphy of the Mesozoic units, the Prebetic Zone is subdivided (from NW to SE) into the External and Internal Prebetic (De Ruig, 1992).

Specifically, the study area is located in the Jumilla region (SE
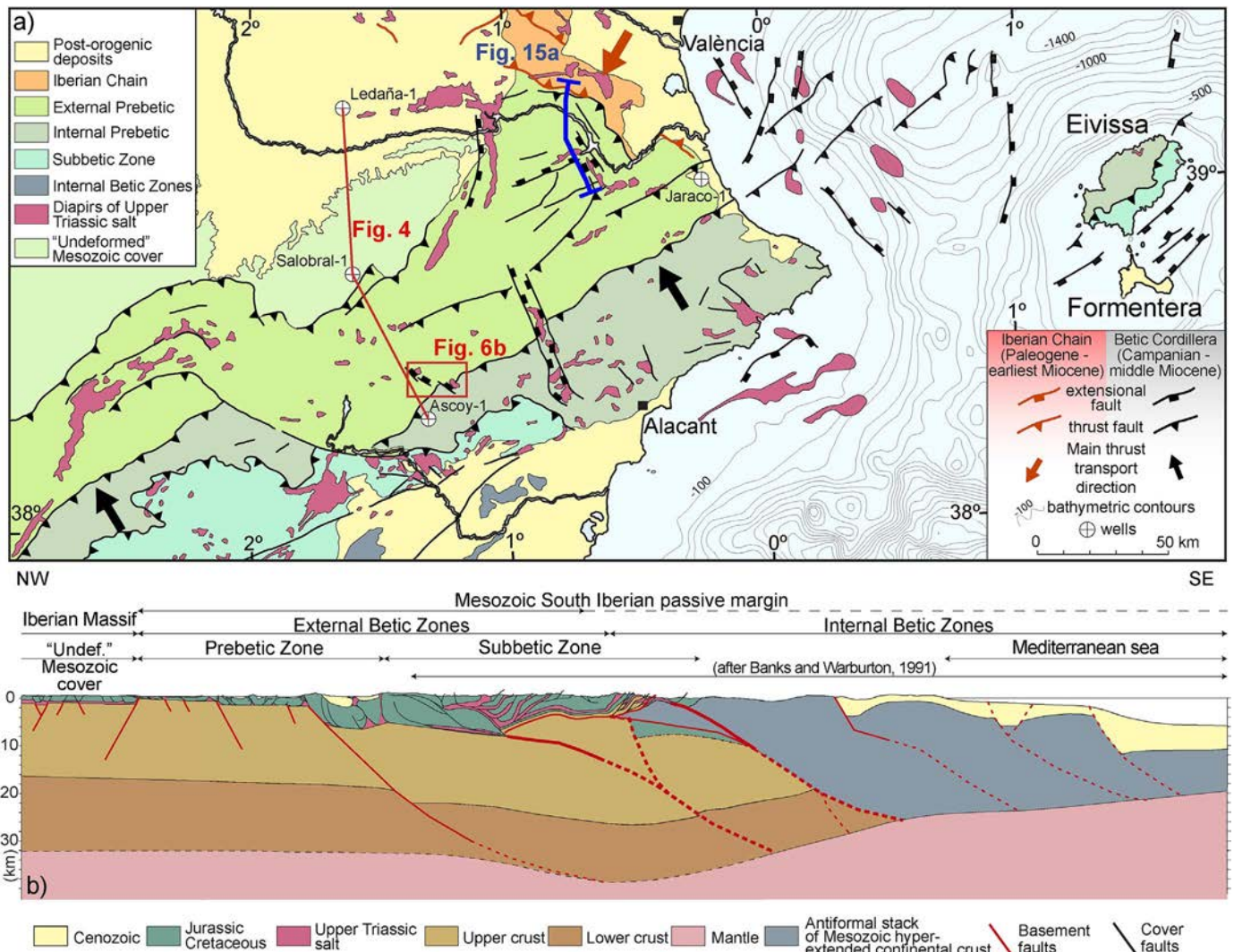
**Fig. 2.** a) Tectonic map of the Eastern Betic Cordillera, Eivissa and Formentera islands. Red line points out the stratigraphic well correlation shown in Fig. 4. Red square corresponds to the location of the study area depicted in Fig. 6b. Blue line indicates the northern part of the cross-section shown in Fig. 15a. b) Regional cross-section across the Eastern Betic Cordillera illustrating the crustal geometry of the orogen (see location in Fig. 1a) (the Internal Betic Zones and the Subbetic Zone are modified from Banks and Warburton, 1991). (For interpretation of the references to color in this figure legend, the reader is referred to the Web version of this article.)

Iberia), comprising a part of the External and Internal Prebetic (see red square in Fig. 2a). This area is characterized by a NW-directed, ENE-WSW trending fold-and-thrust belt in which the Variscan basement to Middle Triassic succession does not crop out and salt diapirs are abundant (Fig. 2b).

### 2.1. General stratigraphy

The outcropping sedimentary record of the study area is composed of Mesozoic to Cenozoic rocks that can be grouped into four well-differentiated tecto-sedimentary packages (Fig. 3):

1) The Upper Triassic evaporitic unit is mostly comprised of halite with intercalations of volcanic, carbonate and detrital rocks (Ortí, 1974). Its preserved normal stratigraphy and original thickness is difficult to determine because it is highly deformed by diapiric structures. Nevertheless, based on well data and composite outcrop sections along the Eastern External Betic Zones, its original thickness is estimated to be ca. 600–700 m (Bartrina et al., 1990; De Torres and Sánchez, 1990). This unit is interpreted to be deposited in a postrift setting related to the breakup of Pangea (e.g. Dercourt et al., 1993). In the study area, this unit acts like a regional décollement level.

2) An uppermost Triassic to Santonian mainly marine platform carbonate cover where the following units can be differentiated (Fig. 3): i) a prerift uppermost Triassic to Middle Jurassic conformable unit depicting a moderate thickness increase towards the SE and a homogeneous stratigraphy, which is mostly composed of marine carbonates; ii) a syn-extensional Upper Jurassic to lower Albian unconformable unit characterized by deepening depositional environments with a thicker succession towards the SE (Vilas et al., 1982; Arias et al., 1993). The largest variations of thickness (Fig. 4) can be observed across the boundary between the Internal and External Prebetic (Azéma, 1977; García-Hernández et al., 1980); and iii) a syn-extensional upper Albian to Santonian unconformable unit with a more homogeneous marine facies association (Figs. 3 and 4), which, to a minor degree, thickens towards the SE (Vilas et al., 2003). Locally, this unit shows sudden thickness increases in the External Prebetic.

3) A Campanian to Eocene unit lying unconformably above the previous sedimentary package (Rodríguez-Estrella, 1977; Martín-Chivelet, 1996). These units are composed of carbonates, mudstones and sandstones that were deposited in platform to continental environments until the Eocene. In general, this unit is interpreted as a syn-orogenic sequence thickening towards the SE where the

**Fig. 3.** Lithostratigraphic chart of the sedimentary facies variation across the External and Internal Prebetic in the Jumilla region. After López-Garrido, 1971; Moseley 1973; Hillebrandt, 1974; Ortí, 1974; Martínez del Olmo et al., 1975; Azéma, 1977; Rodríguez-Estrella, 1977; García-Hernández et al., 1980; Vera et al., 1982; Vilas et al., 1982, 2003; Bartrina et al., 1990; Arias et al., 1993; Guerrera et al., 2014.

foredeep of the Betic orogen was located (Guerrera et al., 2014).

4) Finally, Oligocene to Quaternary terrigenous marine to continental rocks (Fig. 3) lie unconformably above the previous sedimentary packages (Hillebrandt, 1974; Guerrera et al., 2014).

Below the previous outcropping units, the subsalt stratigraphic succession revealed by Jaraco-1 and Salobral-1 wells (located 200 km northeast and 60 km northwest respectively of the study area) is composed of carbonates, shales, sandstones and meta-sedimentary
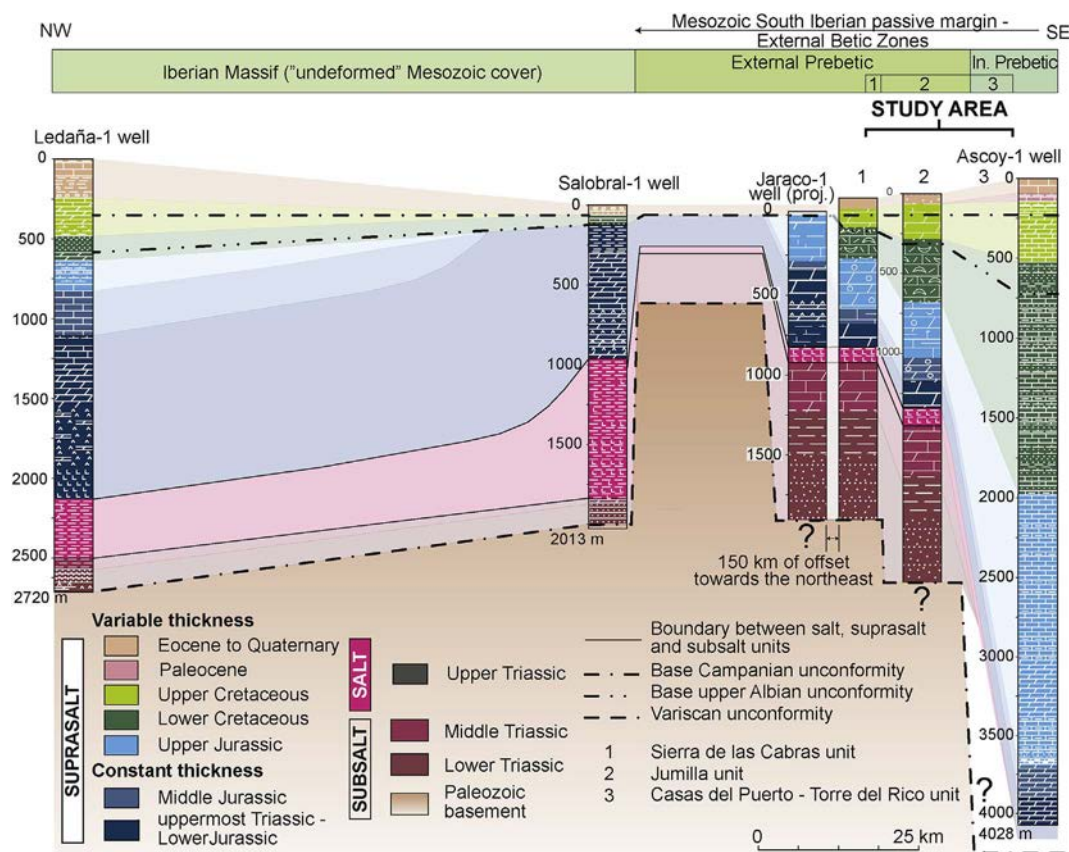
**Fig. 4.** Well correlation throughout the undeformed Mesozoic cover and External and Internal Prebetic (datum of the well correlation is defined at the base of the Campanian unconformity). Note the thickening of the Mesozoic units in the External and Internal Prebetic towards the southeast related to the rifting trend of the Mesozoic South Iberian passive margin. The study area is divided in three differentiated units: (1) Sierra de las Cabras, (2) Jumilla and (3) Casas del Puerto - Torre del Rico. Their synthetic stratigraphic columns are depicted in the well correlation. Refer to legends in Fig. 3 for lithological symbols. Stratigraphic thickness of salt, supra- and subsalt units in the study area and the Salobral-1 obtained from field work and after García-Hernández et al. (1980) and Lanaja et al. (1987). Jaraco-1 well is located approximately 150 km towards the northeast from the study area.

sandstones (Fig. 3). The analysis of the stratigraphic sections intersected by the previous wells (Fig. 4) reveals Middle Triassic marine carbonates and Lower Triassic detrital continental rocks unconformably overlying a meta-sedimentary Paleozoic basement (Lanaja et al., 1987).

### 3. Methodology

To address the goals outlined in this study, both field and subsurface data were integrated into the analysis. Field data include more than 6000 stations distributed over the study area containing structural and stratigraphic data obtained from field work. Subsurface data includes six 2D depth-converted seismic profiles across the External and Internal Prebetic and the sonic and stratigraphic logs of the Ascoy-1 well (see its location in Fig. 2a). The sonic log was used to perform the depth conversion of the seismic profiles and the stratigraphic log was used to interpret the seismic facies according to their lithology and the stratigraphic thicknesses (Fig. 5a and b). Move 2015™ from Midland Valley was used to integrate the surface and subsurface data and to create both the geologic maps (Figs. 6b and 8a) and the cross-sections (Figs. 7a, b and 8b).

The cross-sections, oriented NW-SE perpendicular to the trend of the Betic structures, depict the main structural features of the study area. Field dip data and seismic interpretations were used to constrain the cross-sections. The deep subsalt, salt and suprasalt structures have been interpreted according to widely used constraints in thin-skinned fold-and-thrust belts developed in salt provinces (e.g. Dahlstrom, 1969; Elliott, 1976; Hossack, 1983; Suppe, 1983; Woodward et al., 1985; Rowan and Ratliff, 2012). Depth-to-basement calculations are made using Mesozoic to Cenozoic stratigraphic thicknesses both from well data and field data, combined with seismic data. In addition to these

constrains, we also accept the following assumptions in the construction of the cross-sections: 1) the location in depth of the fold hinges involving the uppermost Triassic to Quaternary sequence determines the depth to the roof of the subsalt basement; and 2) the monoclinal flexures of the Mesozoic suprasalt cover coincident with growth-strata geometries are interpreted to be controlled in depth by extensional subsalt faults. In the construction of the salt structures we assumed that 1) salt structures are no longer active when at depth —they are primary and/or secondary welded (Cramez and Jackson, 2000); 2) progressive thinning of the sedimentary units within the basin is related to primary welding; and 3) thickened young successions lying directly above salt are interpreted to be related to salt collapsed structures.

### 4. Structure of the Prebetic Zone at the Jumilla region

#### 4.1. Salt and suprasalt structure

The study area is characterized by a fold-and-thrust system (Fig. 2a) and currently inactive salt diapirs that are parallel to the ENE-to NE-regional trend of the Betic Cordillera and the Mesozoic South Iberian passive margin (Fig. 1a and b). However, this regional trend is disrupted by the NW-trending Matamoros Basin, which is flanked by the Jumilla and la Rosa diapirs (Fig. 6b).

Based on the wavelength of the ENE-trending folds and the stratigraphy of the suprasalt cover, three different units can be distinguished. From NW to SE they are: the Sierra de las Cabras unit, the Jumilla unit, and the Casas del Puerto-Torre del Rico unit. The first two units are located in the External Prebetic, and the third one is located in the Internal Prebetic (Fig. 6a).

**Fig. 5.** a) Time-depth curve used to perform the depth conversion of the seismic profiles (sonic log of the Ascoy-1 well has been used to obtain the interval velocity and the aver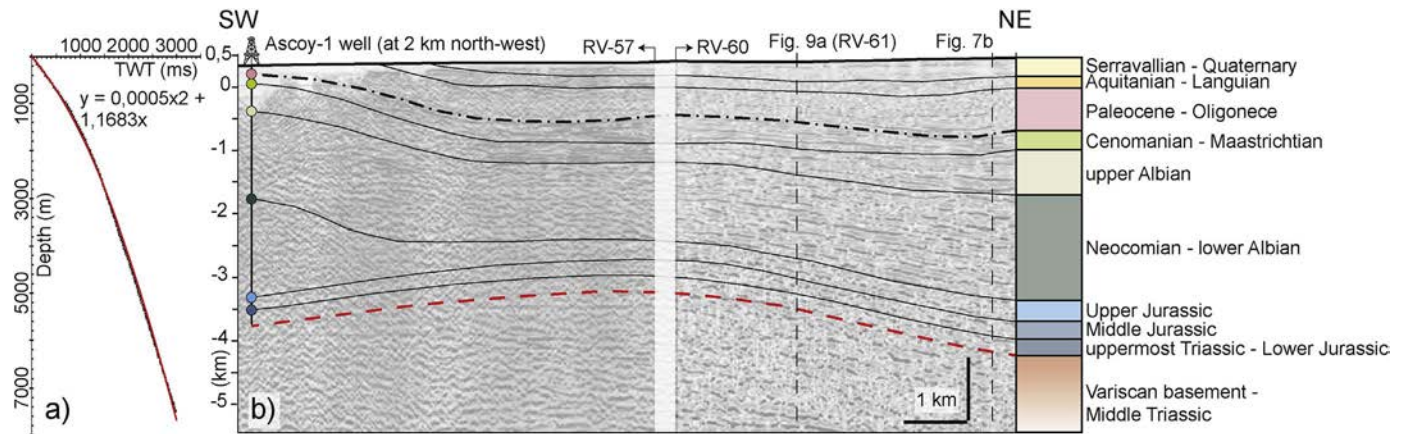age velocity. Processing datum 1050 m). b) Seismostratigraphy of the Mesozoic and Cenozoic cover at the Ascoy-1 well (see the location of the well and the seismic profile RV-57 in Fig. 6a). Colored dots indicate the base of the stratigraphic units intersected by the well. Lithology colors used on the seismic interpretation in Fig. 9 and 10. (For interpretation of the references to color in this figure legend, the reader is referred to the Web version of this article.)

#### 4.1.1. Sierra de las Cabras unit

The Sierra de las Cabras unit is restricted to the northwestern corner of the study area, where mostly Jurassic rocks crop out (Fig. 6b). This unit includes an uppermost Triassic to Cenomanian succession unconformably overlain by the upper Miocene deposits. The structure of this area is characterized by symmetric folds whose amplitude and wavelength decreases suddenly at the southern limit of this unit. These folds also affect the middle Miocene rocks which are less or much less deformed than the underlying Mesozoic rocks. According to the symmetric fold geometry and the rocks involved it is interpreted that these are detachment folds cored by Upper Triassic salt. Taking into account the observed syncline hinge location and the thickness of the folded successions, it has an estimated detachment level located between 0 and 100 m below sea level (Fig. 7a and b).

#### 4.1.2. Jumilla unit

The Jumilla unit is located between the previous northwestern unit and the Sierra Larga-Sopalmo and Carxe, where mostly Cretaceous to Quaternary rocks crop out (Fig. 6b). This unit includes an assumed homogeneous uppermost Triassic to Middle Jurassic succession overlain by Upper Jurassic to Quaternary rocks that display thickness changes across the area. The structure of the northwestern limit of this unit is characterized by a SE-dipping monoclinal flexure (Fig. 7a). This monocline is cut by SE-dipping extensional faults and thrusts, locally affected by short wavelength folds that deform the Upper Cretaceous rocks that are detached from the underlying succession. The Upper Cretaceous rocks deformed by narrow anticlines, together with the presence of Upper Triassic salt at their cores, suggest that these structures correspond to the roof of pre-Albian diapirs or salt walls that were squeezed during the later contractional deformation.

Southeast of this boundary, the structure mainly consists of broad and flat-bottomed synclines and narrow and tight anticlines. These anticlines are characterized by vertical to overturned limbs and are cut by both extensional and contractional faults as well as by some diapiric structures (Fig. 7a and b). Contrasting with the Sierra de las Cabras unit, the folds of the Jumilla unit verge toward the foreland and hinterland. The genetic and structural relationships of these structures can be analyzed in the Sierra de los Bujes anticline located at the northern part of the Jumilla unit (see location in Figs. 6b and 7a and the detailed geological map in 8a). The anticline is cut by a longitudinal NW-directed thrust fault, which displaces minor scale ENE-trending double plunge folds that deform uppermost Triassic to Serravallian sedimentary successions (Fig. 8a). In the hanging wall of the thrust fault there is a minor anticline that deforms an uppermost Jurassic to Lower Cretaceous succession (Fig. 8b). The Mesozoic folded architecture and its

internal geometrical relationships denote that the core of the anticline shows evidence of a salt roller structure that is bounded by SE-dipping listric faults. In the hanging wall of these faults, the syn-extensional Lower Cretaceous to upper Albian sediments display growth strata geometries (Fig. 8a).

According to the qualitative restoration (Fig. 8c), the salt roller developed as a consequence of increasing fault displacement (Fault 3 in Fig. 8) and the subsequent salt inflation in its footwall from Neocomian to upper Albian times. Continued extension promoted salt extrusion and passive diapirism. In the Sierra de los Bujes outcrop, there are isolated and brecciated bodies containing upper Albian rocks adjacent to the Sabina Diapir (Fig. 8a). They are interpreted to be diapir-derived debris flows deposited as a consequence of diapir rise and destabilization of the diapir roof. The near-diapir abrupt facies change from carbonate breccias to sandstones that are upper Albian in age, in addition to the presence of mass-wasting deposits are indicative of hook halokinetic sequences adjacent to the Sabina Diapir (Giles and Rowan, 2012). Afterwards, during compression, the suprasalt cover located over this inflated area was eroded and the extensional faults were deformed by folding and thrusting —a process that triggered localized diapir rejuvenation (e.g. the Sabina diapir, see location in Fig. 8a). In this scenario, contractional folds developed due to salt roller squeezing, in which further compression might have led to thrust deformation (Fig. 8b). The genetic and structural similarities between this fold and other structures along the Jumilla unit suggest a common development process where the fold and thrust vergence can be used as a polarity indicator for each salt roller.

The only folds that seem not to follow this development pattern are the synclines located northwest of the Sierra del Molar and southeast of the Sierra del Buey (Fig. 6b). These folds include Turonian to Maastrichtian anomalous thick successions unconformably lying above upper Cenomanian rocks. Turonian angular unconformities located at the top of the upper Cenomanian succession in the Sierra del Buey are indicative of an uplifted area during the upper Cenomanian. Despite the fact that diapirism occurred during Cretaceous times, these Turonian to Maastrichtian thickened successions are interpreted to be a result of a salt wall collapse as proposed in the cross section depicted in Fig. 7a. The resulting collapse basin was later deformed during the Betic compression as recorded in the Oligocene to lower Miocene growth-strata geometries, which unconformably overlap the Turonian to Maastrichtian successions (Fig. 7a and b). Taking into account the fold hinge location and the general thickness of the involved successions, we interpret the base of the Upper Triassic salt to be nearly horizontal being located at 800–1000 m below sea level (Fig. 7a and b).

**Fig. 6.** a) Relief map depicting the location of the main structural units along the Prebetic and Subbetic Zones in the Jumilla region as well as the Ascoy-1 well and seismic profiles RV-57 and RV-60 in Fig. 5b. b) Geological map of the External and Internal Prebetic in the Jumilla region. The northernmost part integrates data from Baena (1979). Note the location of two cross-sections shown in Fig. 7a and b; a detailed geological map of the south-western part of Sierra de los Bujes shown in Fig. 8a; and the location of the provided depth-converted seismic lines in Figs. 9 and 10.

Fig. 7. Regional cross-sections throughout the Prebetic Zone at the Jumilla region. a) Eastern cross-section. b) Western cross-section. See location in Fig. 6b.
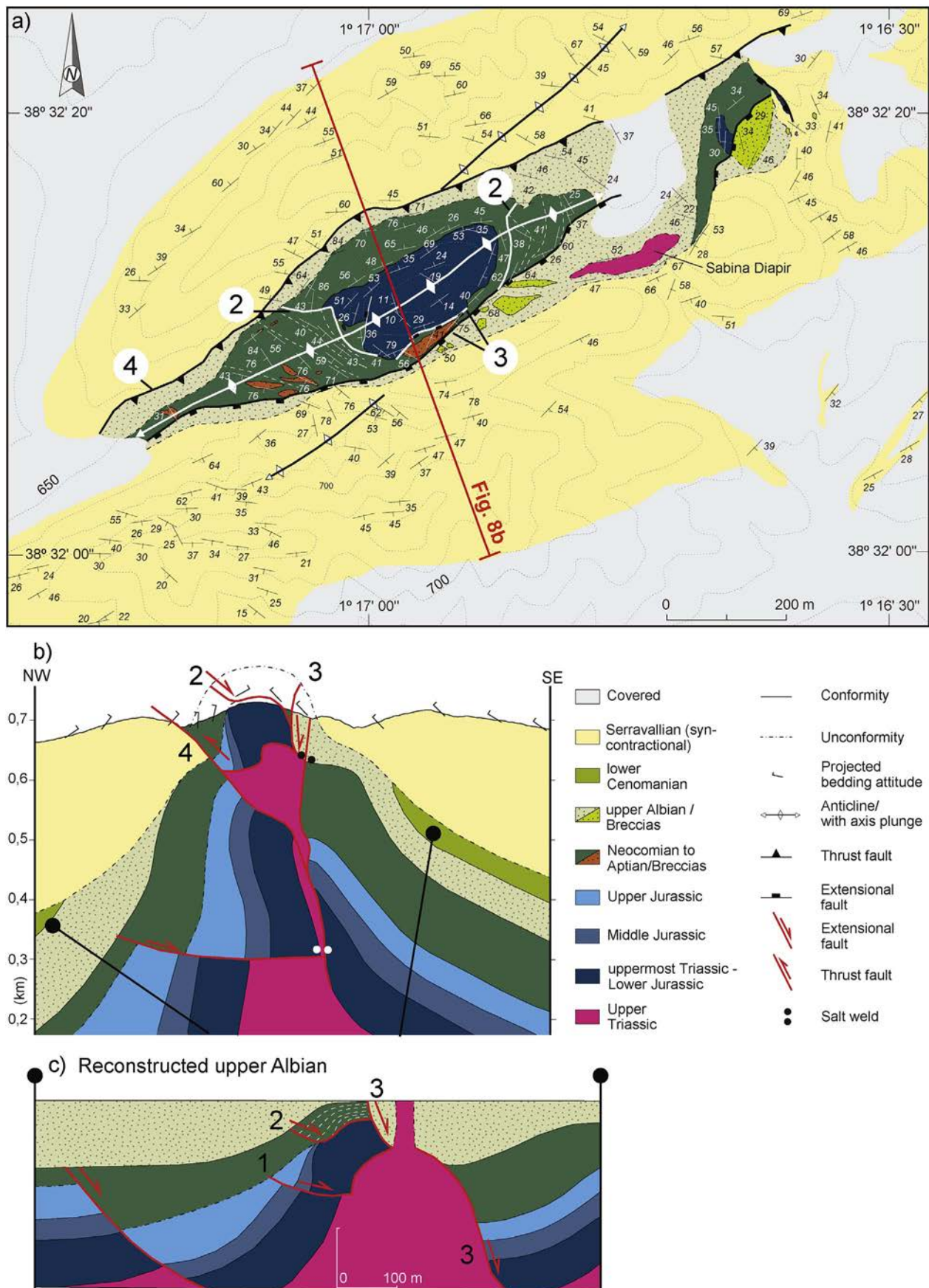
**Fig. 8.** a) Detailed geological map of the Sierra de los Bujes anticline (see location in Fig. 6b). Numbers 1, 2, 3 and 4 indicate the relative age of each fault in a younging order. b) Cross-section showing the internal geometry of the salt roller structure (see location in Fig. 8a). c) Qualitative restoration of cross-section depicted in Fig. 8b for the upper Albian. Number 4 indicates the inversion of the older extensional Fault 1 during the compressional deformation of the salt roller.
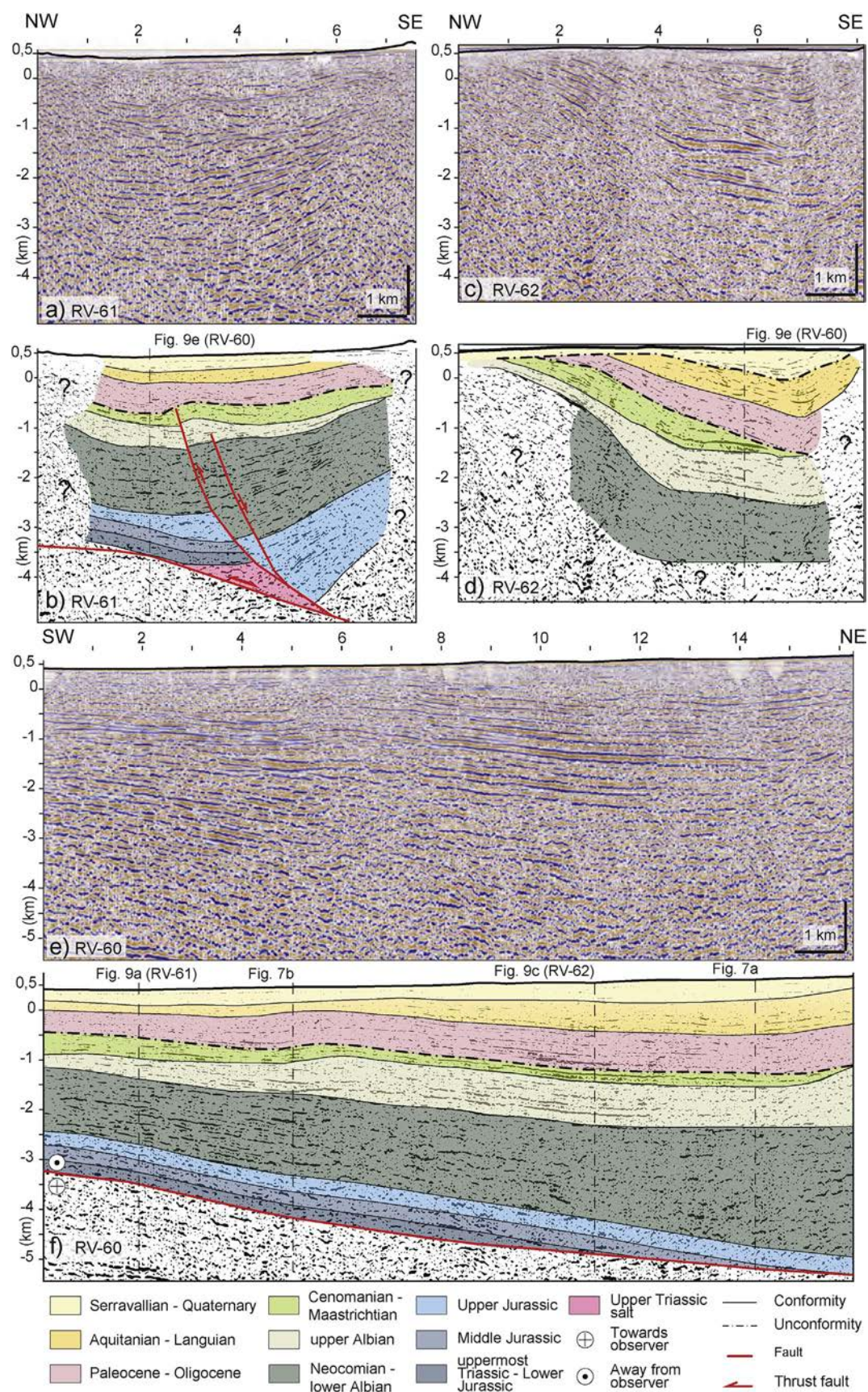
**Fig. 9.** 2D depth-converted seismic profiles located in the Internal Prebetic (Fig. 6b). a) Seismic line RV-61 and b) its interpretation. c) Seismic line RV-62 and d) its interpretation. e) Seismic line RV-60 and f) its interpretation.
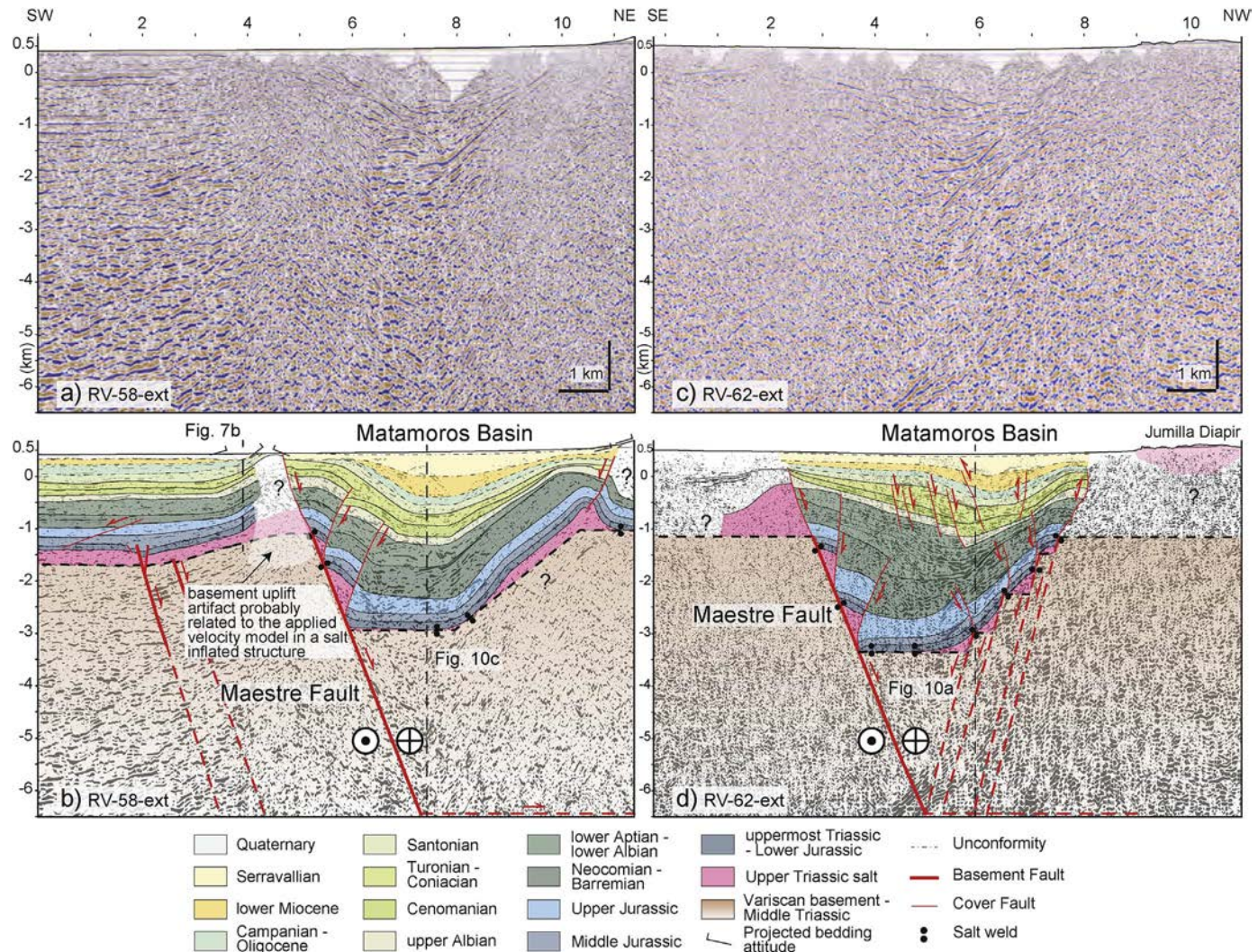
**Fig. 10.** 2D depth-converted seismic profiles with their respective interpretations crossing the Maestre Fault and the Matamoros Basin. a) Seismic line RV-58-ext. b) Seismic line RV-62-ext. See the location of both seismic profiles in Fig. 6b.

### 4.1.3. Casas del Puerto – Torre del Rico unit

Southeast of the previous unit, field and seismic data show the presence of a thicker differentiated Casas del Puerto – Torre del Rico unit (Figs. 6a and 9a, c, and e). This unit is characterized by a thick Upper Jurassic to Campanian succession and a more complete Cenozoic succession including Paleocene and Eocene materials that are not present in the previous units.

Its northwestern limit is located along the Sierra Larga-Sopalmo and Carxe (Fig. 6b). This area is characterized by a system of NW-directed thrust faults developed over a salt inflated area, which includes diapirs (e.g. Carxe Diapir, see its location in Fig. 6b). Toward the SE and in the eastern part of this unit, the geometry of the cover is depicted by a southeast dipping monoclinal fold followed by a nearly horizontal panel (Fig. 9d). In the western part of this unit, the geometry of the seismic reflectors (Fig. 9a) illustrates an anticline deforming the base of the interpreted Cenozoic rocks (Fig. 9b). This fold could be related to the contractional reactivation of an Upper Jurassic to upper Albian suprasalt fault (Fig. 9b). The southern part of Sierra Larga-Sopalmo is also affected by extensional SE-dipping faults (Fig. 6b). Therefore, we interpret a similar origin for the folds related to the inversion of these faults illustrated in Fig. 7b. According to the seismic data and the stratigraphic thickness of the cover, we interpret that the base of the Upper Triassic salt is dipping towards the SE and is located between −3200 m and −5000 m below sea level (Fig. 9f).

In the southern part of the unit there is the contractionally squeezed La Sarsa salt wall (Fig. 6b). This salt structure is covered by Paleocene to Quaternary deposits which together with the salt wall are folded and cut by some minor NW-directed thrusts. The presence of these thrusts is indicative of secondary welding resulting from the squeezing of this salt wall during the Betic compression. The Paleocene to Quaternary sedimentary roof that covers the entire salt wall is a consequence of salt depletion and the formation of primary welds and thus the cessation of the salt wall growth (Fig. 7a).

In summary, the described structures in the Casas del Puerto – Torre del Rico unit were formed before upper Miocene time. The internal deformation of this unit is represented by the Upper Jurassic to upper Albian extensional suprasalt faults (see the interpreted seismic profile in Fig. 9b), but also by folds and thrust faults, and by the squeezing of the La Sarsa salt wall and the Carxe Diapir. The development of the La Sarsa salt wall and the Carxe Diapir is linked to the extensional activity of the suprasalt faults that are Upper Jurassic to upper Albian in age. In the southern part of the Sierra del Carxe, the presence of low angle unconformities at the base of the Campanian and Paleogene rocks and a regressive general trend from hemipelagic to continental facies (Figs. 6b and 7a), suggests the onset of an incipient contractional deformation during this time (Rodríguez-Estrella, 1977; Martín-Chivelet et al., 1997; Vilas et al., 2003; Guerrera et al., 2014).

### 4.2. NW-trending structures of Jumilla – La Rosa

In the Jumilla unit, the lateral continuity of the ENE-trending structures is interrupted by an elongated NW-trending and 2–4 km wide area that extends from the Jumilla Diapir to the southwestern termination of the Sierra del Carxe (Fig. 6b). This area includes two actives and relatively rounded diapirs (Jumilla and La Rosa diapirs) that are located at its northwestern end and are close to the opposite southeastern limits respectively. The diapirs generate up to 134 m (Jumilla Diapir) and 227 m (La Rosa Diapir) of topographic relief over the surrounding Quaternary valleys. Moreover, the near-diapir upper Miocene to Quaternary rocks are deformed by narrow and steep drape-fold geometries that correspond to hook halokinetic sequences, which are common in high rate salt extrusion settings (Giles and Rowan, 2012).

The Mesozoic and Cenozoic structure of this NW-trending elongated area is difficult to determine because of the presence of a broad valley that is filled with Quaternary colluvial and alluvial sediments (Fig. 6b). Despite this, the combination of surficial dip attitudes (Fig. 6b) and seismic data (Fig. 10a and c) allows inferring that this area actually corresponds to a lower Miocene to Quaternary syncline basin (Fig. 10b and d). This basin is bounded by a set of lower Miocene to Quaternary suprasalt and subsalt faults that cut up to the surface. Beneath the unconformably lying Neogene sediments, the Mesozoic rocks also show a synclinal geometry having the same orientation with a horizontal NW-trending fold hinge located on top of the Upper Triassic detachment level (Fig. 10d). The northeastern part of the synclinal basin has a constant dip (Fig. 10b), whereas its southern part is affected by suprasalt faults (Fig. 10b and d). According to the interpreted stratigraphic thicknesses, the base of the syncline basin could be located at ~3200 m below sea level (Fig. 10d).

The detailed geometrical analysis of the Mesozoic and Cenozoic sediments recognized in the seismic profiles (Fig. 10b and d), show that the Matamoros Basin forms a drape syncline that developed during the Upper Jurassic to Santonian over a rollover controlled by the NE-dipping Maestre Fault (see qualitative restoration for the Matamoros Basin in Fig. 11a, b, c, d, and e). Furthermore, during the lower Miocene to Quaternary, the syncline continued to develop through the vertical subsidence of its central part (Fig. 11f and g), which was synchronous to the movement of the supra- and subsalt faults that bound the Matamoros Basin.

### 4.3. Subsalt structure

The subsalt structure is not well imaged in either the seismic profiles or the gravimetric data (Fig. 12). Nevertheless, the geometrical analysis of the outcropping Mesozoic and Cenozoic structures allows inferring the roof of the subsalt basement. The progressive SE-deepening of the inferred Upper Triassic regional detachment along the study area, can be interpreted as associated with basement steps. Whereas the boundary between the Sierra de las Cabras and Jumilla units implies a subsalt step of ~800–1000 m of vertical throw, the boundary between Jumilla and Casas del Puerto – Torre del Rico corresponds to a basement step of ~4000 m of vertical throw, and thereby characterizes the boundary between the External and Internal Prebetic. The characteristic width and rectilinear geometry of the basement steps suggest that the subsalt faults control the NE-SW trend of the Eastern Prebetic Zone. From NW-SE these faults are called: the Jumilla and Sopalmo-Carxe Faults (Fig. 7a and b). In the Bouguer anomaly map, the location of the Jumilla Fault is well depicted, whereas the Maestre, Sopalmo, and Carxe faults can only be inferred (Fig. 12).

The inferred horizontal base of the regional Upper Triassic salt detachment over the faulted blocks suggests a non-rotational planar geometry for these subsalt faults. The thickness variation of the Mesozoic to Cenozoic suprasalt cover along the faulted blocks allows constraining the age of the faulting from Upper Jurassic to Santonian with a later extensional reactivation that is Burdigalian to Langhian in

age. In addition, over the hanging wall of the subsalt faults, the regional base of the syn-orogenic units shows similar (or slightly less) topographic elevation compared to the same syn-orogenic sequence over their footwalls. Therefore, this evidence suggests that basement faults cannot be significantly inverted, and thus a thin-skinned inversion model needs to be assumed.

The subsalt rocks are also deformed by the NE-dipping Maestre Fault (Fig. 10b and d). This subsalt fault constrains the southwestern boundary of the Matamoros Basin. Its geometry is interpreted as a kinked planar fault with an associated basement rollover and a horizontal detachment located at ~-6000 m below sea level (Fig. 10b and d). According to the age of the associated growth strata, this fault was active during the Upper Jurassic to Santonian times with a later extensional reactivation during the lower Miocene to Quaternary times.

## 5. Interaction between sub- and suprasalt deformation during South Iberian passive margin development and its subsequent inversion at the Eastern Prebetic Zone

To address the tectonic evolution of the suprasalt cover in relation to the subsalt basement we use a combination of thick- and thin-skinned styles of deformation. The results of this interpretation are the qualitative restorations shown in Figs. 11 and 13, which illustrate the development of the proximal segment of the Eastern South Iberian passive margin and its subsequent inversion.

In the study area, the major thick-skinned extension started during the Late Jurassic. In this initial stage, the pre-kinematic units (i.e. uppermost Triassic to Middle Jurassic) were affected by a broadly diffused subsalt deformation (Fig. 13a and b). Above the subsalt faults, the cover was deformed by monoclinal drape folds and was stretched by suprasalt faults and reactive diapirs (Fig. 13b). As a result, suprasalt materials mimicked the resultant stepped subsalt geometry using the salt as an effective detachment. Suprasalt rollover structures and associated growth strata also developed on the hanging wall of the suprasalt listric faults (e.g. ramp-flat fault in Sierra de los Bujes, Fig. 8b). Locally, the offset of these listric faults triggered the rise of diapirs on their footwalls (e.g. Sabina Diapir).

As extension progressed, the cover and diapirs together with the suprasalt faults were dragged basinwards becoming progressively incorporated above the hanging wall of the subsalt faults (see this process in Fig. 11). At the same time, folding and faulting was concentrated above the footwalls of the main subsalt faults in which a thinner cover was prone to be easily deformed (Fig. 13c). Moreover, the basinwards translation of the cover triggered the widening of passive diapirs compartmentalizing the cover into different blocks (Fig. 13c and d). However, we interpret passive diapirism to have finished during the upper Cenomanian – lower Turonian after salt depletion and the development of primary welds (Fig. 13d). In this scenario, salt structures collapsed and the corresponding sedimentary depocenters allowed the development of Turonian to middle Miocene salt-withdrawal basins progressively distributed in time along the footwall of the Carxe – Sopalmo faults (e.g. Sierra del Molar, del Buey or Larga-Sopalmo, Fig. 6b).

Summarizing, in the study area, the development of the Eastern South Iberian passive margin was the result of a major NW-SE thick-skinned extension caused by the activation of the SE-dipping Jumilla and Carxe-Sopalmo faults. According to the qualitative restoration illustrated in Fig. 13, the basement was stretched by ~6 km of SE-wards directed subsalt extension resulting in ~13 km of SE-wards suprasalt extension. However, the area was coevally stretched by ~0.8 km of NE-wards directed subsalt extension conducted by the Maestre Fault (Fig. 11g). In this scenario, the Maestre Fault could act as a lateral structure transferring subsalt transtension between the two major Sopalmo and Carxe faults. The location of the Jumilla and La Rosa diapirs would indicate the intersection of this lateral fault with the two regionally-trending extensional faults. The presence of NW-trending subsalt faults is also documented in other parts of the Eastern Prebetic
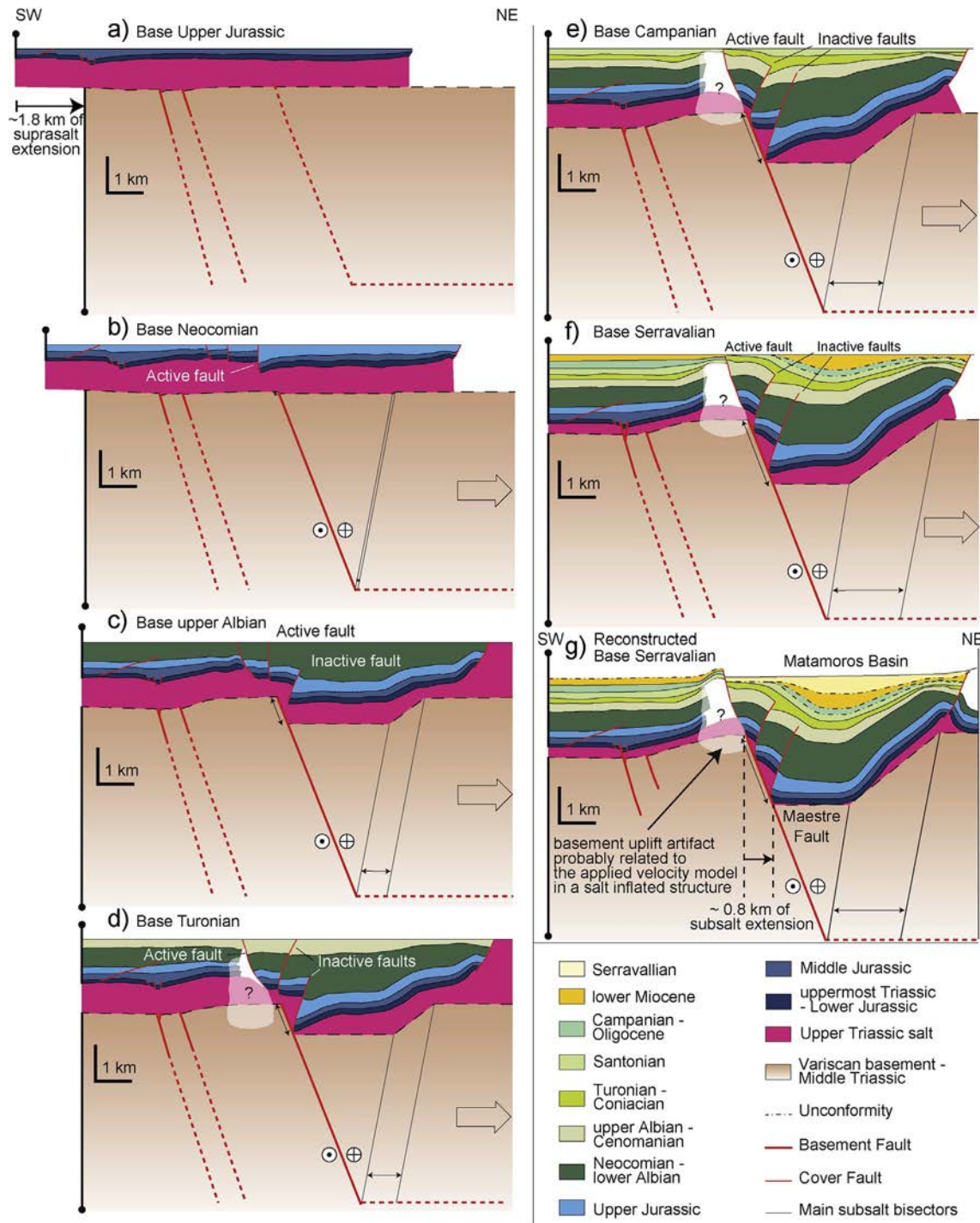
**Fig. 11.** Qualitative sequential restoration of the Matamoros Basin according to the interpreted RV-58-ext seismic profile (see its interpretation in Fig. 10a and its location in Fig. 6b). Note that the dextral strike-slip component of the Maestre transtensional fault has not been taken into account during the qualitative restoration.

Zone (De Ruig, 1992). This orientation could be linked to the E-to NE-directed Mesozoic extension that affected the southeastern Iberian Chain (Roca et al., 1994, 2006), which was synchronous with extension in the Eastern South Iberian passive margin.

After extension, the basinwards stepped subsalt geometry and the salt structures controlled the Betic inversion of the proximal part of the passive margin (Fig. 13g). In the study area, the present-day location of the syn-orogenic units deepening towards the SE demonstrates that the subsalt basement was not involved during the contractional deformation. Therefore, the stepped geometry of the basement allowed for the NW-directed propagation of the thin-skinned contractional

deformation. This shortening was carried out by a thrust fault with a flat-ramp-flat geometry rooted into the detachment level (i.e. Upper Triassic salt).

According to field observations and the interpreted seismic data, the incorporation of the South Iberian passive margin into the external zones of the Betic fold-and-thrust belt encompassed the following phases: a first stage (Campanian to Aquitanian in age) when the contractional deformation was mostly absorbed by squeezing of the pre-existing diapirs, thus generating secondary welds. As compression progressed, the compartmentalized cover became reconnected and thrust faults nucleated at the secondary welds. Field evidence
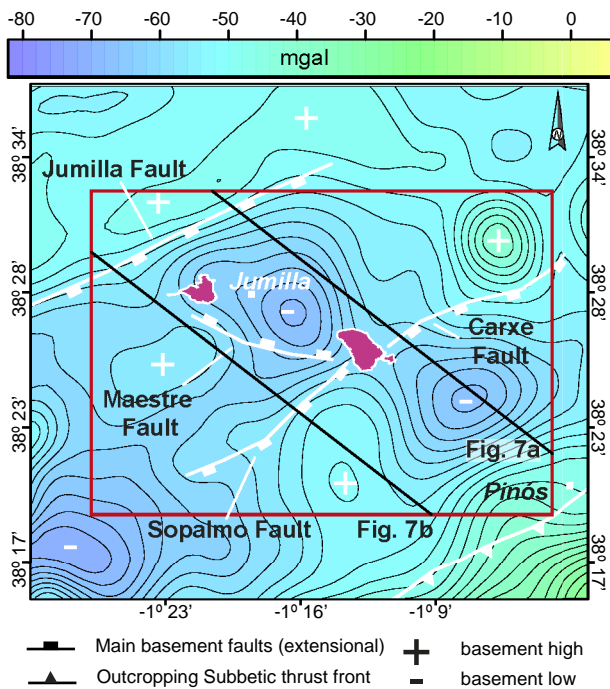
**Fig. 12.** Bouguer Anomaly map of the External and Internal Prebetic in the Jumilla region. Study area located inside the red square. The source of the gravity data is field data from IGME and Castaño (1993); the reference density used is 2.67 g/cm³; topographic correction has been implemented. (For interpretation of the references to color in this figure legend, the reader is referred to the Web version of this article.)

supporting this interpretation takes the form of thrust faults affecting the Sarsa salt wall (Figs. 6b and 7a); a second stage Burdigalian to Langhian in age occurred when the major subsalt faults (e.g. Sopalmo, Carxe and Maestre faults) were extensionally reactivated (Fig. 7a and b). This extension could be linked to the flexural deformation that experienced the forebulge of the orogen as a result of the southwards lithospheric loading of the Eastern Betics. The orogenic loading could have also promoted the tilting of the sub- and suprasalt architecture including the Carxe and Sopalmo faults (Fig. 13g). In addition, the development of a Burdigalian – Langhian salt-withdrawal basin above the upper cut-off of the Sopalmo Fault could have also occurred during its extensional reactivation; and finally, a third stage that is Serravallian in age occurred when the suprasalt cover and the squeezed diapirs were contractionally translated towards the northwest along the salt detachment. In the Internal Prebetic, the SE-dipping Aquitanian to Langhian units are located beneath an unconformity and are onlapped by less dipping Serravallian sediments (see Fig. 9b). This geometrical relationship could be interpreted as a consequence of the northwestern translation of the suprasalt cover, its intersection with the ramp of the thin-skinned thrust fault and the subsequent southeast tilting and erosion during the Serravallian.

## 6. Discussion

### 6.1. The role of the subsalt structure and the prerift salt during South Iberian passive margin development

According to our interpreted tectonic evolution of the study area, prerift salt decoupled the extensional deformation thereby generating two differentiated structural styles, above and below the salt. This scenario is also documented in other parts of the Eastern Prebetic Zone (De Ruig, 1992; Roca et al., 2013), in the Basque-Cantabrian Basin (Carola et al., 2015), in the Bay of Biscay (Ferrer et al., 2012), in the Lusitanian Basin of the North Atlantic (Alves et al., 2002), in the North

Sea (Withjack et al., 1989; Pascoe et al., 1999), in the Rhine Graben (Maurin and Niviere, 2000) as well as in analogue models (Koyi et al., 1993; Ferrer et al., 2014, 2016). In most of these examples, suprasalt extension is mainly accommodated by the development of monoclinal drape folds, suprasalt faults and diapirs.

Considering the previously outlined deformation conditions (see Section 5 for more detail), our cross-sections (Fig. 7a and b) and the qualitative restorations (Figs. 11 and 13), the increase of subsalt fault extension must therefore generate: (1) folding and lengthening of the cover; and (2) accommodation above the hanging wall progressively filled by syn-kinematic units located above the monoclinal drape folds.

Folding of the pre-kinematic cover takes place due to a combination of hanging wall subsidence and coeval salt evacuation towards the fault (Withjack et al., 1989; Pascoe et al., 1999; Cosgrove and Ameen, 2000; Maurin and Niviere, 2000; Richardson et al., 2005; Kane et al., 2010; Duffy et al., 2012). During this process, the wavelength of the resulting extensional drape fold will be controlled by the dip of the subsalt fault (Ferrer et al., 2016). Hence, low-angle subsalt faults (e.g. dipping 30°–40°, Fig. 14a) tend to generate long wavelength extensional drape folds, which deform the overburden and control the broad deposition of syn-kinematic units. In contrast, high-angle subsalt faults (e.g. dipping 60°–70°, Fig. 14b) will result in short wavelength extensional drape folds that restrict the deposition of syn-kinematic units.

In the study area, extensional faults rooted at the top of the salt detachment developed along the monoclinal flanks (maximum stretching area) also constraining diapirism above the footwall of the subsalt faults. (e.g. Fig. 13b). As a result, the progressive incorporation of the suprasalt cover into the hanging wall of the subsalt fault produced the lengthening of the monoclinal flanks (Fig. 14a and b). In addition, low-angle subsalt faults (Fig. 14a) tend to keep suprasalt faults active once they are incorporated into the hanging wall (e.g. Fig. 13c and d). Nonetheless, high-angle subsalt faults (Fig. 14b) tend to favor the clockwise rotation of the suprasalt faults, which appear as reverse faults when these are dragged into the hanging wall of the subsalt fault (e.g. Figs. 11b, c and d).

In all scenarios, subsalt fault displacement produces an increase in the accommodation space over their hanging walls and hence the deposition of syn-extensional units. During this process and as a consequence of salt depletion, primary welding may generate coupling of the cover and the subsalt basement (Withjack and Callaway, 2000). This strengthens the suprasalt cover over the hanging wall and disrupts the continuity of the salt unit.

Therefore, in extension, the location and distribution of the suprasalt deformation changed over time. In the early stages, subsalt faults were associated with short offsets and they could not control suprasalt thicknesses which remained almost constant. Thus, similar thicknesses along the margin promoted a diffused and distributed extensional deformation over the subsalt faults (e.g. Fig. 13b). As extension progressed and subsalt faults offsets increased, there was a corresponding major difference in suprasalt cover thicknesses over the faulted blocks (e.g. Fig. 13c). In this scenario, folding and faulting were concentrated above the footwall of the main subsalt faults, where the cover was thin and hence mechanically weak; and translation with minor folding was concentrated above their hanging walls where the cover was thick and mechanically resistant.

### 6.2. The influence of salt diapirism

The presence of a thick salt (i.e. Upper Triassic salt) beneath a relatively thin pre-kinematic unit (i.e. uppermost Triassic to Middle Jurassic) could facilitate diapiric processes during the early stages of extension. However according to our tectonic model, as extension progressed, diapirs located above the hanging wall of the subsalt faults tended to translate basinwards together with the thickened cover, without concentrating further strain (see translation of the La Sarsa salt wall over time on Fig. 13b, c, and d). In spite of this, the diapirs located
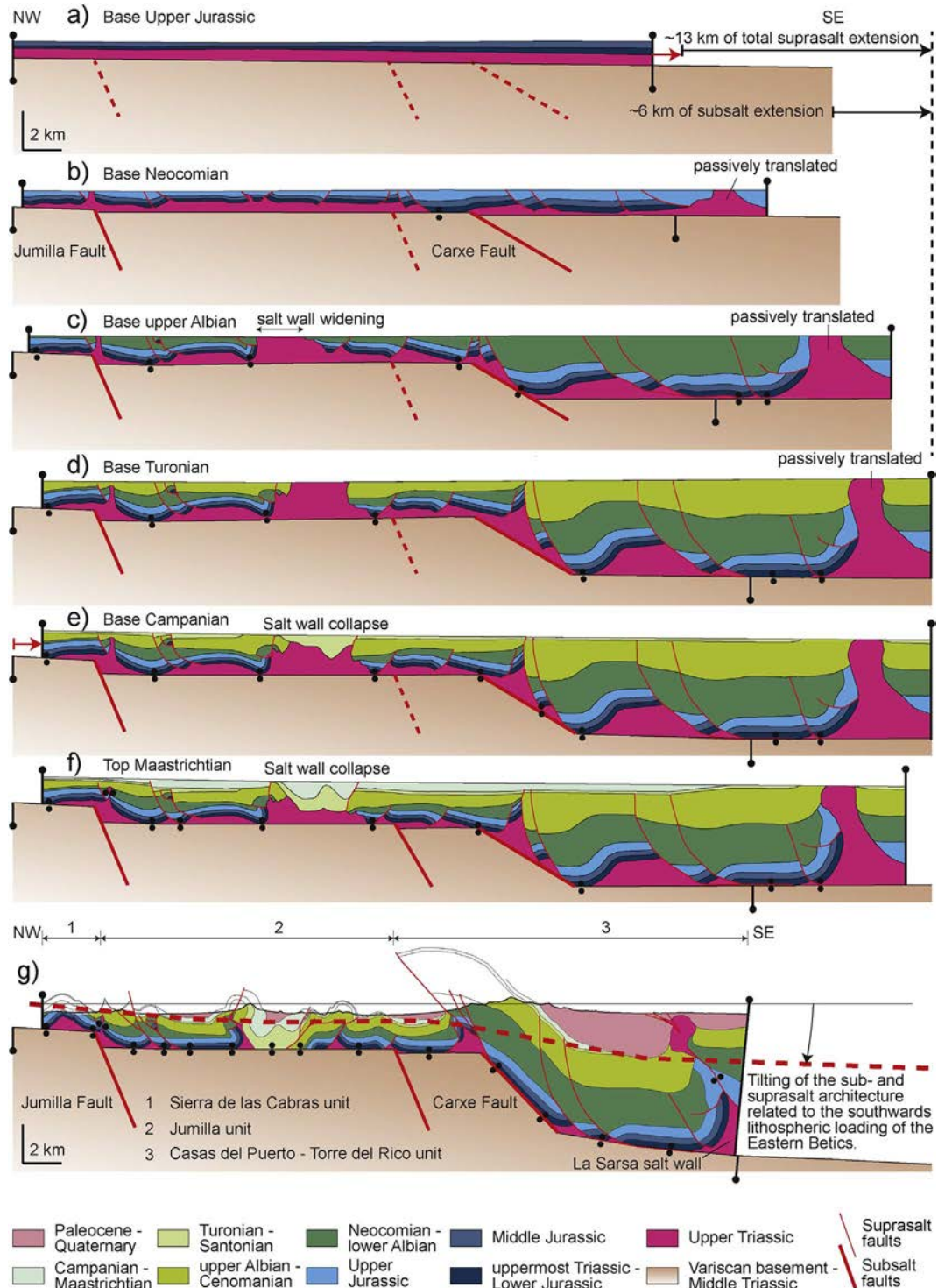
**Fig. 13.** Qualitative sequential restoration for the Eastern Prebetic Zone at the Jumilla region. Fig. 13g corresponds to the regional cross-section shown in Fig. 7a. The original thickness of the Upper Triassic salt is estimated according to Bartrina et al. (1990) and De Torres and Sánchez (1990).

above the footwall, where the sedimentary cover was thin, were not displaced from their original location and instead they concentrated part of the deformation (e.g. widening process in Fig. 13c and d).

The growth of diapirs and salt walls not only play a key role in the deformation of the adjacent suprasalt cover, they also have mechanical implications for the entire segment of the passive margin (Rowan and Vendeville, 2006; Ferrer et al., 2012; Rowan, 2014). Therefore, the regions with diapirs become mechanically weak, nucleating further extensional deformation (mostly non-rigid body transformations or

strain). The capacity to concentrate future extensional deformation will depend on both salt bodies' geometries and the strengths of the adjacent covers. This will be maximum in a thin and weak suprasalt cover with salt bodies oriented orthogonal to the tectonic transport direction; and it will be minimum in a thick, and hence strong, suprasalt cover adjacent to a salt body parallel to tectonic transport with a circular or elongated geometry.

However, ongoing extension and thinning of the cover eventually inhibits further diapir growth, leading to its collapse (e.g. see this
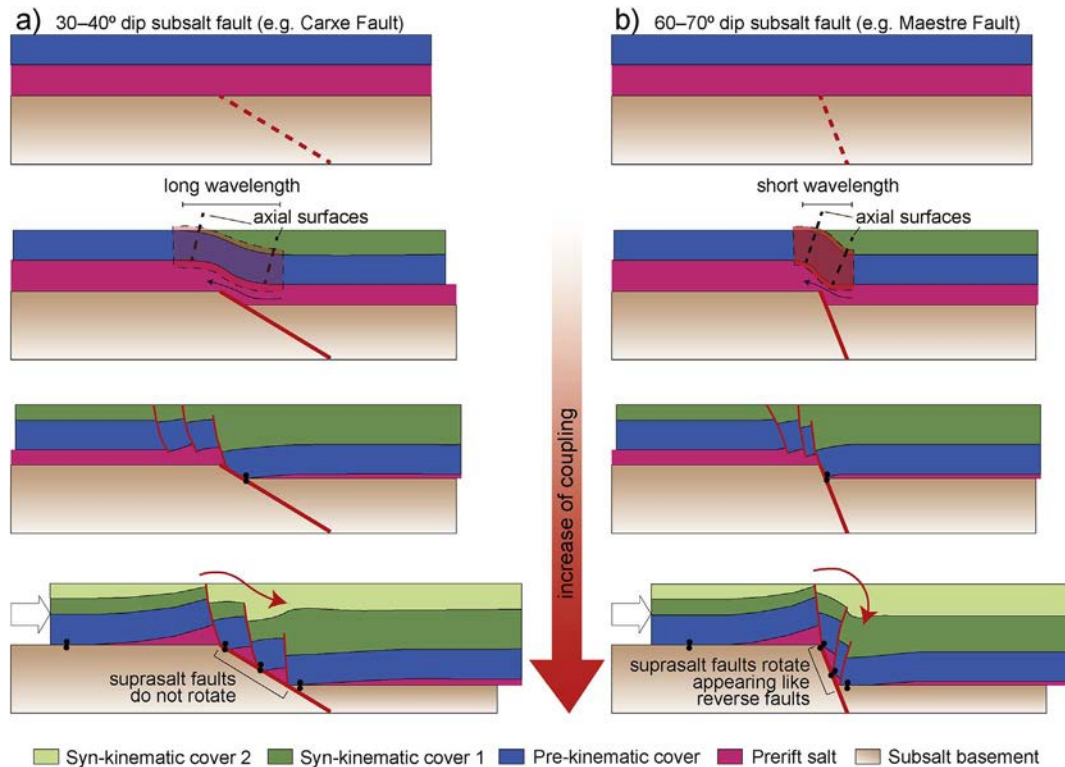
**Fig. 14.** Balanced cross-sections across an ideal monoclinal drape fold system. a) in the case of a 30–40° dip subsalt fault similar to the Carxe Fault; and b) in the case of a 60–70° dip subsalt fault similar to the Maestre Fault.

process in Fig. 14 of Vendeville and Jackson, 1992). The salt structure collapse occurs when the salt supply becomes restricted after depletion and primary weld formation, thus disrupting the salt unit (e.g. see Fig. 13e). Consequently, young sedimentary depocenters are located directly on top of an ancient diapir as it collapses by out-of-plane salt evacuation. Such basins can eventually ground onto the basement and invert to form mock turtle anticlines (e.g. Sierra del Buey in Fig. 7a).

### 6.3. Distinctive contractional suprasalt features linked to the stepped subsalt geometry and the presence of salt structures

#### 6.3.1. Stepped salt detachment

After extension, the resulting salt and suprasalt contractional structure was constrained by the dip direction of the inherited subsalt faults, and by the direction of the thin-skinned shortening. Thus, depending on the dip of subsalt faults (towards the foreland or the hinterland) with respect to the shortening propagation, different contractional structures of the detached cover were developed (Fig. 15a and b).

When the contractional deformation propagated over the hanging wall of a subsalt fault dipping towards the hinterland, a suprasalt ramp anticline was developed over the footwall cut-off of this fault (Fig. 15a and b). Consequently, the fold wavelength will increase towards the hinterland because of the increase of cover thickness. This can be observed by comparing the fold wavelength between the Sierra de las Cabras anticlines with respect to the Sierra Larga-Sopalmo and Carxe anticlines (Fig. 13g).

In contrast, when the contractional deformation propagated over the footwall of a subsalt fault dipping towards the foreland, further advance of shortening was blocked by the footwall cut-off (e.g. see location of the B.T.F in Fig. 15a). Rubinat et al. (2012) and Roca et al. (2013) discussed the role played by this specific subsalt architecture in the junction between the Iberian Chain and the Northeastern Prebetic Zone (Fig. 15a). In this scenario, the pre-existing north-dipping subsalt fault hampered the propagation of the Betic thin-skinned shortening. Consequently, the footwall cut-off of the subsalt fault acted as a

nucleation point in the Betic contractional detachment, which concentrated the entire shortening of the cover (Fig. 15a). In other words, the basal detachment of the cover thrust system did not step down into the Upper Triassic salt of the hanging wall of the north-dipping subsalt fault but ramped up and breached the surface.

#### 6.3.2. Effects of previous salt structures on basin inversion

The incorporation of an ancient passive margin into a foreland fold-and-thrust belt is also restrained by the presence of salt structures (Rowan and Vendeville, 2006). They are weaker than adjacent areas and thus preferentially absorb the shortening during early stages of contractional deformation. In this context, the geometry, width, and number of diapiric structures are the key factors controlling the inversion of the passive margin.

In some locations of the study area, the suprasalt structure was the result of salt roller inversion generating a detachment anticline cored by the salt remnant. Shortening produced the inversion of the suprasalt extensional fault that propagated into the overburden as a thrust fault and controlled the evolution of the hanging wall propagation fold (i.e. the Rajica de Enmedio and Comisario anticlines; see their locations in Fig. 7a and b). In addition, shortening also rejuvenated buried diapirs by squeezing, thus arching their roof (i.e. La Sarsa salt wall, Fig. 7b). As shortening increased, the salt wall could be depleted thus developing secondary welds, eventually evolving into a thrust-weld if shortening progressed (e.g. La Sarsa salt wall, Fig. 7a).

The distribution of previous salt structures along the margin would also control the location of weaker mechanical zones in the suprasalt cover during contraction. For instance, the La Rosa and Jumilla diapirs compartmentalized two thickened suprasalt covers (e.g. Matamoros Basin and Casas del Puerto-Torre del Rico unit, Fig. 15b). In this scenario, shortening was absorbed by rejuvenating the Jumilla Diapir, but also the southeastern La Rosa Diapir, whereas the mechanically resistant thickened covers remained almost undeformed.

The proposed contractional model is consistent with what is observed along the western Betic Cordillera (Flinch et al., 1996; Ramos
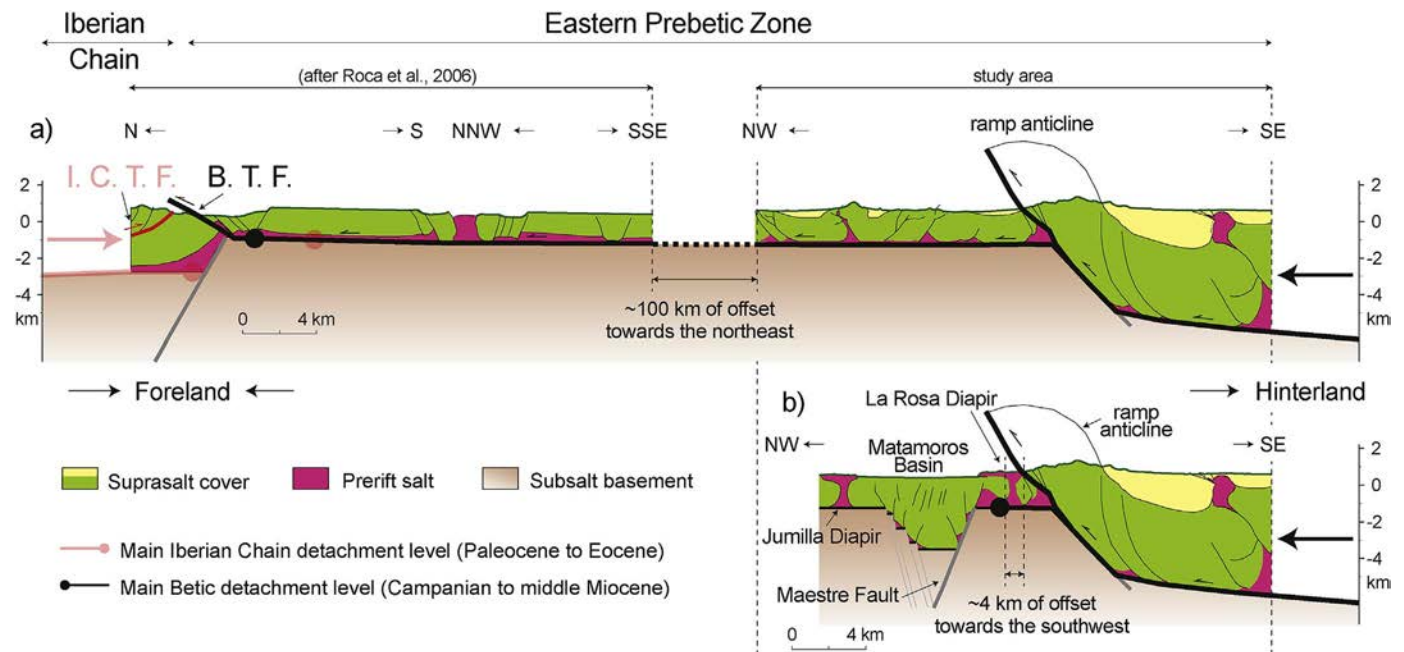
**Fig. 15.** Simplified cross-sections across the Eastern Prebetic Zone. a) structure observed in the junction between the Betic and the Iberian Chain Thrust Fronts (B.T.F. and I.C.T.F., respectively). See the location of the northern part of the cross-section in Fig. 2b. b) structure observed in the study area where the footwall cut-off of the Maestre Fault blocks further propagation of the Betic contractional deformation into the Matamoros Basin. Instead of this, the thin-skinned shortening is absorbed by the rejuvenation of the bounding salt structures.

et al., 2016), the Cotiella Basin (e.g. south central Pyrenees, López-Mir et al., 2014), the Aquitaine Basin (James and Canerot, 1999), the Zagros fold-and-thrust belt (Callot et al., 2012) or the Flinders Ranges (Rowan and Vendeville, 2006) among others where different degrees of inversion of a salt-bearing passive margin led to thin-skinned fold-and-thrust belt development.

## 7. Conclusions

The Eastern Prebetic Zone (SE Iberia), is an outstanding natural laboratory for studying the contractional reactivation of the proximal part of a passive margin containing prerift salt. The structural and stratigraphic analysis of field and subsurface data unravels a series of extensional and contractional structures that can be used to characterize the development of similar passive margins and their later incorporation into thin-skinned fold-and-thrust belts. Therefore, we essentially provide a case study in which:

1  Thick-skinned extension controlled the rate of subsidence and hence the accumulation of sediment over mobile prerift salt. In this scenario, salt acted as a strain localizer by decoupling supra- and subsalt deformation, thus generating two differentiated structural styles —above and below the salt. The subsalt extension controlled suprasalt deformation, and its location and distribution changed over time. In the early stages of extension, the suprasalt deformation was accommodated by the development of monoclinal drape folds, suprasalt faults and diapirs. As extension progressed, folding and faulting were concentrated above the footwall of the main subsalt faults where the cover was thin and mechanically weak. In spite of this, translation with minor folding was concentrated above their hanging walls where the cover was thick and mechanically resistant.

2  Salt also localized strain during the incorporation of the proximal part of the passive margin into the external zones of the fold-and-thrust belt. The preexisting salt structures, weaker than adjacent areas, preferentially absorbed the contractional deformation. The stepped subsalt geometry which resulted from thick-skinned extension also controlled the shortening propagation. Therefore, the degree of strain localization depended on the thickness of the suprasalt

cover and on the dip of subsalt faults relative to the thin-skinned transport direction.

## References

Alves, T.M., Gawthorpe, R.L., Hunt, D.W., Monteiro, J.H., 2002. Jurassic tectono-sedimentary evolution of the northern Lusitanian Basin (offshore Portugal). Mar. Pet. Geol. 19, 727–754. http://dx.doi.org/10.1016/S0264-8172(02)00036-3.

Arias, C., Masse, J.P., Vilas, L., 1993. Caracterización secuencial y bioestratigráfica del Aptiense-Albiense p. p. en la Sierra de Sopalmo, Prebético Interno (Prov. de Murcia). Boletín del Instituto Geológico y Minero de España 104–6, 603–612.

Azéma, J., 1977. Étude géologique des zones externes des cordillères bétiques aux confins des provinces d'Alicante et de Murcie (Espagne). PhD Thesis. Université Pierre et Marie Curie, Paris, pp. 393.

Baena, J., 1979. Mapa Geológico y Memoria explicativa de la Hoja Jumilla (nº 869) del Mapa geológico Nacional a escala 1:50.000. Instituto Geológico y Minero de España, Madrid, pp. 49.

Balanyá, J.C., García-Dueñas, V., 1987. Les directions structurales dans le Domaine d'Alborán de part et d'autre du Détroit de Gibraltar. Comptes Rendus de l'Académie des Sci. de Paris 304, 929–932.

Banks, C.J., Warburton, J., 1991. Mid-crustal detachment in the Betic system of southeast Spain. Tectonophysics 191, 275–289. http://dx.doi.org/10.1016/0040-1951(91)90062-W.

Bartrina, T., Hernández, E., Serrano, A., 1990. Estudio de subsuelo del Trías salino en la Depresión Intermedia. In: Ortí, F., Salvany, J.M. (Eds.), Formaciones evaporíticas de la Cuenca del Ebro y cadenas periféricas y de la zona de Levante, ENRESA. Universitat de Barcelona, pp. 232–238.

Beaumont, C., Muñoz, J.A., Hamilton, J., Fullsack, P., 2000. Factors controlling the Alpine evolution of the central Pyrenees inferred from a comparison of observations and geodynamical models. J. Geophys. Res. 105, 8121–8145. http://dx.doi.org/10.

1029/1999JB900390.

Bernoulli, D., Lemoine, M., 1980. Birth and early evolution of the Tethys: the overall situation. In: 26th International Geological Congress, Paris, pp. 59–96.

Callot, J.-P., Trocmé, V., Letouzey, J., Albouy, E., Jahani, S., Sherkati, S., 2012. Pre-existing salt structures and the folding of the Zagros Mountains. In: In: Alsop, G.I., Archer, S.G., Hartley, A.J., Grant, N.T., Hodgkinson, R. (Eds.), Salt Tectonics, Sediments and Prospectivity, vol. 363. Geological Society of London Special Publications, pp. 545–561. http://dx.doi.org/10.1144/SP363.27.

Canérot, J., Hudec, M.R., Rockenbauch, K., 2005. Mesozoic diapirism in the Pyrenean orogen: salt tectonics on a transform plate boundary. AAPG Bull. 89, 211–229.

Carola, E., Muñoz, J.A., Roca, E., 2015. The transition from thick-skinned to thin-skinned tectonics in the Basque-Cantabrian Pyrenees: the Burgalesa Platform and surroundings. Int. J. Earth Sci. 104, 2215–2239. http://dx.doi.org/10.1007/s00531-015-1177-z.

Castaño, S., 1993. La estructura cortical del area de union de las Cordilleras Ibérica y Béticas. Interpretación geotectónica basada en datos gravimétricos. PhD Thesis. Universidad Complutense de Madrid, Madrid, pp. 302.

Cosgrove, J.W., Ameen, M.S., 2000. A comparison of the geometry, spatial organization and fracture patterns associated with forced folds and buckle folds. In: In: Cosgrove, J.W., Ameen, M.S. (Eds.), Forced Folds and Fractures, vol. 169. Geological Society of London Special Publications, pp. 7–21. http://dx.doi.org/10.1144/GSL.SP.2000.169.01.02.

Cramez, C., Jackson, M.P.A., 2000. Superposed deformation straddling the continental-oceanic transition in deep-water Angola. Mar. Pet. Geol. 17, 1095–1109.

Dahlstrom, C., 1969. Balanced cross sections. Can. J. Earth Sci. 6, 743–757.

De Galdeano, C.S., 1990. Geologic evolution of the betic cordilleras in the western mediterranean, Miocene to the present. Tectonophysics 1772, 107–119. http://dx.doi.org/10.1016/0040-1951(90)90062-D.

De Jong, K., 1990. Alpine tectonics and rotation pole evolution of Iberia. Tectonophysics 184, 279–296. http://dx.doi.org/10.1016/0040-1951(90)90444-D.

De Ruig, M.J., 1992. Tectono-sedimentary Evolution of the Prebetic Fold Belt of Alicante (SE Spain). A Study of Stress Fluctuations and Foreland Basin Deformation. PhD Thesis. Vrije Universiteit, Amsterdam.

De Ruig, M.J., 1995. Extensional diapirism in the eastern prebetic Foldbelt, southeastern Spain. In: In: Jackson, M.P.A., Roberts, D.G., Snelson, S. (Eds.), Salt Tectonics: a Global Perspective, vol. 65. AAPG Memoir, pp. 353–367.

De Torres, T., Sánchez, A., 1990. Espesores de las Facies Keuper en la Rama Castellana de la Cordillera Ibérica y en el Dominio Prebético. In: Ortí, F., Salvany, J.M. (Eds.), Formaciones evaporíticas de la Cuenca del Ebro y cadenas periféricas, y de la zona de Levante. ENRESA - Universitat de Barcelona, Barcelona, pp. 212–218.

Decarlis, A., Maino, M., Dallagiovanna, G., Lualdi, A., Masini, E., Seno, S., Toscani, G., 2014. Salt tectonics in the SW Alps (Italy–France): from rifting to the inversion of the European continental margin in a context of oblique convergence. Tectonophysics 636, 293–314. http://dx.doi.org/10.1016/j.tecto.2014.09.003.

Dercourt, J., Zonenshain, L.P., Ricou, L.E., Kazmin, V.G., Le Pichon, X., Knipper, A.L., Grandjacquet, C., Sbortshikov, I.M., Geyssant, J., Lepvrier, C., Pechersky, D.H., Boulin, J., Sibuet, J.C., Savostin, L.A., Sorokhtin, O., Westphal, M., Bazhenov, M.L., Lauer, J.P., Biju-Duval, B., 1986. Geological evolution of the Tethys belt from the Atlantic to the pamirs since the Lias. Tectonophysics 123, 241–315. http://dx.doi.org/10.1016/0040-1951(86)90199-X.

Dercourt, J., Ricou, L.E., Vrielynck, B. (Eds.), 1993. Atlas Tethys Paleoenvironmental Maps. Gauthier-Villars, Paris.

Dewey, J.F., Pitman III, W.C., Ryan, W.B.F., Bonnin, J., 1973. Plate tectonics and the evolution of the Alpine system. Geol. Soc. Am. Bull. 84, 3137–3180. http://dx.doi.org/10.1130/0016-7606(1973)84<3137: PTATEO>2.0.CO;2.

Dewey, J.F., Helman, M.L., Knott, S.D., Turco, E., Hutton, D.H.W., 1989. Kinematics of the western mediterranean. In: In: Coward, M.P., Dietrich, D., Park, R.G. (Eds.), Alpine Tectonics, vol. 45. Geological Society of London Special Publications, pp. 265–283. http://dx.doi.org/10.1144/GSL.SP.1989.045.01.15.

Duffy, O., Gawthorpe, R.L., Docherty, M., Brocklehurst, S.H., 2012. Mobile evaporite controls on the structural style and evolution of rift basins: Danish Central Graben, North Sea. Basin Res. 24, 1–21. http://dx.doi.org/10.1111/bre.12000.

Egeler, C.G., Simon, O.J., 1969. Orogenic evolution of the betic zone (betic cordilleras, Spain), with emphasis on the nappe structures. Geol. Mijnbouw 48 296–205.

Elliott, D., 1976. The energy balance and deformation mechanisms of thrust sheets. Philos. Trans. Roy. Soc. Lon. Series A Math. Phys. Sci. 283, 289–312.

Ellis, S., Beaumont, C., Jamieson, R.A., Quinlan, G., 1998. Continental collision including a weak zone: the vise model and its application to the Newfoundland Appalachians. Can. J. Earth Sci. 35, 1323–1346.

Fallot, P., 1948. Les Cordillères Bétiques. Estud. Geol. 8, 83–172.

Favre, P., Stampfli, G.M., 1992. From rifting to passive margin: the examples of the Red Sea, Central Atlantic and Alpine Tethys. Tectonophysics 215, 69–97.

Ferrer, O., Jackson, M.P.A., Roca, E., Rubinat, M., 2012. Evolution of salt structures during extension and inversion of the offshore Parentis Basin (eastern Bay of Biscay). In: In: Alsop, G.I., Archer, S.G., Hartley, A.J., Grant, N.T., Hodgkinson, R. (Eds.), Salt Tectonics, Sedimentation and Prospectivity, vol. 363. Geological Society of London Special Publications, pp. 361–380. http://dx.doi.org/10.1144/SP363.16.

Ferrer, O., Roca, E., Vendeville, B.C., 2014. The role of salt layers in the hangingwall deformation of kinked-planar extensional faults: insights from 3D analogue models and comparison with the Parentis Basin. Tectonophysics 636, 338–350. http://dx.doi.org/10.1016/j.tecto.2014.09.013.

Ferrer, O., McClay, K., Sellier, N.C., 2016. Influence of fault geometries and mechanical anisotropies on the growth and inversion of hanging-wall synclinal basins: insights from sandbox models and natural examples. In: Childs, C., Holdsworth, R.E., Jackson, C.A.-L., Manzocchi, T., Walsh, J.J., Yielding, G. (Eds.), The Geometry and Growth of Normal Faults. Geological Society of London Special Publications, pp. 439. http://dx.

doi.org/10.1144/SP439.8.

Flinch, J.F., Bally, A.W., Wu, S., 1996. Emplacement of a passive-margin evaporitic allochthon in the Betic Cordillera of Spain. Geology 24, 67–70. http://dx.doi.org/10.1130/0091-7613(1996)024<0067:EOAPME>2.3.CO;2.

Frizon de Lamotte, D., Raulin, C., Mouchot, N., Wrobel-Daveau, J.-C., Blanpied, C., Ringenbach, J.-C., 2011. The southernmost margin of the Tethys realm during the Mesozoic and Cenozoic: initial geometry and timing of the inversion processes. Tectonics 30, 1–22. http://dx.doi.org/10.1029/2010TC002691.

García-Hernández, M., López-Garrido, A.C., Rivas, P., Sanz de Galdeano, C., Vera, J.A., 1980. Mesozoic palaeogeographic evolution of the external zones of the Betic Cordillera. Geol. Mijnbouw 59, 155–168.

García-Hernández, M., López-Garrido, A.C., Martín-Algarra, A., Molina, J.M., Ruiz-Ortiz, P.A., Vera, J.A., 1989. Las discontinuidades mayores del Jurásico de las Zonas Externas de las Cordilleras Béticas: análisis e interpretación de los ciclos sedimentarios. Cuad. Geol. Iber. 13, 35–52.

Giles, K.A., Rowan, M.G., 2012. Concepts in halokinetic-sequence deformation and stratigraphy. Geol. Soc. Lon. Spec. Publ. 363, 7–31. http://dx.doi.org/10.1144/SP363.2.

Guerrera, F., Mancheño, M.A., Martín-Martín, M., Raffaelli, G., Rodríguez-Estrella, T., Serrano, F., 2014. Paleogene evolution of the external betic zone and geodynamic implications. Geol. Acta 12, 170–192. http://dx.doi.org/10.1344/GeologicaActa2014.12.3.1.

Hanne, D., White, N., Lonergan, L., 2003. Subsidence analyses from the betic Cordillera, southeast Spain. Basin Res. 15, 1–21.

Hillebrandt, A. von, 1974. Bioestratigrafía del Paleógeno en el Sureste de España (Provincias de Murcia y Alicante). Cuad. Geol. Iber. 5, 135–153.

Hossack, J.R., 1983. A cross-section through the Scandinavian Caledonides constructed with the aid of branch-line maps. J. Struct. Geol. 5, 103–111.

Jackson, M.P.A., Vendeville, B.C., 1994. Regional extension as a geologic trigger for diapirism. Geol. Soc. Am. Bull. 106, 57–73. http://dx.doi.org/10.1130/0016-7606(1994)106<0057:REAAGT>2.3.CO;2.

Jackson, C.A.L., Jackson, M.P.A., Hudec, M.R., 2015. Understanding the kinematics of salt-bearing passive margins: a critical test of competing hypotheses for the origin of the Albian Gap, Santos Basin, offshore Brazil. Geol. Soc. Am. Bull. 127, 1730–1751. http://dx.doi.org/10.1130/B31290.1.

James, V., Canerot, J., 1999. Diapirisme et structuration post-triasique des Pyrénées occidentales et de l'Aquitaine méridionale (France). Eclogae Geol. Helv. 92, 63–72.

Jammes, S., Huismans, R.S., 2012. Structural styles of mountain building: controls of lithospheric rheologic stratification and extensional inheritance. J. Geophys. Res. 117, 1978–2012. http://dx.doi.org/10.1029/2012JB009376.

Kane, K.E., Jackson, C.A.L., Larsen, E., 2010. Normal fault growth and fault-related folding in a salt-influenced rift basin: south Viking Graben, Offshore Norway. J. Struct. Geol. 32, 490–506.

Klitgord, K.D., Schouten, H., 1986. Plate kinematics of the central Atlantic. In: Vogt, P.R., Tucholke, B.E. (Eds.), The Geology of North America, the Western North Atlantic Region M. Geological Society of America, pp. 351–378.

Koyi, H., Jenyon, M.K., Petersen, K., 1993. The effect of basement faulting on diapirism. J. Pet. Geol. 16, 285–312.

Lanaja, J.M., Querol, R., Navarro, A., 1987. Contribución de la exploración petrolífera al conocimiento de la geología de España. Instituto Geológico y Minero de España, Madrid, pp. 465.

Lemoine, M., Bas, T., Arnaud-Vanneau, A., Arnaud, H., Dumont, T., Gidon, M., Bourbon, M., de Graciansky, P.C., Rudkiewicz, J.L., Megard-Galli, J., Tricart, P., 1986. The continental margin of the mesozoic Tethys in the western Alps. Mar. Pet. Geol. 3, 179–199. http://dx.doi.org/10.1016/0264-8172(86)90044-9.

López-Garrido, A.C., 1971. Geología de la Zona Prebética al NE de la provincia de Jaén. PhD Thesis. Universidad de Granada, pp. 317.

López-Mir, B., Muñoz, J.A., García Senz, J., 2014. Restoration of basins driven by extension and salt tectonics: example from the Cotiella Basin in the central Pyrenees. J. Struct. Geol. 69, 147–162. http://dx.doi.org/10.1016/j.jsg.2014.09.022.

Martín-Chivelet, J., 1996. Late cretaceous subsidence history of the betic continental margin (Jumilla-Yecla region, SE Spain). Tectonophysics 265, 191–211.

Martín-Chivelet, J., Giménez, R., Luperto Sinni, E., 1997. La discontinuidad del Campaniense basal en el Prebético: ¿Inicio de la convergencia alpina en el Margen Bética? Geogaceta 22, 121–124.

Martínez del Olmo, W., Benzaquen, M., Cabañas, I., Uralde, M.A., 1975. Mapa y memoria explicativa de la Hoja Onteniente (nº 820) del Mapa geológico Nacional a escala 1:50.000. Instituto Geológico y Minero de España, Madrid, pp. 49.

Maurin, J.C., Niviere, B., 2000. Extensional forced folding and decollement of the pre-rift series along the Rhine graben and their influence on the geometry of the syn-rift sequences. In: In: Cosgrove, J.W., Ameen, M.S. (Eds.), Forced Folds and Fractures, vol. 169. Geological Society of London, Special Publications, pp. 73–86. http://dx.doi.org/10.1144/GSL.SP.2000.169.01.06.

Moseley, F., 1973. Diapiric and gravity tectonics in the Pre-betic, (Sierra bernia) southeast Spain. Boletín del Instituto Geológico y Minero de España 84, 114–126.

Muñoz, J.A., 2002. The Pyrenees. In: Gibbons, W., Moreno, T. (Eds.), The Geology of Spain. Geological Society of London, pp. 370–385.

Ortí, F., 1974. El Keuper del Levante español. Estud. Geol. 30, 7–46.

Pascoe, R., Hooper, R., Storhaug, K., Harper, H., 1999. Evolution of extensional styles at the southern termination of the Nordland Ridge, Mid-Norway: a response to variations in coupling above Triassic salt. In: In: Fleet, A.J., Boldy, S.A.R. (Eds.), Petroleum Geology of Northwest Europe, Proceedings of the 5th Conference, vol. 5. pp. 83–90.

Platt, J.P., Allerton, S., Kirker, A., Mandeville, C., Mayfield, A., Platzman, E.S., Rimi, A., 2003. The ultimate arc: differential displacement, oroclinal bending, and vertical axis rotation in the External Betic-Rif arc. Tectonics 22, 1017–1048. http://dx.doi.org/10.1029/2001TC001321.

Puga, E., Fanning, M., Díaz de Federico, A., Nieto, J.M., Beccaluva, L., Bianchini, G., Díaz

Puga, M.A., 2011. Petrology, geochemistry and U-Pb geochronology of the betic ophiolites: inferences for Pangaea break-up and birth of the westernmost Tethys ocean. Lithos 124, 255–272.

Ramos, A., Fernández, O., Terrinha, P., Muñoz, J.A., 2016. Extension and inversion structures in the Tethys-Atlantic linkage zone, Algarve Basin, Portugal. Int. J. Earth Sci. 105, 1663–1679. http://dx.doi.org/10.1007/s00531-015-1280-1.

Richardson, N.J., Underhill, J.R., Lewis, G., 2005. The role of evaporite mobility in modifying subsidence patterns during normal fault growth and linkage, Halten Terrace, Mid-Norway. Basin Res. 17, 203–223. http://dx.doi.org/10.1111/j.1365-2117.2005.00250.x.

Roca, E., Guimerà, J., Salas, R., 1994. Mesozoic extensional tectonics in the southeast Iberian Chain. Geol. Mag. 131, 155–168.

Roca, E., Sans, M., Koyi, H.A., 2006. Polyphase deformation of diapiric areas in models and in the Eastern Prebetics (Spain). AAPG Bull. 90, 115–136. http://dx.doi.org/10.1306/07260504096.

Roca, E., Muñoz, J.A., Ferrer, O., Ellouz, N., 2011. The role of the Bay of Biscay Mesozoic extensional structure in the configuration of the Pyrenean orogen: constraints from the MARCONI deep seismic reflection survey. Tectonics 30, 1–33. http://dx.doi.org/10.1029/2010TC002735.

Roca, E., Beamud, E., Rubinat, M., Soto, R., Ferrer, O., 2013. Paleomagnetic and inner diapiric structural constraints on the kinematic evolution of a salt-wall: the Bicorb-Quesa and northern Navarrés salt-wall segments case (Prebetic Zone, SE Iberia). J. Struct. Geol. 52, 80–95. http://dx.doi.org/10.1016/j.jsg.2013.04.003.

Rodríguez-Estrella, T., 1977. Síntesis geológica del Prebético de la provincia de Alicante. Boletín del Instituto Geológico y Minero de España 88, 183–214 and 88, 273–299.

Rowan, M.G., 2014. Passive-margin salt basins: hyperextension, evaporite deposition, and salt tectonics. Basin Res. 26, 154–182. http://dx.doi.org/10.1111/bre.12043.

Rowan, M.G., Ratliff, R.A., 2012. Cross-section restoration of salt-related deformation: best practices and potential pitfalls. J. Struct. Geol. 41, 24–37.

Rowan, M.G., Vendeville, B.C., 2006. Foldbelts with early salt withdrawal and diapirism: physical model and examples from the northern Gulf of Mexico and the Flinders Ranges, Australia. Mar. Pet. Geol. 23, 871–891. http://dx.doi.org/10.1016/j.marpetgeo.2006.08.003.

Rowan, M.G., Peel, F.J., Vendeville, B.C., 2004. Gravity-driven fold belts on passive margins. In: In: McClay, K.R. (Ed.), Thrust Tectonics and Hydrocarbon Systems, vol. 82. AAPG Memoir, pp. 157–182.

Rubinat, M., Roca, E., Escalas, M., Queralt, P., Ferrer, O., Ledo, J.J., 2012. The influence of basement structure on the evolution of the Bicorb-Quesa Diapir (eastern Betics, Iberian Peninsula): contractive thin-skinned deformation above a pre-existing extensional basement fault. Int. J. Earth Sci. 102, 25–41. http://dx.doi.org/10.1007/s00531-012-0789-9.

Saura, E., Vergés, J., Martín-Martín, J.D., Messager, G., Moragas, M., Razin, P., Gréland, C., Joussiaume, R., Homke, S., Hunt, D.W., 2013. Syn- to post-rift diapirism and minibasins of the Central High Atlas (Morocco): the changing face of a mountain belt. J. Geol. Soc. Lon. 171, 97–105. http://dx.doi.org/10.1144/jgs2013-079.

Schettino, A., Turco, E., 2010. Tectonic history of the western Tethys since the late triassic. Geol. Soc. Am. Bull. 123, 89–105.

Serrano, A., Hernaiz, P.P., Malagón, J., Rodríguez-Cañas, C., 1994. Tectónica distensiva y halocinesis en el margen SO de la cuenca Vasco-Cantábrica. Geogaceta 15, 131–134.

Srivastava, S.P., Schouten, H., Roest, W.R., Klitgord, K.D., Kovacs, L.C., Verhoef, J., Macnab, R., 1990. Iberian plate kinematic: a jumping between Eurasia and Africa. Nature 344, 756–759.

Suppe, J., 1983. Geometry and kinematics of fault-bend folding. Am. J. Sci. 283, 684–721.

Tari, G., Molnar, J., Ashton, P., 2003. Examples of salt tectonics from west Africa: a comparative approach. In: In: Arthur, T.J., MacGregor, D.S., Cameron, N.R. (Eds.), Petroleum Geology of Africa: New Themes and Developing Technologies, vol. 207. Geological Society of London, Special Publications, pp. 85–104.

Tavani, S., Granado, P., 2014. Along-strike evolution of folding, stretching and breaching of supra-salt strata in the Plataforma Burgalesa extensional forced fold system (northern Spain). Basin Res. 1–13. http://dx.doi.org/10.1111/bre.12089.

Ter Borgh, M.M., Oldenhuis, R., Biermann, C., Smit, J.H.W., Sokoutis, D., 2011. The effects of basement ramps on deformation of the Prebetics (Spain): a combined field and analogue modelling study. Tectonophysics 502, 62–74. http://dx.doi.org/10.1016/j.tecto.2010.04.013.

Torres-Roldán, R.L., 1979. The tectonic subdivision of the Betic Zone (Betic Cordilleras, southern Spain): its significance and one possible geotectonic scenario for the westernmost Alpine belt. Am. J. Sci. 279, 19–51.

Vendeville, B.C., Jackson, M.P.A., 1992. The fall of diapirs during thin-skinned extension. Mar. Pet. Geol. 9, 354–371.

Vera, J.A., 2004. Geología de España. SGE-IGME, Madrid.

Vera, J.A., García-Hernández, M., López-Garrido, A.C., Comas, M.C., Ruíz-Ortíz, P.A., Martín-Algarra, A., 1982. El Cretácico de las Cordilleras Béticas. In: García, A. (Ed.), El Cretácico de España. Universidad Complutense de Madrid, Madrid, pp. 515–632.

Vilas, L., Arias, C., Elizaga, E., García de Domingo, A., López-Olmedo, F., 1982. Consideraciones sobre el Cretácico inferior de la zona de Jumilla-Yecla. Cuad. Geol. Iber. 8, 635–649.

Vilas, L., Martin-Chivelet, J., Arias, C., 2003. Integration of subsidence and sequence stratigraphic analyses in the Cretaceous carbonate platforms of the Prebetic (Jumilla–Yecla Region), Spain. Palaeogeogr. Palaeoclimatol. Palaeoecol. 200, 107–129. http://dx.doi.org/10.1016/S0031-0182(03)00447-4.

Withjack, M.O., Callaway, S., 2000. Active normal faulting beneath a salt layer: an experimental study of deformation patterns in the cover sequence. AAPG Bull. 84, 627–651. http://dx.doi.org/10.1306/c9ebce73-1735-11d7-8645000102c1865d.

Withjack, M.O., Meisling, K., Russell, L., 1989. Forced folding and basement-detached normal faulting in the Haltenbanken area, offshore Norway. In: In: Tankard, A.J., Balkwell, H.R. (Eds.), Extensional Tectonics and Stratigraphy of the North Atlantic Margins, vol. 46. AAPG Memoir, pp. 567–575.

Woodward, N.B., Boyer, S.E., Suppe, J., 1985. second ed. An Outline of Balanced Cross-sections, vol. 11 Univ. Tenn. Dep. Geol. Sci., Stud. Geol 170 pp.

Ziegler, P.A., 1982. Geological Atlas of Western and Central Europe. Elsevier, Amsterdam.

Ziegler, P.A., 1989. Evolution of the north Atlantic – an overview. In: In: Tankard, A.J., Balkwell, H.R. (Eds.), Extensional Tectonics and Stratigraphy of the North Atlantic Margins, vol. 46. AAPG Memoir, pp. 111–129.
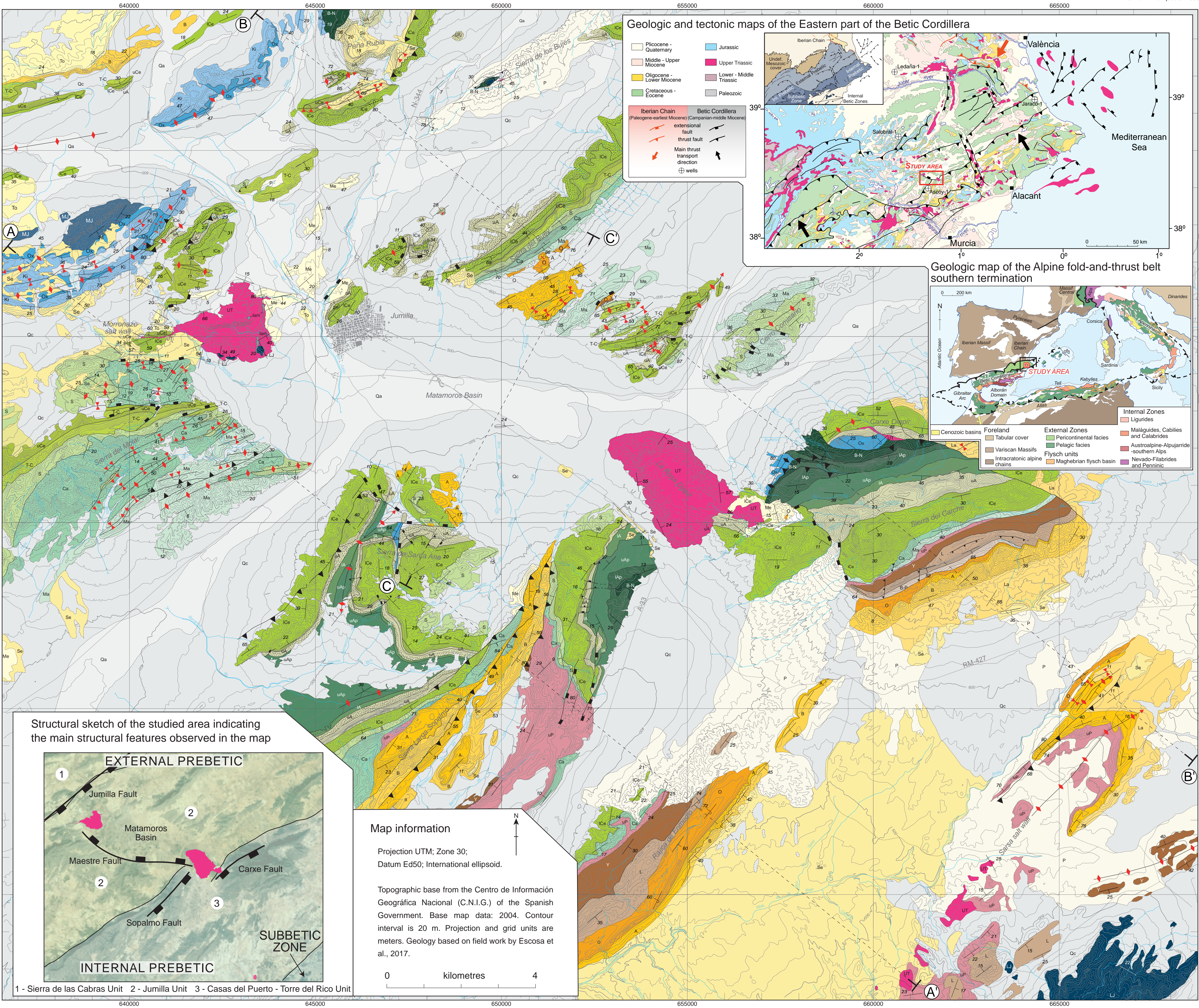
# 1: 50,000 GEOLOGICAL MAP OF THE EASTERN PREBETIC ZONE AT THE JUMILLA REGION (SE IBERIA)

*Frederic Oriol Escosa, Oriol Ferrer and Eduard Roca*

Institut de Recerca Geomodels
Departament de Dinàmica de la Terra i de l'Oceà
Facultat de Ciències de la Terra
Universitat de Barcelona, Barcelona, Spain.
c/ Martí i Franquès s/n. 08028 Barcelona.

UNIVERSITAT DE BARCELONA    geomodels institut de recerca

**Geologic and tectonic maps of the Eastern part of the Betic Cordillera**

Pliocene - Quaternary
Middle - Upper Miocene
Oligocene - Lower Miocene
Cretaceous - Eocene
Jurassic
Upper Triassic
Lower - Middle Triassic
Paleozoic

Iberian Chain (Paleogene-earliest Miocene) / Betic Cordillera (Campanian-middle Miocene)
extensional fault
thrust fault
Main thrust transport direction
wells

València
Mediterranean Sea
Murcia
Alacant

**Geologic map of the Alpine fold-and-thrust belt southern termination**

Cenozoic basins
Foreland: Tabular cover, Variscan Massifs, Intracratonic alpine chains
External Zones: Pericontinental facies, Pelagic facies
Flysch units: Maghrebian flysch basin
Internal Zones: Ligurides, Malàguides, Cabilies and Calabrides, Austroalpine-Alpujarride -southern Alps, Nevado-Filabrides and Peninnic

STUDY AREA

## Geologic Map Units

### Post-orogenic

Qc — Quaternary colluvial
Qa — Quaternary alluvial
P — Pliocene
lam — Pliocene - Messinian (lamproitic rocks)
Me — Messinian  ⎤
To — Tortonian   ⎦ Miocene

### Syn-contractional (coeval to Betic orogen development)

Se — Serravallian ⎤
La — Langhian     ⎥ Miocene
B — Burdigalian   ⎥
A — Aquitanian    ⎦
O — Oligocene
B-P — Barto. - Priab. ⎤
L — Lutetian          ⎥ Eocene
Y — Ypresian          ⎦
uP — upper Paleocene
Ma — Maastrichtian ⎤ Upper
Ca — Campanian     ⎦ Cretaceous

### Syn-extensional (coeval to South Iberian passive margin development)

S — Santonian            ⎤
T-C — Turonian to Coniacian ⎥ Upper
uCe — upper Cenomanian   ⎥ Cretaceous
lCe — lower Cenomanian (marls / dolostones) ⎦
uA — upper Albian (sands / limestones) ⎤
lA — lower Albian                       ⎥
uAp — upper Aptian                      ⎥ Lower
lAp — lower Aptian                      ⎥ Cretaceous
B-N — Barremian Neocomian               ⎦
Ki — Kimmeridgian ⎤ Upper
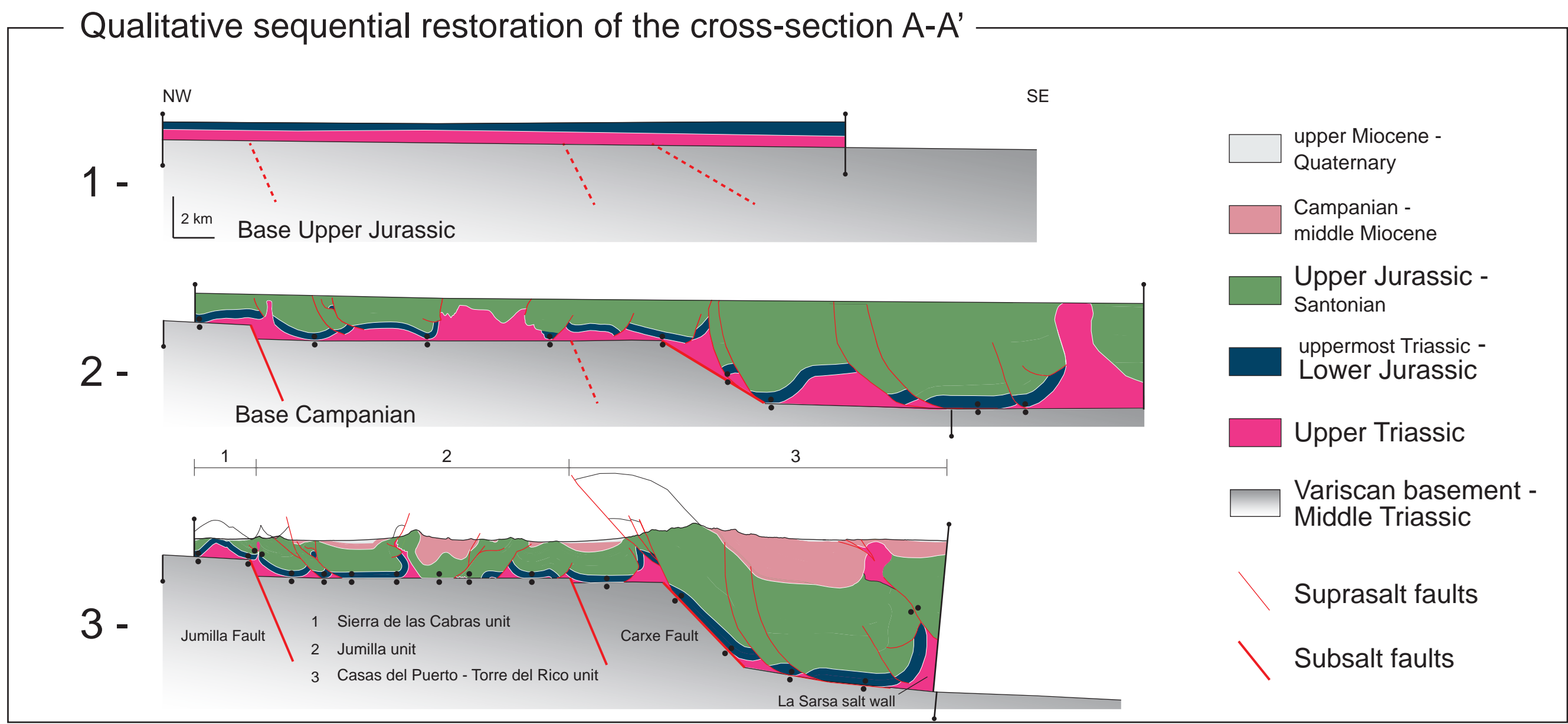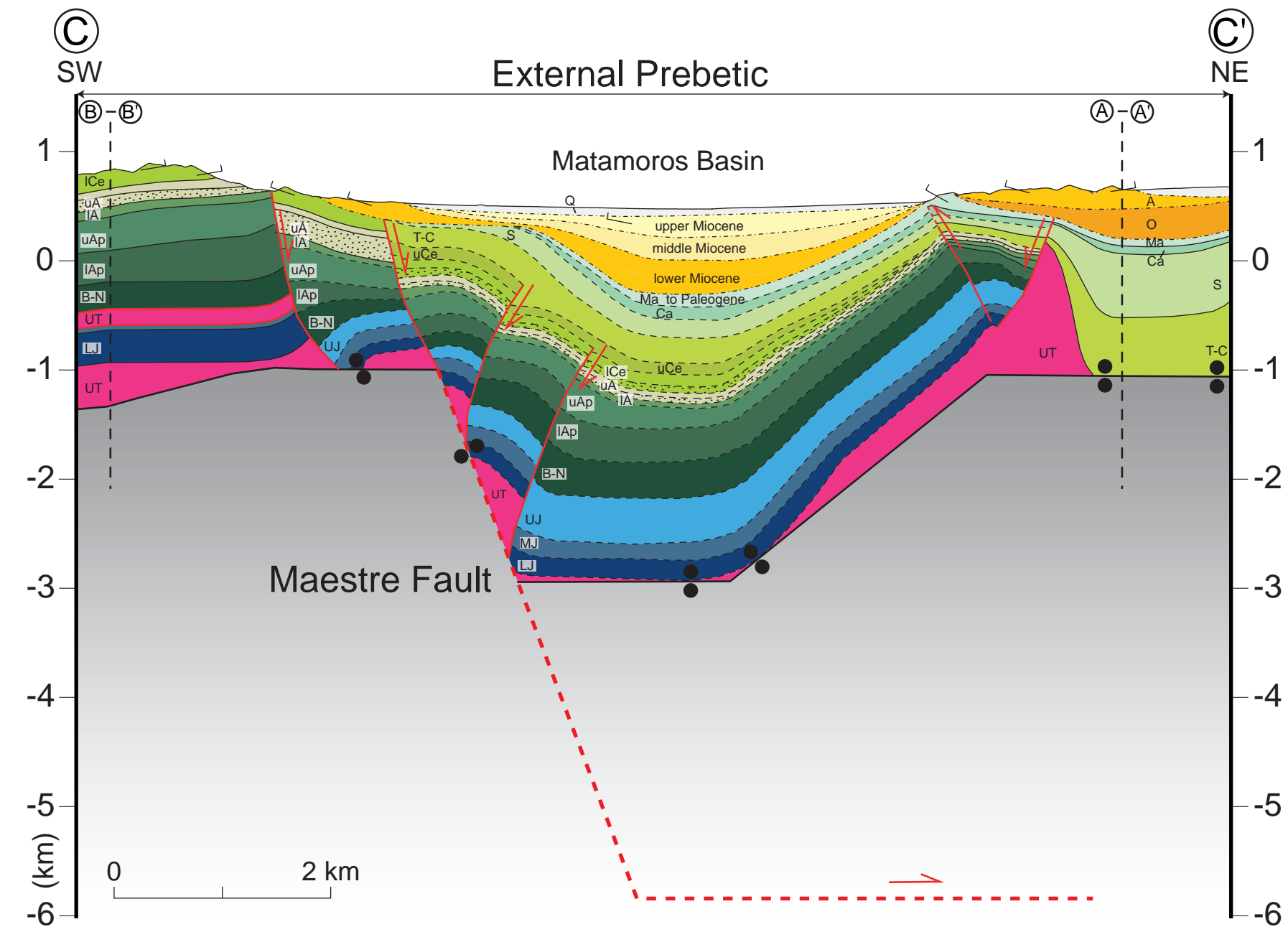Ox — Oxfordian    ⎦ Jurassic

### Pre-extensional

MJ — Middle Jurassic
LJ — uppermost Triassic - Lower Jurassic
UT — Upper Triassic

## Symbols

27 — Normal dip
60 — Overturned dip
— Vertical dip
— Contact
— Unconformity
— Syncline
— Anticline
— Thrust fault
— Extensional fault
— Roads
— Overturned syncline
— Overturned anticline

* The fault symbols depicted in this map reflect the stratigraphical relationship of hanging wall to footwall (i.e. thrust: older over younger; normal: younger over older).

### Structural sketch of the studied area indicating the main structural features observed in the map

EXTERNAL PREBETIC
Jumilla Fault
Matamoros Basin
Maestre Fault
Carxe Fault
Sopalmo Fault
SUBBETIC ZONE
INTERNAL PREBETIC

1 - Sierra de las Cabras Unit   2 - Jumilla Unit   3 - Casas del Puerto - Torre del Rico Unit

### Map information

Projection UTM; Zone 30;
Datum Ed50; International ellipsoid.

Topographic base from the Centro de Información Geográfica (C.N.I.G.) of the Spanish Government. Base map data: 2004. Contour interval is 20 m. Projection and grid units are meters. Geology based on field work by Escosa et al., 2017.

0    kilometres    4

# CROSS-SECTIONS OF THE EASTERN PREBETIC ZONE AT THE JUMILLA REGION (1:50,000 SCALE). *Escosa, F.O.; Ferrer, O. and Roca, E.*



**Color key**

**Post-orogenic**

- Q Quaternary
- P Pliocene
- Me Messinian — Miocene
- To Tortonian — Miocene

**Syn-contractional (coeval to Betic orogen development)**

- Se Serravallian — Miocene
- La Langhian — Miocene
- B Burdigalian — Miocene
- A Aquitanian — Miocene
- O Oligocene
- B-P Barto. - Priab. — Eocene
- L Lutetian — Eocene
- Y Ypresian — Eocene
- uP upper Paleocene
- Ma Maastrichtian — Upper Cretaceous
- Ca Campanian — Upper Cretaceous

**Syn-extensional (coeval to South Iberian passive margin development)**

- S Santonian — Upper Cretaceous
- T-C Turonian - Coniacian — Upper Cretaceous
- uCe upper Cenomanian — Upper Cretaceous
- lCe lower Cenomanian (marls / dolostones) — Upper Cretaceous
- uA upper Albian (sands/ carbonates) — Lower Cretaceous
- lA lower Albian — Lower Cretaceous
- uAp upper Aptian — Lower Cretaceous
- lAp lower Aptian — Lower Cretaceous
- B-N Neocomian Barremian — Lower Cretaceous
- UJ Upper Jurassic

**Pre-extensional**

- MJ Middle Jurassic
- LJ uppermost Triassic - Lower Jurassic
- UT Upper Triassic
- Variscan basement - Middle Triassic

**Sign key**

- Projected bedding attitude
- Unconformity
- Salt weld
- Extensional fault
- Thrust fault
- Inverted fault

**Contact geometry legend**

- inferred geometry
- constrained geometry
- * no vertical exaggeration
- * Quaternary units are not differentiated

Qualitative sequential restoration of the cross-section A-A'

- upper Miocene - Quaternary
- Campanian - middle Miocene
- Upper Jurassic - Santonian
- uppermost Triassic - Lower Jurassic
- Upper Triassic
- Variscan basement - Middle Triassic
- Suprasalt faults
- Subsalt faults